UNIVERSIDAD NACIONAL AUTÓNOMA DE MÉXICO
PROGRAMA DE DOCTORADO EN CIENCIAS BIOMÉDICAS

La respuesta al estrés de retículo endoplásmico en *Dictyostelium discoideum*

TESIS

QUE PARA OPTAR POR EL GRADO DE
DOCTORA EN CIENCIAS

PRESENTA

Eunice Alejandra Domínguez Martín

Directores de tesis
Dr. Roberto Coria Ortega,
Instituto de Fisiología Celular
Universidad Nacional Autónoma de México,
CDMX, México

DR. Ricardo Escalante Hernández
Instituto de Investigaciones Biomédicas "Alberto Sols"
Consejo Superior de Investigaciones Científicas,
Universidad Autónoma de Madrid, Madrid, España

Ciudad Universitaria, Cd. Mx, México, 2018

Universidad Nacional Autónoma de México /
Universidad Autónoma de Madrid

Programa de Doctorado en Ciencias Biomédicas /
Doctorado en Biociencias Moleculares

La respuesta al estrés de retículo endoplásmico en *Dictyostelium discoideum*

Eunice Alejandra Domínguez Martín

Ciudad Universitaria, Cd. Mx., México

Madrid, España

2018

DEPARTAMENTO DE BIOQUÍMICA
FACULTAD DE MEDICINA
UNIVERSIDAD AUTÓNOMA DE MADRID

La respuesta al estrés de retículo endoplásmico en *Dictyostelium discoideum*

EUNICE ALEJANDRA DOMÍNGUEZ MARTÍN

Licenciada en Investigación Biomédica Básica,
Maestra en Ciencias Bioquímicas
por la Universidad Nacional Autónoma de México

DIRECTORES DE TESIS
DR. ROBERTO CORIA ORTEGA,
IFC, UNAM. CDMX, MÉXICO

DR. RICARDO ESCALANTE HERNÁNDEZ
IIB, UAM, MADRID, ESPAÑA.

Instituto de Fisiología Celular
Universidad Nacional Autónoma de México, CDMX, México

Instituto de Investigaciones Biomédicas "Alberto Sols"
Consejo Superior de Investigaciones Científicas, Universidad Autónoma de Madrid, Madrid, España

Dr. Ricardo Escalante Hernández
Científico Titular del Consejo Superior de Investigaciones Científicas en
el Instituto de Investigaciones Biomédicas "Alberto Sols" de Madrid (CSIC/UAM)

CERTIFICA:
que **Eunice Alejandra Domínguez Martín**, Licenciada en Investigación Biomédica Básica por la Universidad Nacional Autónoma de México ha realizado bajo su dirección el trabajo de investigación titulado: **"La respuesta al estrés de retículo endoplásmico en *Dictyostelium discoideum*".**

Dicho trabajo reúne las condiciones requeridas por la legislación vigente, así como la originalidad y calidad científica necesarias para poder ser presentado y defendido con el fin de optar al grado de Doctor por la Universidad Autónoma de Madrid.

Y para que conste donde proceda, firmo el presente documento en Madrid a 4 de septiembre de 2018

Dr. Roberto Coria Ortega
Investigador Titular C,
Instituto de Fisiología Celular,
Universidad Nacional Autónoma de México

CERTIFICA:

que **Eunice Alejandra Domínguez Martín**, Licenciada en Investigación Biomédica Básica por la Universidad Nacional Autónoma de México ha realizado bajo su dirección el trabajo de investigación titulado: **"La respuesta al estrés de retículo endoplásmico en *Dictyostelium discoideum"*.**

Dicho trabajo reúne las condiciones requeridas por la legislación vigente, así como la originalidad y calidad científica necesarias para poder ser presentado y defendido con el fin de optar al grado de Doctor por la Universidad Autónoma de Madrid.

Y para que conste donde proceda, firmo el presente documento en la CDMX, México, el día 30 de julio de 2018

ROBERTO CORIA ORTEGA

AGRADECIMIENTOS

El jurado que evaluó esta tesis para el examen de obtención de grado fue el siguiente:

Dra. Rosa Estela Navarro González, IFC, UNAM.
Dra. Susana Castro Obregón, IFC, UNAM.
Dra. Lourdes Massieu Trigo, IFC, UNAM.
Dr. Leandro Sastre Garzón, IIB, UAM.
Dr. Francisco Portillo Pérez, IIB, UAM.

RESUMEN

El retículo endoplásmico (RE) es el compartimento celular en el cual se pliegan y modifican la mayor parte de las proteínas transmembranales y de secreción. Existe un programa adaptativo que permite mantener la homeostasis de este organelo, principalmente mediante la activación de la vía de respuesta a proteínas mal plegadas (UPR), la cual en animales, se constituye por tres rutas de señalización reguladas respectivamente por las proteínas ATF6 (*Activating Transcription Factor 6*), PERK (*Protein Kinase RNA-like ER Kinase*) e IRE1 (*Inositol-Requiring Enzyme 1*). Estas, comunican al núcleo la presencia de alteraciones en el RE y permiten así, que se incremente la capacidad de plegamiento de proteínas en el RE y activan los mecanismos celulares de degradación. Uno de estos es la autofagia, la cual es mediada por la formación de vesículas de doble membrana que entregan material celular al lisosoma.

En este trabajo se definen por primera vez las rutas involucradas en mantener la homeostasis celular en respuesta al estrés de RE en *Dictyostelium discoideum,* una ameba social que se ha utilizado ampliamente para el estudio de la autofagia y de otras rutas de señalización, ya que ha evolucionado un ciclo de vida complejo, durante el cual amebas aisladas se agregan para desarrollar un organismo multicelular capaz de sobrevivir al ayuno.

En este trabajo se encontró que la tunicamicina (TN) genera estrés de RE en *D. discoideum* y desencadena una reprogramación de la expresión génica, la cual permite aumentar la capacidad de plegamiento del RE y aliviar su carga de proteínas. Aproximadamente el 40% de esta respuesta transcripcional depende de IreA, el único ortólogo de IRE1 en *D. discoideum.* Además de esta ruta, se encontró que, para sobrevivir al estrés de RE, las amebas requieren de BzpD, un factor de transcripción transmembranal similar a ATF6.

Los resultados aquí reportados, muestran que en *D. discoideum,* el estrés de RE induce una respuesta autofágica activada por una ruta independiente a la UPR, la cual resulta esencial para que las células puedan contender con este tipo de estrés. Sin embargo, durante el estrés de RE, se requiere de IreA para que exista un correcto ensamblaje de los autofagosomas en el RE. Proponemos que la incapacidad de las células que carecen de IreA para restaurar la homeostasis en el RE causa alteraciones estructurales severas en el RE, que generan un bloqueo en la formación de los autofagosomas.

ABSTRACT

The Unfolded Protein Response (UPR) is an adaptive pathway that restores homeostasis upon endoplasmic reticulum (ER) stress. ATF6 (*Activating Transcription Factor 6*), PERK (*Protein Kinase RNA-like ER Kinase*) and IRE1 (*Inositol-Requiring Enzyme 1*) are three transmembrane ER-resident proteins that in animals, can sense the folding environment at the ER and communicate the presence of ER-stress to the nucleus. This communication path modulates the protein folding capacity of the cell and activates degradative mechanisms, such as autophagy, a process that sequesters cytoplasmic material in double-membrane vesicles that will fuse and deliver its cargo to the lysosome.

In this work, we present the first study on the pathways involved in maintaining cellular homeostasis upon ER-stress in *Dictyostelium discoideum*, a social amoeba which has evolved a complex life cycle that alternates between unicellular and multicellular phases to survive starvation. *D. discoideum* is recognized as a valuable biomedical model organism alternative to yeast, since it conserves traits that are present in animal cells but that were lost in fungi.

Our data suggests that ER-stress response in *D. discoideum* relies in the combined activation of an UPR-dependent gene expression program and in autophagy. We found that tunicamycin (TN) induces effectively ER-stress in *D. discoideum* and that it elicits a transcriptional reprogramming to increase cellular protein folding capacity and to decrease the ER-protein load. IreA is the only *D. discoideum* IRE1 orthologue, it is essential for cell survival upon ER-stress and to attain about 40% of the TN-induced transcriptional changes. Moreover, we found that *D. discoideum* contains an ATF6-like transcription factor, BzpD, which is also required to cope with ER stress.

The response of *D. discoideum* cells to ER stress relies in the combined activation of an UPR-dependent gene expression program and the autophagy pathway. Both processes are independently activated by ER-stress; however, autophagy requires IreA at a later stage for proper autophagosome formation. We propose that unresolved ER stress in cells lacking IreA causes severe structural alterations of the ER, which lead to a late-stage blockade of autophagosome assembly.

ÍNDICE

INDICE DE ABREVIATURAS

2-DOG	2-deoxi-D-glucosa
AcbA	Proteína de union a la acil coenzyme A (*Acyl-CoA Binding A*)
ADP	Adenosina difosfato
ALR	*Autophagic Lysosome Reformation*
AMP	Adenosina monofosfato
AMPK	Quinasa activada por AMP (*AMP- activated Protein Kinase*)
ATF4	Factor activador de la transcripción 4 (*Activating Trancription Factor 4)*
ATF6	Factor activador de la transcripción 6 (*Activating Transcription Factor 6)*
ATG	Proteína relacionada con la autofagia (A<u>u</u>top<u>ha</u><u>g</u>y-related protein)
ATP	Adenosina trifosfato
BAG6	*BCL2-associated athanogene cochaperone 6*
BECN-1	Beclin-1
BLAST	Herramienta básica de búsqueda por alineamientos locales (*Basic Local Alignment Search Tool*)
BST	Blassticidina
bZIP	Proteínas con un dominio básico seguido de una cremallera de leucinas
CdcD	*similar to Cell Division Cycle mutant*
Cdc48/VCP	*Cell división control protein 48/ Valosin-Containing Protein*
CMA	*Chaperone Mediated Autophagy*
CREB	Factor de transcripción de unión a elementos de respuesta a AMP cíclico (*cAMP resesponse element-binding*)
DMSO	Dimetilsulfóxido
DTT	Ditiotreitol
eIF2α	Subunidad α del factor de inicio de la traducción 2 (*eukaryotic Inititiation Factor 2α*)
ERAD	Degradación asociada al retículo endoplásmico (*Endoplasmic Reticulum Associated Degradation*)
ERGIC	Compartimiento intermedio entre el RE y el Golgi (*Endoplasmic Reticulum-Golgi Intermediate Compartment*)
FIP200	*Focal adhesion kinase family interacting protein of 200 kDa*
GABARAPs	*γ-Aminobutyric acid receptor-associated proteins*
GDP	Guanosina difosfato
GFP	Proteína verde fluorescente (*Green Fluorescent Protein*)
GO	Ontología génica (*Gene Onthology*)
GRP78/BiP	Proteína regulada por glucose de 78kDa (*Glucose regulated protein 78/Binding Protein*)
GTP	Guanosina trifosfato
HOPS	*Homotypic Fusion and Protein Sorting-tethering*
HSP70s	Proteínas de choque térmico *(Heat Shock Proteins)*
IRE1	*Inositol-Requiring Enzyme 1*
JNK	*c-Jun N-terminal kinase*
KEN	Dominio nucleasa de extensión a una quinasa *(Kinase Extension Nuclease)*
LC3	*microtubule- associated protein Light Chain 3*
LNP	Proteínas Lunapark
MBTPS1	*Membrane-Bound Transcription factor Peptidase Site*
MCCC1	Subunidad alfa de la 3-Methilcrotonyl-CoA Carboxilasa

MHC	Complejo Mayor de Histocompatibilidad
MidA	*Mitochondrial Dysfunction A*
MW	Peso molecular
Ndufaf5	*NADH Dehydrogenase [Ubiquinone] 1 alpha subcomplex Assembly Factor 5*
OASIS	*Old Astrocyte Specifically Induced Substance*
ORF	Marco abierto de lectura (*Open Reading Frame*)
OST	Oligosacaril transferasa
PAS	Sitio de ensamblaje del fagóforo (*phagophore-assembly site*)
PCR	Reacción en cadena de la polimerasa
PDIs	Proteínas Disulfuro Isomerasas
PE	Fosfatidiletanolamina
PERK1	*Protein-kinase R-like Endoplasmic Reticulum Kinase*
PgkA	Fosfoglicerato quinasa
PI3P	Fosfatidil inositol 3-fosfato
PtdIns3K	Fosfatidil inositol 3 quinasa
PVDF	Fluoruro de polivinilideno
RE	Retículo endoplasmático
REDOX	Óxido-reducción
RIDD	Proceso de degradación regulado dependiente de IRE1 (*Regulated IRE1-Dependent Decay*)
RNAseq	Secuenciación masiva profunda de RNA
RTNs	Reticulones
SDF-2	*Spore Differentiation Factor*
Sec62	*Secretory protein 62*
SERCA	ATPasa de calcio del retículo sarco/endoplasmático
SNARE	'SNAP (Soluble NSF Attachment Protein) Receptor'
T/A	Temperatura ambiente
TN	Tunicamicina
TOR	*Target of Rapamycin*
Ubq	Ubiquitina
UDP	Uridina difosfato
ULK1	*Unc-51-like kinase 1*
uORF	Marco abierto de lectura río arriba (*upstream Open Reading Frame*)
UPR	Respuesta a proteínas mal plegadas *(Unfolded Protein Response)*
Vmp1	*Vacuole membrane protein 1*
WIPIs	WD-repeat proteins interacting with phophoinositides protein
WT	Silvestre *(Wild Type)*
XBP1	X-box Binding Protein

"It isn't the Universe that's following our logic, it's we that are constructed in accordance with the logic of the Universe. And that gives what I might call a definition of intelligent life: something that reflects the basic structure of the Universe."

— Fred Hoyle, The Black Cloud
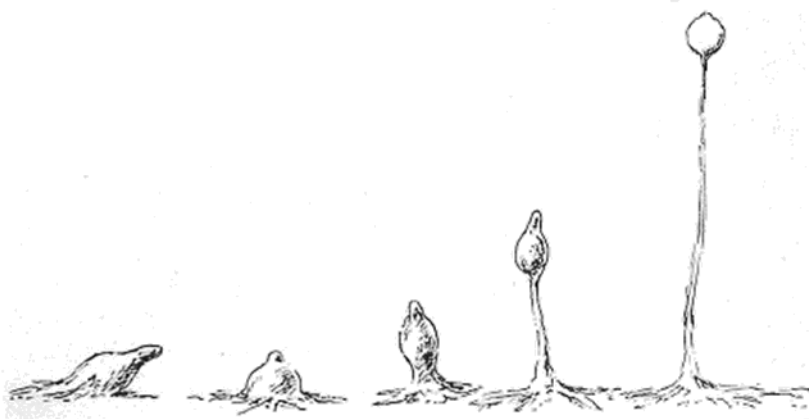
1.-INTRODUCCIÓN

1.1-El retículo endoplásmico (RE) es una red compleja altamente estructurada

El retículo endoplasmático (RE) es un sistema membranoso continuo, aislado del citoplasma, que ocupa una gran proporción del volumen celular, **(Figura 1)** en el que se llevan a cabo una amplia gama de procesos; dentro de ellos, la síntesis de lípidos y el plegamiento de cerca de un tercio de las proteínas celulares, la mayoría de ellas transmembranales o de secreción [1]. El RE se encuentra estructurado en diferentes dominios, los cuales permiten aislar y llevar a cabo de forma eficiente diferentes funciones. En esta estructura membranosa se pueden distinguir dos zonas principales: la envoltura nuclear, formada por una doble membrana laminar, y una zona periférica **(Figura 1A y 1B)** [2]. Dentro de esta última, existen diferentes dominios, uno de estos, presenta una morfología a la que se conoce como de *lámina* o *cisterna;* sin embargo, este dominio se encuentra formado por matrices de túbulos muy empacados que presentan muchas uniones [3]. También, existen láminas verdaderas de baja curvatura, las cuales suelen localizarse en zonas cercanas a la membrana plasmática [4]–[6]. La función de los dominios de cisternas está asociada a la síntesis y plegamiento de proteínas y en esta zona suele observarse una alta densidad de ribosomas asociados [7].

Por otra parte, existe otro domino periférico al cual se le ha asociado con la síntesis de lípidos, en el cual se observa una densidad baja de ribosomas [7]. Esta región está constituida principalmente por túbulos que se interconectan tanto entre ellos, como con las zonas de cisternas **(Figura 1C y 1D)** [2]. Esta red poligonal está sostenida por las proteínas Lunapark (LNP), una familia de proteínas que se encuentra altamente conservada entre organismos, la cual mantiene las interconexiones de la red tubular del RE [8].

En células de mamífero el RE requiere estar asociado al citoesqueleto para mantener su distribución y para que exista una proporción correcta entre túbulos y láminas, [9], [10]. El RE presenta dos tipos de movimientos, los cuales dependen de su asociación con los microtúbulos. Uno de ellos se observa como deslizamientos sobre la red estable de microtúbulos y requiere de los motores moleculares dineína y kinesina; mientras que el otro es mediado por el complejo de unión a la punta (TAC, *Tip Attachment Complex*) y se observa como un movimiento en el cual el RE crece y se constriñe de acuerdo al crecimiento del microtúbulo [10], [11]

Existen también diversas proteínas que participan en mantener la estructura de los diferentes dominios del RE. Una familia de proteínas transmembranales conocidas como reticulones (RTNs) participa en mantener específicamente la alta curvatura presente en los túbulos y en los extremos sobre los que se pliegan las láminas. Los RTNs presentan un dominio conservado y característico en su extremo carboxilo, el cual está formado por dos pases transmembranales separados por una región hidrofílica, cuyo plegamiento es capaz de introducir curvatura en las membranas [12], [13]. Junto con los RTNs, existe otro grupo de proteínas que interviene en mantener la estructura del RE, las Atlastinas. Estas proteínas son un grupo de GTPasas que actúan en los eventos de fusión que suceden entre membranas homotípicas del RE [14]–[16].
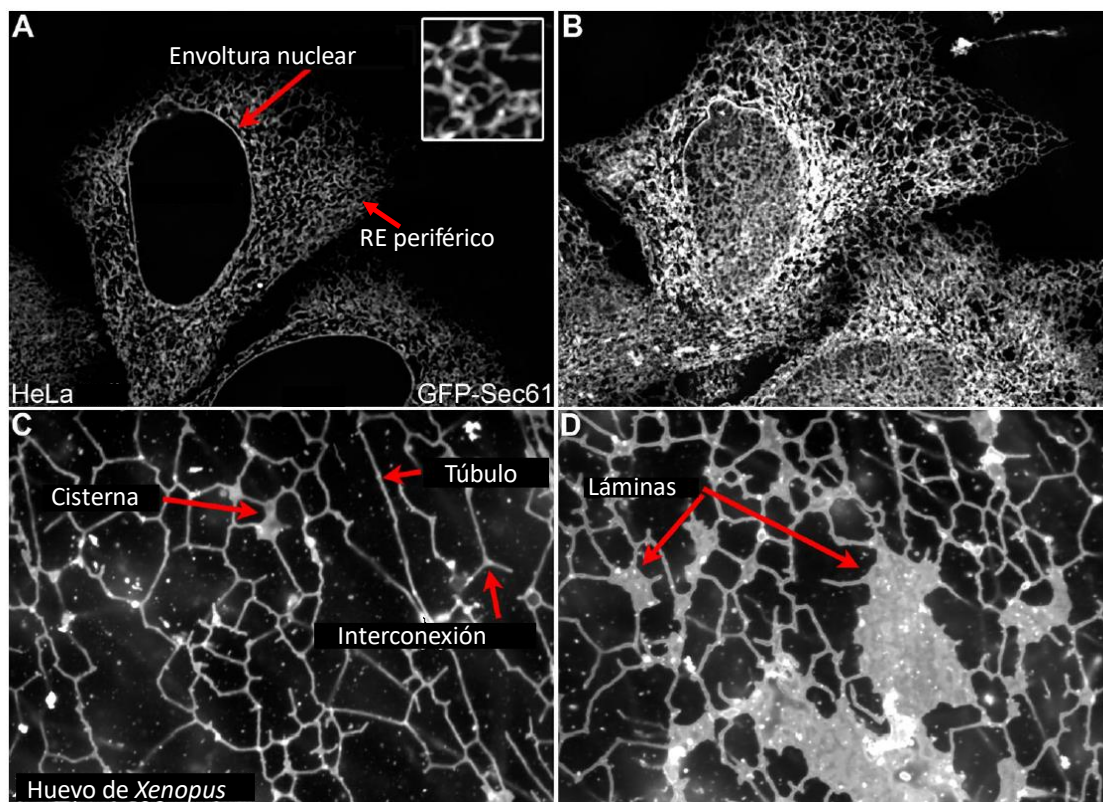
Figura 1. (A) El retículo endoplásmico (RE) se puede dividir en dos regiones principales: la membrana nuclear y el RE periférico. Vista medial del RE de una célula HeLa teñido mediante la expresión de Sec61B (proteína residente del RE que participa en la traslocación de proteínas) fusionada a la GFP. El recuadro muestra un acercamiento de la red poligonal del RE en esta célula. **(B)** Vista cortical de las mismas células en A. **(C y D)** Estructura de la red que conforma el RE periférico. Se puede apreciar que esta región está formada por túbulos y zonas en forma de cisternas o de láminas. Todas las zonas están interconectadas. RE reconstituido artificialmente a partir de extractos de huevos de *Xenopus*. Modificado de Schwarz, D. S.; 2016 [17].

1.2-El RE es un sitio ideal para el plegamiento de proteínas

El ambiente al interior del RE es altamente oxidante y contiene una alta concentración de calcio (Ca^{2+}) con respecto al medio citosólico. Es también muy viscoso, ya que contiene una alta densidad molecular. Además, en este organelo se encuentran concentradas una gran cantidad de chaperonas y de proteínas involucradas en la glicosilación y el plegamiento de proteínas, lo cual, en suma, permite que el plegamiento de las proteínas sea altamente eficiente.

La mayoría de las proteínas transmembranales y solubles que siguen la ruta de secreción sufren diversas modificaciones en el RE. Una de ellas es la unión covalente de carbohidratos en los grupos amida de algunos residuos de asparagina (*N*-glicosilación). Este proceso es mediado por la oligosacaril transferasa (OST) y consiste en la transferencia cotraduccional de un oligosacárido, el cual es ensamblado previamente sobre un acarreador lipídico que se encuentra insertado en la membrana del RE, el dolicol fosfato. LA *N*-glicosilación incrementa la estabilidad y solubilidad de las proteínas, además de que permite que estas sean reconocidas por algunas chaperonas y evita que sean retrotranslocadas [18].

En el RE existen dos sistemas de chaperonas. Uno de ellos contiene a GRP78/BiP (*Glucose Regulated Protein 78/Binding Protein*), una chaperona residente del RE que pertenece a la familia de las chaperonas de choque térmico de 70kDa, HSP70s (*Heat Shock Proteins*)[19]. Este grupo de chaperonas reconoce y se une a las regiones hidrofóbicas de las proteínas, de esta forma evita que estas regiones queden expuestas y que puedan interferir así, con el proceso de plegamiento. La actividad de esta chaperona depende de su estado de unión con ATP o ADP [20]. El otro sistema de chaperonas en el RE está formado por las proteínas tipo lectinas, calnexina y calreticulina. Estas chaperonas reconocen la presencia tanto de regiones no plegadas, como de sitios *N*-glicosilados [21].

Al interior del RE se encuentran también otros grupos de proteínas que no pertenecen a la familia de las chaperonas, pero cuya participación resulta esencial durante el proceso de plegamiento de las proteínas. Dentro de estas se encuentran las peptidil-prolil cis/trans-isomerasas que catalizan la isomerización cis/trans de los enlaces peptídicos en los que interviene el aminoácido prolina. Además, existe una familia de enzimas que participan en la formación y remodelado de los puentes disulfuro, formada por las proteínas disulfuro isomerasas (PDIs) [22], [23].

1.3-La vía de respuesta al estrés de RE

Se puede definir como estrés celular a cualquier condición en la cual se ve alterada la homeostasis de una célula y ante la cual se genera una respuesta de supervivencia para reparar y sobrevivir al daño. Existen diferentes condiciones fisiológicas celulares que alteran las funciones del RE y que causan que se incremente la proporción de proteínas mal plegadas en su interior; entre ellas, se encuentran los cambios en la concentración de calcio intracelular, la disminución en la concentración de ATP intracelular, el aumento en la demanda de proteínas de secreción, la disminución de la capacidad de glicosilación de proteínas, así como las deficiencias en el transporte de proteínas.

Experimentalmente se utilizan diversos agentes capaces de interferir con los procesos que se requieren para el correcto plegamiento de proteínas en el RE y que, como consecuencia, generan un estrés **(Figura 2)**. Para afectar el plegamiento de proteínas, es común el uso de agentes reductores tales como el ditiotreitol (DTT) y el β-mercaptoetanol, los cuales interfieren con la formación de puentes disulfuro intra e intermoleculares. También se utilizan agentes que interfieren con la *N*-glicosilación de las proteínas, tales como la 2-deoxi-D-glucosa (2-DOG) y la tunicamicina (TN). La 2-DOG es un análogo de la glucosa que al ser incorporado en el oligosacárido evita que continúe la adición de más carbohidratos en la cadena. La TN es un antibiótico nucleotídico que inhibe a la UDP- *N*-acetil glucosamina-1-P-transferasa, la cual cataliza la transferencia de la *N*-acetil glucosamina fosfato desde el UDP (uridina difosfato) hacia el dolicol difosfato, el cual es el primer paso en la formación del oligosacárido. Por otra parte, también es común el uso de drogas que afectan la concentración de calcio en el RE, tales como la tapsigargina, la cual funciona como un inhibidor no competitivo de la ATPasa de calcio del retículo sarco/endoplasmático (SERCA). Esta metodología es ampliamente utilizada en células de mamífero; sin embargo, no es funcional en los organismos que carecen de esta bomba de calcio, como es el caso las levaduras [24]–[26].

Las condiciones que ocasionan un aumento en la concentración de proteínas mal plegadas en el RE causan una pérdida de la homeostasis y, por lo tanto, generan estrés de RE. Para poder contender con esto, las células han evolucionado un sistema de señalización, al cual se conoce como la respuesta a proteínas mal plegadas (UPR, *Unfolded Protein Response*), la cual permite por un lado aumentar la capacidad de plegamiento del RE, y por el otro disminuir la carga de proteínas en este compartimiento. Esta respuesta se genera mediante una reprogramación transcripcional, aunada a una disminución en la traducción de proteínas y a un aumento en la capacidad degradativa celular **(Figura 3)** [27]–[30].
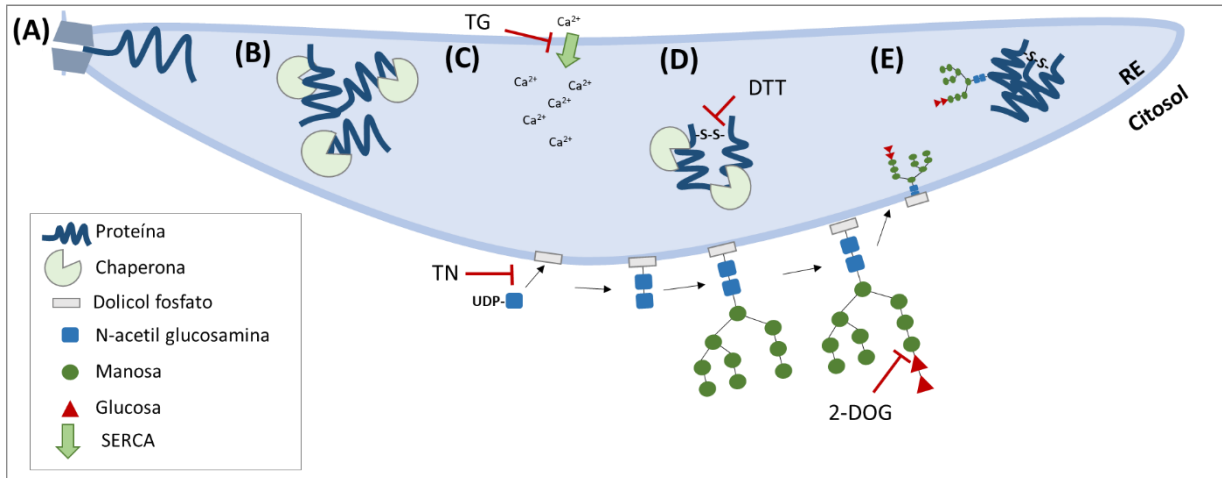
Figura 2. Efecto del ditiotreitol (DTT), la tunicamicina (TN), la 2-deoxy-D-glucosa (2-DOG) y la tapsigargina sobre el plegamiento de proteínas en el RE. **(A)** Las proteínas son translocadas al RE, en donde serán plegadas y sufrirán diversas modificaciones, tales como la adición de oligosacáridos y la formación de puentes disulfuro inter e intramoleculares. **(B)** Conforme las proteínas son transportadas al interior del RE, se unen a ellas las chaperonas y otras proteínas que participan en generar modificaciones postraduccionales. **(C)** Para que el proceso de plegamiento de proteínas al interior del RE sea exitoso, se requiere la actividad de las bombas de Ca^{2+}. La tapsigargina funciona como un inhibidor no competitivo de SERCA, ATPasa que permite la entrada de Ca^{2+} del citosol al RE. **(D)** Dentro de las chaperonas de RE, se encuentra la proteína disulfuro isomerasa (PDI), la cual participa en la formación de puentes disulfuro inter e intramoleculares. El DTT actúa como un agente reductor de los puentes disulfuro, por lo que evita que las proteínas adquieran un plegamiento correcto. **(E)** Otra modificación postraduccional que sufren las proteínas en el RE para poder ser plegadas es la *N*-glicosilación. Tanto la TN como la 2-DOG interfieren con este proceso. La TN, evita el primer paso de formación del oligosacárido ya que inhibe a la enzima que cataliza la transferencia de la N-acetil glucosamina fosfato desde el UDP (uridina difosfato) hacia el dolicol difosfato. La 2-DOG, es incorporada en la cadena de oligosacáridos, pero evita que puedan adicionarse más carbohidratos a la cadena.

En células de mamífero se ha descrito que existen al menos tres rutas de señalización que pueden sentir el ambiente de plegamiento en el lumen del RE. Estas rutas están constituidas por las proteínas transmembranales IRE1, ATF6 y PERK1 (respectivamente *Inositol-Requiring Enzyme 1, Activating Transcription Factor 6* y *Protein-kinase R-like Endoplasmic Reticulum Kinase*). Estas proteínas residentes del RE detectan alteraciones en el ambiente del RE y son capaces de generar las respuestas adaptativas requeridas para mantener la homeostasis **(Figura 3)**.

Junto con la UPR existe también un sistema, conocido como ERAD (*Endoplasmic Reticulum Associated Degradation*), el cual permite retrotranslocar al citosol y degradar mediante el proteasoma a las proteínas que no han podido ser plegadas correctamente en el lumen del RE [31]. Durante este proceso, se requiere de la actividad de las chaperonas del RE, tales como HSP40 y GRP78, las cuales unen a los péptidos mal plegados al interior del RE y los entregan a los complejos que catalizan respectivamente su poliubiquitinación y retrotranslocación [31], [32] Posteriormente, la extracción de las proteínas mal plegadas será asistida por un complejo que está compuesto por la ATPasa de la familia AAA, Cdc48/VCP/p97 (*Cell división control protein 48/ Valosin-Containing Protein*) y otras proteínas

adaptadoras, así como por otras ATPasas que forman parte de la subunidad regulatoria del proteasoma [33], [34]. Una vez en el citosol, las proteínas son reconocidas por chaperonas como el complejo BAG6 (*BCL2-associated athanogene cochaperone 6*) y entregadas al proteasoma [35].

En las secciones que se encuentran a continuación, se describe el mecanismo de activación y la actividad de cada una de las rutas reguladas por estas proteínas ante un estrés de RE.
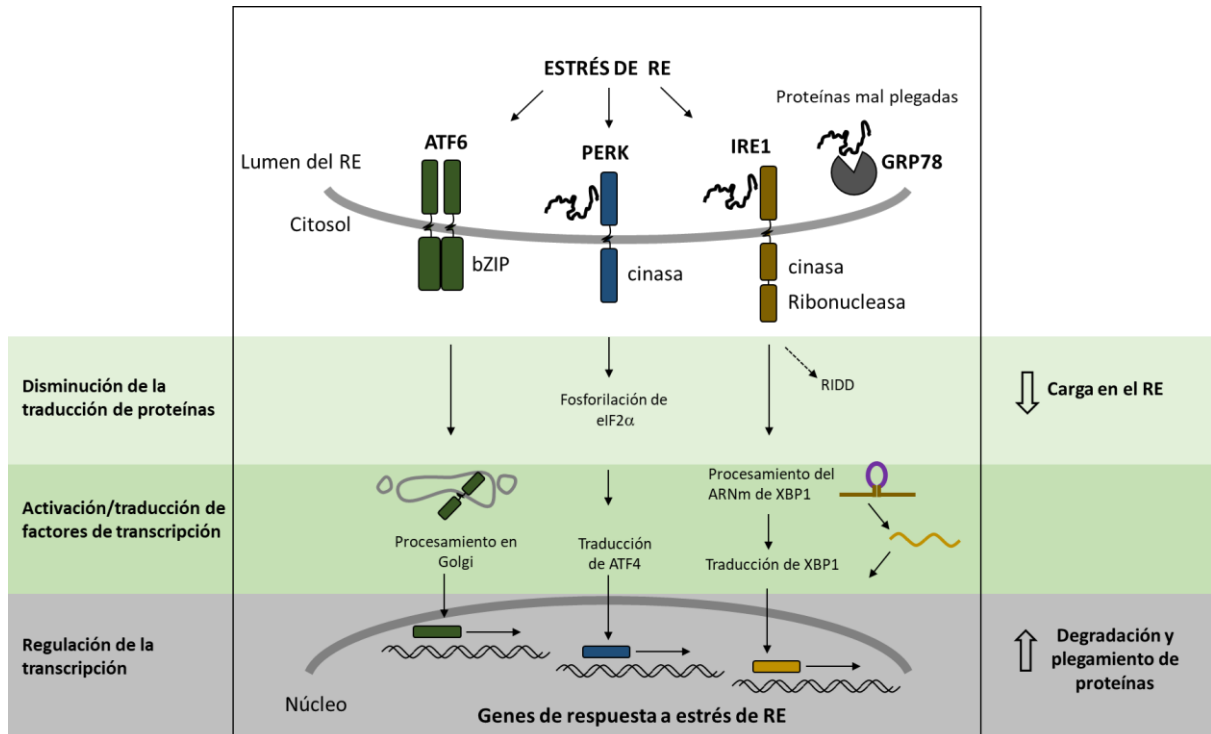
Figura 3. La vía de respuesta a proteínas mal plegadas (UPR) es la encargada de activar la respuesta adaptativa que recuperará la homeostasis celular mediante una reducción de la carga de proteínas en el RE, y al incrementar la capacidad de degradación y de plegamiento de proteínas. En mamíferos existen tres proteínas transmembranales de RE que pueden sentir el ambiente de plegamiento: ATF6 (*Activating Transcription Factor* 6), PERK (*Protein Kinase RNA-Like ER Kinase*) e IRE1 (*Inositol-Requiring Enzyme* 1). Ante un incremento en la carga de proteínas mal plegadas en el RE, los tres sensores pierden su interacción con la chaperona GRP78, lo cual permite su activación. Además, PERK e IRE1 pueden interactuar directamente con péptidos mal plegados mediante su dominio luminal. Las tres rutas de la UPR participan en generar una reprogramación transcripcional, la cual se logra mediante la activación o la traducción de factores de transcripción que participan en incrementar la expresión de genes involucrados con la recuperación de la homeostasis del RE. Tanto PERK como IRE1 participan en atenuar la traducción de proteínas, respectivamente mediante la fosforilación de la subunidad α del factor de inicio de la traducción 2 (eIF2α) y mediante la degradación de mensajeros regulada dependiente de IRE1 (RIDD). Figura modificada de Domínguez-Martín, E., *et al*., 2018 [36].

1.3.1-IRE1 es una quinasa y ribonucleasa conservada evolutivamente

Dentro de los sensores de estrés de RE, IRE1 es el único que está conservado en todas las familas de eucariotas que se han estudiado. En *Saccharomyces cerevisiae* existe un solo ortólogo de IRE1 y la UPR depende únicamente de esta ruta de señalización, mientras que en animales y en plantas IRE1 participa en conjunto con otras proteínas para generar una respuesta; sin embargo, esta ruta resulta esencial para que se genere una respuesta adecuada al estrés de RE [37], [38]. En humanos y en *A. thaliana* se expresan dos isoformas de IRE1 que presentan una alta similitud en su secuencia proteica, pero tienen un patrón de expresión diferencial dependiendo del tipo de tejido [39]–[42].

IRE1 es una proteína transmembranal tipo I cuya porción amino terminal (N-terminal) funciona como un sensor de proteínas mal plegadas al interior del RE. Por otra parte, su región citoplasmática contiene dos dominios con función enzimática, uno de estos dominios actúa como una quinasa de serinas y treoninas y el otro, como una ribonucleasa tipo KEN (*Kinase Extension Nuclease*) **(Figura 4A)** [43], [44].

En condiciones de homeostasis, la fracción N-terminal de IRE1 se mantiene asociada con la chaperona GRP78. Esta asociación se pierde al aumentar la concentración de proteínas mal plegadas en el RE ya que esta condición incrementa la ocupación de la chaperona con proteínas sin plegar; esto permite que IRE1 pase a un estado competente para la activación, en la cual es capaz de formar dímeros y posteriormente oligómeros [45], [46] **(Figura 4B)**. Durante su activación, IRE1 interacciona también con fragmentos de proteínas mal plegadas mediante un surco que se forma en su extremo N-terminal por efecto de la dimerización. Este surco tiene cierta similitud estructural con el complejo mayor de histocompatibilidad (MHC) y presenta una gran afinidad por péptidos compuestos por aminoácidos básicos o hidrofóbicos [47], [48]. La interacción con péptidos no estructurados fortalece la formación de oligómeros de IRE1, lo cual permite que pase a un estado completamente activo que consiste en una alta capacidad de autotransfosforilación y consecuentemente un aumento en su actividad de ribonucleasa.

Cuando el dominio KEN de IRE1 se encuentra activo, cataliza la escisión de un intrón no canónico contenido en el RNA mensajero de un factor de transcripción de la familia las proteínas que contienen un dominio básico seguido de una cremallera de leucinas (bZIP). En humanos y otros metazoarios, este factor de transcripción se conoce como XBP1 (*X-box Binding Protein*), mientras que en *A. thaliana* se conoce como bZIP60 y en *S. cerevisiae* como Hac1p **(Figuras 4D y E)**. Para producir el mensajero maduro del bZIP, se requiere también de la participación de la ligasa de tRNAs Rlg1/RtcB [49]. La escisión del intrón permite la traducción del mensajero maduro y la síntesis de la forma activa del factor de

transcripción (XBP1/bZIP60/Hac1p), el cual se internaliza en el núcleo y para permitir la reprogramación de la transcripción celular **(Figura 4E)**.
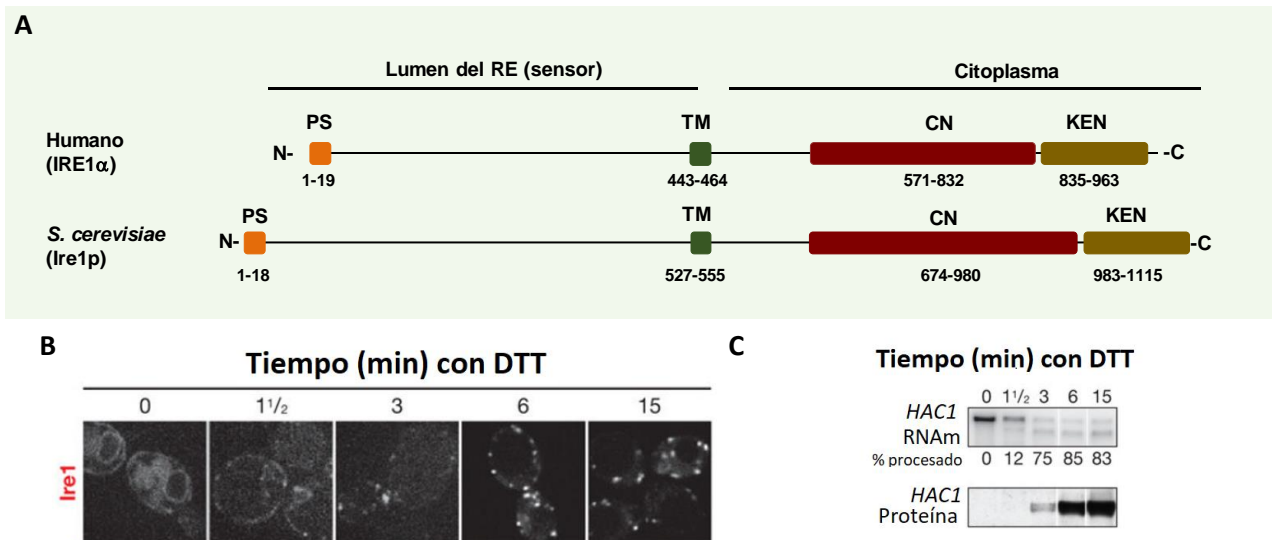
Figura 4. **(A)** Diagrama comparativo de los dominios de IRE1 de Humano (IRE1α) y de *S. cerevisiae*. PS (péptido señal), TM (transmembranal), CN (quinasa) y KEN (dominio kinase extension nuclease). **(B)** Ante un estrés de RE Ire1 forma oligómeros. Células de *S. cerevisiae* expresando a Ire1 fusionado a la proteína mCherry fueron tratadas durante los tiempos indicados con ditiotreitol (DTT) y visualizadas mediante microscopía confocal. Figura modificada de Aragón, T.; *et al*, 2009 [50]. **(C)** El procesamiento del RNAm de *Hac1* tiene lugar cuando Ire1 se encuentra formando oligómeros. Northern blot contra el mensajero (RNAm) de *Hac1* y un Western blot para detectar los niveles de proteína de Hac1. Muestras tomadas a los tiempos indicados tras el tratamiento con DTT como en B. Figura modificada de Aragón, T.; *et al*, 2009 [50].

La familia de los bZIPs se encuentra representada en todos los organismos eucariontes y se caracteriza por la presencia de una región rica en aminoácidos básicos capaz de interaccionar con el DNA seguida de una región de una cremallera de leucinas, la cual permite la formación de dímeros entre proteínas que contienen este dominio [51]. XBP1, Hac1p y bZIP60 forman parte de esta familia de factores de transcripción; sin embargo, presentan muy poca homología a nivel de secuencia proteica entre ellas. Como puede observarse en la **Figura 5A**, la homología entre la secuencia proteica de la forma no activa de estos factores de transcripción se restringe casi exclusivamente a la zona que contiene el dominio bZIP. La forma no procesada tanto de *Xbp1* (*Xbp1u*), como de *bZIP60*, se expresan constitutivamente y codifican una proteína transmembranal tipo II que se mantiene anclada al RE [52]–[54]. El anclaje del dominio transmembranal de XBP1u al RE permite acercar el RNA mensajero al sitio en el que puede ser procesado por IRE1 [52], [53], [55]. El procesamiento del RNA mensajero de *Xbp1* y de *bZIP60* permite que se traduzca una proteína soluble, la cual puede ser transportada al núcleo **(Figura 5B)**.

Por otra parte, el homólogo de XBP1 en levaduras, Hac1p, no se expresa en su forma inactiva, ya que el mensajero inmaduro presenta una estructura terciaria en la región del intrón no canónico, la cual evita

que el mensajero pueda traducirse [56], [57]. A pesar de estas diferencias, los intrones contenidos en los mensajeros de los factores de transcripción que son procesados por IRE1 presentan una estructura similar entre especies, así como algunos motivos conservados en la región del sitio que es reconocido y procesado por IRE1 [58].
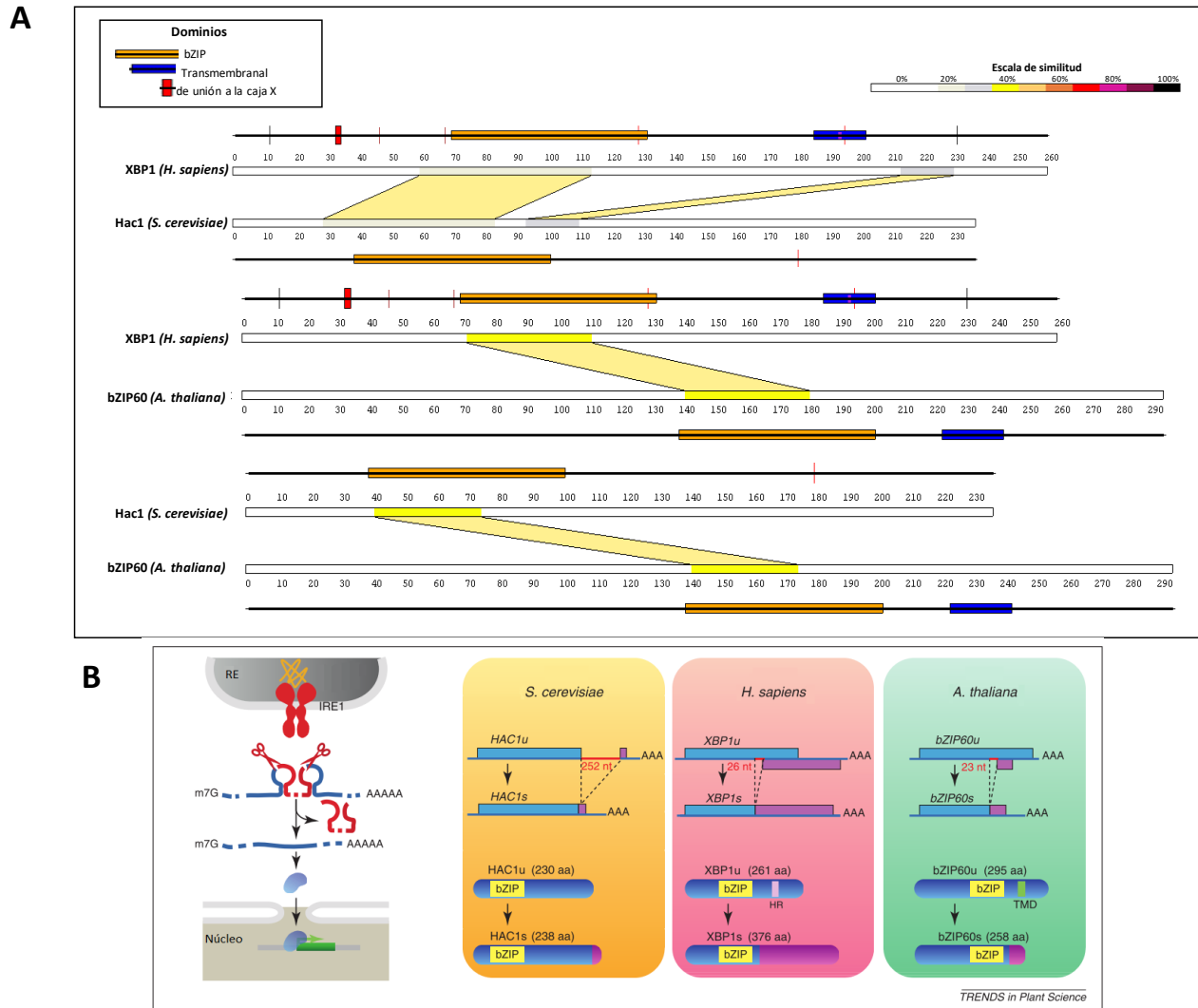
Figura 5. (A) Diagramas de los alineamientos locales entre las secuencias proteicas, respectivamente de XBP1, Hac1 y bZIP60. El código de color representa la similitud que existe entre ambas secuencias. Los alineamientos fueron generados con el programa *SIM alignment* y fueron visualizados con LALNVIEW. **(B)** IRE1 procesa un intrón no canónico contenido en el mRNA de una proteína tipo bZIP, lo cual permite la traducción de un factor de transcripción activo. El procesamiento varía dependiendo del organismo. Respectivamente IRE1 procesa a XBP1 en humanos, a Hac1 en levaduras y a bZIP60 en plantas. Figura modificada de Iwata, Y. y Koizumi, N., 2012 [59].

En plantas, animales y en algunas levaduras, se ha observado que IRE1 es capaz de degradar algunos mensajeros que codifican para proteínas que serán translocadas al RE mediante su actividad de

endorribonucleasa, por un proceso al cual se le conoce como degradación regulada dependiente de IRE1 (RIDD, *Regulated IRE1-Dependent Decay*)[60]–[63]. En plantas el proceso de RIDD permite disminuir la carga de proteínas de secreción que serán translocadas al RE [64], mientras que en células de mamífero este proceso media la degradación selectiva de algunos mensajeros y participa en la ejecución de un programa de muerte por apoptosis cuando el estrés es sostenido, [30], [65]. Por otra parte, el proceso de RIDD es la única respuesta al estrés de RE dependiente de Ire1 en la levadura *Schizosaccharomyces pombe* [62].

Los RNAs mensajeros que son degradados mediante RIDD y el RNA mensajero de XBP1 contienen una secuencia consenso la cual define el sitio reconocido y procesado por IRE1. Esta suele estar contenida en una región del mensajero que presenta una estructura secundaria conservada de tallo-asa[30], [65]. Sin embargo, aunque el sitio reconocido por IRE1 está conservado en ambos casos y la misma actividad catalítica de IRE1 es la misma, la degradación mediante RIDD y el procesamiento del mensajero de XBP1 presentan ciertas diferencias significativas [66]. Por ejemplo, se ha observado en células de mamífero que la degradación del mensajero BLOC1S1 ocurre a una velocidad menor que el procesamiento de XBP1 y que este mensajero se degrada sólo ante la presencia de un estrés prolongado [67]. Además, se ha sugerido que en estas células se requiere de la actividad de PERK para que algunos de los mensajeros puedan ser degradados [65].

1.3.2- PERK regula la traducción de proteínas

PERK es una proteína transmembranal de RE que presenta ciertos rasgos estructurales similares a IRE1. Esta quinasa presenta un dominio N-terminal alojado en el lumen del RE capaz de dimerizarse para formar una estructura similar al MHC y mediante esta región es capaz de interaccionar con péptidos mal plegados. También, en esta porción de la proteína existe una región mediante la cual puede interactuar con la chaperona GRP78 en ausencia de estrés, mientras que en su porción citoplasmática contiene un dominio de quinasa [68], [69].

Ante un aumento en la concentración de proteínas mal plegadas en el RE, PERK y GRP78 pierden su asociación, lo cual permite que PERK forme dímeros. Con esto se activa como quinasa y se autofosforila, esto aumenta su actividad catalítica y le permite fosforilar a la subunidad α del factor 2 de inicio de la traducción (eIF2α) **(Figura 3)** [70], [71].

El eIF2 es un complejo multimérico formado por tres subunidades (α, β, γ) el cual, para su activación, requiere asociarse al GTP. De esta manera puede unirse al RNA de transferencia de la metionina y así,

permite la formación del complejo de pre-inicio de la traducción 43s, el cual incluye también a otros factores de iniciación y a la subunidad pequeña del ribosoma. Cuando el tRNA de la metionina encuentra el codón de inicio, se recluta al factor de inicio de la traducción 5 (eIF5) el cual facilita la hidrólisis del GTP. Para que el factor eIF2 asociado al GDP sea reciclado, debe volver a cargarse con GTP. Esta reacción es catalizada por el intercambiador de nucleótidos eIF2B [72]. Cuando la subunidad α de eIF2 se encuentra fosforilada, se une a un sitio regulatorio en eIF2B para inhibir su actividad. Esto, produce una disminución en el reciclaje del eIF2 y consecuentemente, una disminución en la tasa global de traducción de proteínas, lo cual a su vez, permite disminuir la carga de proteínas en el RE [73].

Por otra parte, la fosforilación de eIF2α permite la traducción selectiva de algunas proteínas, las cuales presentan en el extremo no traducido 5´de su RNA mensajero uno o varios marcos abiertos de lectura pequeños (uORFs). En condiciones normales los uORFs titulan a los ribosomas y bajan la tasa de traducción del ORF codificante. En condiciones de estrés de RE los complejos de inicio de la traducción presentan una vida media mayor, a consecuencia de que la concentración de eIF2-GTP es reducida debido a una disminución en su tasa de reciclaje. Este efecto, permite que aumente la frecuencia de traducción del ORF codificante de los mRNAs que presentan uORFs [72]. Una de las proteínas que se regulan de esta manera es el factor de transcripción tipo bZIP, ATF4 (*Activating Trancription Factor 4),* cuyo mensajero contiene dos uORFs regulatorios [74]. ATF4 pertenece a la familia de factores de transcripción de unión a elementos de respuesta a AMP cíclico (CREBs) y al traducirse en condiciones de estrés permite que se generen cambios transcripcionales que se requieren para la recuperación de la homeostasis celular [75], [76].

1.3.3-ATF6 es un factor de transcripción que se transporta del RE al Golgi

El factor de transcripción ATF6 se expresa como un precursor que se encuentra anclado a la membrana del RE mediante un dominio transmembranal. En su extremo N-terminal, ubicado en el citoplasma, contiene un dominio de unión a DNA tipo bZIP; contiene también dominios de activación transcripcional y secuencias de localización nuclear[77]. En su extremo C-terminal, el cual se encuentra en el lumen del RE, contiene dos cisteínas con las cuales puede formar dímeros u oligómeros [78]. Además, en esta región contiene dos secuencias de reconocimiento de transporte a Golgi. En condiciones de homeostasis, estas secuencias se encuentran enmascaradas por su interacción con la chaperona GRP78 [79]. Cuando se induce estrés de RE, las proteínas mal plegadas titulan a GRP78, ATF6 se libera y quedan así expuestas sus secuencias de transporte. Al mismo tiempo, las cisteínas se reducen y ATF6 se transporta al Golgi en forma monomérica **(Figura 3)**. En el Golgi, ATF6 sufre un procesamiento que es catalizado por las

proteasas transmembranales MBTPS1 y MBTPS2 (*Membrane-Bound Transcription factor Peptidase Site 1 y 2*) [80]. De esta forma, el dominio citosólico de ATF6 se libera y se transporta al núcleo, en donde participa en la reprogramación transcripcional que permite a las células adaptarse al estrés de RE. Parte de esta respuesta se debe a que ATF6 retroalimenta la vía de IRE1 aumentando la expresión de GRP78 y de XBP1 [81].

Recientemente se han identificado otros factores de transcripción que se localizan en la membrana del RE, los cuales contienen un dominio bZIP y un dominio de activación transcripcional. Estos factores, al igual que ATF6, son procesados por las proteasas MBPTPS1 y MBPTPS2. Estos factores constituyen una familia conocida como OASIS (*Old Astrocyte Specifically Induced Substance*), la cual incluye a los factores de transcripción OASIS, BBF2H7, CREBH, CREB4 y LUMAN/CREB3 [82]–[84]. Los factores OASIS presentan características similares a ATF6 y también se procesan en respuesta a la inducción de estrés de RE; sin embargo, en humanos se expresan diferencialmente dependiendo del tipo de tejido, en contraste con ATF6 cuya expresión es ubicua. [83], [84]. Los mecanismos de regulación de estas proteínas, así como su papel fisiológico aún no han sido esclarecidos del todo.

1.4-La autofagia es un proceso complejo de degradación celular

La autofagia es un mecanismo catabólico conservado evolutivamente que permite transportar componentes celulares al interior de los organelos acídicos (los lisosomas en mamíferos, la vacuola en plantas y levaduras), con el objetivo de que sean degradados por la acción de las hidrolasas. Este proceso permite a las células mantener la homeostasis durante el crecimiento y resulta esencial para algunos procesos de desarrollo y diferenciación celular, así como en la respuesta ante diversos tipos de estrés [85]–[89]. Dependiendo del mecanismo mediante el cual se entrega el material celular al lisosoma o la vacuola, los procesos autofágicos se clasifican en i) macroautofagia, ii) microautofagia o iii) autofagia mediada por chaperonas (CMA, *Chaperone Mediated Autophagy*).

La macroautofagia (a la cual nos referiremos a lo largo de este texto como *autofagia*) consiste en la formación de vesículas de doble membrana, conocidas como autofagosomas que, tras secuestrar material celular, se fusionan con los organelos acídicos [90].

Existen mecanismos complejos mediante los cuales los autofagosomas pueden reconocer y secuestrar de forma específica sólo ciertos cargos celulares (a los cuales nos referiremos como *cargos* a lo largo del texto) [91], [92]. Mediante esta autofagia selectiva se pueden degradar organelos que hayan sufrido algún tipo de daño, agregados proteicos o incluso patógenos intracelulares. Durante este proceso, el

material celular que será degradado es marcado mediante la adición de ciertos ligandos como la ubiquitina. Posteriormente estos cargos celulares serán reconocidos por proteínas receptoras, como es el caso de p62/SQSTM1 (*SeQueSTrosoma*) en animales y en *D. discoideum* y de Atg19 en levaduras [93]–[95], que a su vez interactúan con proteínas que forman parte de la membrana del autofagosoma. Esto permite que, durante la formación de la vesícula, se envuelva el material seleccionado [92], [96].

Por otra parte, la microautofagia es un proceso por el cual el lisosoma o la vacuola forman invaginaciones en su membrana para internalizar directamente material celular [97]. Aunque existen evidencias de que este proceso sucede en células de mamífero, los mecanismos moleculares involucrados sólo han sido descritos en levaduras [97], [98]. Finalmente, existe un mecanismo mediante el cual se translocan directamente al lisosoma algunas proteínas solubles. Este proceso, que se conoce como autofagia mediada por chaperonas, sólo ha sido observado en células animales [99][100].

Durante condiciones regulares de crecimiento las células requieren de un nivel basal de autofagia para mantener su homeostasis; sin embargo, este proceso es inducido fuertemente como respuesta ante diferentes condiciones de estrés celular, tales como el ayuno, la hipoxia, cambios en la homeostasis de óxido-reducción, perturbaciones de la proteostasis, entre otros [87], [101]–[104]. Tanto las rutas implicadas, como las proteínas que participan en el proceso de formación de los autofagosomas han sido estudiadas principalmente durante el ayuno, ya que la autofagia resulta vital para que las células reciclen nutrientes y puedan así, sobrevivir a este estrés. La inducción de la autofagia durante una privación de nutrientes depende de la actividad de quinasas de serinas y treoninas que están implicadas en la regulación de la homeostasis celular; siendo las más conocidas TOR (*Target of Rapamycin*) y AMPK (*5′ AMP- activated protein kinase*) [105].

La formación de los autofagosomas es un proceso complejo que sucede en varias etapas, durante el cual participan varios complejos proteicos cuyo reclutamiento y actividad se regulan temporalmente **(Figura 6).** En mamíferos, la primer fase comprende el reclutamiento de la maquinaria de inducción de la autofagia a varios puntos específicos del RE que suelen estar enriquecidos en contactos con la mitocondria y con la membrana plasmática [106]–[108]. Esto conlleva a la formación de un subdominio conocido como omegasoma, el cual funciona como plataforma para la nucleación y ensamblaje del fagóforo, una estructura con forma de copa, la cual se elongará para formar la vesícula cerrada de doble membrana que se fusionará al lisosoma. En levaduras, este proceso sucede en proximidad con el RE y con la vacuola, en un solo sitio al que se conoce como PAS (phagophore-assembly site) [109], [110].

En las siguientes secciones se discutirán con detalle la participación de los complejos proteicos que participan durante la formación de los autofagosomas.

1.4.1-El complejo ATG1/ULK1 regula la inducción y nucleación del fagóforo

Una gran parte de las proteínas que participan en la formación de los autofagosomas fueron descubiertas gracias a una serie de estudios genéticos en levaduras, a partir de los cuales, se han identificado los respectivos homólogos en diferentes organismos. Para facilitar su nomenclatura tanto en levaduras, como otros organismos, se utilizan las siglas ATG (*AuTophaGy-related protein*) para nombrar a la mayoría de las proteínas que son esenciales para la formación de los autofagosomas. La primera que se identificó como indispensable para la autofagia fue la proteína ATG1, también conocida como ULK1 (*Unc-51 Like Kinase 1*) en mamíferos. Esta quinasa de serinas y treoninas se asocia con otras proteínas en un complejo cuyos componentes no están conservados entre organismos, por lo que existen variaciones significativas entre levaduras y mamíferos. En levaduras este complejo está constituido, además de ATG1, por Atg17, Atg13 y Atg29, mientras que en mamíferos está formado por ATG101 y FIP200 (*Focal Adhesion Kinase Family Interacting Protein of 200kDa*). El único elemento común en ambos grupos de organismos es ATG13 [111].

En condiciones normales de crecimiento, tanto en levaduras como en mamíferos, TOR interacciona y al mismo tiempo fosforila a ATG1 y a ATG13, lo cual mantiene inactivo al complejo ATG1. En condiciones de ayuno, TOR se inactiva y esto, induce la liberación de las formas no fosforiladas de ATG1 y ATG13. La forma libre de ATG1 entonces, puede autofosforilarse y a su vez fosforilar a otros miembros del complejo incluyendo a ATG13. Esto promueve la formación del complejo activo [112]–[115] [116]. ATG1 fosforila también a otras proteínas autofágicas, como a ATG9, una proteína transmembranal que participa en la elongación del autofagosoma y en el reclutamiento de complejo de la fosfatidil inositol 3 quinasa (PtdIns3K) en el RE [117]. Además, el complejo ATG1 activa mediante fosforilación a ATG6/Beclin-1(BECN-1)[118].

Figura 6. Diagrama de las diferentes etapas durante la formación de un autofagosoma en una célula de mamífero. Ante un estímulo inductor de autofagia, como el ayuno, TOR (*Target of Rapamycin*) deja de fosforilar a ULK1 (*Unc-51-Like Kinase 1*), lo cual permite que esta quinasa se active, se autofosforile, y pueda fosforilar a los otros miembros del complejo (ATG13 y FIP200 (*Focal Adhesion Kinase Family Interacting Protein of 200 kDa*))*,* con los cuales se ensamblará. El complejo ULK1 permite a su vez, que se reclute al complejo de la fosfatidil inositol 3 quinasa (PtdIns3K), el cual catalizará la formación de fosfatidil inositol 3-fosfato (PI3P) en regiones específicas del RE (omegasoma). Además, este lípido sirve como plataforma para reclutar a otros efectores. Para que la membrana del fagóforo se elongue se requiere del reclutamiento de los sistemas de conjugación, compuestos por ATG4, el complejo de ATG12-ATG5/ATG16L1 y las proteínas de la familia ATG8, LC3 (*Microtubule- Associated Protein Light Chain* 3) y GABARAPs (γ-*Aminobutyric Acid Receptor-Associated Proteins*). LC3 y GABARAPs sufrirán un procesamiento mediado por ATG4 para ser lipidadas con fosfatidiletanolamina (PE). La doble membrana de los autofagosomas se constituye de material membranal que es entregado por vesículas, algunas de ellas ricas en ATG9, que provienen de diversas fuentes. Tras una fase de maduración durante la cual se desasociarán la mayoría de las proteínas ATG, el autofagosoma se fusiona con el lisosoma para degradar su cargo. Este material será reutilizado o secretado y finalmente, se regenerarán los lisosomas (Modificada de Dikic, I.; Elazar, Z. 2018).

1.4.2-La producción de PI3P es necesaria para la nucleación del autofagosoma

Una vez que el complejo ATG1 se encuentra activo y se ubica en el RE, sucede una fase durante la cual se fosforila el fosfatidil inositol (PI) de la membrana de este organelo para inducir un enriquecimiento de fosftadil inositol 3-fosfato (PI3P) [106]. Esta reacción es catalizada por el complejo de la PtdIns3K, el cual está constituido por la enzima Vps34/PIK3C3, por ATG6/BECN-1 y por la quinasa de serinas y treoninas Vps15/PIK3R4 [119]. El PI3P permite que se recluten al sitio de nucleación del autofagosoma otras proteínas efectoras que participan en la formación de esta vesícula, tales como ATG18/WIPI-1 (*WD-*

repeat proteins interacting with phophoinositides). Todo este proceso, promueve la formación del omegasoma, una estructura característica en el RE que acuna la formación del fagóforo [120].

1.4.3-La elongación del autofagosoma requiere de ATG9 y de dos sistemas de conjugación

Tras la formación del omegasoma, la membrana del fagóforo se elongará a partir de varias fuentes de membrana. Ester proceso requiere de la participación de la proteína autofágica ATG9, la cual está involucrada en proveer al fagóforo de membranas. Estas pueden provenir del Golgi, del compartimiento intermedio entre el RE y el Golgi (ERGIC), de endosomas de reciclaje u otras fuentes de membrana [121]– [123]. En levaduras, se ha observado que existe un complejo que permite el contacto entre el RE y el autofagosoma en formación, este está constituido por ATG18 y ATG2, que se encuentran asociados constitutivamente. Este complejo permite a su vez, la asociación de ATG9 mediante la interacción de este con ATG2 [124].

Durante el proceso de formación del fagóforo se requiere también de dos sistemas que presentan un mecanismo de conjugación similar al del sistema de ubiquitinación de proteínas y cuyos componentes se encuentran altamente conservados entre organismos. En levadura uno de los sistemas está constituido por dos proteínas que presentan homología estructural con la ubiquitina, ATG8 y ATG12 [125], [126], las cuales se modifican para formar respectivamente, un producto de ATG8 unido covalentemente con la fosfatidiletanolamina (PE) y un conjugado en el que se unen ATG12 con ATG5 [127].

El conjugado ATG12-ATG5 facilita la lipidación de ATG8 y para su formación, requiere por un lado de la actividad de ATG7, una enzima tipo E1 que activa a ATG12, y por el otro de ATG10, una enzima tipo E2 que promueve la reacción de conjugación [128]. En mamíferos, a su vez, ATG12-ATG5 forma un complejo con ATG16L1. Esta interacción permite reclutar al conjugado al fagóforo gracias a la interacción que existe entre ATG16L1 y WIPI2b [129]. En el caso de las levaduras, ATG16 es reclutada mediante ATG21 [130].

Tanto en las células de levadura, como en las de animales, los miembros de la familia ATG8 (LC3) se sintetizan como proteínas precursoras que son procesadas constitutivamente por la proteasa de cisteínas ATG4. El procesamiento de estas proteínas permite la exposición de un residuo de glicina, lo cual permite que se conjugue con la PE. Este proceso de lipidación de ATG8 es mediado por ATG7 y por la enzima tipo E2, ATG3 [131]. ATG8-PE suele localizarse en la cara interna del fagóforo, lo cual permite generar curvatura en la membrana y regular el tamaño del autofagosoma. Además, los miembros de la

familia ATG8 (LC3) resultan esenciales para el reclutamiento de componentes celulares, ya que pueden interactuar con los receptores de cargos, tales como p62/SQSTM1 [132], [133]. Se ha sugerido también, que ATG8 participa en reclutar de proteínas que se requieren para la maduración de la vesícula y durante el proceso de sellado de la membrana del autofagosoma [134].

1.4.4-El material secuestrado por los autofagosomas se degrada en los lisosomas

Durante la última fase, durante la cual madura el autofagosoma, se disocian los complejos proteicos que participaron en el proceso de nucleación del fagóforo y en la etapa final, los autofagosomas se fusionan con los lisosomas o la vacuola. Para que esto suceda, se requiere del reclutamiento de la GTPasa Ypt7/RAB7 [135]. Esta proteína interacciona con el complejo HOPS (*Homotypic Fusion and Protein Sorting-tethering*), el cual induce cambios en la curvatura de la membrana [136], y junto con ciertos miembros de familia SNARE, participa en la fusión de las membranas [137]. Esto, permite que el material secuestrado por el autofagosoma se libere al organelo acídico y se degrade. En el caso del ayuno, el material degradado es transportado al citosol en donde puede reutilizarse para la construcción de nuevos componentes celulares.

Además de su función catabólica, la autofagia participa en rutas no canónicas de secreción. Por ejemplo, en levaduras se requiere de los componentes de la maquinara autofágica para la secreción de Acb1, y en el caso de células de mamífero para la secreción de la interleucina-1B. Por otra parte, en algunos casos el contenido de los autofagolisosomas, en vez de procesarse completamente, puede ser secretado; e incluso se ha observado que pueden secretarse mitocondrias o patógenos intracelulares que fueron secuestradas por autofagosomas [138]. Los mecanismos mediante los cuales suceden los procesos de secreción asociados a la autofagia aún no han sido esclarecidos. Se ha observado que en algunos casos los autofagosomas y los autolisosomas se pueden fusionar con cuerpos multivesiculares (endosomas tardíos con vesículas intraluminales), los cuales pueden fusionarse con la membrana plasmática; sin embargo, no se ha descartado que los autofagosomas puedan fusionarse directamente con esta membrana [138]–[140].

1.4.5-Los lisosomas se regeneran

Aunque las fases involucradas en la formación de los autofagosomas han sido ampliamente estudiadas, los procesos tardíos de la autofagia han caracterizados pobremente. Recientemente en células de mamífero, se ha comenzado a caracterizar cómo sucede la regeneración de los lisosomas, mecanismo al

que se conoce como "*Autophagic Lysosome Reformation*" (ALR). Durante este proceso, se generan estructuras tubulares a partir de los autofagolisososmas. De estas, brotarán vesículas con proteínas transmembranales características de los lisosomas, pero que carecen de un pH ácido. Estos protolisosomas madurarán para formar lisosomas con capacidad degradativa mediante un mecanismo que aún es desconocido. Para que este proceso suceda, se requiere tanto de la reactivación de mTOR, como de la presencia del acarreador lisosomal de azúcares *Spinster*. Además, se ha observado que se requiere que la membrana del autofagolisosoma se enriquezca en PI(4,5)P2 y que la proteína clatrina sea reclutada a esta vesícula [141], [142].

1.4.6- La autofagia se induce ante el estrés de RE

Se ha reportado ampliamente que la autofagia se induce en respuesta al estrés de RE. Las primeras observaciones sobre este efecto provienen de estudios realizados en levaduras [104], [143] y posteriormente, se ha comprobado que esta respuesta se encuentra ampliamente conservada entre organismos. Se ha sugerido que la autofagia inducida por el estrés de RE funciona como una estrategia para controlar la expansión de este organelo, además de que permite incrementar la capacidad de degradación de los agregados proteicos [143]–[146].

En plantas y en mamíferos se ha observado que la inducción de la autofagia ante el estrés de RE requiere de la actividad de IRE1 [147], [148]. En mamíferos, se ha planteado que esta quinasa media la activación de la ruta de JNK (*c-Jun N-terminal kinase*) y de esta forma se dispara la respuesta autofágica [147]. Sin embargo, la ruta de señalización de JNK se encuentra solamente en animales y no está conservada en otros organismos, por lo que no aún no se ha esclarecido si IRE1 participa en la inducción de la autofagia en organismos carentes de la vía JNK. Por otra parte, se ha planteado que, tras un estrés de RE, Sec62 funciona como un receptor que permite degradar selectivamente ciertas porciones del RE de forma independiente de la ruta de la UPR [149]. Esto sugiere que existen condiciones en las que la autofagia puede inducirse y regularse de forma independiente a la UPR.

1.5-*Dictyostelium discoideum* como organismo modelo

 La mayor parte de los descubrimientos en el área de la biología celular se han logrado gracias a los estudios realizados en organismos modelo; principalmente con microorganismos, debido a que presentan tiempos cortos de duplicación y resultan de fácil manipulación. Dentro de ellos, la levadura

Saccharomyces cerevisiae es uno de los organismos más estudiados y que más ha aportado al campo. Sin embargo, durante la evolución de este organismo, han aparecido características únicas que se encuentran poco conservadas o ausentes en otros organismos, lo cual impide que algunos de los mecanismos moleculares descubiertos en la levadura puedan ser extrapolados. El estudio de otros organismos ha permitido entonces, complementar el conocimiento que se tiene de ciertos procesos celulares complejos.

Dictyostelium discoideum es una ameba social que se encuentra clasificada en el filo Amebozoa, un grupo que divergió antes de la separación de los hongos y los animales [150]. Este organismo fue descrito por primera vez por Kenneth Raper en 1935 y desde ese momento ha sido ampliamente estudiado. Esta ameba presenta algunos mecanismos moleculares implicados en procesos celulares que se encuentran conservados con animales, pero que se han perdido o han divergido significativamente en las levaduras. En *D. discoideum* se han estudiado ampliamente la quimiotaxis, la fagocitosis y ciertas rutas de señalización y de comunicación intercelular [151], [152]. Por este motivo, este organismo ha servido para estudiar la etiología de algunas enfermedades humanas, como la lipofuscinosis ceroide neuronal, la chorea-acantocytosis, la enfermedad de Alzheimer, entre otras [153]. Además, se ha utilizado para identificar y probar nuevas drogas [154]–[156], así como para estudios relacionados con los mecanismos de infección, ya que presenta ciertas similitudes con las células fagocíticas animales involucradas en la respuesta inmune innata [157], [158].

Además de esto, *D. discoideum* presenta un ciclo de vida particular que alterna entre una fase unicelular y una multicelular, la cual culmina en la formación de un cuerpo fructífero constituido por diferentes tipos celulares. La alternancia entre la fase unicelular y multicelular le permite a este organismo adaptarse y sobrevivir a condiciones de ayuno, así como colonizar nuevos nichos. Este proceso se describe con mayor detalle en la sección siguiente.

1.5.1-D. discoideum presenta un ciclo de vida complejo

D. discoideum suele habitar el suelo de bosques templados en donde se alimenta por fagocitosis de bacterias y levaduras. Mientras existan fuentes de alimento, estas amebas se mantienen en su forma vegetativa, dividiéndose mediante fisión. Sin embargo, cuando los nutrientes escasean las células detienen su crecimiento vegetativo y comienzan un proceso de desarrollo y diferenciación que les permitirá sobrevivir la ausencia de nutrientes. Este proceso es regulado por la secreción de diferentes moléculas. Una de ellas es el cAMP (Adenosin monofosfato cíclico), un mensajero de señalización extracelular que actúa como un quimio-atrayente. La secreción de esta y otras moléculas induce la

migración y agregación de alrededor de 10^5 amebas. Este agregado pasará por varias fases de diferenciación, una de ellas como un gusano móvil microscópico (*slug*) capaz de detectar fuentes lumínicas y diferencias en la concentración de amonio. El proceso de diferenciación culmina en la formación de un cuerpo fructífero construido por diferentes tipos celulares, que forman un tallo de células muertas sobre el cual se sostiene un soro lleno de esporas. Bajo condiciones ambientales y nutricionales adecuadas, las esporas se liberan y germinan como amebas **(Figura 7).** En condiciones controladas, el ciclo completo se lleva a cabo durante un tiempo aproximado de entre 24 y 28hrs [159]–[162].

1.5.2-La autofagia es esencial para el proceso de desarrollo de *D. discoideum*

El desarrollo de *D. discoideum* sucede como una respuesta de supervivencia al ayuno, por lo que la única fuente de nutrientes es la autofagia. Por este motivo, cualquier deficiencia en este proceso causa defectos durante el desarrollo [89], [163], [164]. Se han aislado una serie de mutantes que presentan bloqueos en diferentes etapas de la autofagia y se ha observado que presentan diferentes fenotipos de desarrollo. Estos, varían desde una falta completa de agregación, hasta la formación de estructuras con múltiples tallos y pocas esporas viables (fenotipo conocido como *multitip*) **(Figura 8)**.
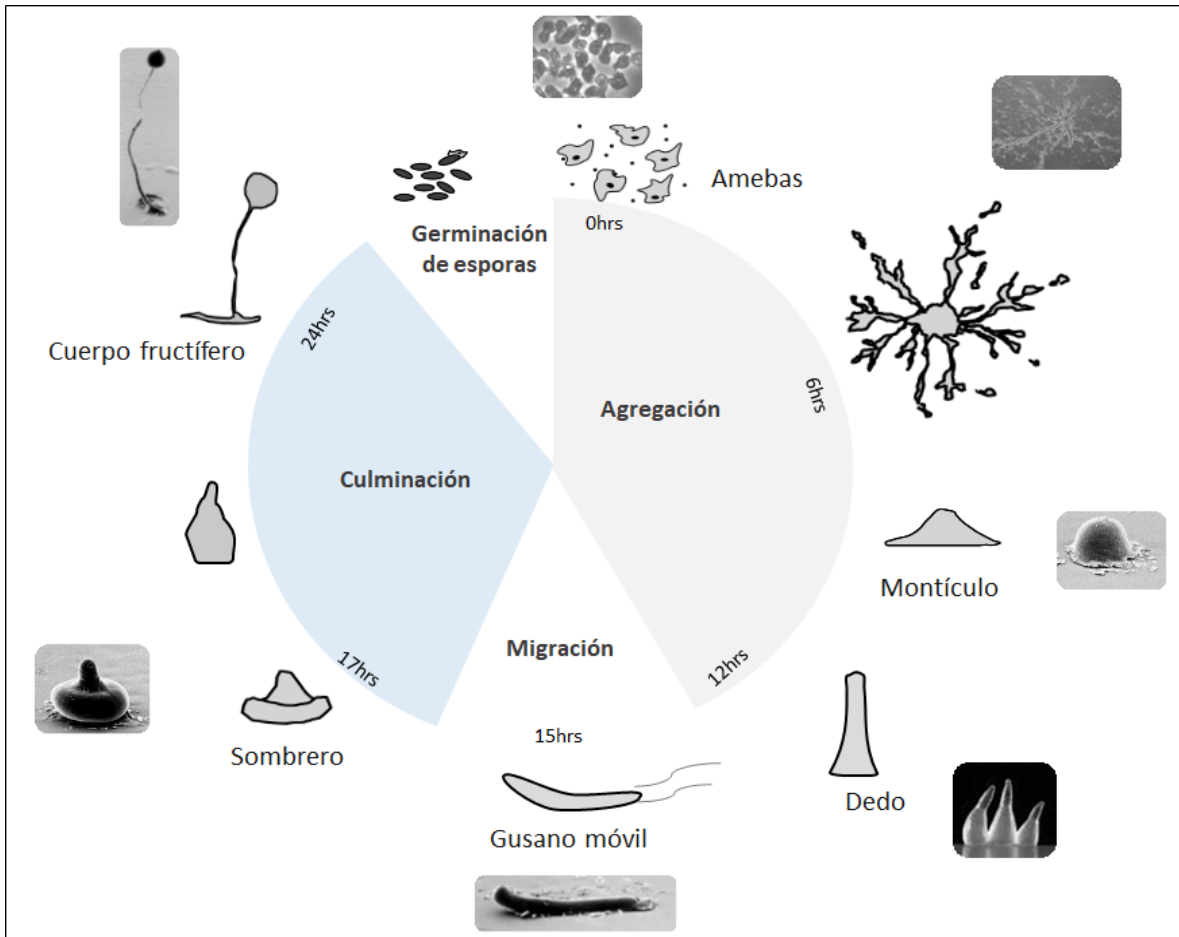
Figura 7. Diagrama del ciclo de vida de *Dictyostelium discoideum*. Las amebas unicelulares se alimentan fagocitando levaduras y bacterias. Cuando el alimento escasea, las células de *D. discoideum* secretan señales extracelulares que les permiten agregarse mediante movimientos quimiotáxicos. Estos agregados celulares sufren un proceso de desarrollo y diferenciación comprendido por varias fases, el cual culmina en la formación de un cuerpo fructífero, compuesto por un tallo de células muertas que sostiene un soro lleno de esporas. Cuando las condiciones ambientales son apropiadas, estas esporas germinarán nuevamente como amebas.

De esta forma, se han identificado a los ortólogos del complejo ATG1 [165], de la PtdIns3K [166] y de los sistemas de conjugación [167]–[169]. Además, en *D. discoideum* se ha identificado que ciertas proteínas cuya función era desconocida, participan durante la autofagia. Entre estas, se encuentran TipC [170], Vmp1 [93], [171], Ndufaf5 y MidA [172]. Todos estos trabajos han demostrado que *D. discoideum* representa un buen organismo modelo para el estudio de la autofagia.

Aún no se ha esclarecido si durante el desarrollo de *D. discoideum* se requiere de la autofagia solamente para proveer de nutrientes a las células y mantener así la homeostasis celular, o si también participa durante los procesos de señalización, ya que se ha observado por ejemplo que, AcbA, una proteína precursora de uno de los factores de diferenciación de las esporas (SDF-2), es secretada mediante un proceso no convencional que requiere de la autofagia [173]. Además, el desarrollo del tallo del cuerpo fructífero requiere que las células que sufran una forma específica de muerte autofágica [174], [175].
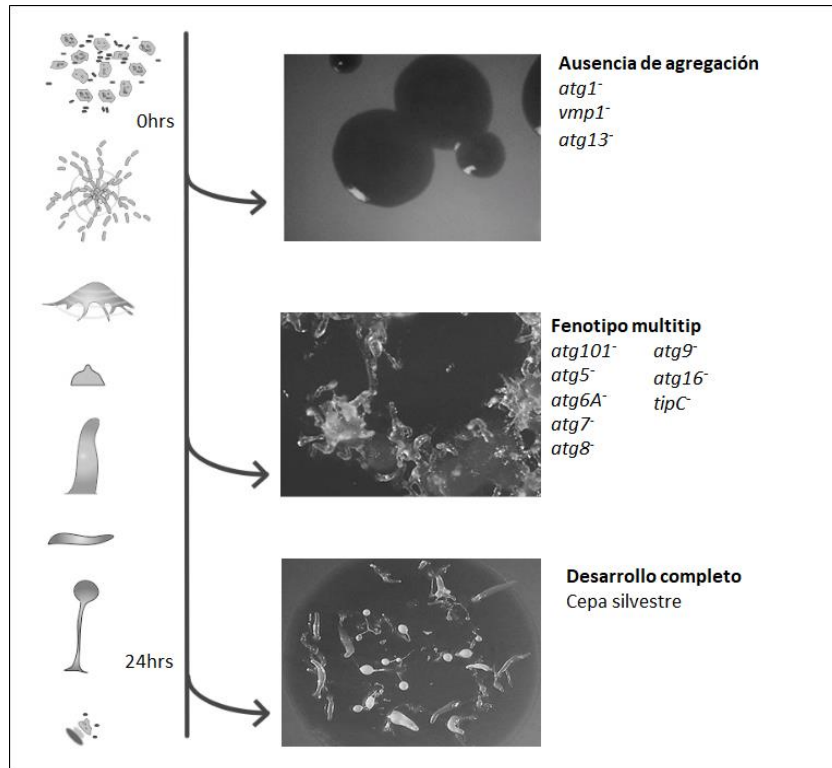
Figura 8. Imágenes representativas de los fenotipos que presentan algunas mutantes de *D. discoideum* con defectos en la autofagia durante el desarrollo. Se muestra un diagrama con las fases de desarrollo y fotografías representativas que corresponden respectivamente a la cepa *atg13⁻, tipC⁻* y AX4 silvestre (comenzando por el panel superior). Figura modificada de Mesquita, A. et al. 2017 [163].

1.5.3-El RE de una ameba social

La estructura del RE de *D. discoideum* puede visualizarse fácilmente mediante microscopia confocal o mediante microscopía electrónica. Como puede observarse en la **Figura 9**, en el RE de *D. discoideum* pueden distinguirse tanto la membrana perinuclear, como la zona periférica. Esta última está formada por una red de túbulos esparcidos por toda la célula y por cisternas situadas en la zona más cercana a la membrana plasmática. A la fecha, son escasos los estudios sobre los procesos que mantienen la estructura del RE de *D. discoideum*; sin embargo, en su genoma se encuentra al menos un miembro de la familia RTN (*rtnlc/DDB_G0293088*), un ortólogo de la proteína de las uniones LUNAPARK (*DDB_G0289961*), y uno de la familia Sey1 (*DDB_G0279823)*, una GTPasa que participa en la fusión homotípica de membranas del RE. En *D. discoideum* se ha descrito que Sey1 se requiere para que la bacteria *Legionella pneumophila* pueda replicarse intracelularmente [176]*.

El proceso de plegamiento de proteínas en el RE, así como las rutas que participan en mantener la homeostasis de este organelo aún no se han estudiado en *D. discoideum*. Sin embargo, se ha visto que

la Calreticulina y la Calnexina, dos chaperonas de RE, tienen un papel importante durante la fagocitosis [21]. También, se han identificado en este organismo los ortólogos de algunas otras chaperonas de RE, tales como Dd-GRP94 de la familia HSP90 [177] y dos miembros de la familia de las proteínas disulfuro isomerasa (PDI) [178], [179].
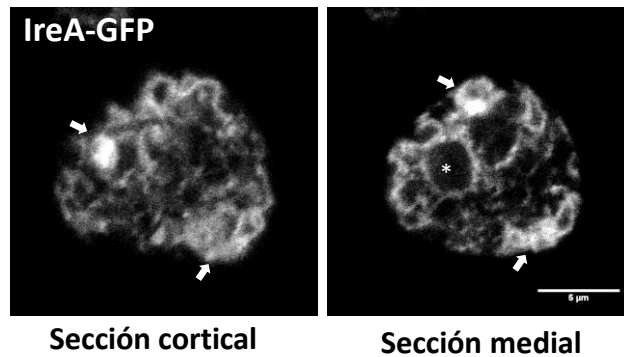
Figura 9. El retículo endoplásmico (RE) de *D. discoideum*. Imágenes obtenidas por microscopía confocal de células silvestres AX4 (WT) vivas expresando una proteína de RE, fusionada a la GFP. Se muestra una sección cortical y una medial. Las flechas señalan zonas con morfología de cisterna y el asterisco marca el núcleo. Se pueden apreciar una red de túbulos esparcida por toda la célula. (Escala 5μM) (Figura modificada de Domínguez-Martín, E.; et al. 2018 [36]).

2. OBJETIVOS

1. Establecer las condiciones para inducir estrés de retículo endoplásmico en *D. discoideum*.
2. Determinar si existen homólogos de IRE1 y ATF6 en *D. discoideum* y definir el papel que juegan durante el estrés de RE.
3. Caracterizar la respuesta transcripcional que genera el estrés de RE en *D. discoideum*.
4. Analizar si en *D. discoideum* la autofagia se induce y es regulada por la ruta de respuesta al estrés de RE.
5. Definir si en *D. discoideum* el ortólogo de IRE1 está involucrado en regular la autofagia durante el estrés de RE y durante el ayuno.

3.-MATERIALES Y MÉTODOS

3.1- Cepas

La cepa AX4 de *D. discoideum* se utilizó para todos los experimentos y para generar todas las mutantes que se estudiaron en este trabajo. Las cepas mutantes *ireA⁻*, *bzpD⁻*, *bzpJ⁻* y *mbtps2⁻* se obtuvieron mediante la inserción por recombinación homóloga del gen de resistencia a la Blasticidina (BST) [180]. Para esto, se generaron construcciones en las que el gen BST fue flanqueado por dos regiones homólogas del gen que se deseaba interrumpir. Un listado con todas las cepas que se utilizaron se encuentra en la **Tabla 1**.

Cepa	Descripción
AX4	Tiene el genotipo *axeA1, axeB1, axeC1* que le permiten el crecimiento axénico. Proviene de la cepa AX3 [181]
ireA-	Presenta una deleción de 998 bases generada al transformar células con el amplificado obtenido de amplificar la construcción pGEM-ireA::BST con los oligonucleótidos IreA1 e IreA2. El gen de resistencia a Blasticidina (BST) se insertó entre los sitios EcoRV del ORF de IreA.
atg1- atg13- atg101-*	Mutantes generadas reportadas en [165]. Los genes *atg1, atg13* y *atg101* se interrumpieron respectivamente mediante la inserción del gen BST.
bzpD-	Cepa en la que se generó una deleción de 400 bases y la inserción del gen BST, al transformar células con el amplificado resultado de la amplificación con los oligonucleótidos bzpD3 y bzpD6 la construcción pRS313-bzpD::BST.
bzpJ-	Cepa en las que el gen bzpJ sufrió una deleción de 717 bases al insertarse el gen BST. Las células se transformaron con el amplificado obtenido de amplificar la construcción pRS313-bzpJ::BST con los oligonucleótidos bzpJ(KO)-3 y bzpJ(KO)-6.

Tabla 1. Cepas utilizadas durante la realización de este trabajo. En el caso de las mutantes generadas durante el desarrollo de este trabajo, se especifica si la inserción del casete de resistencia a blasticidina (BST) generó alguna deleción. Se incluye la referencia al trabajo en el cual se reportaron las cepas mutantes que no fueron obtenidas para este trabajo.

3.2- Construcciones y vectores

Todos los oligonucleótidos que se utilizaron para generar, mediante PCR, los diferentes amplificados que se utilizaron durante este trabajo están enlistados en la **Tabla 2** y tanto las construcciones, como los vectores utilizados para los experimentos reportados en este trabajo se encuentran descritos a continuación en la **Tabla 3**.

Nombre	Secuencia	Unión	Gen
ddIreA-107 (FWD)	ATGTAGGGATCCAAAAACTACAGAATTTCG	-107	DDB_G0267650
IreA1 (FWD)	ATATTATTCCCGCGCCGCATTAATGTT	758	DDB_G0267650
IreA2 (RV)	CAGGTAAAATGCGGCCGCAAGTTTGTTCT	3092	DDB_G0267650
IreA3 (FWD)	GATAGTCATGGTTGGCAACCAGCAG	2525	DDB_G0267650
IreA4 (FWD)	GTAAGATCTATGACTTTTTCAAAA	-9	DDB_G0267650
IreA5 (RV)	ATTACTAGTATAATATTGAACAAAATATTGATC	3209	DDB_G0267650
K603N-IreA (FWD)	GGTAGAAAAGTTGCAGTTAATAGAATGTTATCACAATTTG	2040	DDB_G0267650
K603N-IreA (RV)	CAAATTGTGATAACATTCTATTAACTGCAACTTTTCTACC	2078	DDB_G0267650
N927A-IreA (FWD)	GACCTTTTACGTGTCATTAGAGCTAAATTCAACCATTATAG	3008	DDB_G0267650
N927A-IreA (RV)	CTATAATGGTTGAATTTAGCTCTAATGACACGTAAAAGGTC	3050	DDB_G0267650
bzpd-1 (FWD)	AAAGGATCCGACAAAATGGATATTGATTACGAAAATG	-14	DDB_G0278379
bzpd-2 (RV)	TCTACTAGTATGATTTGTAAATATTGAAGAAGCTGAAG	2759	DDB_G0278379
bzpD-3 (FWD)	GGGAACAAAAGCTGGGTACCGGGCCCCCCCTAGAAGCTAAACACAATCAGCATC	35	DDB_G0278379
bzpD-4 (RV)	CCCGGGAAGCTTATCGATACCGTCGACCTCACAGAAGAATCAGAAGAAGATGAAG	1044	DDB_G0278379
bzpD-5 (FWD)	CATATGCCGATGGTTAATTCCTGCAGCCCAGAATCGTGAAAGTGCACAACTC	1441	DDB_G0278379
bzpD-6 (RV)	AATTGGAGCTCCACCGCGGTGGCGGCCGCTACTAGTATGATTTGTAAATATTGAAGAAG CTGAAG	2740	DDB_G0278379
bzpJ-1 (FWD)	AAAGGATCCATGGTTGAATTAGAATCAATG	-9	DDB_G0274993
bzpJ-2 (RV)	CCCACTAGTTTAATTTAAAGGTGAAAGTGGGG	2540	DDB_G0274993
bzpJ(KO)-3 (FWD)	GGGAACAAAAGCTGGGTACCGGGCCCCCCCCGGCCATAGTGCAAATAGTAGTGCAC	130	DDB_G0274993
bzpJ(KO)-4 (RV)	CCCGGGAAGCTTATCGATACCGTCGACCTCGAATGGGGTGATGATGATGGTG	753	DDB_G0274993
bzpJ(KO)-5 (FWD)	CATATGCCGATGGTTAATTCCTGCAGCCCGCACTCAATGAACGTAATAGTGGTG	1465	DDB_G0274993
bzpJ(KO)-6 (RV)	AATTGGAGCTCCACCGCGGTGGCGGCCGCTTTATTTAAAGGTGAAAGTGGGGGAGAATC	2543	DDB_G0274993

Tabla 2. Lista de los oligonucleótidos que se utilizaron durante la realización de este trabajo. Se muestra la coordenada en la que cada oligonucleótido se une en el gen respectivo. Se muestra también el número de acceso con el cual se encuentra identificado en la base de datos del genoma de *D. discoideum* el gen respectivo.

Vector	Descripción
pGEM-IreA	El amplificado del gen *IreA* obtenido con los oligonucleótidos ddIreA-107 y IreA5 se clonó en el vector comercial pGEM-t easy (PROMEGA).
pGEM-ireA::BST	Construcción en la que se introdujo el fragmento SmaI/KpnI del vector pBluescriptII-*BlasticidinR* entre los sitios EcoRV del pGEM-IreA.
pDM323	Vector extracromosomal de expresión que permite fusionar la proteína verde fluorescente (GFP) al extremo C- terminal del producto que se inserte en su sitio de multiclonaje. Contiene el gen de Neo que confiere resistencia al G418 cuando se expresa en *D. disdoideum* [182].
pDM317	Vector extracromosomal de expresión que permite fusionar la proteína verde fluorescente (GFP) al extremo N- terminal del producto que se inserte en su sitio de multiclonaje. Contiene el gen de *Neo* que confiere resistencia al G418 cuando se expresa en *D. disdoideum* [182].
pDM324	Vector extracromosomal de expresión que permite fusionar la proteína roja fluorescente (mRFPmars) al extremo C- terminal del producto que se inserte en su sitio de multiclonaje. Contiene el gen de Neo que confiere resistencia al G418 cuando se expresa en *D. disdoideum* [182].
pDM358	Vector extracromosomal de expresión que contiene el gen de *Hyg* el cual confiere resistencia a la higromicina al transformarse en *D. disdoideum* [182].
pDM323-IreA	El amplificado del gen *IreA* obtenido con los oligonucleótidos ddIreA-107-IreA5 fue clonado entre los sitios BglII/SpeI del pDM323.
pDM323-IreA^{K603N}	Versión del pDM323-IreA en la que se generó mediante mutagénesis dirigida con los oligonucleótidos K603N-IreA, una mutación puntual para cambiar la lisina 603 por una asparagina.
pDM323-IreA^{N927A}	Versión del pDM323-IreA en la que se generó mediante mutagénesis dirigida con los oligonucleótidos N927A-IreA, una mutación puntual para cambiar la asparagina 927 por una alanina.
pDM317-BzpD	El amplificado del gen *bzpD* obtenido con los oligonucleótidos EDbzpd-1 y EDbzpd-2 clonado en el plásmido pDM317.
pDM317-BzpJ	El amplificado del gen *bzpJ* obtenido con los oligonucleótidos EDbzpJ-1 y EDbzpJ-2 clonado en el plásmido pDM317.
pDM358-GFP-PgkA	La construcción GFP-PgkA descrita previamente en [165], [183] clonada en el plásmido pDM358.
pJSK489	La construcción GFP-Atg18 clonada en el vector pDM448. Vector donado por J. King y descrita en [87].
pRS313-bzpD::BST	Construcción generada mediante la técnica de gap-repair. Contiene clonados los dos fragmentos del gen *BzpD* obtenido por PCR con los oligonucleótidos bzpD-3 y bzpD-4, y con bzpD-5 y bzpD-6. Estos fragmentos flanquean el fragmento entre ClaI y PstI del plásmido pLPBLP, el cual contiene al gen BST.
pRS313-bzpJ::BST	Construcción generada mediante la técnica de gap-repair. Los fragmentos del gen *BzpJ* obtenidos por PCR con los oligonucleótidos bzpJ(KO)-3 y bzpJ(KO)-4, y con bzpJ(KO)-5 y bzpJ(KO)-6, flanquean el fragmento entre ClaI y PstI del plásmido pLPBLP, que contiene el gen BST.
pDM325-Gol	Se clonó el gen *gol* (golvesin) en el vector pDM324 y posteriormente se cambió el gen *Neo* contenido entre los sitios BamHI/XhoI por el gen *Hyg* proveniente del pDM358.
pGEX-4T-DdGrp78	El marco de lectura del gen *DDB_G0276445* (*GRP78*) clonado en el vector para expresión inducible en *E.coli* pGEX-4T1.

Tabla 3. Lista de todos los vectores que se utilizaron para la realización de este trabajo.

3.3-Anticuerpos utilizados

Para los ensayos de Western blot y de inmunofluorescencia se utilizaron los anticuerpos enlistados en la **Tabla 4**.

Blanco	Anticuerpo	Dilución usada
Grp78	Anti-Grp78 (Santa Cruz Biotechnology, sc-1050: goat anti-human GRP78 (N-20), descontinuado)	1:2000 (WB)
GFP	Anti-GFP (*Sigma-Aldrich*, G1544)	1:10000 (WB)
CdcD	Anti-cdcD (Vcp /P97) (rabbit anti-Dictyostelium CdcD. Provisto por el Dr. Ludwig Eichinger [165]).	1:10000 (WB)
MCCC1	Estreptavidina conjugada a la peroxidasa de rábano.	1:100 000 (WB)
PDI	Anti-PDI (mouse anti-Dictyostelium PDI. Provisto por el Dr. Pierre Cosson)	1:1000 (IF)
Ubiquitina	Anti-Ubiquitina (Cell Signaling ((P4D1) #3936: mouse/rabbit anti-human ubiquitin)	1:500 (IF)
Isótopos de IgG	Anticuerpo secundario conjugado al fluorocromo Alexa fluor 546 (rojo) (Invitrogen, A-11003, goat anti-mouse)	1:1000 (WB)
Isótopos de IgG	Anticuerpo secundario conjugado a la peroxidasa de rábano (Santa Cruz Biotechnology, Sc2020 Donkey anti goat).	1:10 000 (WB)
Isótopos de IgG	Anticuerpo secundario conjugado a la peroxidasa de rábano (Santa Cruz Biotechnology, Sc2004, Goat anti rabbit).	1:10 000 (WB)

Tabla 4. Anticuerpos utilizados para los experimentos de inmunodetección reportados en este trabajo. Se especifica si el anticuerpo se utilizó para Western Blot (WB) o para inmunofluorescencia (IF).

3.4-Metodologías de DNA recombinante

Estrategias de clonación

Las construcciones mencionadas en la **Tabla 3**, se generaron mediante la técnica clásica de clonación que depende del uso de enzimas de restricción y de la ligasa de DNA del bacteriófago T4 [184]. Se utilizó también la técnica de Gap-repair, la cual permite el ensamblaje, mediante recombinación homóloga, de varios fragmentos de DNA en un plásmido. Esta técnica consiste en cotransformar levaduras con fragmentos de DNA que contienen en sus extremos 3´ y 5´ regiones que son homólogas a los fragmentos contiguos o al vector, con los cuales se desea realizar la fusión. Además, se incluye el plásmido en el cual se desea hacer la clonación. En este caso se utilizó el pRS313. Los detalles de esta técnica se encuentran publicados en [185].

Mutagénesis dirigida

Para generar las construcciones pDM323-IreA^{K603N} y pDM323-IreA^{N927A}, se diseñaron respectivamente dos juegos de oligonucleótidos complementarios (K603N-IreA (FWD) y K603N-IreA (RV), N927A-IreA (FWD) y N927A-IreA (RV)) que se utilizaron para realizar una reacción de PCR con el kit de amplificación de la enzima KAPA HiFi (*KAPA BIOSYSTEMS*), en la cual se utilizó como templado el vector pGEM-IreA. En

cada reacción se utilizó cada uno de los oligonucleótidos a una concentración final de 5μM, dNTPs a 300μM (mezcla 10mM contenida en el kit) y de 3-5ng de plásmido, en un volumen final de 25μl. El programa de amplificación utilizado fue el siguiente: desnaturalización inicial de 5min a 95ºC; 15 ciclos de amplificación en los que se usó una desnaturalización de 20s a 98ºC, 30s de alineamiento a 60ºC y 270s de amplificación a 65ºC, y finalmente se realizó un ciclo de amplificación por 5min a 65ºC. Posteriormente, esta reacción se digirió durante 2hrs con 10unidades de la enzima DpnI (Invitrogen) y se purificó todo el producto por columna (*QIAquick Extraction kit, Qiagen*) y se transformaron células de *E. coli* DH5a con 25μl del producto. Se seleccionaron varias transformantes, de las cuales se obtuvo el plásmido por miniprep y se evaluó la presencia de la mutación puntual por secuenciación. Posteriormente se subclonó el producto del plásmido pGEM-t al pDM323 como se especifica en la **Tabla 3** para la construcción pDM323-IreA.

3.5-Metodologías para el manejo de *D. discoideum*

Todos los protocolos para la preparación de los medios aquí descritos y para el manejo de *D. discoideum* se encuentran detallados en la página *http: dictybase.org*

Condiciones de cultivo y desarrollo

Las células de *D. discoideum* se crecieron siempre a 22ºC en incubadores estándar para microbiología. Para los cultivos líquidos (crecimiento axénico) se utilizó el medio HL5 (FORMEDIUM HLB0102), el cual se suplementó con glucosa al 1% y con un cóctel de penicilina y estreptomicina (10 000 U /ml penicilina and 10 000 mg/ml estreptomicina; Gibco). Para crecer las amebas en asociación con bacterias se utilizaron placas de medio sólido SM (1% glucosa (Sigma), 1% peptona (Difco), 0.1% extracto de levadura, 4mM 139 MgSO4, 13mM KH2PO4, 3mM K2HPO4 y 2%agar), en las que se esparcía *Klebsiella aerogenes* (cepa Ka) antes de depositar las células. Para inducir ayuno, se utilizó el buffer PDF (20mM KCl, 9mM K2HPO4, 13mM KH2PO4, 1mM CaCl2, 1mM MgSO4, pH 6.4).

Para los experimentos de desarrollo se colectaron por centrifugación (1000 rpm por 5 min) $5x10^7$ células que estaban creciendo de forma axénica en HL5. Posteriormente se suspendieron en buffer PDF y se depositaron en filtros de nitrocelulosa (Millipore, HABP04700) que se mantuvo humedecido con PDF sobre papel filtro.

Se utilizó Blasticidina (10μg/ml), G418 (10μg/ml) e higromicina (25μg/ml) respectivamente como antibióticos para la selección de células transformantes.

Tratamientos

Las drogas utilizadas se prepararon en soluciones concentradas que se mantuvieron congeladas (-20ºC). La tunicamicina (TN) se diluyó en DMSO (stock a 1µg/ml); y se prepararon en agua tanto el ditiotreitol (DTT) (stock a 1M), como la 2-deoxi-D-glucosa (2-DOG) (stock a 2M). Para los tratamientos, las drogas se diluyeron a la concentración deseada en medio HL5 al momento del experimento. Las células fueron tratadas siempre mientras se encontraban creciendo de forma axénica durante la fase exponencial.

Transformación

Para transformar amebas de *D. discoideum*, se lavaron y se electroporaron 5x10^6 células por celda, con 2-10 µg de DNA linear. Estas células fueron lavadas previamente con buffer H50. Este protocolo de transformación ha sido descrito previamente en [186]. El proceso de selección se llevó a cabo en placas para cultivo celular estándar de 60 o de 100mm. Las células se mantuvieron en medio HL5 suplementado con el antibiótico de selección necesario por aproximadamente 4-8 días. Tras este tiempo, las células transformadas con plásmidos fueron mantenidas en placas de cultivo líquido con medio fresco HL5 suplementado con el antibiótico necesario (G418 o higromicina). Mientras que las células en las que se deseaba generar la inserción de fragmentos de DNA se esparcieron en placas de agar SM en presencia de *K. aerogenes* para aislar clonas. Se evaluó mediante PCR de colonia si los eventos de recombinación fueron exitosos. Para esto, se extrajo el DNA a partir de amebas que se tomaron de la zona de crecimiento de las clonas que se encontraban creciendo en placas de SM. Para esto se utilizó la solución de extracción *Master amp DNA* (Epicentre) siguiendo las instrucciones del proveedor. Se utilizó 1µl del extracto de DNA para 50µl de solución de PCR.

Para comprobar la interrupción del locus se siguió la estrategia mostrada respectivamente en cada caso.

3.6- Ensayos de viabilidad mediante goteo de diluciones seriales

Antes de comenzar con los tratamientos se ajustaron a 1x10^6 células/ml los cultivos, los cuales se encontraban creciendo en líquido durante la fase exponencial (2-3x10^6 células/ml). Posteriormente, los cultivos ajustados fueron tratados con la droga señalada (DTT, 2-DOG o TN) a las concentraciones especificadas y durante los tiempos referidos. Posteriormente, se prepararon diluciones seriales 1:10 de estas células en medio HL5 fresco y se depositaron gotas (4µl) de estas diluciones sobre placas de agar SM en las que se había esparcido previamente *K. aerogenes*. Se tomaron fotos de las placas después de incubarlas a 22ºC durante 5-7 días dependiendo del experimento.

3.7- Extracción de RNA y secuenciación masiva de RNA

Se ajustaron las células a una densidad de $1x10^6$ células/ml y se trataron durante 16hrs con $2\mu g$/ml de TN o con el vehículo (DMSO), los cuales se disolvieron en HL5. Posteriormente las células se centrifugaron y se lavaron con PDF. El RNA se extrajo con un protocolo estándar con Trizol (Sigma). Los ensayos de secuenciación masiva profunda de RNA (RNAseq) se realizaron en la Unidad de Biología Molecular del Instituto de Fisiología Celular, UNAM, CDMX, México. El ensamblaje y análisis de los datos obtenidos se realizó en la Unidad de Cómputo de este mismo instituto. Para esto se utilizó el software TopHat y Cufflinks [187]. Las listas de genes que presentaron diferencias significativas en la abundancia de sus transcritos entre las diferentes condiciones se obtuvieron con el mismo software mediante el análisis de dos réplicas. Los datos crudos pueden obtenerse de la base de datos GEO del NCBI usando el número de acceso GSE104409.

Las listas de genes que presentaron cambios significativos se filtraron para obtener solamente los transcritos que se encontraban representados por al menos 1 mensajero por célula. De acuerdo con Parikh, A., *et al*. [188], bajo nuestras condiciones, 15 cuentas normalizadas representarían un mensajero. Los genes que cuya expresión mostró una tasa de cambio mayor o igual a 2.5 veces (Log2 de la tasa de cambio ≥ 1.3 ó ≤ -1.3) entre las condiciones analizadas, se evaluaron y clasificaron con la herramienta DAVID [189], la cual permite generar grupos de términos de ontología (gene onthology, GO) que se encuentren enriquecidos en una lista de genes. Se generaron los grupos de enriquecimiento de GO para las categorías de proceso biológico, componente celular y dominios proteicos.

3.8- Preparación de células para inmunofluorescencia

Se ajustaron cultivos de células creciendo de forma axénica, durante la fase exponencial, a una densidad de $1x10^6$ células/ml y se aplicó el tratamiento deseado. Posteriormente se depositaron $300\mu l$ de células por pozo, en una placa de 8 pozos Ibidi m-Slide la cual había sido tratada previamente con una solución de poli-L-lisina (1mg/ml en agua destilada) aproximadamente por 12hrs y que fue lavada con buffer PDF (ver sección 3.5 Metodologías para el manejo de *D. discoideum*) justo antes de su uso. Estas células se incubaron a 22ºC, y transcurrido el tiempo deseado de tratamiento, se retiró el medio y se fijaron por 15min con 2% de paraformaldehido en PDF (preparado a partir de un stock de PFA al 10% en agua y una solución de PDF 10x). Se lavó el exceso de PFA en la preparación y se incubó por 30min en buffer de bloqueo (0.5% de NP-40 y Albúmina sérica bovina al 2% en buffer PDF) a temperatura ambiente (T/A). Posteriormente se incubó toda la noche a 4ºC con una dilución del anticuerpo primario deseado **(Tabla 4)** preparada en buffer de bloqueo. Se lavó el exceso de anticuerpo primario y se incubó con anticuerpo

secundario **(Tabla 4)** diluido en buffer de bloqueo por 30min a T/A. Se lavó el exceso de anticuerpo y se aplicó PDF con azida de sodio hasta el momento de visualización o se cubrió cada pozo con un cubreobjetos fijado con ProLong Gold Antifade Mountant (*Thermo Fisher*).

En todos los casos los lavados se efectuaron con PDF y la tinción con 4 ',6-diamino-2-fenilindol (DAPI) se realizó de forma estándar, incubando las preparaciones durante 2min a T/A con una solución 1:2000 preparada en PDF.

3.9-Microscopía

Se utilizó un microscopio confocal invertido espectral Zeiss LSM710. Para todos los casos, las células fueron ajustadas a la densidad deseada, se trataron dependiendo del experimento y se transfirieron a placas de 8 pozos Ibidi m-Slide. Para los experimentos con células vivas, las placas se mantuvieron a 22°C hasta el momento de su visualización. La preparación para inmunofluorescencia se detalla en la sección previa.

3.10- Western blot

Para obtener extractos totales de proteína, las células por analizar se centrifugaron, se lavaron con PDF y se suspendieron en buffer de lisis (10 mM Tris/HCl pH 7.5, 150 mM NaCl, 0.5 mM EDTA, 0.5% NP-40, 0.05% SDS) suplementado con inhibidores de proteasas (*Sigma-Aldrich*, P8340). Posteriormente, la suspensión se incubó durante 30 min en hielo y se centrifugó (15 min., 4°C). Se cuantificó la concentración de proteína de los sobrenadantes obtenidos utilizando el kit comercial BCA (*Thermo Fisher Scientific*). Los extractos totales celulares se separaron mediante electroforesis desnaturalizante en geles de poliacrilamida en presencia de SDS (SDS-PAGE) y se transfirieron a membranas de PVDF (*Millipore*) que fueron bloqueadas por 1hr en Buffer TBS (Tris Buffered Saline) adicionado con tween al 0.05% (TBSt) adicionado con leche al 5%. Según el experimento, se utilizaron los anticuerpos contenidos en la **Tabla 4** diluidos en TBSt con leche al 5% o al 9%. Los lavados se realizaron con TBSt. Los análisis de densitometría se realizaron con el programa Image-J. Estas medidas se utilizaron para determinar los niveles arbitrarios de proteína. Para esto, dependiendo del ensayo, se utilizó la señal de MCCC1 o de la GFP-PgkA como control de carga para normalizar.

3.11- Ensayos para evaluar la autofagia

Para evaluar la inducción de la autofagia se transformaron las células con el plásmido pJSK489 y se visualizaron mediante microscopía confocal *in-vivo* tras haber sido tratadas como se indica en cada

experimento. El número de células que presentaba acumulaciones de GFP-Atg18 se cuantificó manualmente con la ayuda del programa Image-J. Para esto, se analizaron las proyecciones máximas y las fotos individuales.

La capacidad de degradación autofágica se evaluó utilizando un protocolo modificado del ensayo de proteólisis descrito previamente para *D. discoideum* [164], [183]. Para esto, se utilizaron células transformadas con el vector pDM358-GFP-PgkA. En todos los experimentos se utilizaron células creciendo en fase exponencial. Los cultivos se ajustaron a una densidad de $1x10^6$ células/ml y se trataron con TN 2 μg/ml o su vehículo (DMSO) por 8hrs. Durante las últimas 2horas de tratamiento con TN, se añadieron dos pulsos de 150mM NH_4Cl a partir de un stock preparado en agua a 2M. Tras este tratamiento, las células se colectaron y se lisaron para poder realizar el análisis mediante Western blot, como se encuentra descrito en la sección previa.

3.12-Análisis bioinformáticos

Todas las secuencias de *D. discoideum* se obtuvieron de la base de datos de su genoma Dictybase [190]. Los análisis de BLAST (Basic Local Alignment Search Tool) se realizaron también en la herramienta provista por esta misma página. Las secuencias proteicas se obtuvieron de la base de datos UNIPROT. Para los alineamientos locales de dos proteínas se utilizó la herramienta SIM [191] y los resultados se visualizaron con LALNVIEW [192]. Los alineamientos múltiples se realizaron con CLUSTAL OMEGA [193].

3.13- Análisis estadísticos

Se graficaron utilizando el software GraphPad Prism 5 los promedios, desviación estándar y significancia de al menos tres ensayos independientes de cada experimento. Dependiendo de las variables del experimento, la significancia estadística se analizó con este mismo programa mediante la prueba de t de Student, ANOVA de una vía con la prueba de Dunnet o de dos vías con la prueba de Bonferrioni.

4.- RESULTADOS

4.1- Inducción de estrés de RE en *D. discoideum*

Dado que no existían reportes previos en los que se hubiese caracterizado la respuesta al estrés de RE en *D. discodeum*, se analizó el efecto de la TN, la 2-DOG y el DTT. Estas tres drogas se han utilizado ampliamente como inductores de ERE en levaduras y en mamíferos [26], [194]. Para esto, se crecieron células de *D. discoideum* de forma axénica hasta que alcanzaron la fase media exponencial (a una densidad aproximada de $2x10^6$ células/ml) y posteriormente se trataron durante 16hrs con TN (2μg/ml), con 2-DOG (200mM) o con DTT (1.5mM). Estas concentraciones se eligieron con base en las concentraciones comúnmente utilizadas para inducir estrés de RE en mamíferos [26]. El efecto de estos tratamientos sobre la viabilidad celular en *D. discodeum* se evaluó mediante un ensayo que se adaptó a partir de los experimentos de goteo que se utilizan comúnmente en levaduras [24], [195]. Para esto, se prepararon diluciones seriales (por un factor de 10) de células de *D. discodeum* a partir de los cultivos de amebas tratadas con las drogas, y se depositaron alícuotas de estas diluciones sobre un césped de bacterias esparcido sobre una placa de agar. Este ensayo permite evaluar la capacidad de las amebas para recuperar el crecimiento en asociación con bacterias tras haber sufrido un tratamiento. También, se evaluaron los efectos de las drogas en la morfología celular mediante microscopía óptica.

De las tres drogas que se emplearon, sólo el tratamiento con TN tuvo un efecto en la viabilidad y en la morfología de las células **(Figura 10A)**. En el ensayo de goteo, solo las diluciones con la mayor densidad celular produjeron un halo de crecimiento y las células adquirieron una forma redondeada y refringente; además de que perdieron adherencia y cesaron de dividirse. Con estos datos se puede concluir que solamente la TN fue capaz de generar un estrés y de afectar la viabilidad celular, en cambio la 2-DOG y el DTT parecen que no generar ningún efecto en estas células, al menos en las concentraciones empleadas.
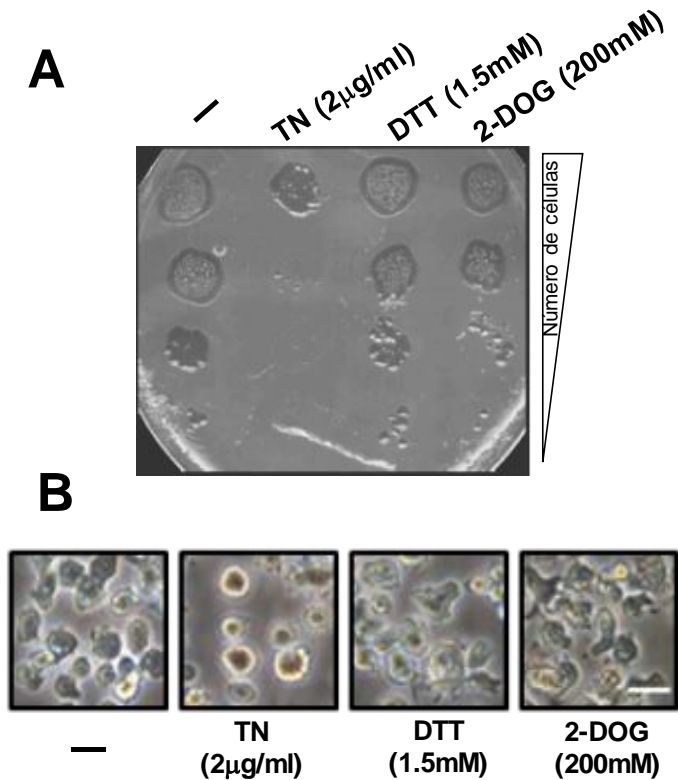
Figura 10. Inducción de estrés de RE en células de *D. discoideum*. **(A)** Ensayo para analizar el efecto sobre la viabilidad celular de un tratamiento con DTT, 2-DOG, TN o vehículo (DMSO). Se trataron amebas en crecimiento axénico con las drogas indicadas durante 16hrs y se depositaron gotas de las diluciones seriales preparadas con estas células sobre una placa de SM en la que se había esparcido previamente *K. aerogenes*. La placa se incubó a 22°C y se fotografió 7 días después. **(B)** Imágenes adquiridas mediante microscopía de luz de las células en A, antes de realizar el ensayo de goteo (escala 10μM). En ambos casos se muestran fotografías significativas de tres ensayos independientes.

En otros organismos se ha descrito ampliamente que el estrés de RE incrementa la expresión tanto de las chaperonas residentes del RE, como de los componentes la ERAD [33], [196]. Dentro de las chaperonas cuya expresión aumenta significativamente en respuesta al estrés de RE se encuentra GRP78, una proteína de RE que participa tanto en el plegamiento de proteínas, como en la regulación de la UPR [197]. Mediante un análisis de BLAST, identificamos que en *D. discoideum* existe un ortólogo de GRP78 (*DDB_G0276445*) y encontramos que esta proteína comparte un 67% de identidad con su respectivo ortólogo de humano. En el caso de la ERAD, una de las proteínas cuya expresión es inducida ante el estrés de RE es la AAA ATPasa Cdc48/VCP/p97, la cual, en levaduras, participa en la retrotranslocación de proteínas [198]. En *D. discoideum* se ha descrito que CdcD es el ortólogo de esta ATPasa y existe un anticuerpo que se ha generado específicamente para detectar esta proteína [198].

Dados estos antecedentes, evaluamos si en *D. discoideum* un tratamiento con TN, 2-DOG o DTT causaba cambios en la expresión de Grp78 y de CdcD. Para esto, se analizaron mediante Western blot, los extractos totales de las células que fueron tratadas con las drogas mencionadas **(Figura 11)**. Se utilizaron

respectivamente un anticuerpo generado para detectar GRP78 de humano y el anticuerpo anti-CdcD de *D. discoideum* **(Tabla 4)**.

Para confirmar que el anticuerpo anti-GRP78 de humano fuese capaz de detectar al ortólogo de *D. discoideum,* se realizó un ensayo en el cual se sobreexpresó en bacterias la Grp78 de *D. discoideum (DDB_G0276445)*. Al analizar mediante Western blot los extractos totales de bacterias en las que se indujo la expresión de Grp78, se observó que el anticuerpo generado contra el ortólogo de humano fue capaz de detectar una proteína cuya migración está en el rango de los 72kDa **(Figura 11A).**

Al realizar ensayos de inmunodetección de Grp78 de extractos de células de *D. discoideum* que fueron tratadas con TN, se observó la presencia de tres bandas **(Figuras 11B, E y G, señaladas como *a* y *b*)**. Una de ellas, la que migró en la posición de mayor peso molecular, corresponde con el tamaño estimado a partir de la secuencia proteica del ortólogo en *D. discoideum* de Grp78 (72kDa) y con la banda que se observó en la prueba de sobreexpresión en bacterias. Al analizar mediante densitometría varios ensayos de Western blot, se observó que la proteína que migró en esta posición fue la única que presentó un incremento en su expresión tras un tratamiento con TN. Las otras dos proteínas detectadas por el anticuerpo contra GRP78 de humano en los extractos celulares de *D. discoideum*, presentaron un peso molecular cercano al estimado para las chaperonas citosólicas de la familia de las Hsc70, HspB (70kDa) y HspE (69kDa). No se observaron cambios significativos en la expresión de ninguna de estas dos proteínas ante los tratamientos evaluados **(Figuras 11B, C, E, F, G y H)**.

Figura 11. Página siguiente (A) El anticuerpo contra Grp78 de humano reconoce al ortólogo de *D. discoideum*. Se transformaron células de *Escherichia coli* BL21 con el vector pGEX-4T1-DdGrp78, se indujo con IPTG la expresión de la proteína en cultivos de cuatro colonias diferentes y posteriormente se analizaron los extractos totales de proteína de estas células mediante Western blot. Se incluyó como control un extracto total de amebas de *D. discoideum* tratadas con TN. **(B)** Western blot que muestra la expresión de Grp78 y CdcD en células tratadas con las drogas especificadas durante 16hrs. **(C)** Cuantificación por densitometría de las bandas observadas en el panel B. El gráfico muestra el promedio y la desviación estándar de 3 experimentos relativo al nivel observado en la condición control (vehículo). El nivel de Grp78 y CdcD se ajustó usando el control de carga (MCCC1). **(D)** Ensayo en el que se analizó la viabilidad de células tratadas con diferentes concentraciones de TN durante 16hrs. **(E)** Western blot en el que se observa la expresión de Grp78 y CdcD ante un tratamiento con diferentes concentraciones de TN y **(F)** gráfico que muestra el promedio y la desviación estándar de la cuantificación de 7 experimentos realizada como en D. **(G)** Western blot en el que se muestra la expresión de Grp78 y CdcD tras diferentes tiempos de tratamiento con 2mg/ml de TN y **(H)** gráfico que muestra el promedio y la desviación estándar de la cuantificación de 3 experimentos, realizada como en D. En todos los casos se muestran fotografías representativas de un experimento y los asteriscos en los gráficos denotan las diferencias estadísticamente significativas.
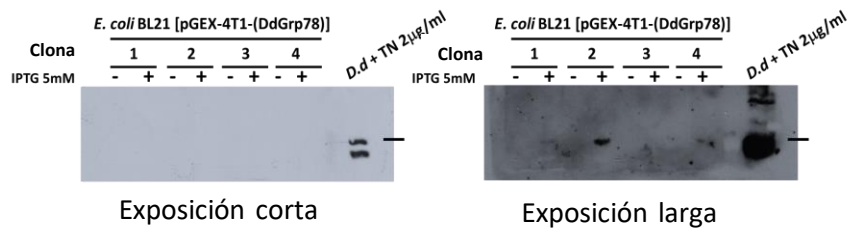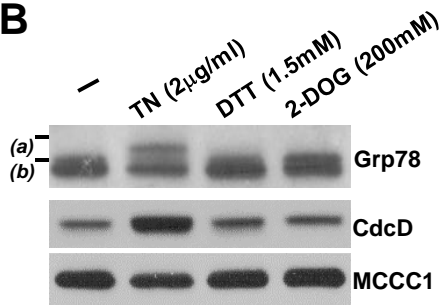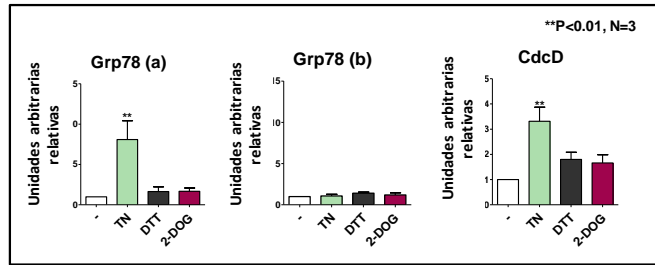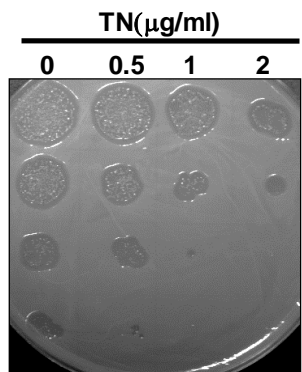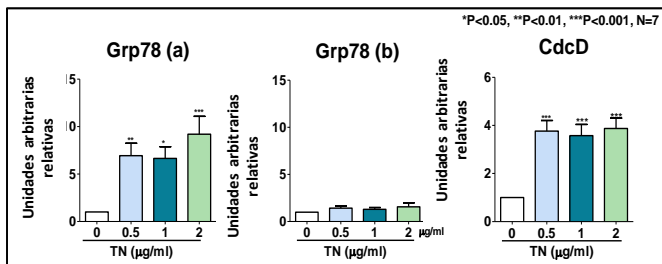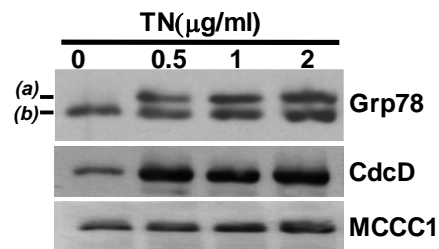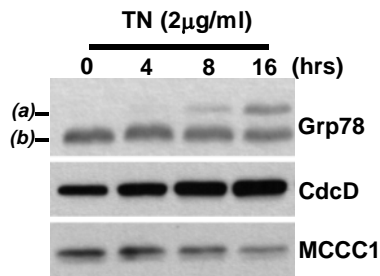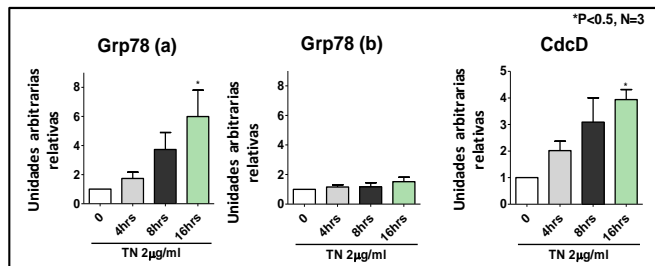
En el caso de CdcD, se observó que la TN indujo significativamente su expresión, de forma similar a lo que se observó para Grp78 **(Figuras 11B, C, E, F, G y H)**. La expresión tanto de Grp78 como de CdcD se incrementó de forma proporcional al tiempo de tratamiento con TN **(Figuras 11G y H)**. Además, se encontró que el incremento en la expresión de ambas proteínas se da desde concentraciones tan bajas como 0.5 μg/ml de TN, aunque la viabilidad celular se vio afectada a partir de concentraciones mayores a 1μg/ml, como puede observarse en las **Figuras 11D y E**.

Los datos obtenidos a partir de todas las pruebas mostradas anteriormente, en las que se utilizaron diferentes inductores de estrés de RE, nos mostraron que es posible utilizar un tratamiento con TN para generar de forma experimental este tipo de estrés en *D. discoideum*. En cambio, la 2-DOG y el DTT a las concentraciones probadas, no causaron efectos significativos en la viabilidad celular, ni en la expresión de Grp78, ni de CcdD. Se ha reportado que la 2-DOG se internaliza muy pobremente en las células de *D. discoideum* [199], motivo por el cual posiblemente no sea capaz de causar estrés de RE en estas células. Por su parte, cuando el DTT se administra a concentraciones mayores a la que se muestran, altera fuertemente el equilibrio de óxido-reducción (REDOX) celular y causa efectos pleiotrópicos más allá del estrés de RE, por lo que no se realizaron más ensayos con concentraciones mayores de esta droga.

4.2-Identificación de las proteínas ortólogas de la UPR en *D. discoideum*

El hecho de que en *D. discoideum* la TN generara cambios morfológicos celulares, así como una inducción de la expresión de Grp78 y de CdcD, sugiere que debe existir una ruta de señalización capaz de generar una respuesta a este estímulo. Por lo tanto, se procedió a identificar si en *D. discoideum* existían proteínas ortólogas de los diferentes componentes de la vía de la UPR. Para esto, se realizó una búsqueda mediante BLAST (*Basic Local Alignment Search Tool*) empleando la herramienta albergada en la página web de la base de datos del genoma de *D. discoideum (www.dictybase.org)* [190]. Para esto, se utilizaron las secuencias de aminoácidos de las proteínas IRE1, XBP1/Hac1p/bZIP60, ATF6/bZIP28 y PERK, respectivamente de humano, de *S. cerevisiae* y de *A. thaliana.* Con este análisis se identificó que en esta ameba existe un solo ortólogo de IRE1 codificado por el gen *DDB_G0267650/ireA*. Sin embargo, este análisis no nos permitió identificar ortólogos de los factores de transcripción XBP1 y ATF6 **(Tabla 5).**

Proteína	Localizador	Tamaño *	Resultado	Tamaño *	*E-value*
Xbp1/Hac1p	P17861 (XBP1_HUMAN)	261/376	ND		
	P41546 (HAC1_YEAST)	230/238			
	Q9C7S0 (BZP60_ARATH)	258/295			
Ire1p/Ern1	O75460 (ERN1_HUMAN)	977	IreA	984	4e-69
	P32361 (IRE1_YEAST)	1 115			1e-75
	Q93VJ2 (IRE1B_ARATH)	881			2e-78
ATF6	P18850 (ATF6A_HUMAN)	670	ND		
	Q9SG86 (BZP28_ARATH)	675			
PERK	Q9NZJ5 (E2AK3_HUMAN)	1,116	IfkA *	2 258	4e-30
			IfKB*	1 358	2e-30

Tabla 5. Resultados del análisis que se realizó para identificar los posibles homólogos de las vías de respuesta a estrés de retículo endoplásmico utilizando la herramienta BLAST de la base de datos *de D. discoideum*. * IfkA e IfkB se ha descrito que representan ortólogos de Gcn2

Esta búsqueda nos arrojó, con un muy buen valor de *E-value*, a IfkA y a IfkB como ortólogos de PERK en *D. discoideum*; sin embargo, estas proteínas carecen del dominio transmembranal típico que caracteriza a PERK; además, ya se ha descrito que estas proteínas representan ortólogos de Gcn2 [200], [201], una quinasa que en levaduras se ha identificado que, al igual que PERK, puede fosforilar a la subunidad alfa del eIF2 [202].

Por otra parte, esta búsqueda no arrojó ningún posible ortólogo de XBP1, ni de ATF6. Sin embargo, en el genoma de *D. discoideum* se encuentran anotados 19 factores de transcripción que contienen un dominio bZIP **(Tabla 6)**, por lo que se realizó un análisis de la secuencia proteica de cada uno de los posibles bZIPs para determinar si alguno de ellos presenta un dominio transmembranal o una zona altamente hidrofóbica en la región carboxilo. Esta característica estructural suele definir a este tipo de factores de transcripción. Se encontró que tres de estas proteínas, bzpC, bzpD y bzpJ, contienen un cruce transmembranal, mientras que seis de ellas, bzpH, bzpM, bzpO, bzpQ, bzpR y bzpS, contienen una zona hidrofóbica en su extremo carboxilo.

Posteriormente durante este trabajo, se analizó el papel de BzpD y BzpJ en la respuesta al estrés de RE, dado que fueron los únicos con un probable cruce transmembranal, y porque han sido anotados en la base de datos como posibles factores de transcripción de la familia ATF6 **(Tabla 6)**; BzpD como un posible ortólogo de la isoforma C de Atf6 de *Drosophila* y BzpJ como ortólogo de CREB3, un factor de transcripción de la familia de ATF6 que en mamíferos se ha observado que responde al estrés de RE [203], [204].

bZIP	TM	ZH	Función reportada/ortólogos
dimA	No	No	Regulador transcripcional implicado en la respuesta a la señalización por DIF-1 durante el desarrollo [205], [206].
dimB	No	No	Participa en la expresión de los genes pretallo en respuesta a DIF-1 durante el desarrollo [207].
bzpC	Si	Si	-
bzpD	Si	Si	Ortólogo del gen Atf6-C de *Drosophila*.
bzpE	No	No	-
bzpF	No	No	Factor de transcripción tipo CREB que participa en la señalización de la vía de PKA [208]. Ortólogo de YAP6 de levadura.
bzpG	No	No	Ortólogo de los factores de transcripción HY5-like y AtbZip64 de *A. thaliana*.
bzpH	No	Si	-
bzpI	No	No	-
bzpJ	Si	Si	Ortólogo de los factores de transcripción de humano Luman/CREB3 y de ABSCISIC ACID-INSENSITIVE 5-like protein 7 de *A. thaliana*.
bzpK	No	No	-
bzpL	No	No	Ortólogo de BZIP18 de *A. thaliana*
bzpM	No	Si	-
bzpN	No	No	Factor de transcripción homólogo a GCN4 de levadura [208].
bzpO	No	Si	-
bzpP	No	No	-
bzpQ	No	Si	-
bzpR	No	Si	Factor de transcripción que se expresa cuando la subunidad alfa del eIF2 se encuentra fosforilado. La mutante nula de este gen presenta un fenotipo similar a la mutante de eIF2alfa que no puede fosforilarse[201].
bzpS	No	Si	-

Tabla 6. Análisis de los factores de transcripción codificados en el genoma de *D. discoideum* que presentan un dominio básico seguido de una cremallera de leucinas (bZIP). Se muestra la información sobre la presencia de regiones transmembranales (TM) o zonas hidrofóbicas (ZH), la función que ha sido anotada para estas proteínas en la base de datos del genoma de *D. discoideum,* así como si existen posibles ortólogos de esa proteína en otros organismos.

4.3- Caracterización de la ruta de IreA

4.3.1- IreA es una quinasa/ribonucleasa transmembranal residente del RE en *D. discoideum*

IreA de *D. discoideum* es una proteína transmembranal tipo II de 984 aminoácidos la cual contiene en su extremo amino (N), una secuencia de 26 aminoácidos que presenta las características de una señal de direccionamiento al RE **(Figura 12A)**. Esta proteína presenta un peso molecular (MW) de aproximadamente 112 kDa y contiene en su región carboxilo (C) terminal citoplasmática los dos dominios característicos de los ortólogos de IRE1: uno de quinasa de serinas y treoninas (residuos del 575 al 851), seguido de uno de ribonucleasa KEN (residuos del 854 al 984).

Al analizar mediante un alineamiento global múltiple la secuencia proteica de los ortólogos de IRE1, encontramos que la similitud entre las proteínas de las diferentes especies es aproximadamente de un 30%. Por otra parte, al evaluar las secuencias mediante alineamientos locales, se observó que la mayor identidad entre los ortólogos de IRE1 se encuentra restringida en la porción citoplasmática de las proteínas; específicamente en la región que contiene los dominios de quinasa y de ribonucleasa **(Figura 12A)**. Mediante este análisis se encontró que, de las proteínas evaluadas, las porciones citoplasmáticas de IreA de *D. discoideum* y de IRE1α de humano son las que muestran mayor similitud.

Para determinar la localización de IreA se generó una construcción utilizando el plásmido de expresión para *D. discoideum* pDM323 **(Tabla 3)**, en la que se etiquetó a IreA con la GFP en su extremo C-terminal (IreA-GFP). Posteriormente, esta proteína de fusión se expresó en amebas silvestres (WT). En las imágenes de microscopía confocal de la **Figura 12C** se puede observar que IreA-GFP se distribuyó en un patrón reticular, el cual coincide con la distribución de la proteína disulfuro isomerasa (PDI). Esta proteína, que se detectó mediante inmunofluorescencia en este ensayo, se utiliza comúnmente en *D. discoideum* como un marcador de RE, ya que es una chaperona que reside en el lumen de este organelo [178], [179]. También se puede observar que IreA-GFP se localizó rodeando a la señal de DAPI lo que indica que tiene también una distribución perinuclear. Todo esto muestra que IreA es una proteína que se localiza en el RE.
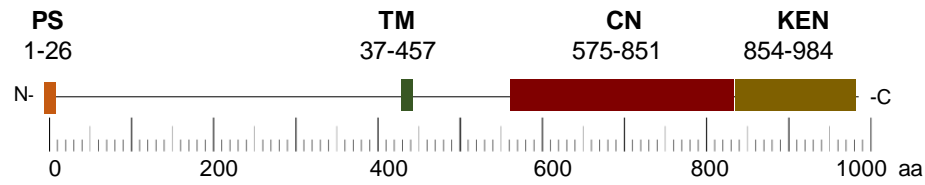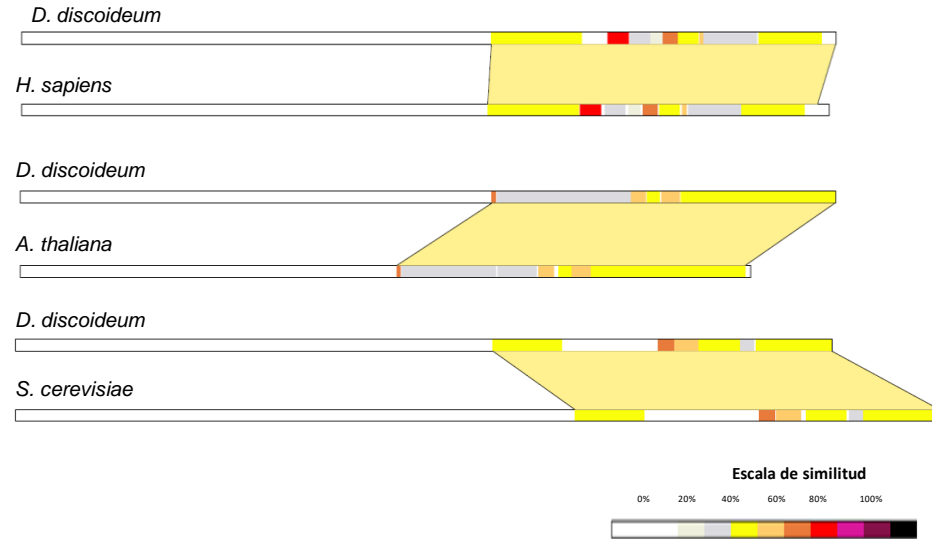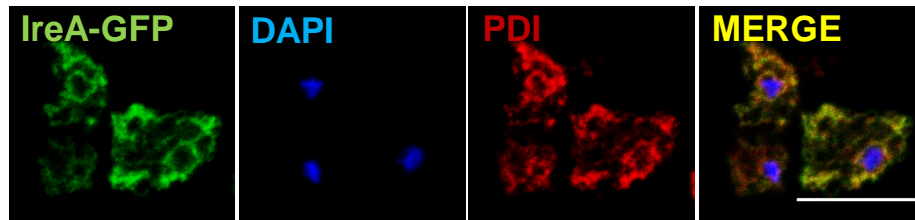
Figura 12. (A) Esquema de los dominios de IreA. PS (péptido señal), TM (transmembranal), CN (quinasa) y KEN (dominio *Kinase Extension Nuclease*). **(B)** Diagramas de los alineamientos locales entre las secuencias proteicas de los ortólogos de IRE1, respectivamente de *D. discoideum*, *H. sapiens* y *A. thaliana*. El código de color representa la similitud que existe entre ambas secuencias. Los alineamientos fueron generados con el programa SIM alginment y analizados con LALNVIEW. **(C)** Fotos obtenidas por microscopía confocal de amebas de *D. discoideum* WT expresando la construcción de IreA fusionada a la GFP (IreA-GFP). Estas células se fijaron y se prepararon para detectar por inmunofluorescencia a la Proteína Disulfuro Isomerasa (PDI) (en rojo), chaperona de RE que se utiliza como marcador de este organelo en *D. discoideum*. Los núcleos se tiñeron con DAPI.

4.3.2-IreA es necesaria para contender con el estrés de RE inducido con TN

Para evaluar el papel de IreA en la respuesta a estrés de RE y su posible participación en el proceso de desarrollo de *D. discoideum,* se generó una cepa mutante de esta proteína. Para esto, se interrumpió el locus de *ireA* mediante la inserción de un gen de resistencia a la Blasticidina (BST) [180]. De esta forma, se generó una deleción de 998 pares de bases en este locus. La inserción del casete BST y la ausencia de expresión del RNA mensajero se corroboró mediante PCR y RT-PCR respectivamente **(Figura 13).**
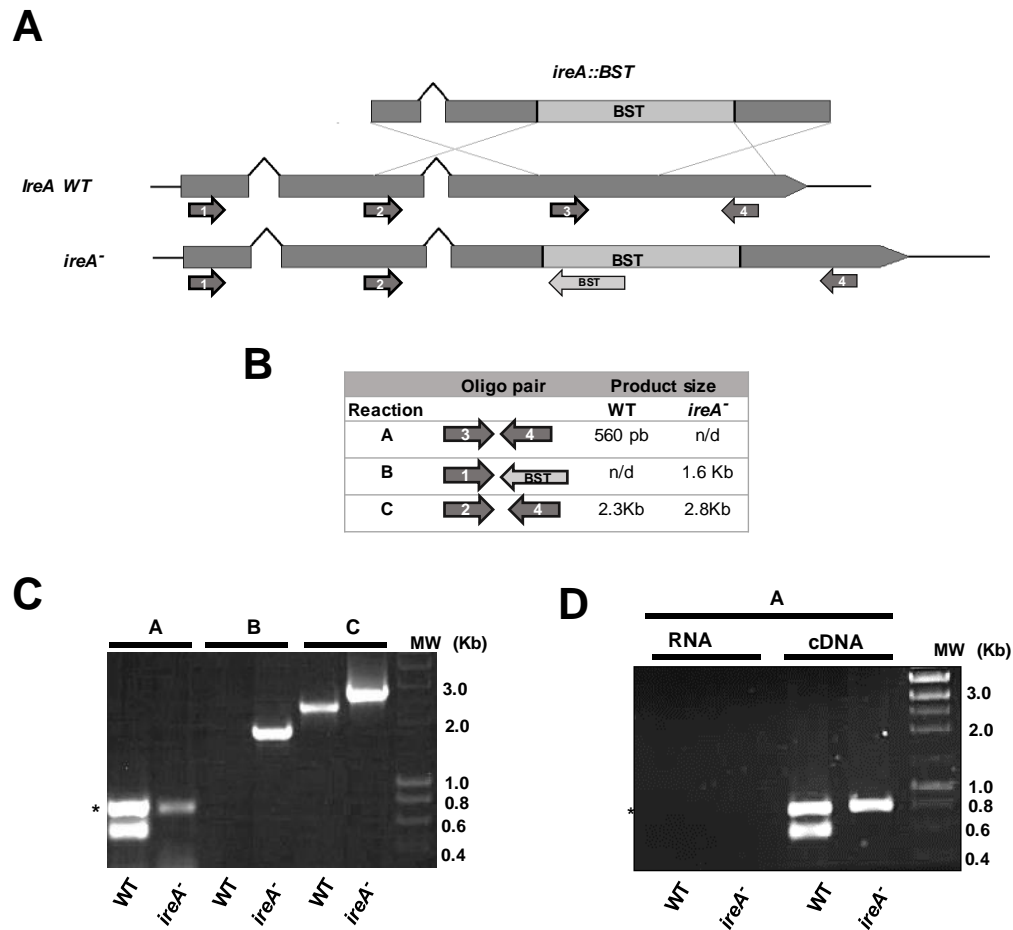
Figura 13. Interrupción del locus de *ireA*. **(A)** Diagrama de la metodología usada para generar la mutante *ireA*⁻. Se muestra el sitio en el que se insertó mediante recombinación homóloga la construcción generada para interrumpir el locus con un casete que contiene el gen de resistencia a la Blasticidina *(ireA::BST)* y se muestran los sitios en los que se unen los diferentes oligonucleótidos que se utilizaron para verificar mediante PCR la interrupción y la inserción de BST en *ireA*. **(B)** Tabla que muestra el tamaño de los productos que se obtienen al usar las parejas de oligonucleótidos señaladas en A. **(C** y **D)** Productos que se obtuvieron al amplificar mediante PCR el **(C)** DNA o **(D)** el cDNA de las cepas especificadas. *Amplificado de un gen no relacionado que se incluyó como un control de la reacción de PCR.

La cepa *ireA*⁻ no presentó defectos significativos durante el crecimiento axénico, ni en asociación con bacterias. Únicamente, se detectó en los ensayos de desarrollo en filtro, los cuales se llevan a cabo en ausencia completa de nutrientes, que la cepa *ireA*⁻ se mantuvo más tiempo en la fase migratoria de gusano. Sin embargo, las células de la mutante *ireA*⁻ lograron completar el ciclo de desarrollo y formaron cuerpos fructíferos normales y con esporas viables **(Figura 14A)**. Esto indica que la ausencia de IreA no genera efectos drásticos ni en la diferenciación y ni durante el desarrollo.

Para evaluar el efecto de la TN sobre la morfología de las células de la cepa *ireA*⁻ se realizaron observaciones de microscopia óptica y se analizó la viabilidad de estas células mediante un ensayo de goteo de diluciones seriadas de células como el que se describió en secciones previas. Con estos ensayos encontramos que un tratamiento con TN por 16hrs causa que las células *ireA*⁻ se redondeen y se observen refringentes. También, pudo observarse que en esta cepa, este tratamiento causó lisis celular **(Figura 14B)**. Por otra parte, los tratamientos con TN por 4, 8 y 16hrs evitaron por completo que las células mutantes *ireA*⁻ pudieran crecer en placas de agar que contenían un césped bacteriano **(Figura 14C)**. Finalmente, observamos que en las células *ireA*⁻ tratadas por 16hrs con TN la expresión de Grp78 y de CdcD fue menor que en la cepa WT tratada bajo las mismas condiciones **(Figuras 14D y E)**.

Todos estos resultados indican que en *D. discoideum,* IreA resulta indispensable para que las células puedan contender con un tratamiento que genera estrés de RE y sugieren que esta proteína participa en una ruta de señalización involucrada en mantener la homeostasis del RE.
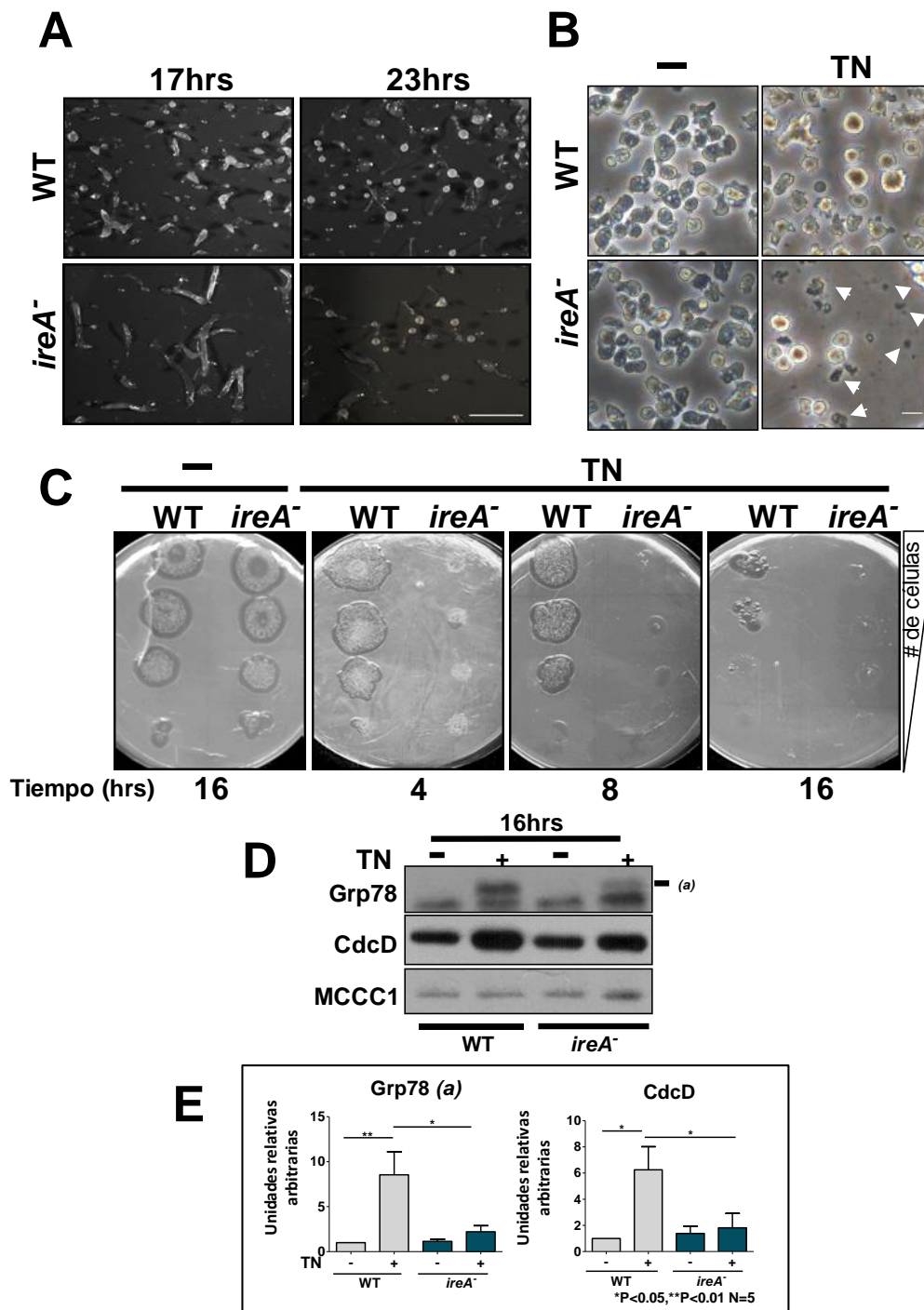
Figura 14. Fenotipo de la mutante *ireA*. **(A)** Efectos de la ausencia de IreA sobre el desarrollo. Se muestran fotografías representativas de células tras 17 y 23hrs en un filtro de nitrocelulosa en buffer PDF, ensayo que permite que se desarrollen (escala 1mm). **(B)** Fotografías obtenidas mediante microscopía óptica de amebas de *D. discoideum* WT o *ireA*- tras haber sido tratadas por 16hrs con TN (2μg/ml) o su vehículo (DMSO). Las flechas indican restos celulares (escala 10μM). **(C)** Ensayo de goteo de diluciones seriales de células para evaluar la viabilidad de la cepa WT e *ireA*- tras un tratamiento con TN (2μg/ml) durante los tiempos indicados. **(D)** Imagen representativa de un ensayo de Western blot para evaluar la expresión de Grp78 y CdcD en las cepas WT e *ireA*- tras un tratamiento con TN (2μg/ml). **(E)** Gráfico del promedio y la desviación estándar del análisis densimétrico de 5 experimentos, relativo al nivel observado en la condición control (vehículo) de la cepa WT. Todas las muestras se ajustaron con respecto a su control de carga (MCCC1). Los asteriscos denotan las diferencias significativas.

4.3.3-Los dominios de quinasa y de ribonucleasa de IreA se requieren para responder al estrés de RE

Para examinar la participación de los dominios de quinasa y de ribonucleasa de IreA durante la respuesta al estrés de RE, se generaron de forma independiente una mutante puntual sin actividad de quinasa y una mutante puntual sin actividad de ribonucleasa. La inactivación del dominio de quinasa se consiguió al remplazar un residuo conservado de lisina localizado en el sitio de unión a ATP por un residuo de asparagina (*ireA^{K603N}*). Para generar una mutante sin actividad de ribonucleasa, se sustituyó una asparagina conservada en el sitio activo del dominio KEN por una alanina (*ireA^{N927A}*) **(Figura 15A).** En otros organismos, se ha comprobado que las mutaciones correspondientes inactivan eficientemente tanto la actividad de quinasa como de ribonucleasa [209], [210].

Se generaron construcciones para expresar ambas mutantes puntuales fusionadas a la GFP **(Tabla 3)** y se transformaron células *ireA^{-}* respectivamente con la construcción que contenía la forma WT (IreA-GFP), o con una de las mutantes puntuales (ireA^{K603N}-GFP o ireA^{N927A}-GFP). Posteriormente, se examinó mediante microscopía confocal la expresión y la localización de estas versiones de IreA en células que fueron preparadas para inmunofluorescencia para poder detectar a la PDI. Observamos que, al igual que la forma WT de IreA, ambas mutantes puntuales se expresaron correctamente y se localizaron en el RE **(Figura 15B)**.
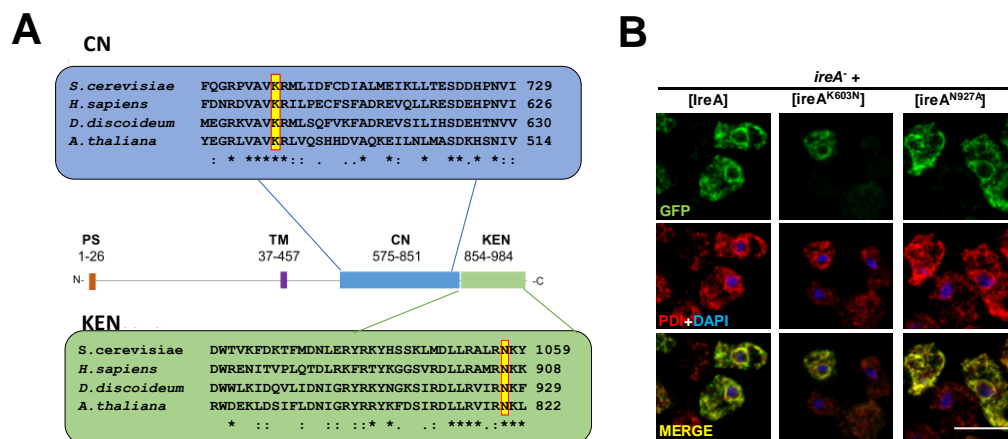
Figura 15. (A) Diagrama en el que se muestran los aminoácidos conservados de IreA que se mutaron para inactivar respectivamente su dominio de quinasa (CN) (sustitución de la K603 por N) o el dominio de ribonucleasa (KEN) (cambio de la N927 por A). Se muestra un alineamiento de los ortólogos de IRE1 de *S. cerevisiae*, *H. sapiens, D. discoideum* y *A. thaliana* de estas zonas conservadas. **(B)** Imágenes obtenidas mediante microscopía confocal de células expresando respectivamente la forma silvestre de IreA fusionada a la GFP, o las formas mutadas de esta proteína con los cambios K603N o N927A. Las células se prepararon para detectar mediante inmunofluorescencia a la PDI (rojo) y para teñirlas con DAPI.

Posteriormente, se siguió mediante microscopía confocal *in-vivo* la expresión y localización de las tres formas de IreA durante diferentes tiempos de tratamiento con TN. Se ha descrito que la actividad de IRE1 en mamíferos y en levaduras se regula de manera dependiente a su estado de oligomerización. En ambos casos, IRE1 transita de una forma monomérica a una forma oligomérica durante un estímulo de estrés y cuando la célula comienza el proceso de adaptación, esta retoma su forma monomérica [211], [212]. Como puede observarse en la **Figura 16A**, en *D. discoideum* las tres formas de IreA que se probaron fueron capaces de formar oligómeros al ser tratadas con TN (que se observan como puntos en la **Figura 16A**). Aproximadamente el 40% de las células que expresaban la forma WT de IreA presentaron puntos sobre el RE entre las 2 y las 4hrs de tratamiento con TN. Como se observa en la **Figura 16B**, el porcentaje de células en las que se pudo observar la formación de oligómeros de IreA difirió dependiendo de si expresaban la forma WT o alguna de las mutantes puntuales. En comparación con la cepa que expresaba la forma WT de IreA, un porcentaje significativamente menor de células presentó oligómeros en la cepa que expresaba la forma sin actividad de quinasa (ireA^{K603N}), mientras que casi el total de las células que expresaban la forma con la ribonucleasa inactiva (ireA^{N927A}) presentaron oligómeros en todos los tiempos de tratamiento que fueron analizados.

Las observaciones anteriores indican que las formas mutantes de IreA probablemente mantienen su estructura, ya que son capaces de oligomerizarse ante el estrés de RE. Por lo que analizamos el efecto de la expresión de estas formas mutantes sobre la viabilidad celular ante un tratamiento con TN. Para esto, se realizó un ensayo de goteo de diluciones seriadas como el que se ha descrito anteriormente. Se observó que, sólo las células que expresaban la forma silvestre de IreA fueron capaces de crecer en placas de agar con bacterias tras un tratamiento con TN, mientras que las mutantes puntuales carentes respectivamente de las actividades de quinasa y de ribonucleasa, se comportaron como la cepa *IreA⁻*; es decir que ambas cepas fueron altamente sensibles al tratamiento con este antibiótico **(Figura 16C).** De la misma manera, la expresión de Grp78 y de CdcD solo aumentó ante un tratamiento con TN en las células que expresaban la forma WT y no en las que expresaban las mutantes puntuales de IreA **(Figuras 16D y E)**.

Las células *ireA⁻* que expresaban las formas mutantes de IreA (K603N o N297A) no sólo no fueron capaces de reestablecer el crecimiento tras un estrés de RE sino que además, fueron incapaces de mantener la estructura del RE. Como se observa en las **Figuras 16A** y **16F**, el RE de las células que expresaban la forma WT de IreA, conservaron la estructura del RE durante el tratamiento con TN. Sin embargo, se observó que en un porcentaje significativo de las células que expresaban las formas mutantes puntuales de IreA, el RE perdió su estructura y se pudieron apreciar regiones en las que los túbulos se colapsaron.

Todos estos datos en conjunto muestran que las formas mutantes de IreA sin actividad de quinasa o de ribonucleasa, son capaces de sentir las condiciones de estrés, ya que pueden formar oligómeros. Sin embargo, sugieren que cuando IreA no presenta actividad de quinasa o de ribonucleasa, no puede disparar la respuesta al estrés y por consiguiente, la estructura del RE y su homeostasis se ven comprometidas. Además, se observó que el proceso de formación y disociación de los oligómeros resultó defectuoso en las mutantes puntuales de IreA analizadas. Esto sugiere que se requiere que IreA se encuentre completamente activa para regular su propia dinámica de oligomerización, y posiblemente su señalización.
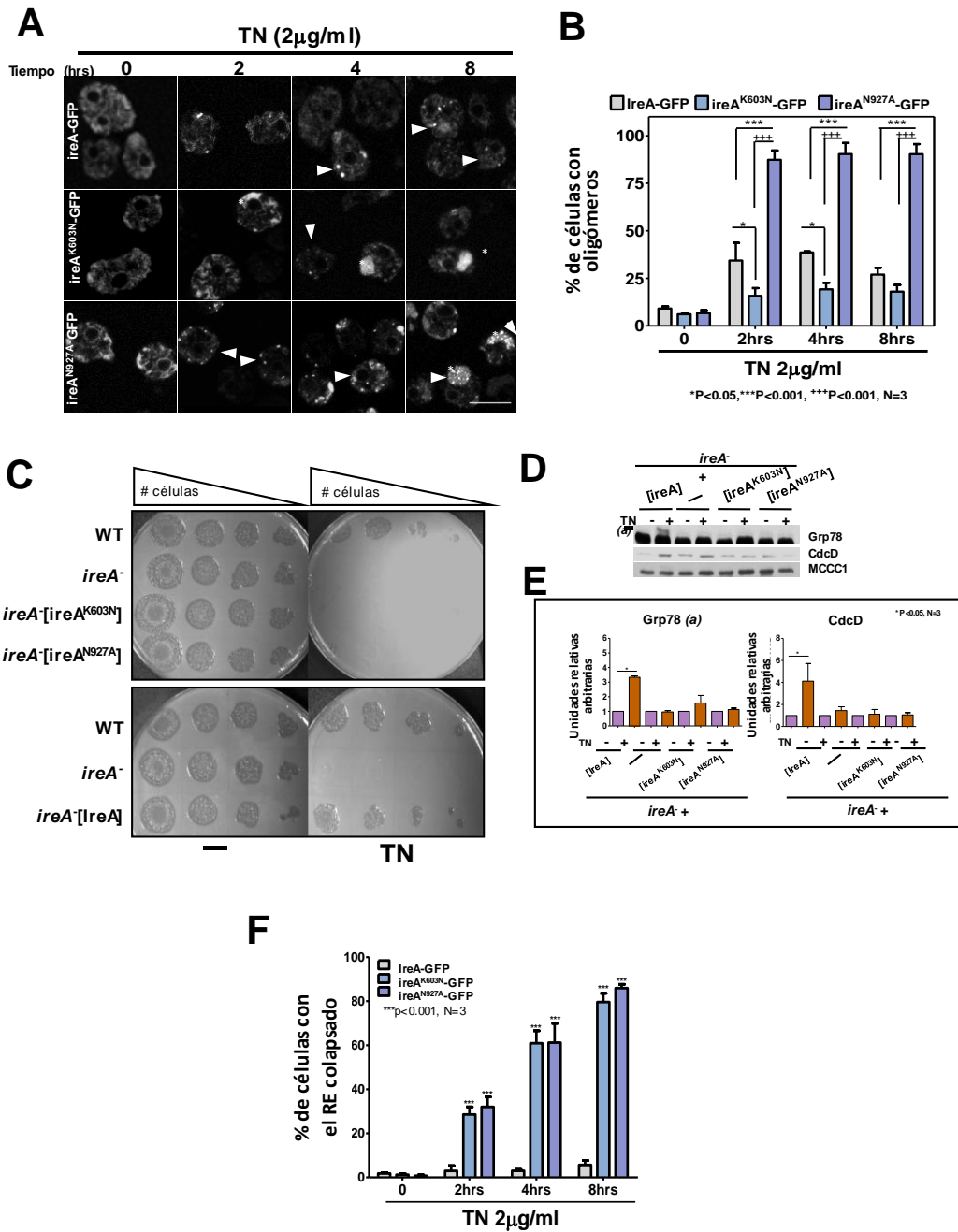
Figura 16. Los dominios de quinasa y de ribonucleasa de IreA en la respuesta al estrés de RE. **(A)** Imágenes de microscopía confocal que muestran la localización de IreA y su conformación en oligómeros. Células *ireA*- que expresaban respectivamente las construcciones IreA-GFP, IreA[K603N]-GFP o IreA[N927A]-GFP fueron tratadas con TN y evaluadas *in-vivo* cada dos horas por microscopía confocal. **(B)** Cuantificación del porcentaje de células con oligómeros de IreA en (A). Se muestra el promedio y la desviación estándar de 3 experimentos. **(C)** Ensayo de goteo de células *ireA*- que expresaban respectivamente las construcciones IreA-GFP, IreA[K603N]-GFP o IreA[N927A]-GFP, tras haber sido tratadas con TN durante 16h. **(D)** Western blot que muestra la expresión de Grp78 y CdcD tras un tratamiento con TN en células que expresaban respectivamente las construcciones IreA-GFP, IreA[K603N]-GFP o IreA[N927A]-GFP. **(E)** Gráfico de la cuantificación por densitometría de tres experimentos como en (D). Se muestra el promedio y la desviación estándar. **(F)** Se cuantificó el porcentaje de células que mostraban túbulos colapsados en tres experimentos como en (A). Se graficó el promedio y la desviación estándar. Para todos los gráficos los asteriscos denotan diferencias estadísticas significativas.

4.3.4-La respuesta transcripcional al estrés de RE depende parcialmente de IreA

En otros organismos, una parte significativa de la respuesta al estrés de RE consiste en una reprogramación transcripcional que le permite a la célula readaptar su capacidad de plegamiento de proteínas en el RE y aumentar los procesos celulares de degradación. Para evaluar si en *D. discoideum* un tratamiento con TN causa cambios transcripcionales, realizamos un ensayo de secuenciación profunda de RNA poliadenilado (RNAseq). Para esto, se utilizó RNA de células WT o *ireA*[-], tratadas previamente con 2µg/ml de TN o con su vehículo (DMSO) durante 16hrs. En los resultados obtenidos con este ensayo, se observó que en una cepa WT, la TN ocasionó cambios en la abundancia de 433 transcritos, lo cual equivale a aproximadamente 3.5% de los genes en *D. discoideum*. Dentro de estos, se observó que aumentó la expresión de 166, mientras que hubo una disminución en 267 **(Figuras 17A y B).**

Con el objetivo de definir los procesos celulares en los que se generaron cambios transcripcionales, se analizó el grupo de genes cuya expresión cambión con el tratamiento con TN. El análisis se generó con la herramienta *DAVID gene ontology enrichment clustering tool*. Este programa arroja términos de ontología génica (GO) que se encuentran enriquecidos en una lista de genes dada y genera grupos de términos que se encuentren asociados. Se analizaron los términos GO contenidos únicamente en las siguientes categorías: *proceso biológico, dominio proteico* y *componente celular.* En **la Figura 17** se muestra un resumen de los resultados obtenidos a partir de este análisis y los datos completos de cada grupo se encuentran en el Apéndice I. Como puede observarse en la **Figura 17**, el conjunto de transcritos cuya abundancia aumentó ante un tratamiento con TN está principalmente enriquecido en genes asociados a procesos biológicos involucrados en la respuesta a estrés de RE, al plegamiento de proteínas y a la homeostasis REDOX. Además, se observó que este conjunto está enriquecido significativamente en genes asociados a procesos de degradación dependiente de ubiquitinación.

Figura 17. (Página siguiente). Análisis de los procesos celulares que en *D. discoideum* se ven afectados tras un tratamiento con tunicamicina (TN). **(A y B)** La TN indujo un incremento en la abundancia de 166 transcritos **(A)** y la disminución de 267 **(B)**. Cada uno de estos conjuntos de genes se analizó mediante la herramienta informática DAVID para obtener las categorías de términos ontológicos (GO) que se encontraron enriquecidas. Los grupos de categorías GO obtenidas tanto para el conjunto de los transcritos cuya expresión incrementó, como para el que disminuyó, se graficaron dependiendo de su nivel de enriquecimiento y de su probabilidad (P-value ≥ 0.05). Se muestran las categorías GO obtenidas para "*Proceso Biológico*" **(C y D)**, "*Dominios Proteicos*" **(E y F)** y "*Componente celular*" **(G y H)**. Las estrellas marcan las categorías GO en las que >45% de los genes contenidos dependen de IreA para cambiar su expresión. El tamaño de la burbuja es proporcional al número de genes que contiene. Se utilizó el mismo color para las categorías que pertenecen a un mismo grupo de enriquecimiento.

A

- Dependientes de IreA
- Independientes de IreA
- Transcritos cuya expresión disminuyó con TN

166 transcritos que aumentó su expresión con TN

76
90

B

- Dependientes de IreA
- Independientes de IreA
- Transcritos cuya expresión aumentó con TN

267 transcritos que disminuyó su expresión con TN

92
175

C Proceso Biológico

Respuesta a estrés de RE
Plegamiento
Homeostasis redox
Transporte
Ubiquitinación ★

P-value
Enriquecimiento
★ >45% de gens dependientes de IreA

D Proceso Biológico

Endocitosis ★
Catálisis de peptidoglicano
Catálisis de lípidos
Fototaxis ★
Fagocitosis
Defensa contra bacterias ★
Morfogénesis celular ★
Respuesta a hiperósmosis ★
Citocinesis

P-value
Enriquecimiento
★ >45% de genes dependientes de IreA

E Dominios proteicos

Sitio conservado de tiorredoxina
Ubiquitina ★
alfa/beta hidrolasa ★
Dominio DNA-J
Enzima de conjugación de ubiquitina
Transportador ABC ★

P-value
Enriquecimiento
★ >45% de genes dependientes de IreA

F Dominios proteicos

Carboxilesterasa tipo B ★
Hidrolasa de glucósidos
Actina
Saposina B
CMP/dCMP deaminasa
Hidrolasa de nucleótidos ★

P-value
Enriquecimiento
★ >45% de genes dependientes de IreA

G Componente celular

Retículo endoplásmico
Complejo de uniquitina ligasa ★
Citoplasma ★

P-value
Enriquecimiento
★>45% de genes dependientes de IreA

H Componente celular

Membrana plasmática
Borde lider celular
Zona de contacto célular
Espacio extracelular
Filamento actina
Vesícula fagocítica
Polo celular
Membrana ★

P-value
Enriquecimiento
★ >45% of IreA-dependent genes

76

Por otra parte, se encontró que el conjunto de transcritos cuya abundancia disminuyó en respuesta a la TN, está enriquecido en genes asociados a procesos relacionados con el metabolismo de carbohidratos, con la defensa contra infecciones bacterianas y con el catabolismo de lípidos. Otros genes cuya transcripción disminuye y que no pertenecen a estos grupos, son aquellos que codifican para proteínas secretadas o que residen en membranas.

Al analizar el transcriptoma de la mutante *ireA*⁻ pudimos determinar que esta quinasa se requiere para que se generen cerca del 40% de los cambios transcripcionales que se observan en respuesta a un tratamiento con TN y se encontró que esta quinasa está involucrada en regular la expresión principalmente de genes que están relacionadas con procesos degradativos, y principalmente se relaciona con el proceso de ubiquitinación. Observamos también que, IreA participa en disminuir la carga proteica en el RE, ya que se requiere para que baje la expresión de un porcentaje significativo de genes que codifican proteínas que transitan por el RE.

En condiciones de crecimiento en ausencia de estrés de RE, la contribución de IreA en la regulación de la expresión génica no es significativa, ya que en su ausencia sólo se afectó la expresión de 25 genes.

En conjunto, los datos obtenidos a partir del ensayo de transcirptómica sugieren que en *D. discoideum* el estrés de RE causa una reprogramación transcripcional, la cual permite a la célula aumentar su capacidad de plegamiento de proteínas e incrementar los procesos degradativos. Además, este cambio transcripcional sirve para disminuir la carga de proteínas en el RE. A partir de estos datos, se puede inferir que de forma homóloga a lo que sucede en otros organismos, la ruta mediada por IreA es necesaria para que puedan generarse una porción significativa de los cambios transcripcionales inducidos por el estrés de RE. Nuestras observaciones sugieren que IreA se requiere para que se incremente la abundancia de transcritos involucrados principalmente en procesos de degradación de proteínas y para disminuir la de transcritos que codifican proteínas que transitan por el RE.

4.4- La autofagia en la respuesta a estrés de RE en *Dictyostelium*

4.4.1- El estrés de RE induce autofagia

Se ha descrito ampliamente, en varios organismos, que el estrés de RE induce autofagia, por lo que evaluamos si esta respuesta se encuentra conservada en *D. discoideum.* Para esto, se trataron con 2μg/ml de TN, durante 4, 8 y 16hrs, células WT que expresaban la proteína de fusión GFP-Atg18. Posteriormente, las células tratadas con este antibiótico se analizaron mediante microscopia confocal *in-vivo,* ya que se ha descrito que en *D. discoideum* se pueden observar como puntos discretos fluorescentes los sitios en que se recluta transitoriamente a Atg18-GFP ante un estímulo que induce la autofagia [164], [213].   Con este ensayo, observamos que la TN generó un incremento significativo en el porcentaje de células con puntos de GFP-Atg18 y que la proporción de estas células con puntos fue aumentando proporcionalmente con el tiempo de tratamiento **(Figuras 18A y B)**.

Para realizar una evaluación más completa de la autofagia, es necesario determinar si un aumento en la población de células con estructuras que contienen a Atg18 se encuentra asociado a un incremento en la capacidad de degradación celular mediada por la autofagia, o si es consecuencia de un bloqueo en la tasa de degradación de autofagosomas. Por este motivo analizamos el flujo autofágico de células de *D. discoideum* que fueron tratadas con TN. Para esto se utilizó un ensayo que se desarrolló gracias a la resistencia relativa que presenta la GFP a la degradación lisosomal. Esta característica permite que pueda determinarse la capacidad autofágica de las células si se cuantifica la proporción de GFP libre que se acumula a partir de inducir la proteólisis de una proteína citoplasmática que se encuentre fusionada a la GFP. En el caso de *D. discoideum* se ha desarrollado un protocolo en el cual se evalúa la degradación de la proteína citoplasmática de fusión PgkA-GFP. Sin embargo, para poder detectar la GFP libre se debe disminuir el pH lisosomal, que en estas células suele ser menor a 3.5 [214], adicionando NH_4Cl [164], [183].

Como puede observarse en la **Figura 18C y 18D**, la GFP libre se acumuló en una mayor proporción en las células que fueron tratadas con TN, lo cual indica que se generó un incremento en la capacidad de degradación mediada por autofagia. Encontramos también, que la degradación que se observó de la PgkA-GFP ante un tratamiento con TN se debió a un proceso autofágico, ya que en una mutante *atg1*[-] no se observó acumulación de GFP libre **(Figura 18C)**.

En conjunto, los datos de flujo autofágico, junto con la observación de que la TN incrementa la proporción de autofagosomas, indican que en *D. discoideum* hay una inducción de la autofagia que permite a las células degradar cargos citoplásmicos en respuesta a un estrés de RE.
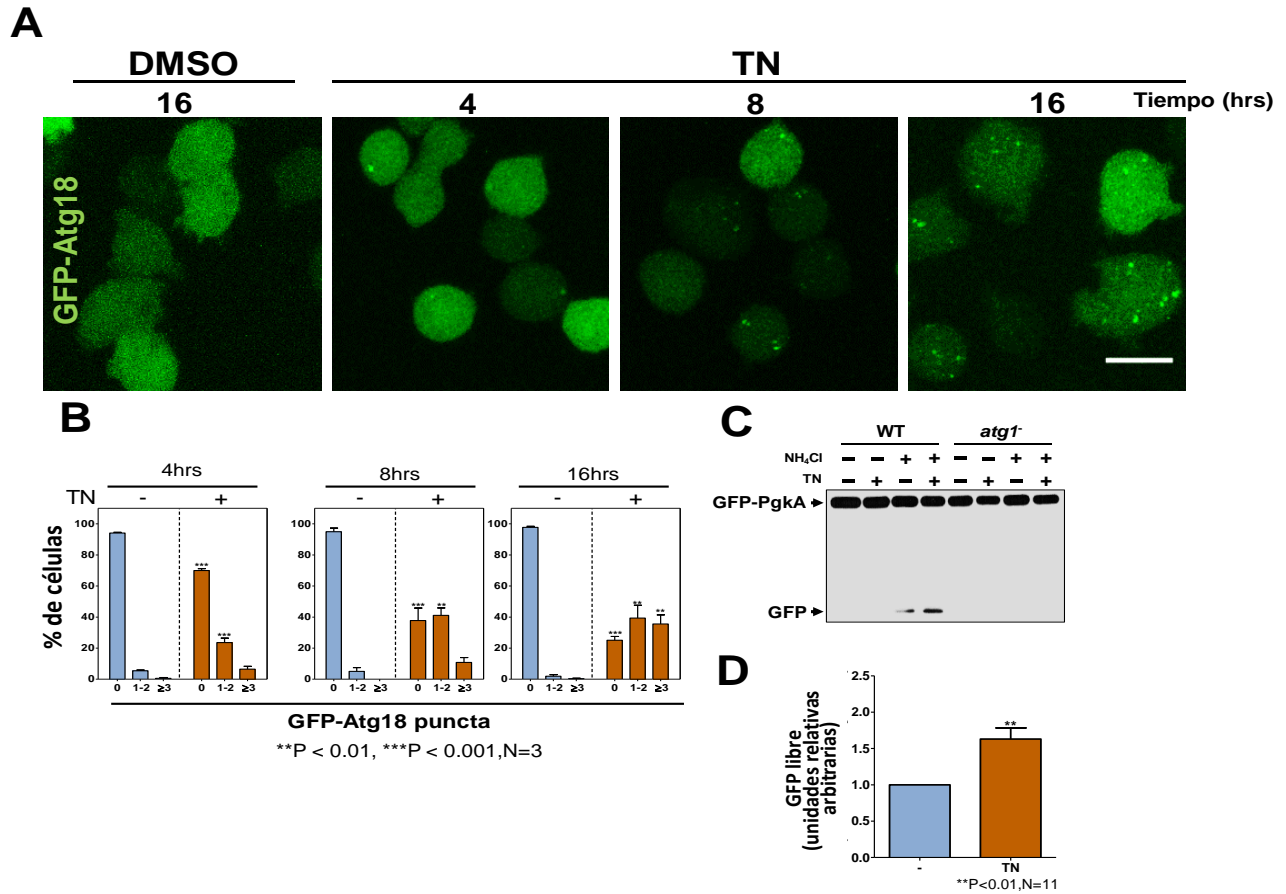
Figura 18. La TN induce una respuesta autofágica en *D. discoideum*. **(A)** La inducción de la autofagia se determinó evaluando células que expresaban la construcción GFP-Atg18. Estas se trataron con TN y se observaron mediante microscopía confocal *in-vivo* a los tiempos indicados. Se muestra la proyección máxima de imágenes representativas de este ensayo. **(B)** Se cuantificó el porcentaje de células tratadas como en (A) que contenían 0, 1 ó 2, y más de 3 puntos de GFP-Atg18 y se muestra el gráfico del promedio y la desviación estándar obtenidos a partir de tres experimentos. **(C)** Ensayo de proteólisis para definir la capacidad degradación autofágica de células WT y *atg1⁻* que fueron tratadas con TN por 8hrs. Se evaluó mediante Western blot la acumulación de GFP libre en extractos de células que expresaban la construcción GFP-PgkA. Estas células se trataron con TN o su vehículo, en presencia o ausencia de NH_4Cl. **(D)** Cuantificación de la banda de la GFP libre de 11 ensayos de proteólisis como en (C). Se muestra el promedio y la desviación estándar. Como control de carga se usó la banda de la GFP-PgkA y el nivel de expresión se muestra de forma relativa a la condición con vehículo.

4.4.2-La autofagia contribuye a la supervivencia ante un tratamiento con TN

Dado que encontramos que el estrés de RE induce una respuesta autofágica en *D. discoideum,* procedimos a determinar si este proceso degradativo es necesario también para que las células puedan contender con este tipo de estrés. Para esto, se probaron cepas mutantes que carecen de la actividad de algunas de las proteínas que pertenecen, respectivamente, al complejo ATG1/ULK1 (*atg1*⁻, *atg13*⁻ y *atg101*⁻) y al sistema de conjugación (*atg7*⁻) **(Figura 19B)**. Estas mutantes se han estudiado previamente y se ha descrito que presentan diferentes defectos en la autofagia [165], [167], [169]. Las cepas *atg1*⁻ y *atg13*⁻ son incapaces de inducir la autofagia **(Figura 19B)**, y por lo tanto presentan un bloqueo total en la formación de autofagosomas, mientras que las cepas *atg101*⁻ y *atg7*⁻ presentan sólo un bloqueo parcial, por lo que pueden inducir autofagia a bajos niveles. Se trataron células de las cepas *atg1*⁻, *atg13*⁻, *atg101*⁻ y *atg7*⁻ con TN durante 16hrs, y posteriormente se evaluó su viabilidad mediante un ensayo de goteo en placas de agar con un césped de bacterias.

Como puede observarse en la **Figura 19A**, las cepas *atg1*⁻, *atg13*⁻ y *atg101*⁻, presentaron una deficiencia en el crecimiento en asociación con bacterias después de haber sido tratadas con TN. La sensibilidad de estas cepas al antibiótico resultó ser proporcional al grado de bloqueo autofágico que presentan, es decir, las cepas *atg1*⁻y *atg13*⁻ son más sensibles que la cepa *atg101*⁻. En cambio, la ausencia de *Atg7* no generó sensibilidad a TN.

De forma paralela, se evaluó el efecto que tiene la inactivación de Vmp1 en el crecimiento durante un tratamiento con TN. Vmp1 es una proteína transmembranal de RE cuya ausencia produce efectos pleiotrópicos en *D. discoideum*. Uno de ellos es un defecto severo de la autofagia [171], [215]. La función de esta proteína se ha asociado con la regulación de los sitios de contacto entre el RE y otros organelos [216] y con la distribución de algunos fosfolípidos [217]. A las células de la mutante *vmp1*⁻ , no se les puede mantener por tiempos prolongados en cultivo líquido, por lo que las pruebas con esta cepa se realizaron solamente por un tiempo máximo de 8hrs. Observamos, que en presencia de 2μg/ml de TN las células *vmp1*⁻ no presentaron un defecto visible en su capacidad de crecimiento en asociación con bacterias **(Figura 19C)**. Todos estos datos sugieren que, para sobrevivir a un tratamiento con TN, en *D. discoideum* se requiere de procesos autofágicos asociados principalmente a la función del complejo ATG1, y que posiblemente estos son independientes del sistema de conjugación y de la función de Vmp1.
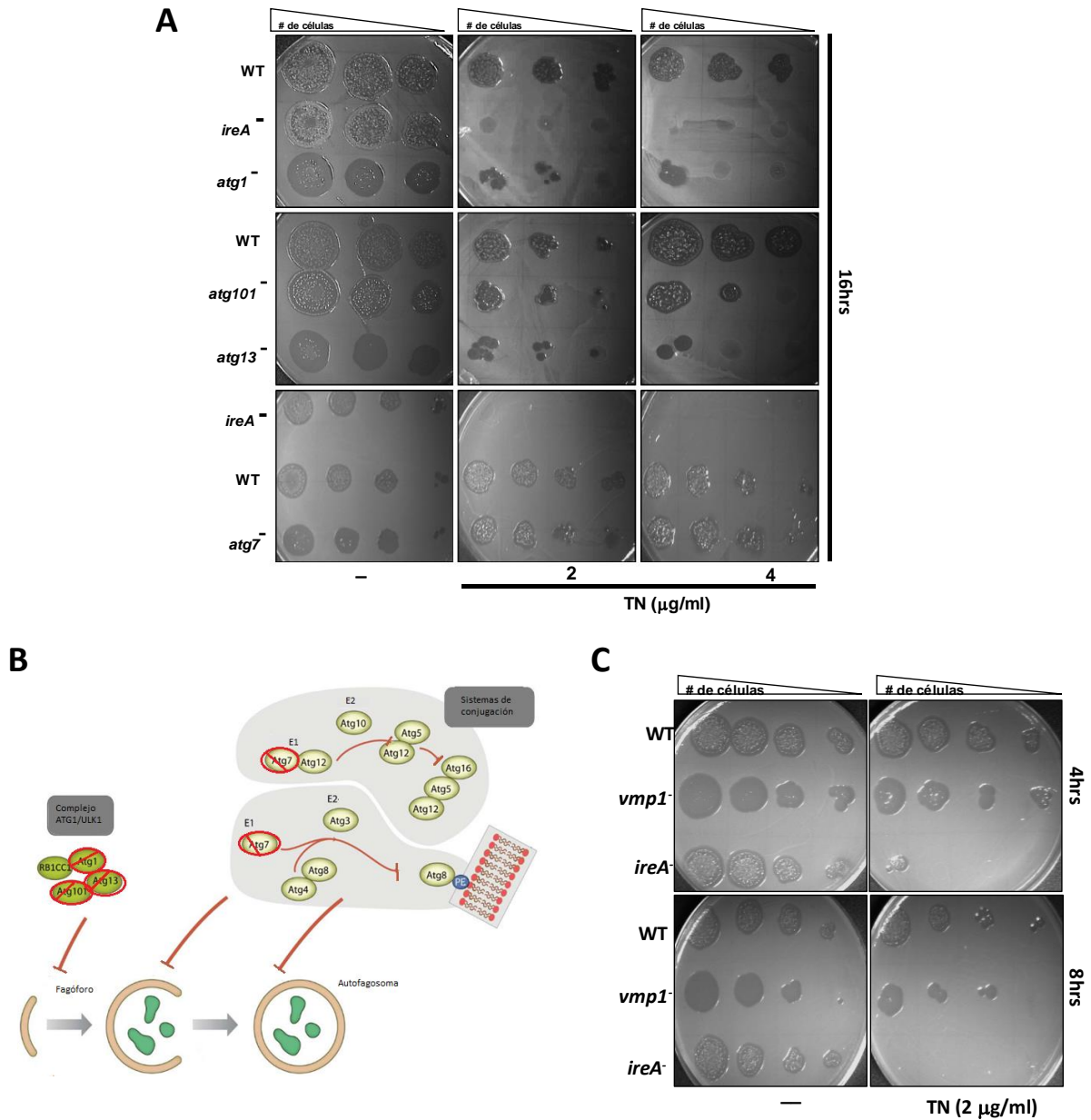
Figura 19. (A) Ensayos de goteo para evaluar la viabilidad de las cepas *atg1⁻, atg13⁻, atg101⁻ y atg7⁻* ante un tratamiento con TN. **(B)** Diagrama de las proteínas que forman el complejo ATG1 y el sistema de conjugación en *D. discoideum*. Se muestran resaltados con un círculo rojo los componentes que carecen las células de las cepas que se probaron en (A).
(C) Ensayo de viabilidad de la cepa *vmp1⁻* tras un tratamiento con TN. **(A y B)** Las cepas indicadas fueron tratadas durante el tiempo y la concentración especificada de TN, o con su vehículo (DMSO). Se realizaron diluciones seriales de los cultivos tratados y se depositaron gotas de estos sobre placas de agar en las cuales se había esparcido previamente *K. aerogenes*. Se muestran fotografías representativas de tres experimentos, que se tomaron tras incubar las placas a 22°C por 5-7 días.

4.4.3- IreA es dispensable para inducir la autofagia en respuesta al estrés de RE

Se ha reportado que tanto en plantas como en mamíferos se requiere de IRE1 para la inducción de la autofagia en respuesta al estrés de RE [147], [148], por lo que en este trabajo evaluamos si esto mismo ocurre en *D. discoideum*. Para esto, seguimos mediante microscopía confocal *in-vivo* los efectos de un tratamiento con TN sobre el proceso de formación de autofagosomas en células de la mutante *ireA*⁻, las cuales expresaban al gen híbrido GFP-Atg18 **(Figura 20A).** Se observó que, en respuesta al tratamiento con TN, las células de la mutante *ireA*⁻ fueron capaces de inducir la autofagia **(Figura 20A).** Además, encontramos que la proporción de células de la cepa mutante que presentaron puntos de GFP-Atg18 fue significativamente mayor a la que se observó en las células WT **(Figura 20B).** Observamos también, que la proporción de células de la cepa *ireA*⁻ con puntos de GFP-Atg18 aumentó de forma directamente proporcional al tiempo de tratamiento con TN. Por otra parte, una observación importante que resultó de estos ensayos fue que los autofagosomas de la mutante *ireA*⁻ son más conspicuos y alargados en comparación con los que se observan en la cepa WT **(Figura 20A)**.
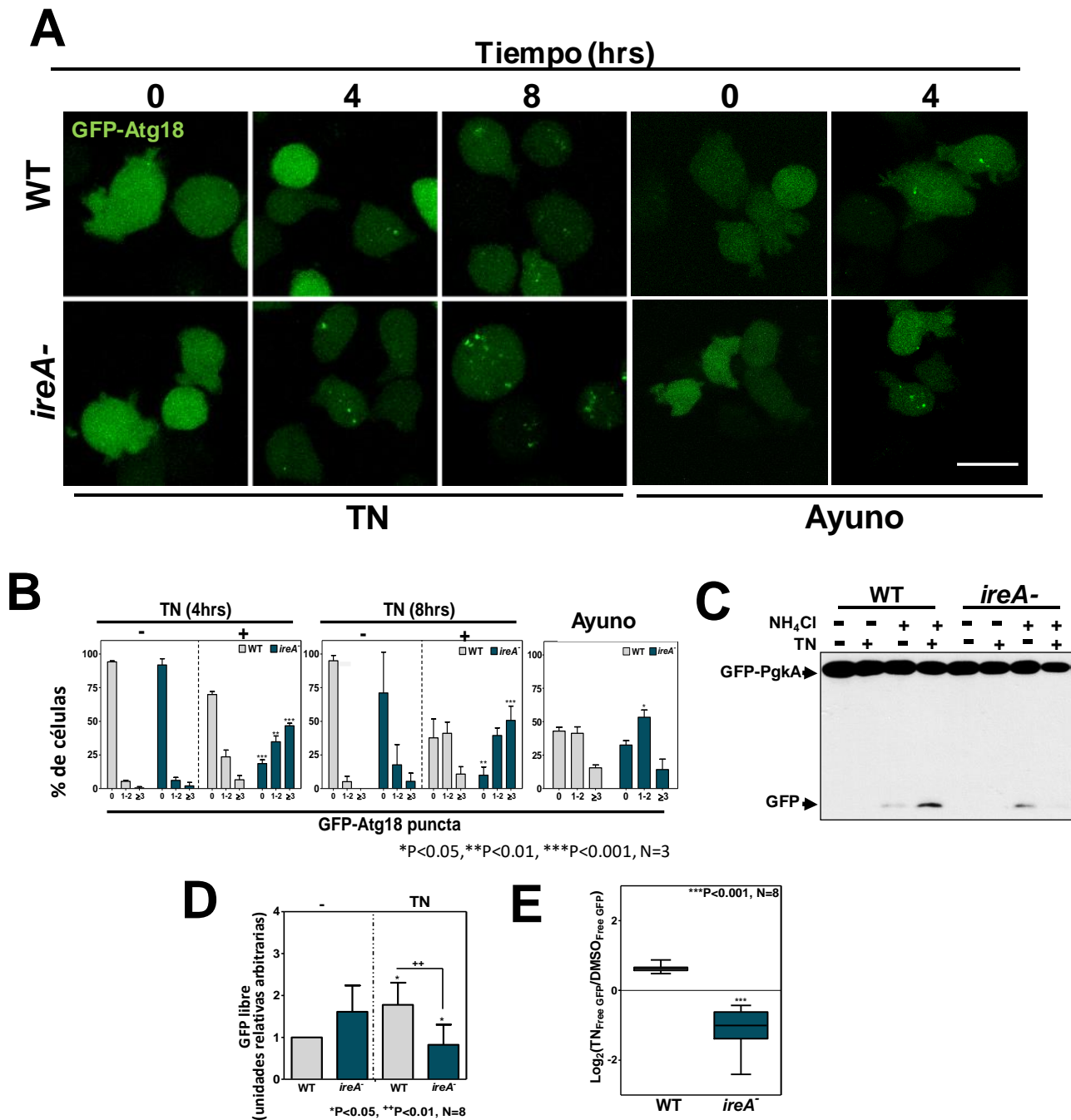
Figura 20. (A) Fotografías de microscopía confocal de células WT e i*reA*- expresando la construcción GFP-Atg18, durante un tratamiento con TN por los tiempos especificados (escala 10μM). **(B)** Se cuantificó el porcentaje de células en las que GFP-Atg18 se acumuló y se clasificaron dependiendo de si presentaban 0, 1 ó 2, y ≥3 puntos por célula y se graficó el promedio y la desviación estándar. **(C)** Ensayo de proteólisis de la GFP-PgkA en células WT e *ireA*- que fueron tratadas por 8hrs con TN en presencia y ausencia de NH$_4$Cl. **(D)** Se cuantificó el nivel de GFP libre acumulada mediante densitometría y se graficó el promedio y la desviación estándar de 8 experimentos. Se normalizó contra el nivel de GFP-PgkA y todos los datos se refirieron al nivel de expresión en la cepa WT sin tratamiento. **(E)** Media y desviación estándar del Log$_2$ de los datos en (D). En todos los gráficos, los asteriscos denotan diferencias estadísticamente significativas.

Con el objetivo de determinar si en la mutante *ireA⁻* el reclutamiento de GFP-Atg18 que se observa en respuesta a un tratamiento con TN participa en la formación de autofagosomas funcionales, se evaluó la capacidad de degradación autofágica de esta cepa. Para esto, se utilizó el ensayo de proteólisis de la PgkA-GFP. Mediante este experimento, encontramos que la cepa *ireA⁻* no es capaz de aumentar su capacidad de degradación autofágica ante un tratamiento con TN, ya que presenta una menor acumulación de GFP libre en esta condición, en comparación con la que se observa en ausencia de estrés **(Figuras 20 C, D y E)**. Estos datos indican que las células de la mutante *ireA⁻* aún son capaces de inducir la formación de autofagosomas en presencia de TN pero, a diferencia de las células silvestres, presentan un bloqueo que evita que se puedan degradar cargos citoplasmáticos.

Para profundizar en éste fenómeno, evaluamos el flujo autofágico en una cepa mutante *ireA⁻* que expresaba las mutantes puntuales de IreA que carecen respectivamente, de la actividad de quinasa (IreA^{K603N}), o de la de ribonucleasa (ireA^{N927A}). La TN indujo una acumulación de GFP libre en la cepa que expresa la forma silvestre de IreA; pero encontramos que, esto no ocurrió en las cepas que expresaban las mutantes puntuales **(Figuras 21A y B)**. Estos datos sugieren que las células requieren de ambas funciones de IreA para incrementar su capacidad de degradación autofágica ante un tratamiento con TN.
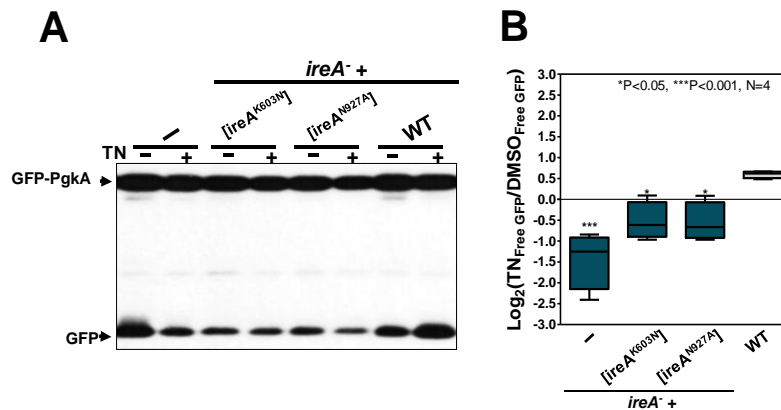
Figura 21. El defecto autofágico de la cepa *ireA⁻* no se recupera al expresar las mutantes puntuales de IreA. **(A)** Western blot en el que se aprecia la acumulación de GFP libre en células *ireA⁻* que expresaban la forma sin actividad de quinasa (ireA^{K603N}), la forma de ribonucleasa inactiva (ireA^{N927A}) o la forma silvestre (WT) de IreA. Las células se trataron con TN durante 8hrs y se agregó NH$_4$Cl durante las últimas dos horas de tratamiento. **(B)** Gráfico que muestra el incremento en la acumulación de GFP libre que se genera tras un tratamiento con TN. Se analizó mediante densitometría el nivel de GFP libre y se graficó el promedio y la desviación estándar del Log$_2$ de la tasa entre el nivel con TN y el nivel en el control (DMSO). Los asteriscos señalan las diferencias estadísticamente significativas.

Estudios previos han mostrado que, cuando la degradación autofágica es deficiente, se acumulan de forma anómala agregados proteicos citoplasmáticos que se encuentran ubiquitinados . Esto, puede deberse a que la autofagia participa directamente en la degradación de agregados proteicos ubiquitinados o a que, cuando la autofagia es defectuosa, los agregados destinados a ser degradados por esta ruta, permanecen expuestos por tiempos muy prolongados [218]. En *D. discoideum* se ha observado

que la acumulación de proteínas agregadas ubiquitinadas se puede correlacionar con deficiencias autofágicas y su detección se ha utilizado como un ensayo complementario para evaluar la capacidad de degradación autofágica [93], [164]. Por este motivo, analizamos la presencia de agregados ubiquitinados en células tanto de la cepa WT, como de la *ireA⁻*, con el objetivo de corroborar los efectos causados por un tratamiento con TN en la capacidad de degradación autofágica. En ambos casos se utilizaron células que expresaban la construcción GFP-Atg18. Para esto, se trataron las células WT e *ireA⁻* con TN (2μg/ml) durante 8hrs, se prepararon para inmunofluorescencia y se visualizaron mediante microscopía confocal. Como puede observarse en las fotografías de la **Figura 22**, sólo las células *ireA⁻* presentaron agregados visibles de proteínas ubiquitinadas y este efecto, se observó sólo en presencia de TN. Estos resultados, sugieren que la mutante *ireA⁻* presenta una fuerte deficiencia en los procesos de degradación de proteínas con esta marca. También se puede observar en esta preparación, que algunos agregados ubiquitinados colocalizaron con estructuras elongadas marcadas con GFP-Atg18 **(Figura 22)**, lo cual sugiere que en presencia de TN, en la mutante *ireA⁻* se puede comenzar el proceso de formación de los autofagosomas, pero estos son incapaces de completar los procesos de degradación característicos de la autofagia.

En mamíferos y en *D. discoideum* se ha observado que Atg18/WIPI-1 se recluta de forma transitoria a los sitios de nucleación de los autofagosomas [87], [219]. Sin embargo, se ha observado que en las mutantes autofágicas que presentan un bloqueo posterior a esta fase, Atg18/WIPI-1 se mantiene acumulado en estructuras alargadas que persisten en el tiempo. Por lo tanto, el estudio de la dinámica de este marcador permite detectar un posible bloqueo en fases tardías de la formación de los autofagosomas [171], [220]. Con el objetivo de determinar si en la mutante *ireA⁻* existe un bloqueo en fases tardías de la autofagia, se analizó la dinámica que presenta Atg18 en estas células, tras un tratamiento con TN. Para esto se siguió durante 900s, por microscopía confocal *in-vivo*, la señal de GFP-Atg18 en células WT e *ireA⁻* que fueron tratadas con TN durante 7hrs. En las células WT la señal de GFP-Atg18 estuvo presente sólo durante algunos segundos (30-80s) **(Figura 23)**, mientras que en las células de la mutante *ireA⁻*, GFP-Atg18 se acumuló en estructuras elongadas que fueron visibles incluso hasta los 900s **(Figura 23)**. Estas observaciones sugieren que, durante un estrés de RE, las células *ireA⁻* presentan defectos en etapas tardías en la formación de los autofagosomas. Lo cual, coincide con la capacidad degradativa deficiente que presenta la cepa *ireA⁻* durante un tratamiento que genera estrés de RE.
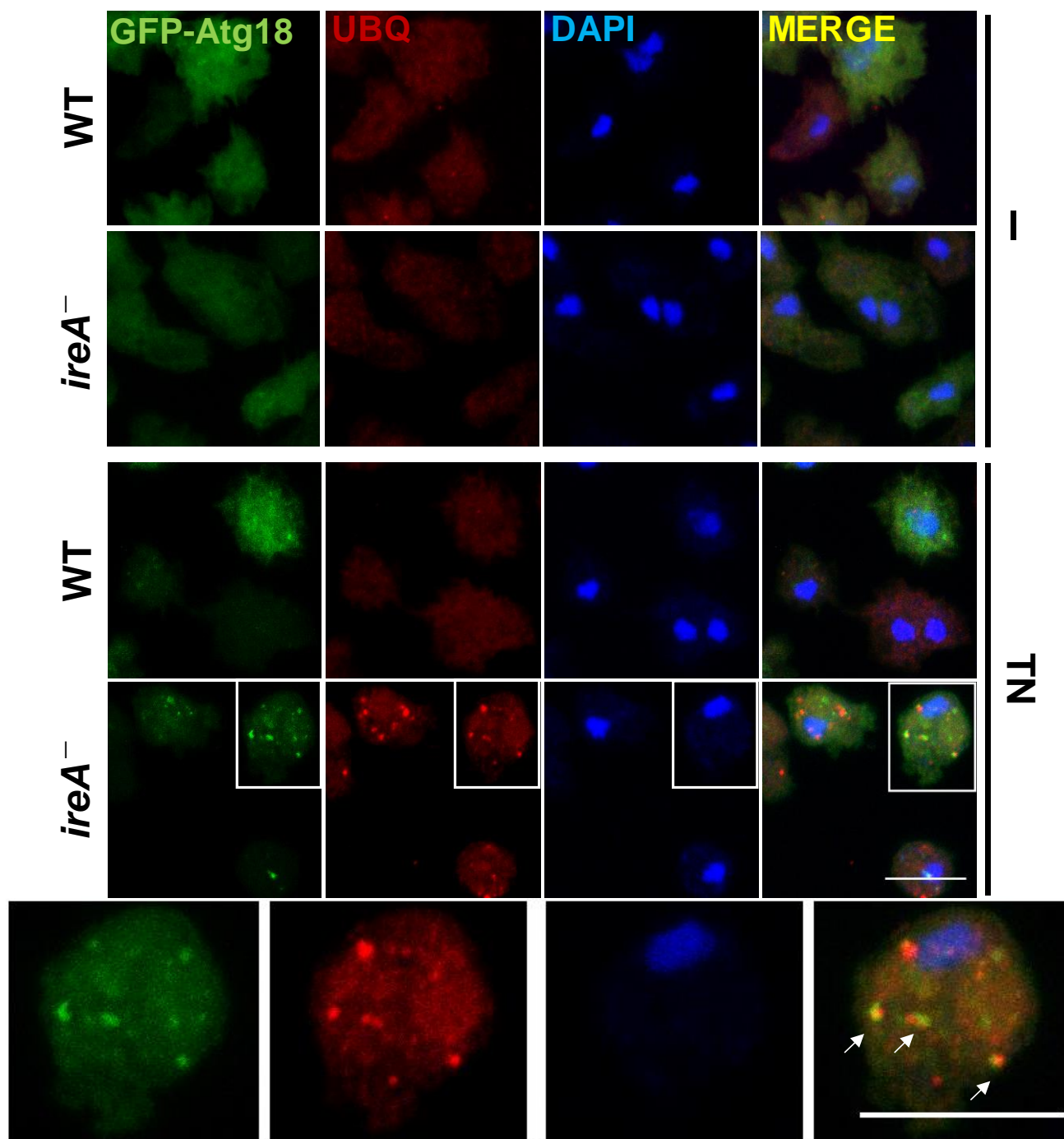
Figura 22. Las células *ireA*⁻ acumulan agregados proteicos ubiquitinados al ser tratadas con TN. Fotografías de células WT o *ireA*⁻ que expresaban a la GFP-Atg18 y que fueron tratadas con TN por 8hrs o con su vehículo y que se prepararon para detectar mediante inmunofluorescencia a la ubiquitina (rojo). Las imágenes se adquirieron por microscopía confocal. Los núcleos se tiñeron con DAPI. Se muestra un acercamiento de la célula de la cepa *ireA*⁻ marcada por un recuadro. Las flechas indican puntos en los que la señal de la ubiquitina y la de GFP-Atg18 colocalizan (Escala 10μM).
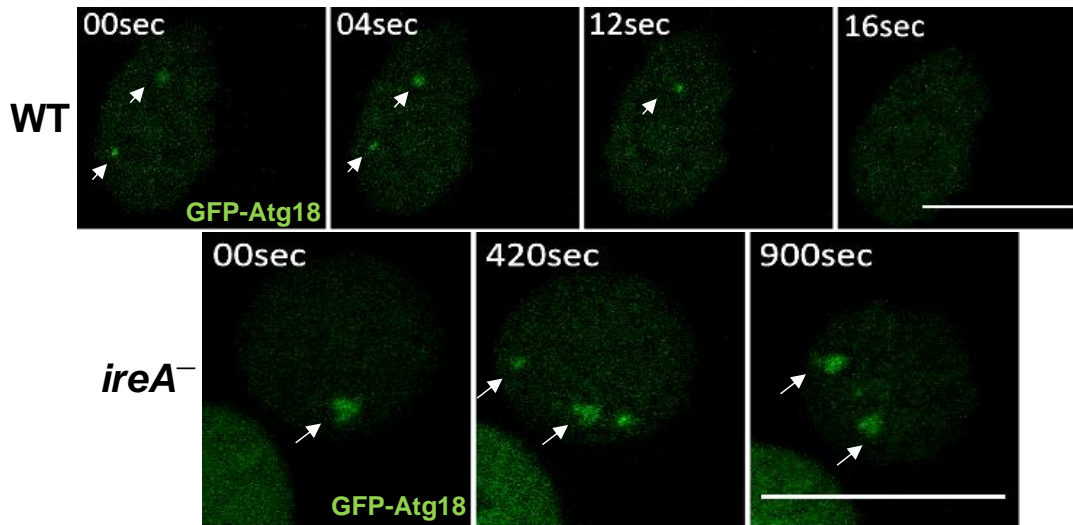
Figura 23. Las estructuras de GFP-Atg18 observadas en las células *ireA*⁻ tras un tratamiento con TN resultan aberrantes y persistentes. Fotografías obtenidas de células de las cepas WT o *ireA*⁻, que expresaban la construcción GFP-Atg18, tras haber sido tratadas con TN durante 7hrs. La señal de este marcador se siguió *in-vivo* y se videograbó durante 900s.

En levadura se ha observado que la membrana del RE se remodela ante un estrés de RE [143], [221]. Cuando analizamos los efectos transcripcionales causados por la TN en *D. discoideum*, encontramos que este tratamiento causó un cambio importante en la expresión de genes involucrados con el metabolismo de lípidos, lo cual sugiere que parte de la respuesta al estrés de RE en este organismo involucra cambios en la composición de la membrana del RE. Por otra parte, es importante mencionar que en *D. discoideum* y en mamíferos este organelo funciona como una plataforma para el ensamblaje de los autofagosomas [87], [107], [222].

Estas observaciones nos llevaron a plantear que las perturbaciones que presenta la mutante de *ireA*⁻ en la estructura del RE podrían interferir con el proceso de formación de los autofagosomas. Para probar esta hipótesis, se evaluó de forma simultánea la localización de Atg18 y la morfología del RE en células que fueron tratadas con TN. Para esto, se prepararon, para detectar a la PDI mediante inmunofluorescencia, células que expresaban la construcción GFP-Atg18. Como puede observarse en la **Figuras 24A y B** el RE de las células *ireA*⁻ tratadas con TN presentó alteraciones severas; la presencia de túbulos es escasa y se aprecian colapsados en una sola estructura, la cual se acumula principalmente en la zona perinuclear. Se observó también que la mayoría de las estructuras aberrantes de GFP-Atg18 que se acumulan en las células *ireA*⁻ (puntos conspicuos en la imagen), se localizan en zonas de RE que se encuentra colapsado. Estas observaciones sugieren que la mutante *ireA*⁻ presenta una incapacidad para reestructurar el RE, lo cual ocasiona un defecto severo en el ensamblaje de los autofagosomas **(Figuras 24A y B)**. Esto a su vez, explicaría la deficiencia que presenta esta cepa para degradar cargos autofágicos durante el estrés de RE.

A

GFP-Atg18   DAPI   PDI   MERGE

WT

ireA⁻

I

WT

ireA⁻

TN

B

GFP-Atg18+ PDI

ireA⁻

TN
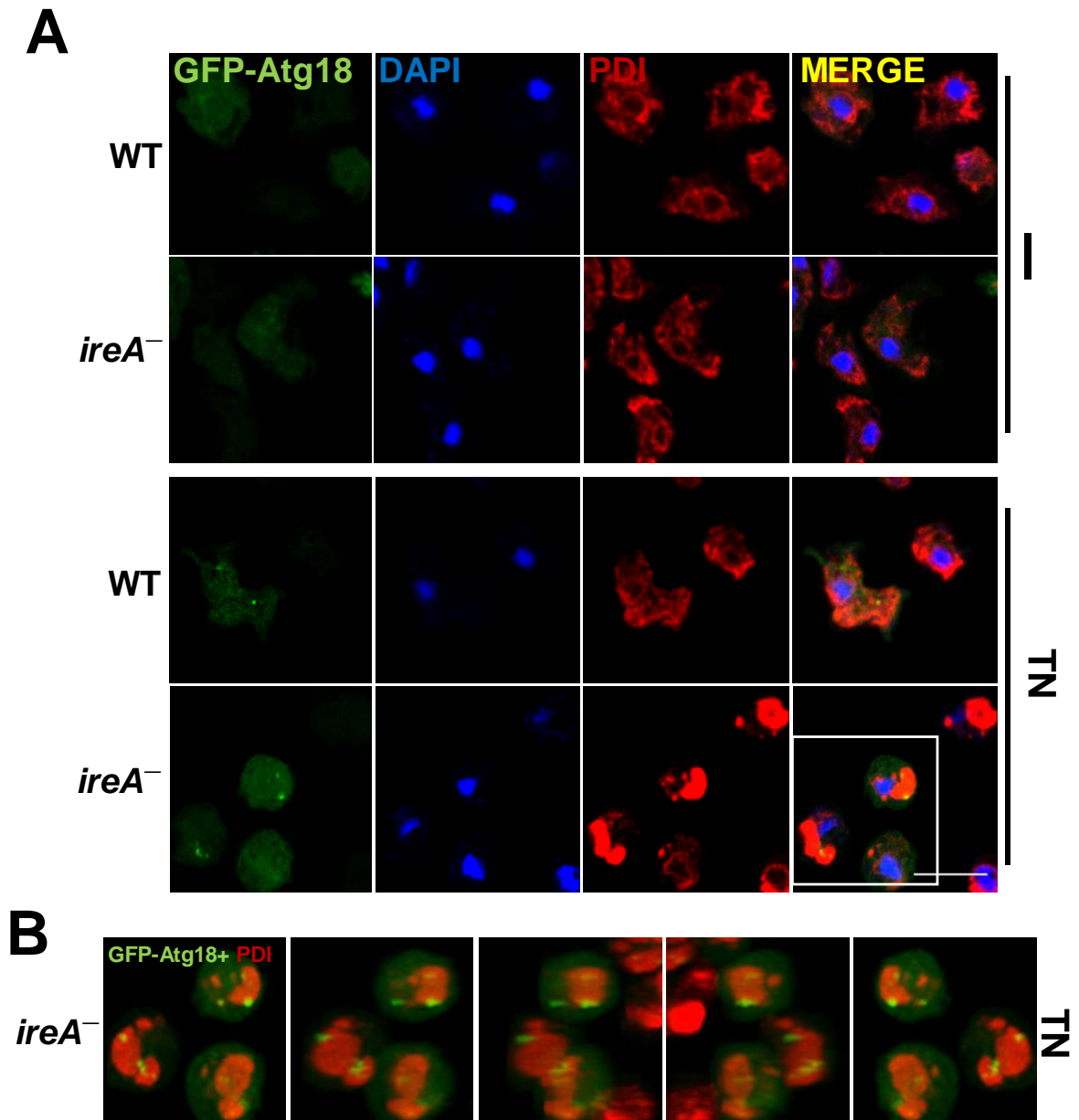
Figura 24. (A) Fotografías de células WT e *ireA*⁻, que fueron tratadas con TN o DMSO durante 8hrs y posteriormente se prepararon para detectar mediante inmunofluorescencia a la PDI (rojo). Se muestran fotografías representativas obtenidas por microscopía confocal. **(B)** Se generó una proyección en 3D de las fotografías en (A) y se muestran algunas vistas que se obtuvieron al girar esta proyección.

4.5- BzpD participa en la respuesta al estrés de RE

4.5.1- Análisis informático de las secuencias proteicas de BzpC, BzpD y BzpJ

En mamíferos y en plantas la UPR está compuesta por rutas adicionales a la de IRE1 que se requieren para generar la respuesta transcripcional inducida por el estrés de RE. En *D. discoideum*, los resultados obtenidos del análisis de expresión génica sugieren que, durante la reprogramación de la expresión génica generada en respuesta a un tratamiento con TN, participan vías alternas a la de IreA. Por este motivo, se evaluó mediante BLAST si en el genoma de esta ameba se encontraban codificados posibles ortólogos de ATF6. Como se describió en la **sección 3.2** y en la **Tabla 5**, se encontró que BzpC, BzpD y BzpJ contienen un dominio transmembranal que es característico de los activadores transcripcionales tipo ATF6. También se encontró que en el genoma de *D. discoideum* se encuentran codificados ortólogos de MBPTS1 (*mbpts1/DDB_G0282397*) y de MBPTS2 (*mbpts2/DDB_G0275939*), las dos proteasas de Golgi que en otros organismos participan en el procesamiento de ATF6 [223].

Al analizar la secuencia de aminoácidos de estas tres proteínas transmembranales, buscando motivos que suelen estar conservados en los homólogos de ATF6, tales como los sitios de reconocimiento de las proteasas MBPTS1 y MBPTS2 y las secuencias de localización nuclear (NLS) **(Figura 25A)**, encontramos que las tres proteínas (BzpC, BzpD y BzpJ) contienen secuencias de localización nuclear y también que las tres presentan posibles sitios de reconocimiento de MBPTS1 (S1P); sin embargo, sólo BzpD contiene el motivo de reconocimiento de MBPTS2 (S2P). Esta última, es la proteasa que cataliza el corte del segmento transmembranal de ATF6, lo cual permite su liberación de la membrana del retículo [223]. Se encontró también que BzpJ contiene una posible secuencia de exportación dependiente de COP-II en su región citoplasmática.

Mediante un alineamiento global utilizando la herramienta informática CLUSTAL omega se encontró que la proteína que presenta mayor homología con ATF6 de humanos es BzpD **(Figura 25B)**. Por su parte, BzpJ es la que resultó presentar un mayor porcentaje de identidad con ATF6 de Drosophila y con bZIP28 de *A. thaliana*.

A
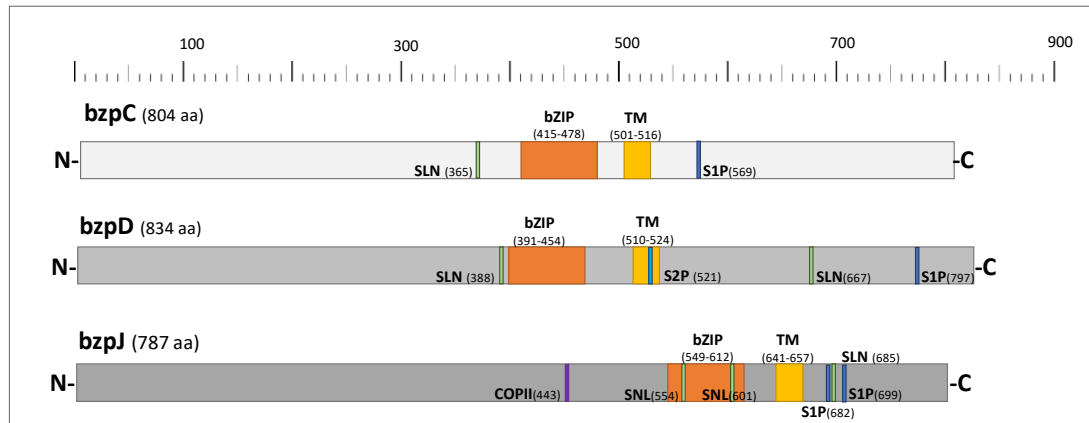
B

	Hs_ATF6α	Dm_ATF6c	bZIP28	BzpC	BzpD	BzpJ
Hs_ATF6α	100%	26.53%	16.63%	14.57%	19.05%	15.90%
Dm_ATF6c	26.53%	100%	17.66%	20.24%	17.29%	20.53%
bZIP28	16.63%	17.66%	100%	18.99%	18.22%	22.76%
BzpC	14.57%	20.24%	18.99%	100%	26.70%	29.01%
BzpD	19.05%	17.29%	18.22%	26.70%	100%	24.95%
BzpJ	15.90%	20.53%	22.76%	29.01%	24.95%	100%

Figura 25. (A) Diagrama que muestra los dominios identificados en las secuencias de BzpC, BzpD y BzpJ. Las proteínas se dibujaron a escala. Se indican los residuos en los cuales se encuentran los dominios especificados. SLN (secuencia de localización nuclear), bZIP (dominio básico seguido de una cremallera de leucinas), TM (transmembranal), S1P (sitio reconocido por MBPTS1), S2P (sitio reconocido por MBPTS2), COPII (secuencia de exportación COP-II). **(B)** Tabla que muestra el porcentaje de identidad entre las proteínas señaladas. Resultados obtenidos a partir de un alineamiento global realizado con el programa CLUSTAL omega.

4.5.2- BzpD y BzpJ se localizan en el RE

Para definir la localización subcelular de BzpC, BzpD y BzpJ se generaron construcciones en las que se fusionó la GFP al extremo N-terminal de cada una de estas proteínas. Al analizar su localización mediante microscopia confocal, se encontró que tanto GFP-BzpD como GFP-BzpJ se encuentran en el RE. En estas preparaciones se detectó mediante inmunofluorescencia a la PDI, la cual, como se mencionó anteriormente, se utiliza como marcador de RE en *D. discoideum* **(Figura 26)**. Observamos que aunque GFP-BzpD y GFP-BzpJ se localizaron en el RE, su distribución resultó ser diferente . BzpD se localizó por toda la red del RE y colocalizó casi totalmente con la PDI, mientras que BzpJ se distribuyó en un patrón punteado y sólo sobre ciertas zonas del RE **(Figura 26)**. Esto sugiere que, aunque la secuencia estas dos proteínas comparte algunas características, podrían estar cumpliendo diferentes funciones en el RE, ya que presentan diferencias claras en su patrón de localización.

En cambio, no fue posible detectar a la GFP-BzpC. Esto puede deberse posiblemente a que la expresión de esta proteína puede estar siendo regulada a nivel postraduccional, también es posible que la etiqueta utilizada interfiera con su expresión o que esta no se sintetice en las condiciones de crecimiento que se utilizaron. Por este motivo, y también debido a la baja identidad que BzpC presenta con los homólogos de ATF6 no se continuo con su análisis.
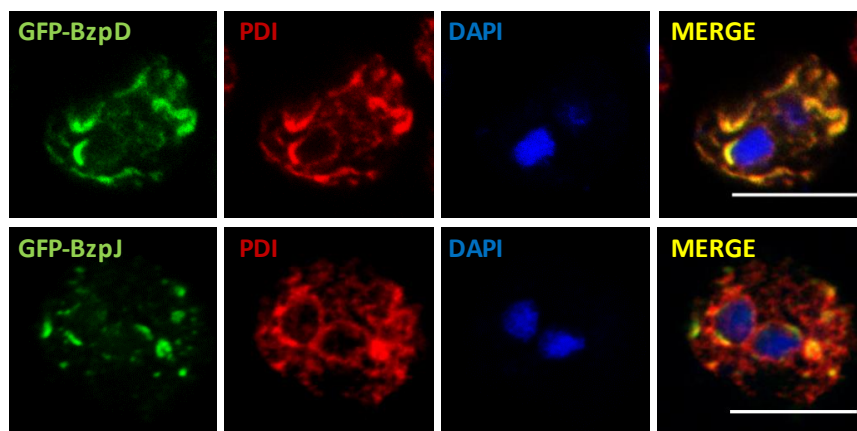
Figura 26. Localización subcelular de BzpD y BzpJ. Fotografías de células WT expresando respectivamente las construcciones GFP-BzpD o GFP-BzpJ que fueron prepadas para detectar a la PDI (rojo) mediante inmunofluorescencia. Para la detección de núcleos, las células se tiñeron con DAPI y se visualizaron mediante microscopía confocal (escala 10µM).

4.5.3- BzpD se requiere para contender con el estrés de RE

Para evaluar si BzpD y BzpJ se requieren durante la respuesta al estrés de RE, se construyeron cepas mutantes de estas proteínas **(Figura 27)**. Para esto se integró mediante recombinación homologa el casete de resistencia a la BST en los locus respectivos **(Figura 27)**. En el caso de *bzpD,* esto generó una deleción de 400 pares de bases **(Figura 27A),** y en el locus *bzpJ* una de 717 pares de bases **(Figura 27B)**. La integración de BST en ambos casos se comprobó mediante PCR **(Figuras 27C y D)**.
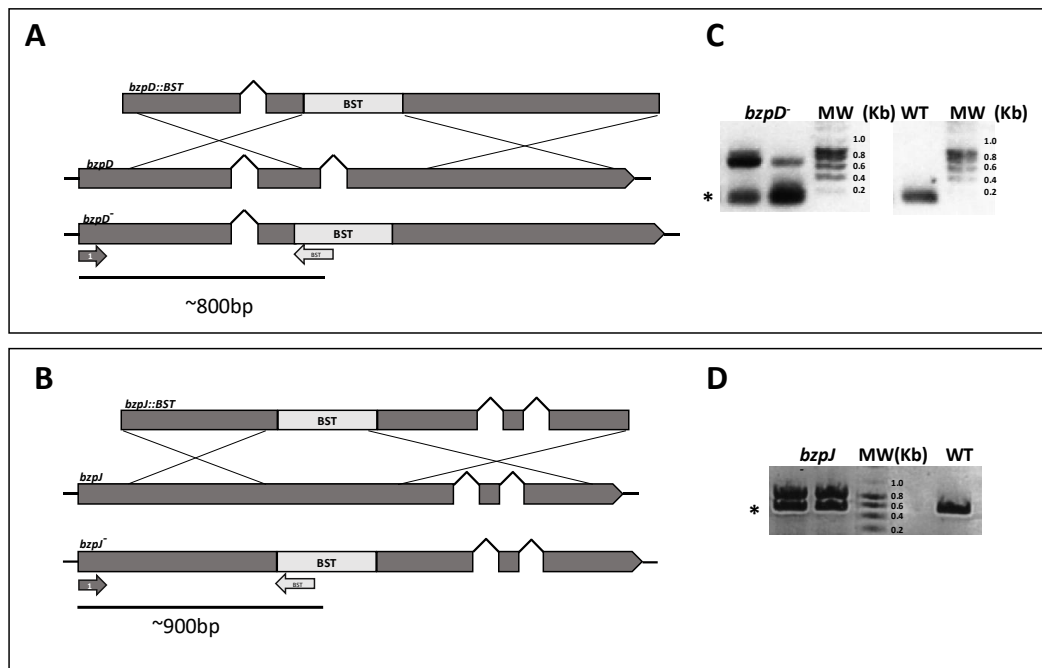
Figura 27. Metodología para interrumpir el locus de *bzpD* y el de *bzpJ*. Los diagramas en **(A)** y en **(B)** muestran las construcciones utilizadas para generar las interrupciones. Estas se generaron mediante la inserción por recombinación homóloga del gen de resistencia a la blasticidina (BST) en el locus indicado. En **(A)** se muestra la construcción para *bzpD*⁻ y **(B)** para *bzpJ*⁻. Se ilustran los oligonucleótidos que se utilizaron para comprobar mediante PCR la integración de BST en el locus, y el tamaño esperado del amplificado que se obtendría con ellos. En **(C)** y **(D)** se muestra el producto obtenido de amplificar con los oligonucléotidos indicados en A y B, mediante PCR, el DNA genómico de dos clonas mutantes respectivamente de **(C)** *bzpD*⁻ y **(D)** *bzpJ*⁻ y de células WT. *Amplificado de un gen no relacionado que se incluyó como control.

Como puede observarse en la **Figura 28A** y **B**, un tratamiento con TN por 16hrs afectó visiblemente la morfología de las células de ambas mutantes. Este tratamiento produjo que las células se tornaran redondeadas y refringentes, y se observó la aparición de detritus. Lo cual es indicativo de lisis celular. Sin embargo, el efecto de la TN sobre la morfología celular en estas mutantes no resultó ser tan severo como el que presentó la cepa *ireA*⁻.

Por otra parte, un tratamiento de 16hrs con TN afectó la capacidad de retomar el crecimiento en asociación con bacterias de la mutante *bzpD*⁻, pero no de la mutante *bzpJ*⁻ **(Figura 28C)**. Aunque las células de la mutante *bzpD*⁻ resultaron ser sensibles al estrés de RE, su sensibilidad a la droga no fue tan severa como la que presentó la mutante *ireA*⁻.

Cuando *D. discoideum* se desarrolla en presencia de bacterias, se pueden observar al mismo tiempo las diferentes fases de desarrollo. En la parte central de la colonia, en la cual las amebas han consumido las bacterias por completo, se encuentran los cuerpos fructíferos; mientras que, en la zona periférica de la colonia, se encuentran las amebas que están consumiendo bacterias; las fases intermedias de desarrollo pueden observarse entre estas dos zonas. Una de estas fases es la de gusano, que en la cepa silvestre tiene una movilidad reducida y no abandona la zona de crecimiento colonial **(Figura 28E)**, en cambio en la mutante *bzpD*⁻, el gusano presentó una migración anómala, ya que tendió a recorrer mayores distancias y frecuentemente abandonó la zona de crecimiento.
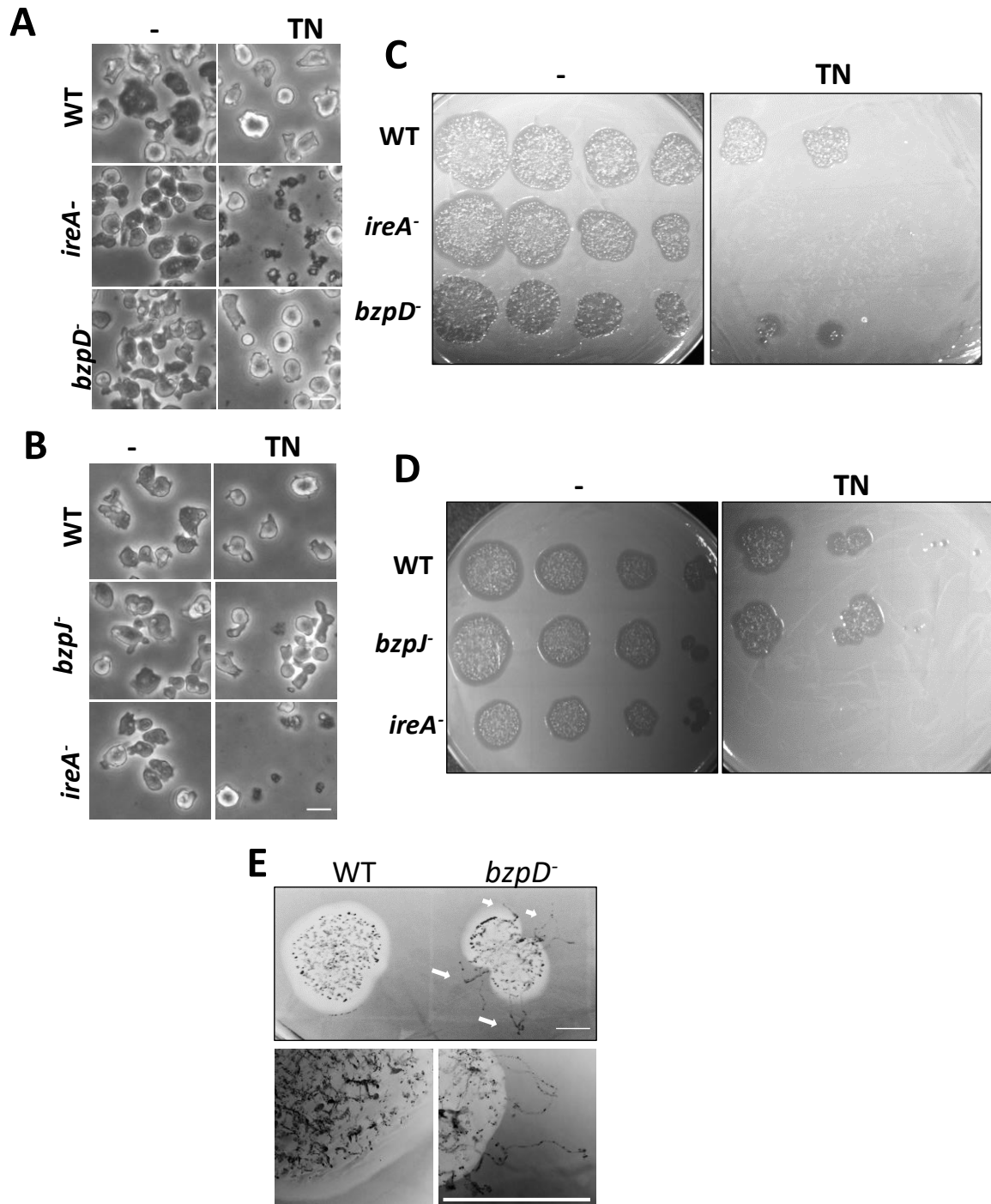
Figura 28. Análisis para determinar la sensibilidad a la TN de las cepas *bzpD*⁻ y *bzpJ*⁻. Se muestran en **(A)** y en **(B)** fotografías de células de las cepas indicadas (microscopía óptica), que fueron tratadas con TN o con su vehículo (DMSO) durante 16hrs. **(C** y **D)** Se analizó la viabilidad de estas células eran capaces de restablecer el crecimiento en asociación con bacterias después de ser tratadas con TN y se muestran los resultados obtenidos en **(C)** para *bzpD*⁻y en **(D)** para *bzpJ*⁻. **(E)** Fotografías de las colonias formadas por células de las cepas WT y *bzpD*⁻ creciendo sobre una placa de medio sólido en la que se esparció previamente *K. aerogenes*. Las flechas señalan los rastros de migración de los gusanos. Se muestra en la parte inferior un acercamiento de la zona de crecimiento de amebas de las cepas WT y *bzpD*⁻ (Escala 1cm). En todos los casos, se muestran fotografías representativas de tres experimentos independientes.

La expresión del gen silvestre BzpD en la mutante *bzpD*⁻ logró revertir tanto la sensibilidad a la TN, como la migración anómala durante la fase de gusano **(Figura 29)**, lo cual indica que este factor transcripcional se requiere para generar una respuesta adecuada al estrés de RE y para regular la transición durante la fase de gusano en el proceso de desarrollo.

A

B
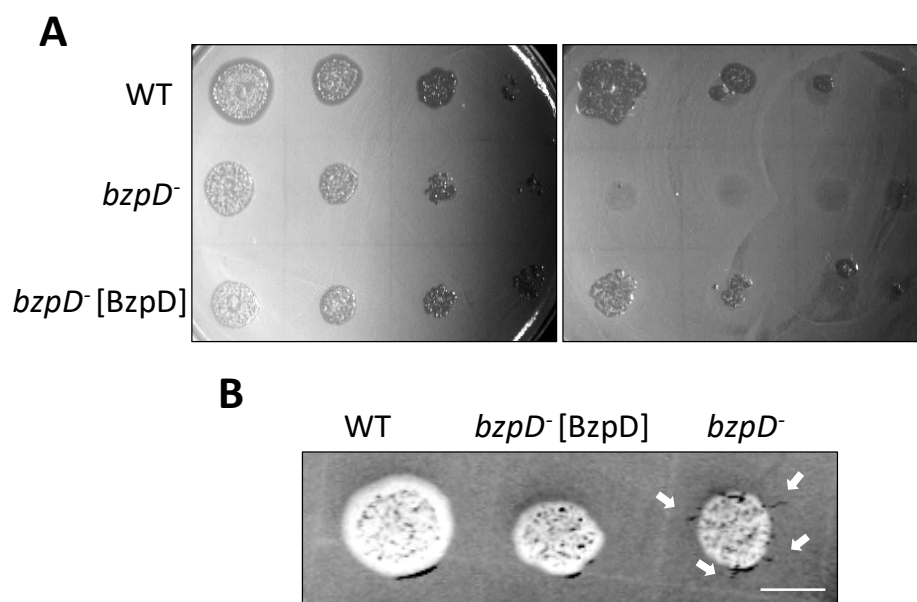
Figura 29. Efectos fenotípicos de la sobreexpresión de GFP-BzpD en la mutante *bzpD*⁻. (A) Ensayo de goteo para analizar el efecto sobre la viabilidad de células de las cepas indicadas tras un tratamiento con TN durante 16hrs. (B) Fotografías de las colonias formadas por células de las cepas señaladas creciendo sobre una placa de medio sólido en presencia de *K. aerogenes*. Las flechas señalan los rastros de migración de gusanos. En todos los casos, se muestran fotografías representativas de tres experimentos independientes.

4.5.4- BzpD se procesa en Golgi y se transporta al núcleo ante un tratamiento con TN

Cuando se somete a células de mamífero a un estrés de RE, ATF6 se transporta al Golgi en donde es procesada secuencialmente por las proteasas MBTPS1 y MBTPS2. De esta forma se libera su segmento N-terminal, el cual contiene el dominio bZIP y la secuencia de localización nuclear [77]. Por este motivo, analizamos si BzpD transita por el Golgi ante un estrés de RE. Para esto, se siguió su localización tras un tratamiento con TN en células en las que se marcó el Golgi mediante la expresión de la proteína Golvesina fusionada a la proteína roja fluorescente (Gol-RFP) [224]. Se trataron con TN células que expresaban tanto a la Gol-RFP, como a GFP-BzpD y se observaron mediante microscopía confocal *in-vivo* durante 150 minutos **(Figura 30A)**. Inicialmente (entre los 60 y 150 min) se observó que BzpD colocaliza con Gol-RFP, lo cual indica que se encuentra en el Golgi **(Figura 30A)**. Posteriormente, a tiempos mayores de

tratamiento con TN se observó que BzpD colocalizó con los núcleos teñidos con DAPI. Esta observación indica que GFP-BzpD fue transportada al núcleo **(Figura 30B)**.

Una vez que detectamos que BzpD transita por el Golgi y se acumula en el núcleo ante un tratamiento con TN, examinamos si esta proteína sufría un procesamiento para generar una forma soluble, de forma análoga a como sucede con ATF6. Para esto, se analizaron por Western blot extractos totales de células de las cepas WT e *ireA*⁻ que expresaban a GFP-BzpD y que fueron tratadas con TN durante 2, 4 y 6hrs. En todas las condiciones, se detectó una proteína de aproximadamente 80kDa **(Figura 31)** que coincide con el peso molecular del fragmento citoplasmático de BzpD fusionado a la GFP (84kDa, del residuo del 1 al 501). La proteína completa que tiene un peso molecular aproximado de 118kDa (incluyendo a la GFP) se observó que se expresa pobremente y fue difícil detectarla mediante esta técnica con las condiciones utilizadas.

Como puede observarse el procesamiento de BzpD fue independiente de IreA, ya que ocurre aún en la mutante que carece de esta quinasa; sin embargo, es dependiente de TN, lo cual indica que sólo ocurre en condiciones de estrés de RE.

Estos datos muestran que BzpD es una proteína tipo bZIP que se requiere para que las células puedan responder a condiciones de estrés de RE y que se procesa en respuesta a un tratamiento con TN. El procesamiento incluye su relocalización en el núcleo, tras haber transitado por el Golgi. En conjunto, todas estas observaciones sugieren que BzpD cumple en *D. discoideum* las funciones que ATF6 realiza en otras especies.
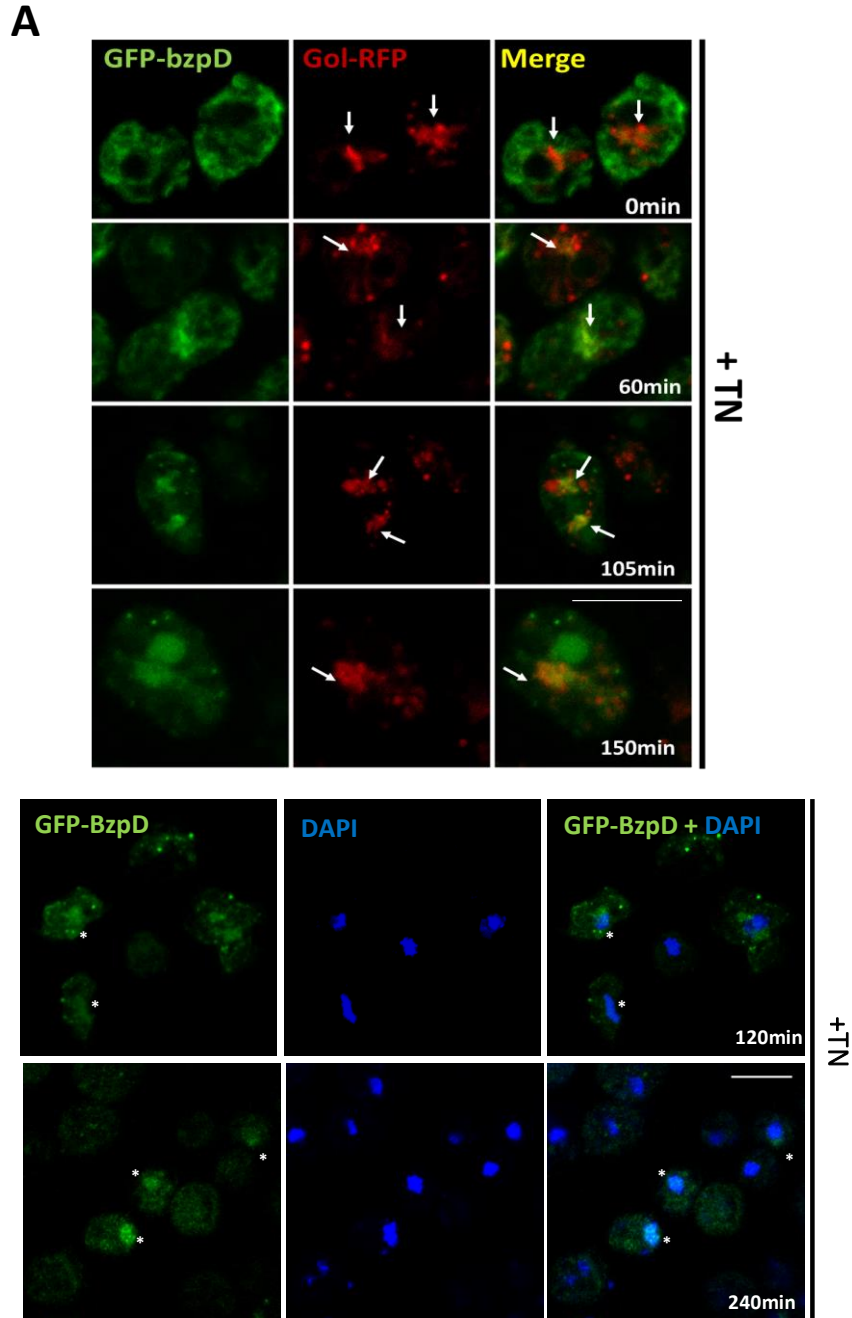
Figura 30. BzpD transita por el Golgi y se acumula en el núcleo ante un tratamiento con TN. **(A)** Imágenes adquiridas mediante microscopía confocal *in-vivo* que muestran la localización de GFP-BzpD y Gol-RFP en células WT que fueron tratadas con TN durante los tiempos señalados. Las flechas blancas señalan las zonas en las que se observa colocalización entre GFP-BzpD y Gol-RFP. **(B)** Células que expresaban la GFP-BzpD fueron tratadas con TN por los tiempos señalados y posteriormente se fijaron y se tiñeron con DAPI para detectar núcleos. Los asteriscos marcan las células en las que se detecta colocalización entre GFP-BzpD y el núcleo (escala 10μM).
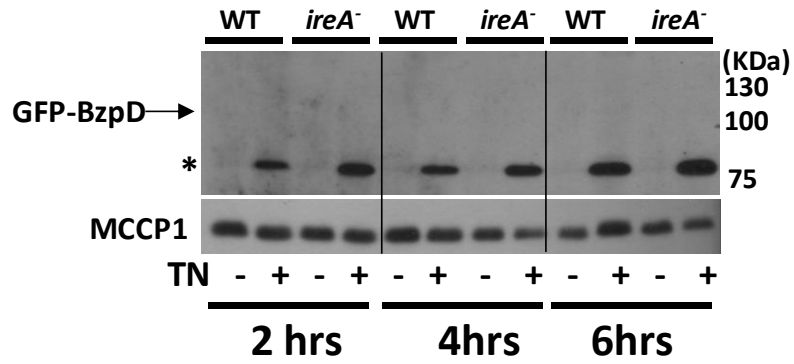
Figura 31. BzpD se procesa ante un tratamiento con TN. Se muestra un ensayo representativo de un Western blot en donde se analizaron extractos de células que expresaban a GFP-BzpD, respectivamente de la cepa WT (IreA +) o *ireA⁻*, y que fueron tratadas con TN o su vehículo durante los tiempos indicados. La detección de MCCCP1 se utilizó como control de carga.

5.-DISCUSIÓN

5.1- La TN induce estrés de RE en *D. discoideum*

En este trabajo se presenta la primera descripción que se ha hecho de la respuesta al estrés de RE en *D. discoideum*. Para esto, establecimos las condiciones tanto para inducir estrés de RE, como para poder detectar su inducción. También, mostramos las rutas que participan en esta respuesta. Encontramos que la TN es el mejor inductor de estrés de RE en *D. discoideum* pues, además de afectar la viabilidad de estas células, genera un incremento en la expresión de Grp78 y de CdcD; dos proteínas que participan en la respuesta a este tipo de estrés. La TN actúa como un antibiótico que bloquea la glicosilación de proteínas en el RE, ya que inhibe a la enzima que transfiere la *N*-acetilglucosamina fosfato al dolicol fosfato [225]. En contraste, otro agente que interfiere de manera diferente con la glicosilación de proteínas, la 2-DOG, no causó efectos significativos en *D. discoideum*. Existen observaciones previas que sugieren que la 2-DOG es internalizada pobremente en estas células y por esto, posiblemente no fue capaz de inducir estrés de RE [199]. El DTT, a la concentración probada, tampoco generó efectos significativos en *D. discoideum*. Sin embargo, no se probaron concentraciones mayores de este agente reductor debido a que suele tener efectos deletéreos en las células.

5.2- *D. discoideum* requiere de la ruta de IreA para contender con el estrés de RE

Para identificar a los posibles ortólogos de la ruta de respuesta a estrés de RE, se realizó un análisis bioinformático con el cual se encontró que en el genoma de *D. discoideum* existe un sólo ortólogo respectivamente de *grp78*, la chaperona de RE que regula a la UPR, y de *ire1*, una de las proteínas que es capaz de sentir cambios en el ambiente de plegamiento en el RE. El ortólogo de IRE1 de *D. discoideum,* IreA, presenta una mayor similitud con la proteína de humano que con la de *S. cerevisiae*, lo cual podría sugerir que la ruta de IRE1 es evolutivamente más cercana entre *D. discoideum* y humano, que entre humano y levadura. Esto hace a *D. discoideum* un organismo útil para estudios comparativos de la respuesta a estrés de RE en humano.

Como en otros organismos, IreA se localiza en el RE y resulta esencial para que las células de *D. discoideum* puedan contender con el estrés de RE; para esto, requiere tanto de su actividad de quinasa, como de ribonucleasa. Además, IreA es capaz de formar oligómeros ante un tratamiento con TN y es capaz de oligomerizarse aun cuando presenta mutaciones puntuales en su dominio de quinasa, o en el

de ribonucleasa. Posiblemente debido a que la superficie de oligomerización de IreA no se ve afectada por estas mutaciones, de forma similar a como sucede en otros organismos [211], [226]. La formación de oligómeros de IRE1 se encuentra conservada en todos los organismos que se han estudiado, por lo que es posible que este mecanismo de señalización haya surgido tempranamente durante la evolución y se haya mantenido durante la especialización de la ruta en las diferentes especies.

En levaduras y en mamíferos el tiempo durante el cual IRE1 se mantiene ensamblada en su forma oligomérica se correlaciona con el periodo durante el cual esta proteína se encuentra activa [50], [212]. En *D. discoideum*, IreA forma oligómeros aproximadamente a las 2hrs después de un tratamiento con TN, por lo que inferimos que se activa en esta ventana de tiempo. A partir de estos datos de oligomerización inferimos también que, la adaptación de IreA al estrés parece tener lugar aproximadamente a las 8hrs de tratamiento. Tras este tiempo, puede detectarse un incremento en la expresión de proteínas de respuesta a estrés y comienza a disminuir el número de células que presentan oligómeros de IreA.

En levaduras se ha demostrado que mutantes de IRE1 que carecen de las actividades de quinasa y de ribonucleasa presentan oligómeros que persisten en el tiempo, aun cuando las mutaciones no afectan la región de oligomerización [227]. De forma similar en *D. discoideum* la mutante de IreA que tiene un defecto en su actividad de ribonucleasa se mantiene persistentemente en el estado oligomérico. Posiblemente debido a que esta mutación perturba su interacción con el sustrato de su dominio de ribonucleasa. Por otra parte, cuando IreA carece de su actividad de quinasa parece presentar una menor capacidad para oligomerizarse. Estas observaciones, sugieren que aunque los dominios con actividad enzimática de IreA juegan un papel importante en la regulación de su propio ensamblaje como oligómero.

Nuestros datos sugieren que *D. discoideum* carece de un ortólogo del factor XBP1/Hac1; sin embargo, se ha reportado que los factores de transcripción de la familia de los bZIP han divergido ampliamente durante la evolución [51], [228], por lo que no se puede aún descartar que IreA procese el RNA mensajero de algún factor bZIP, cuya secuencia primaria presente poca similitud con los factores tipo XBP1.

5.3-La TN induce cambios transcripcionales que son parcialmente dependientes de IreA

Los datos obtenidos a partir del análisis de expresión, sugieren que en *D. discoideum*, ante un estrés de RE, se dispara una reprogramación de la expresión génica similar a la que sucede en otros organismos [27][229]. Un tratamiento con TN genera en esta ameba, un incremento en la expresión de genes que

codifican proteínas relacionadas con en el plegamiento, tales como las chaperonas DnaJ, la Calreticulina (CrtA) y las PDIs. También hay un aumento en la abundancia de transcritos relacionados con procesos degradativos, principalmente relacionados con la ubiquitinación de proteínas. También se incrementó la expresión de p62/SQSTM1, una proteína que participa en la autofagia. Todo esto sugiere que, para contender con un estrés de RE, las células de *D. discoideum* requieren incrementar su capacidad de plegamiento y activar procesos degradativos, principalmente asociados a la ubiquitinación.

Por otra parte, las células disminuyen su carga en el RE disminuyendo la abundancia de un número significativo de transcritos que codifican para proteínas de secreción o que requieren de procesos de plegamiento en la membrana del RE. En estos grupos se encuentran proteínas asociadas a la fagocitosis y a la endocitosis. Esto, sugiere que ante un estrés de RE las células de *D. discoideum* disminuyen la internalización de alimento, lo cual podría estar ocasionando una interrupción del crecimiento mientras la célula restablece su homeostasis.

En *Schizosaccharomyces pombe* y en *Candida glabrata* no existen homólogos de Hac1/XBP1, y se ha observado que la respuesta al estrés de RE está mediada únicamente por el proceso de degradación de mensajeros dependiente de IRE1 (RIDD) [62], [230]. Los datos aquí presentados indican que en *D. discoideum*, la respuesta al estrés de RE que depende de IreA genera tanto una disminución en la abundancia de ciertos transcritos, como un incremento en la expresión de otros, lo cual sugiere que en esta ameba podrían actuar en paralelo, la regulación de la transcripción a través de un factor (aún desconocido) y un proceso de RIDD. Si esto es así, la vía de respuesta a estrés de RE de *D. discoideum*, tendría más similitudes funcionales con mamíferos que con *S. cerevisiae*.

5.4- La autofagia se induce en respuesta al estrés de RE en *Dictyostelium*

Se ha reportado ampliamente y en diferentes especies, que el estrés de RE induce autofagia [231]. En *D. discoideum* esta respuesta también está presente y en este organismo la autofagia resulta esencial para que las células puedan sobrevivir a este tipo de estrés. Sin embargo, el proceso autofágico requerido para la adaptación al estrés de RE requiere solamente del complejo de la quinasa ATG1, mientras que el sistema el sistema de conjugación y la proteína de RE Vmp1, resultan dispensables. Previamente se ha observado que se pueden formar autofagosomas en células de mamífero que carecen de ATG5 o de ATG7, ambas, proteínas que participan en el proceso de conjugación [144], [232]. Además, se ha reportado que en *S. cerevisiae*, en respuesta al estrés de RE, se degradan porciones del este organelo sin que se requiera la participación de ATG1 o de componentes del sistema de conjugación [233]. Esto, junto

con nuestros datos, abre la posibilidad de que la autofagia que se requiere durante la respuesta al estrés de RE dependa únicamente del complejo ATG1, y que la formación de autofagosomas durante esta respuesta suceda mediante rutas alternativas al sistema de conjugación.

A diferencia de lo que ocurre en plantas y mamíferos, en *D. discoideum* existe un sólo ortólogo de IRE1. Esta característica facilita diseccionar el papel de esta quinasa en varios procesos celulares, dentro de ellos la inducción de la autofagia. En este trabajo se describe por primera vez que la inactivación de IreA en *D. discoideum* no impide que se inicie se induzca la formación de autofagosomas en presencia de estrés de RE [147], [148], en contraste con lo que se ha reportado en plantas y mamíferos; en donde IRE1 resulta ser esencial para que pueda llevarse a cabo dicha inducción. Sin embargo, las células de *D. discoideum* si requieren de IreA para que la autofagia sea eficiente. En particular, la mutante *ireA*⁻ presenta una disminución en su capacidad para degradar cargos citoplasmáticos durante el estrés de RE. Además, en estas células, Atg18 se acumula anómalamente en agregados prematuros, elongados, que permanecen asociados al RE y que resultan ser persistentes en el tiempo. Posiblemente, estas estructuras representan autofagosomas que no logran ensamblarse correctamente, por lo que se mantienen asociados al RE y son incapaces de degradar cargos.

Dado que el RE funciona como la plataforma sobre la cual se ensamblan las vesículas autofágicas [106]–[109], cualquier alteración en el RE puede causar defectos en el proceso de formación de autofagosomas. Por ejemplo, en levaduras, se ha observado que la biogénesis de los autofagosomas se ve afectada cuando existe un desbalance en la homeostasis del RE a causa de alteraciones en su composición lipídica [234]. También, este efecto se observa tanto en células de mamífero, como de *D. discoideum* que carecen de Vmp1. La ausencia de esta proteína causa deficiencias en el RE y esto, a su vez genera defectos severos en pasos tempranos en la formación de los autofagosomas [171]. Nuestros datos muestran que existe un efecto similar en *D. discoideum* durante el estrés de RE cuando IreA está ausente o inactiva. En este caso, las células pierden la capacidad para recuperar la homeostasis del RE y esto causa alteraciones severas en el proceso de formación de los autofagosomas. Todo esto sugiere que, durante el estrés de RE, IreA se requiere para mantener una estructura adecuada del RE, lo cual resulta esencial para que puedan ensamblarse autofagosomas funcionales.

5.5-Participación de BzpD en la respuesta a estrés de RE

En *D. discoideum* solo el 45% de los cambios transcripcionales generados por un tratamiento con TN dependen de la actividad de IreA. Esto quiere decir que más de un 50 % de la reprogramación transcripcional que genera el estrés de RE en este organismo dependen de una o varias vías alternativas. En mamíferos la UPR está constituida por tres ramas, una de ellas depende de ATF6, un factor de transcripción tipo bZIP que se libera de la membrana del RE cuando incrementa la carga de proteínas mal plegadas al interior de este organelo [38], [235]. Sin embargo, al analizar por BLAST el genoma de *D. discoideum,* no logramos identificar ortólogos de este factor de transcripción. Posiblemente este resultado se deba a que los factores de transcripción tipo bZIP han divergido ampliamente durante la evolución, de forma que mediante análisis filogenéticos no ha sido posible establecer que existan ortólogos de la familia ATF6/HAC1 fuera del dominio opisthokonta [51], [236]. Sin embargo, en *A. thaliana* se ha identificado que existen homólogos funcionales tanto de XBP1, como de ATF6 [54], [237], [238].

Al analizar si dentro de las 19 proteínas en las que se ha identificado un dominio bZIP en *D. discoideum* podía identificarse alguna que presentase características estructurales similares a ATF6, dedujimos que BzpC, BzpD y BzpJ podrían ser buenos candidatos, pues estas tres proteínas presentan un cruce transmembranal y al menos una secuencia de localización nuclear, características típicas de los factores tipo ATF6. Cuando evaluamos con más detalle estas proteínas encontramos que, aunque la identidad de las secuencias proteicas de BzpD y ATF6 es muy baja, resultan ser factores de transcripción análogos. En *D. discoideum*, BzpD responde ante el estrés de RE de forma muy similar a ATF6, se transporta al Golgi, se procesa proteolíticamente y se acumula en el núcleo. Además, su ausencia genera sensibilidad a un tratamiento con TN. Finalmente, el hecho de que en *D. discoideum* existan ortólogos de las dos proteasas de Golgi que participan en el procesamiento de ATF6 en otras especies (MBPTS1 y MBPTS2) sugiere que el mecanismo de activación de este factor de transcripción podría estar conservado en *D. discoideum*.

La traslocación de BzpD al Golgi sucede aproximadamente después de 60min en presencia de TN. En cambio, la activación de IreA (estimada por la formación de oligomeros) comienza a partir de las 2hrs de tratamiento. Esta diferencia temporal, sugiere que la respuesta mediada por BzpD es más rápida que la de IreA, por lo que es posible que, este factor de transcripción participe más tempranamente en el proceso de adaptación al estrés de RE. Estas diferencias en la temporalidad pueden deberse al mecanismo mediante el cual se regulan respectivamente estas dos rutas. Mientras que BzpD se produce constitutivamente y se puede activar rápidamente al ser procesada, la señalización mediada por la ruta

de IreA posiblemente dependa de una paulatina acumulación de péptidos mal plegados y de cambios en la membrana del RE que permitan su oligomerización y su activación.

Aunque se ha planteado que la respuesta al estrés de RE mediada por los factores de transcripción tipo bZIP que son liberados de la membrana del RE apareció sólo en ciertas líneas evolutivas superiores, como la de los animales [51], [84], [228], [236], en este trabajo se muestra que en *D. discoideum*, un organismo que apareció antes de la divergencia de los opistocontos, existe una ruta homóloga constituida por la proteína BzpD. Esto sugiere que este sistema de señalización surgió de forma temprana durante la evolución, pero divergió y se especializó ampliamente. La divergencia en la secuencia de estos factores de transcripción puede deberse, entre otras cosas, a que la composición del genoma de los diferentes organismos causó que la secuencia de aminoácidos de los factores de transcripción tipo bZIP se ajustara pera permitir la interacción entre los dominios de unión al DNA y las secuencias promotoras de cada organismo. Por ejemplo, el genoma de *D. discoideum* está compuesto en un 70% por adeninas (A) y timinas (T) [239], lo que podría relacionarse al hecho de que los factores de transcripción de éste organismo presente secuencias muy particulares de aminoácidos.

En el caso de *D. discoideum*, además de las rutas que responden a un incremento en la concentración de proteínas mal plegadas en el RE, es posible que existan factores de transcripción de la familia de los bZIP, como BzpJ, los cuales sean capaces de regular otros aspectos que se requieren para mantener la homeostasis del RE. Probablemente, estos factores puedan ser activados por diferentes estímulos y que generen diferentes respuestas transcripcionales, como es el caso del factor de transcripción de humanos SREBP (Sterol regulatory element-binding proteins), el cual detecta cambios en la composición lipídica del RE y regula específicamente la síntesis de esteroles [240], [241], o el de bZIP17 de *A. thaliana*, que participa en la respuesta al estrés salino [242]. La caracterización de esos factores podría ampliar el panorama de la regulación de la homeostasis del RE.

6.-Modelo de la vía de respuesta a estrés de RE en *D. discoideum*

Los datos obtenidos en este trabajo permiten plantear el modelo de la **Figura 32**, la cual muestra que en *D. discoideum* la respuesta al estrés de RE está regulada por las proteínas transmembranales de RE, IreA y BzpD. Estas están involucradas en generar una reprogramación de la expresión génica que permitirá aumentar la capacidad de degradación celular y la de plegamiento de proteínas. Además, esta respuesta permite disminuir la carga de proteínas en el RE. Por otra parte, la respuesta al estrés de RE requiere de la inducción de la autofagia. Esta inducción resulta ser independiente de IreA. Sin embargo, se requiere la presencia de esta proteína para que se recupere la homeostasis del RE y por lo tanto para que los autofagosomas puedan formarse adecuadamente.
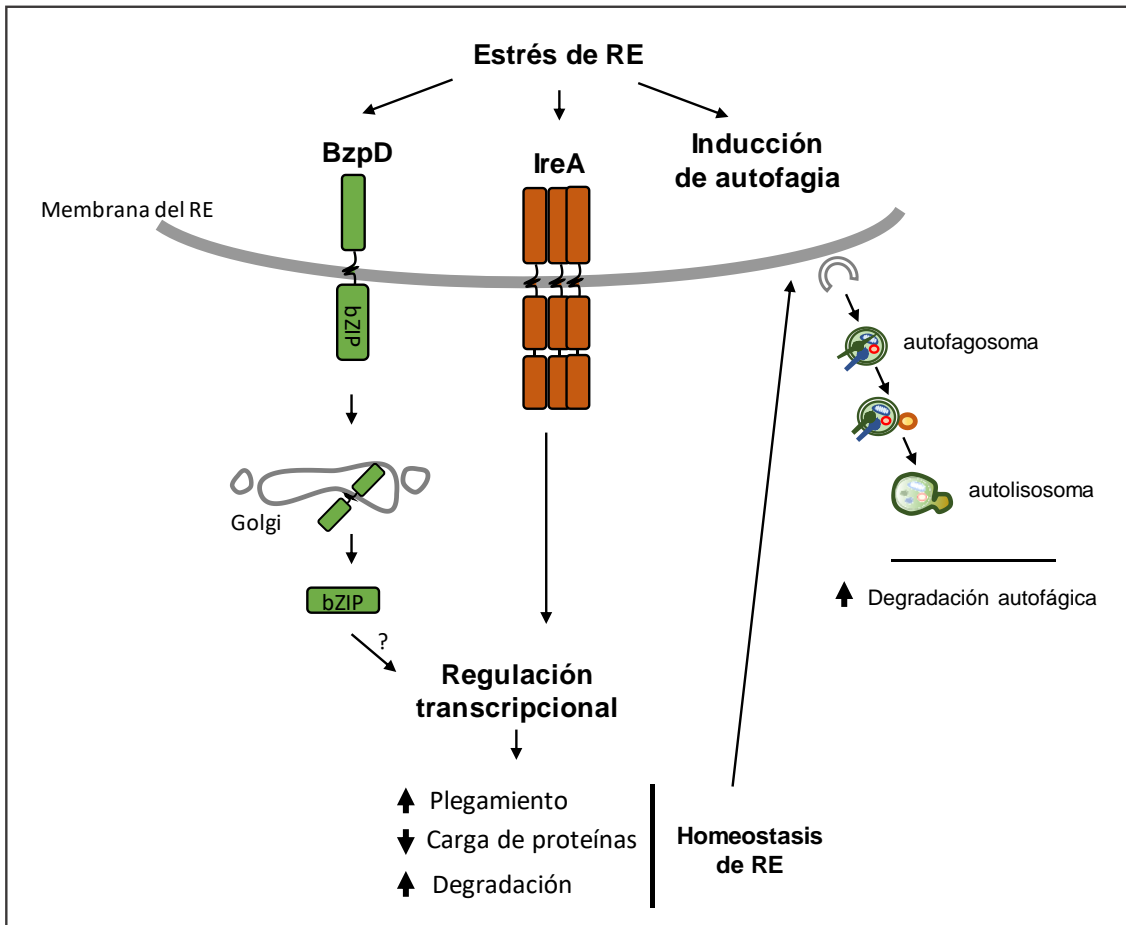
Figura 32. Modelo de la ruta de respuesta a estrés de RE en *D. discoideum*.

7.-CONCLUSIONES

1. La TN es capaz de inducir la expresión de marcadores de estrés de RE, así como de generar cambios morfológicos y de afectar la viabilidad de las células de *D. discoideum*. Los efectos de la TN, tanto sobre la expresión de marcadores, como sobre la viabilidad celular, dependen del tiempo y la concentración de tratamiento con este antibiótico.

2. IreA es el único ortólogo de IRE1 en *D. discoideum* y su actividad resulta indispensable para contender con el estrés de RE.

3. Para señalizar, IreA se asocia transitoriamente en oligómeros. La regulación de la dinámica de formación y disociación de estos oligómeros requiere que IreA se encuentre activa como quinasa y como ribonucleasa.

4. En *D. discoideum*, un tratamiento con TN genera una reprogramación de la expresión génica que permite, por un lado, incrementar la capacidad degradativa de las células y la de plegamiento de proteínas y por el otro, disminuye la carga de proteínas en el RE. Esta respuesta depende parcialmente de IreA, la cual se requiere principalmente para incrementar la degradación de proteínas mediante procesos relacionados a la ubiquitinación y para aligerar la carga del RE.

5. Ante un tratamiento con TN, las células de *D. discoideum* inducen la autofagia y el complejo ATG1 resulta indispensable para lograr una respuesta completa de supervivencia ante este estrés.

6. IreA es dispensable para que pueda inducirse la formación de autofagosomas en presencia de TN. Sin embargo, la degradación autofágica no es funcional cuando IreA está ausente o inactiva, debido a que las células no pueden mantener la homeostasis del RE.

7. BzpD participa en la respuesta al estrés de RE y se regula mediante un mecanismo análogo al de ATF6 de mamíferos. Ante un tratamiento con TN BzpD se transporta al Golgi, se procesa y se transporta al núcleo.

8. REFERENCIAS

[1] E. Snapp, "Endoplasmic Reticulum Biogenesis: Proliferation and Differentiation," in *The Biogenesis of Cellular Organelles*, C. Mullins, Ed. Landes Bioscience, Kluwer Academic / Plenum Publishers, 2005, pp. 63–95.

[2] L. M. Westrate, J. E. Lee, W. A. Prinz, and G. K. Voeltz, "Form Follows Function: The Importance of Endoplasmic Reticulum Shape," *Annu. Rev. Biochem.*, vol. 84, no. 1, pp. 791–811, 2015.

[3] J. Nixon-Abell *et al.*, "Increased spatiotemporal resolution reveals highly dynamic dense tubular matrices in the peripheral ER.," *Science*, vol. 354, no. 6311, pp. aaf3928-aaf3928, Oct. 2016.

[4] R. Fernández-Busnadiego, Y. Saheki, and P. De Camilli, "Three-dimensional architecture of extended synaptotagmin-mediated endoplasmic reticulum–plasma membrane contact sites," *Proc. Natl. Acad. Sci.*, vol. 112, no. 16, pp. E2004–E2013, 2015.

[5] M. W. Hetzer, "The Nuclear Envelope," *Cold Spring Harb. Perspect. Biol.*, vol. 2, no. 3, pp. a000539–a000539, 2010.

[6] M. Terasaki *et al.*, "Stacked endoplasmic reticulum sheets are connected by helicoidal membrane motifs," *Cell*, vol. 154, no. 2, pp. 285–96, 2013.

[7] Y. Shibata, G. K. Voeltz, and T. A. Rapoport, "Rough Sheets and Smooth Tubules," *Cell*, vol. 126, no. 3, pp. 435–439, 2006.

[8] S. Chen, T. Desai, J. A. McNew, P. Gerard, P. J. Novick, and S. Ferro-Novick, "Lunapark stabilizes nascent three-way junctions in the endoplasmic reticulum," *Proc. Natl. Acad. Sci.*, vol. 112, no. 2, pp. 418–423, 2015.

[9] C. M. Waterman-Storer and E. D. Salmon, "Endoplasmic reticulum membrane tubules are distributed by microtubules in living cells using three distinct mechanisms," *Curr. Biol.*, vol. 8, no. 14, pp. 798–807, 1998.

[10] P. S. Gurel, A. L. Hatch, and H. N. Higgs, "Connecting the cytoskeleton to the endoplasmic reticulum and Golgi," *Curr. Biol.*, vol. 24, no. 14, pp. 660–672, 2014.

[11] B. Bola and V. Allan, "How and why does the endoplasmic reticulum move?," *Biochem. Soc. Trans.*, vol. 37, no. Pt 5, pp. 961–5, 2009.

[12] T. Oertle, M. Klinger, C. A. O. Stuermer, and M. E. Schwab, "A reticular rhapsody: phylogenic evolution and nomenclature of the RTN/Nogo gene family.," *FASEB J.*, vol. 17, no. 10, pp. 1238–47, Jul. 2003.

[13] N. Zurek, L. Sparks, and G. Voeltz, "Reticulon short hairpin transmembrane domains are used to shape ER tubules," *Traffic*, vol. 12, no. 1, pp. 28–41, 2011.

[14] T. Y. Liu *et al.*, "Lipid interaction of the C terminus and association of the transmembrane segments facilitate atlastin-mediated homotypic endoplasmic reticulum fusion," *Proc. Natl. Acad. Sci.*, vol. 109, no. 32, pp. E2146–E2154, 2012.

[15] J. A. McNew, H. Sondermann, T. Lee, M. Stern, and F. Brandizzi, "GTP-Dependent Membrane Fusion," *Annu. Rev. Cell Dev. Biol.*, vol. 29, no. 1, pp. 529–550, 2013.

[16] X. Bian *et al.*, "Structures of the atlastin GTPase provide insight into homotypic fusion of

endoplasmic reticulum membranes," *Proc. Natl. Acad. Sci.*, vol. 108, no. 10, pp. 3976–3981, 2011.

[17]   D. S. Schwarz and M. D. Blower, "The endoplasmic reticulum: Structure, function and response to cellular signaling," *Cell. Mol. Life Sci.*, vol. 73, no. 1, pp. 79–94, 2016.

[18]   C. Xu and D. T. W. Ng, "Glycosylation-directed quality control of protein folding," *Nat. Rev. Mol. Cell Biol.*, vol. 16, no. 12, pp. 742–752, 2015.

[19]   L. Halperin, J. Jung, and M. Michalak, "The many functions of the endoplasmic reticulum chaperones and folding enzymes," *IUBMB Life*, vol. 66, no. 5, pp. 318–326, 2014.

[20]   A. Korennykh and P. Walter, "Structural Basis of the Unfolded Protein Response," *Annu. Rev. Cell Dev. Biol.*, vol. 28, no. 1, pp. 251–277, 2012.

[21]   A. Müller-Taubenberger, a N. Lupas, H. Li, M. Ecke, E. Simmeth, and G. Gerisch, "Calreticulin and calnexin in the endoplasmic reticulum are important for phagocytosis.," *EMBO J.*, vol. 20, no. 23, pp. 6772–82, Dec. 2001.

[22]   T. Gidalevitz, F. Stevens, and Y. Argon, "Orchestration of secretory protein folding by ER chaperones," *Biochim. Biophys. Acta - Mol. Cell Res.*, vol. 1833, no. 11, pp. 2410–2424, 2013.

[23]   I. Braakman and D. N. Hebert, "Protein folding in the endoplasmic reticulum," *Cold Spring Harb. Perspect. Biol.*, vol. 5, no. 5, p. a013201, 2013.

[24]   S. Back, M. Schröder, K. Lee, K. Zhang, and R. J. Kaufman, "ER stress signaling by regulated splicing: IRE1/HAC1/XBP1," *Methods*, vol. 35, no. 4, pp. 395–416, 2005.

[25]   C. M. Oslowski and F. Urano, *Measuring ER stress and the unfolded protein response using mammalian tissue culture system*, 1st ed., vol. 490, no. C. Elsevier Inc., 2011.

[26]   D. J. Cox, N. Strudwick, A. A. Ali, A. W. Paton, J. C. Paton, and M. Schröder, *Measuring signaling by the unfolded protein response*, vol. 491. 2011.

[27]   K. J. Travers, C. K. Patil, L. Wodicka, D. J. Lockhart, J. S. Weissman, and P. Walter, "Functional and genomic analyses reveal an essential coordination between the unfolded protein response and ER-associated degradation," *Cell*, vol. 101, no. 3, pp. 249–58, Apr. 2000.

[28]   D. Ron and P. Walter, "Signal integration in the endoplasmic reticulum unfolded protein response," *Nature Reviews Molecular Cell Biology*, vol. 8, no. 7. pp. 519–529, 2007.

[29]   D. Scheuner *et al.*, "Translational control is required for the unfolded protein response and in vivo glucose homeostasis.," *Mol. Cell*, vol. 7, no. 6, pp. 1165–76, 2001.

[30]   M. Maurel, E. Chevet, J. Tavernier, and S. Gerlo, "Getting RIDD of RNA: IRE1 in cell fate regulation," *Trends Biochem. Sci.*, vol. 39, no. 5, pp. 245–254, 2014.

[31]   S. S. Vembar and J. L. Brodsky, "One step at a time: endoplasmic reticulum-associated degradation," *Nat. Rev. Mol. Cell Biol.*, vol. 9, no. 12, pp. 944–957, 2008.

[32]   L. Lemus and V. Goder, "Regulation of Endoplasmic Reticulum-Associated Protein Degradation (ERAD) by Ubiquitin," *Cells*, vol. 3, no. 3, pp. 824–847, 2014.

[33]   D. H. Wolf and A. Stolz, "The Cdc48 machine in endoplasmic reticulum associated protein degradation," *Biochim. Biophys. Acta - Mol. Cell Res.*, vol. 1823, no. 1, pp. 117–124, 2012.

[34]   C. Lipson *et al.*, "A proteasomal ATPase contributes to dislocation of Endoplasmic Reticulum-associated Degradation (ERAD) substrates," *J. Biol. Chem.*, vol. 283, no. 11, pp. 7166–7175, 2008.

[35]   A. Ruggiano, O. Foresti, and P. Carvalho, "ER-associated degradation: Protein quality control and

beyond," *J. Cell Biol.*, vol. 204, no. 6, pp. 869–879, 2014.

[36]   E. Domínguez-Martín, M. Hernández-Elvira, O. Vincent, R. Coria, and R. Escalante, "Unfolding the Endoplasmic Reticulum of a Social Amoeba: Dictyostelium discoideum as a New Model for the Study of Endoplasmic Reticulum Stress," *Cells*, vol. 7, no. 6, p. 56, Jun. 2018.

[37]   H. Wu, B. S. H. Ng, and G. Thibault, "Endoplasmic reticulum stress response in yeast and humans," *Biosci. Rep.*, vol. 34, no. 4, pp. 321–330, 2014.

[38]   R. Chakraborty, J. H. Baek, E. Y. Bae, W. Y. Kim, S. Y. Lee, and M. G. Kim, "Comparison and contrast of plant, yeast, and mammalian ER stress and UPR," *Appl. Biol. Chem.*, vol. 59, no. 3, pp. 337–347, 2016.

[39]   A. Bertolotti *et al.*, "Increased sensitivity to dextran sodium sulfate colitis in IRE1β-deficient mice," *J. Clin. Invest.*, vol. 107, no. 5, pp. 585–593, 2001.

[40]   M. B. Martino *et al.*, "The ER stress transducer IRE1β is required for airway epithelial mucin production," *Mucosal Immunol.*, vol. 6, no. 3, pp. 639–654, May 2013.

[41]   N. Koizumi, I. M. Martinez, Y. Kimata, K. Kohno, H. Sano, and M. J. Chrispeels, "Molecular characterization of two Arabidopsis Ire1 homologs, endoplasmic reticulum-located transmembrane protein kinases.," *Plant Physiol.*, vol. 127, no. 3, pp. 949–62, 2001.

[42]   S. J. Noh, C. S. Kwon, and W. I. Chung, "Characterization of two homologs of Ire1p, a kinase/endoribonuclease in yeast, in Arabidopsis thaliana," *Biochim. Biophys. Acta - Gene Struct. Expr.*, vol. 1575, no. 1–3, pp. 130–134, 2002.

[43]   K. P. K. Lee, M. Dey, D. Neculai, C. Cao, T. E. Dever, and F. Sicheri, "Structure of the Dual Enzyme Ire1 Reveals the Basis for Catalysis and Regulation in Nonconventional RNA Splicing," *Cell*, vol. 132, no. 1, pp. 89–100, Jan. 2008.

[44]   D. Ron and S. R. Hubbard, "How IRE1 reacts to ER stress.," *Cell*, vol. 132, no. 1, pp. 24–6, Jan. 2008.

[45]   Y. Kimata *et al.*, "Two regulatory steps of ER-stress sensor Ire1 involving its cluster formation and interaction with unfolded proteins," *J. Cell Biol.*, vol. 179, no. 1, pp. 75–86, 2007.

[46]   D. Oikawa, Y. Kimata, and K. Kohno, "Self-association and BiP dissociation are not sufficient for activation of the ER stress sensor Ire1.," *J. Cell Sci.*, vol. 120, no. Pt 9, pp. 1681–8, May 2007.

[47]   B. M. Gardner and P. Walter, "Unfolded proteins are Ire1-activating ligands that directly induce the unfolded protein response.," *Science (80-.).*, vol. 333, no. 6051, pp. 1891–4, Sep. 2011.

[48]   G. E. Karagöz, D. Acosta-Alvear, H. T. Nguyen, C. P. Lee, F. Chu, and P. Walter, "An unfolded protein-induced conformational switch activates mammalian IRE1," *Elife*, vol. 6, pp. 1–29, 2017.

[49]   T. N. Gonzalez, C. Sidrauski, S. Dörfler, and P. Walter, "Mechanism of non-spliceosomal mRNA splicing in the unfolded protein response pathway.," *EMBO J.*, vol. 18, no. 11, pp. 3119–32, Jun. 1999.

[50]   T. Aragón *et al.*, "Messenger RNA targeting to endoplasmic reticulum stress signalling sites," *Nature*, vol. 457, no. 7230, pp. 736–740, Feb. 2009.

[51]   K. Jindrich and B. M. Degnan, "The diversification of the basic leucine zipper family in eukaryotes correlates with the evolution of multicellularity Genome evolution and evolutionary systems biology," *BMC Evol. Biol.*, vol. 16, no. 1, pp. 1–12, 2016.

[52]   C. Chen *et al.*, "Signal peptide peptidase functions in ERAD to cleave the unfolded protein response regulator XBP1u.," *EMBO J.*, vol. 33, no. 21, pp. 2492–506, 2014.

[53] K. Yanagitani *et al.*, "Cotranslational Targeting of XBP1 Protein to the Membrane Promotes Cytoplasmic Splicing of Its Own mRNA," *Mol. Cell*, vol. 34, no. 2, pp. 191–200, 2009.

[54] Y. Nagashima, K. Mishiba, E. Suzuki, Y. Shimada, Y. Iwata, and N. Koizumi, "Arabidopsis IRE1 catalyses unconventional splicing of bZIP60 mRNA to produce the active transcription factor.," *Sci. Rep.*, vol. 1, no. 1, p. 29, Dec. 2011.

[55] K. Yanagitani, Y. Kimata, H. Kadokura, and K. Kohno, "Translational Pausing Ensures Membrane Targeting and Cytoplasmic Splicing of XBP1u mRNA," *Science (80-.).*, vol. 331, no. 6017, pp. 586–589, Feb. 2011.

[56] L. Sathe, C. Bolinger, M. Amin-Ul Mannan, T. E. Dever, and M. Dey, "Evidence that base-pairing interaction between intron and mRNA leader sequences inhibits initiation of HAC1 mRNA translation in yeast," *J. Biol. Chem.*, vol. 290, no. 36, pp. 21821–21832, 2015.

[57] U. Rüegsegger, J. H. Leber, and P. Walter, "Block of HAC1 mRNA translation by long-range base pairing is released by cytoplasmic splicing upon induction of the unfolded protein response," *Cell*, vol. 107, no. 1, pp. 103–114, 2001.

[58] K. B. Hooks and S. Griffiths-Jones, "Conserved RNA structures in the non-canonical Hac1/Xbp1 intron.," *RNA Biol.*, vol. 8, no. 4, pp. 552–6, 2011.

[59] Y. Iwata and N. Koizumi, "Plant transducers of the endoplasmic reticulum unfolded protein response," *Trends Plant Sci.*, vol. 17, no. 12, pp. 720–727, 2012.

[60] J. Hollien and J. S. Weissman, "Decay of Endoplasmic Reticulum-Localized mRNAs During the Unfolded Protein Response," *Science (80-.).*, vol. 313, no. 5783, 2006.

[61] J. Hollien, J. H. Lin, H. Li, N. Stevens, P. Walter, and J. S. Weissman, "Regulated Ire1-dependent decay of messenger RNAs in mammalian cells," *J. Cell Biol.*, vol. 186, no. 3, pp. 323–331, 2009.

[62] P. Kimmig *et al.*, "The unfolded protein response in fission yeast modulates stability of select mRNAs to maintain protein homeostasis.," *Elife*, vol. 1, p. e00048, Jan. 2012.

[63] S. Hayashi, Y. Wakasa, K. Ozawa, and F. Takaiwa, "Characterization of IRE1 ribonuclease-mediated mRNA decay in plants using transient expression analyses in rice protoplasts," *New Phytol.*, vol. 210, no. 4, pp. 1259–1268, 2016.

[64] K. -i. Mishiba *et al.*, "Defects in IRE1 enhance cell death and fail to degrade mRNAs encoding secretory pathway proteins in the Arabidopsis unfolded protein response," *Proc. Natl. Acad. Sci.*, vol. 110, no. 14, pp. 5713–5718, 2013.

[65] K. Moore and J. Hollien, "Ire1-mediated decay in mammalian cells relies on mRNA sequence, structure, and translational status," *Mol. Biol. Cell*, vol. 26, no. 16, pp. 2873–2884, 2015.

[66] A. B. Tam, A. C. Koong, and M. Niwa, "Ire1 Has Distinct Catalytic Mechanisms for XBP1/HAC1 Splicing and RIDD," *Cell Rep.*, vol. 9, no. 3, pp. 850–858, 2014.

[67] M. D. Bright, D. N. Itzhak, C. P. Wardell, G. J. Morgan, and F. E. Davies, "Cleavage of *BLOC1S1* mRNA by IRE1 Is Sequence Specific, Temporally Separate from *XBP1* Splicing, and Dispensable for Cell Viability under Acute Endoplasmic Reticulum Stress," *Mol. Cell. Biol.*, vol. 35, no. 12, pp. 2186–2202, 2015.

[68] W. Cui, J. Li, D. Ron, and B. Sha, "The structure of the PERK kinase domain suggests the mechanism for its activation," *Acta Crystallogr. Sect. D Biol. Crystallogr.*, vol. 67, no. 5, pp. 423–428, 2011.

[69] J. Zhou *et al.*, "The crystal structure of human IRE1 luminal domain reveals a conserved dimerization interface required for activation of the unfolded protein response," *{PROCEEDINGS Natl. Acad. Sci.*

UNITED STATES Am., vol. {103}, no. {39}.

[70]   H. P. Harding *et al.*, "Regulated translation initiation controls stress-induced gene expression in mammalian cells," *Mol. Cell*, vol. 6, no. 5, pp. 1099–1108, 2000.

[71]   J. B. DuRose, D. Scheuner, R. J. Kaufman, L. I. Rothblum, and M. Niwa, "Phosphorylation of Eukaryotic Translation Initiation Factor 2 Coordinates rRNA Transcription and Translation Inhibition during Endoplasmic Reticulum Stress," *Mol. Cell. Biol.*, vol. 29, no. 15, pp. 4295–4307, 2009.

[72]   R. C. Wek, "Role of eIF2α Kinases in Translational Control and Adaptation to Cellular Stress," *Cold Spring Harb. Perspect. Biol.*, p. a032870, 2018.

[73]   D. Scheuner *et al.*, "Control of mRNA translation preserves endoplasmic reticulum function in beta cells and maintains glucose homeostasis," *Nat. Med.*, vol. 11, no. 7, pp. 757–764, 2005.

[74]   K. M. Vattem and R. C. Wek, "Reinitiation involving upstream ORFs regulates ATF4 mRNA translation in mammalian cells," *Proc. Natl. Acad. Sci.*, vol. 101, no. 31, pp. 11269–11274, 2004.

[75]   K. Ameri and A. L. Harris, "Activating transcription factor 4," *Int. J. Biochem. Cell Biol.*, vol. 40, no. 1, pp. 14–21, 2008.

[76]   D. T. Rutkowski and R. J. Kaufman, "All roads lead to ATF4," *Dev. Cell*, vol. 4, no. 4, pp. 442–444, 2003.

[77]   M. Li *et al.*, "ATF6 as a transcription activator of the endoplasmic reticulum stress element: thapsigargin stress-induced changes and synergistic interactions with NF-Y and YY1.," *Mol. Cell. Biol.*, vol. 20, no. 14, pp. 5096–106, Jul. 2000.

[78]   S. Nadanaka, T. Okada, H. Yoshida, and K. Mori, "Role of Disulfide Bridges Formed in the Luminal Domain of ATF6 in Sensing Endoplasmic Reticulum Stress," *Mol. Cell. Biol.*, vol. 27, no. 3, pp. 1027–1043, 2007.

[79]   J. Shen, X. Chen, L. Hendershot, and R. Prywes, "ER stress regulation of ATF6 localization by dissociation of BiP/GRP78 binding and unmasking of golgi localization signals," *Dev. Cell*, vol. 3, no. 1.

[80]   J. Ye *et al.*, "ER Stress Induces Cleavage of Membrane-Bound ATF6 by the Same Proteases that Process SREBPs," *Mol. Cell*, vol. 6, pp. 1355–1364, 2000.

[81]   R. F. Hillary and U. Fitzgerald, "A lifetime of stress : ATF6 in development and homeostasis," pp. 1–10, 2018.

[82]   S. Kondo, A. Saito, R. Asada, S. Kanemoto, and K. Imaizumi, "Physiological unfolded protein response regulated by OASIS family members, transmembrane bZIP transcription factors," *IUBMB Life*, vol. 63, no. 4, pp. 233–239, 2011.

[83]   R. Asada, S. Kanemoto, S. Kondo, A. Saito, and K. Imaizumi, "The signalling from endoplasmic reticulum-resident bZIP transcription factors involved in diverse cellular physiology," *J. Biochem.*, vol. 149, no. 5, pp. 507–518, 2011.

[84]   A. Saito, "Physiological functions of endoplasmic reticulum stress transducer OASIS in central nervous system," *Anat. Sci. Int.*, vol. 89, no. 1, pp. 11–20, 2014.

[85]   S. Cenci, "Autophagy, a new determinant of plasma cell differentiation and antibody responses," *Molecular Immunology*. 2014.

[86]   S. Besteiro, R. A. M. Williams, G. H. Coombs, and J. C. Mottram, "Protein turnover and differentiation in Leishmania," *International Journal for Parasitology*. 2007.

[87]   J. S. King, D. M. Veltman, and R. H. Insall, "The induction of autophagy by mechanical stress,"

Autophagy, vol. 7, no. 12, pp. 1490–1499, 2011.

[88]   M. Hamasaki, T. Noda, M. Baba, and Y. Ohsumi, "Starvation triggers the delivery of the endoplasmic reticulum to the vacuole via autophagy in yeast.," *Traffic*, vol. 6, no. 1, pp. 56–65, Jan. 2005.

[89]   J. Calvo-garrido *et al.*, "Autophagy in Dictyostelium : Genes and pathways , cell death and infection.," *Autophagy*, vol. 66, no. August, pp. 686–701, 2010.

[90]   I. Tanida, "Autophagy basics," *Microbiol. Immunol.*, vol. 55, no. 1, pp. 1–11, 2011.

[91]   G. Zaffagnini and S. Martens, "Mechanisms of Selective Autophagy," *J. Mol. Biol.*, vol. 428, no. 9, pp. 1714–1724, 2016.

[92]   D. Gatica, V. Lahiri, and D. J. Klionsky, "Cargo recognition and degradation by selective autophagy," *Nat. Cell Biol.*, vol. 20, no. 3, pp. 233–242, 2018.

[93]   J. Calvo-Garrido and R. Escalante, "Autophagy dysfunction and ubiquitin-positive protein aggregates in Dictyostelium cells lacking Vmp1," *Autophagy*, vol. 6, no. 1, pp. 100–109, 2010.

[94]   S. V. Scott, J. Guan, M. U. Hutchins, J. Kim, and D. J. Klionsky, "Cvt19 is a receptor for the cytoplasm-to-vacuole targeting pathway," *Mol. Cell*, vol. 7, no. 6, pp. 1131–1141, 2001.

[95]   M. Lippai and P. Low, "The role of the selective adaptor p62 and ubiquitin-like proteins in autophagy," *Biomed Res. Int.*, vol. 2014, 2014.

[96]   A. L. Anding and E. H. Baehrecke, "Cleaning House: Selective Autophagy of Organelles," *Dev. Cell*, vol. 41, no. 1, pp. 10–22, 2017.

[97]   W. W. Li, J. Li, and J. K. Bao, "Microautophagy: Lesser-known self-eating," *Cell. Mol. Life Sci.*, vol. 69, no. 7, pp. 1125–1136, 2012.

[98]   D. Mijaljica, M. Prescott, and R. J. Devenish, "Microautophagy in mammalian cells: Revisiting a 40-year-old conundrum," *Autophagy*, vol. 7, no. 7, pp. 673–682, 2011.

[99]   S. Kaushik and A. M. Cuervo, "Chaperone-mediated autophagy: A unique way to enter the lysosome world," *Trends Cell Biol.*, vol. 22, no. 8, pp. 407–417, 2012.

[100]   F. Li and R. D. Vierstra, "Autophagy: A multifaceted intracellular system for bulk and selective recycling," *Trends Plant Sci.*, vol. 17, no. 9, pp. 526–537, 2012.

[101]   G. Kroemer, G. Mariño, and B. Levine, "Autophagy and the Integrated Stress Response," *Mol. Cell*, vol. 40, no. 2, pp. 280–293, 2010.

[102]   R. C. Russell, H.-X. Yuan, and K.-L. Guan, "Autophagy regulation by nutrient signaling.," *Cell Res.*, vol. 24, no. 1, pp. 42–57, 2014.

[103]   G. Filomeni, D. De Zio, F. Cecconi, D. De Zio, and F. Cecconi, "Oxidative stress and autophagy: the clash between damage and metabolic needs," *Cell Death Differ.*, vol. 22, no. 3, pp. 377–388, 2015.

[104]   T. Yorimitsu, U. Nair, Z. Yang, and D. J. Klionsky, "Endoplasmic Reticulum Stress Triggers Autophagy," *J. Biol. Chem.*, vol. 281, no. 40, pp. 30299–30304, 2006.

[105]   E. a. Dunlop and a. R. Tee, "mTOR and autophagy: A dynamic relationship governed by nutrients and energy," *Semin. Cell Dev. Biol.*, vol. 36, pp. 121–129, 2014.

[106]   E. L. Axe *et al.*, "Autophagosome formation from membrane compartments enriched in phosphatidylinositol 3-phosphate and dynamically connected to the endoplasmic reticulum," *J. Cell Biol.*, vol. 182, no. 4, pp. 685–701, 2008.

[107]   M. Hamasaki *et al.*, "Autophagosomes form at ER-mitochondria contact sites," *Nature*, vol. 495, no.

7441, pp. 389–393, 2013.

[108] A. C. Nascimbeni *et al.*, "ER–plasma membrane contact sites contribute to autophagosome biogenesis by regulation of local PI3P synthesis," *EMBO J.*, vol. 36, no. 14, pp. 2018–2033, 2017.

[109] M. Graef, J. R. Friedman, C. Graham, M. Babu, and J. Nunnari, "ER exit sites are physical and functional core autophagosome biogenesis components.," *Mol. Biol. Cell*, vol. 24, no. 18, pp. 2918–31, 2013.

[110] K. Suzuki, M. Akioka, C. Kondo-Kakuta, H. Yamamoto, and Y. Ohsumi, "Fine mapping of autophagy-related proteins during autophagosome formation in Saccharomyces cerevisiae.," *J. Cell Sci.*, vol. 126, no. Pt 11, pp. 2534–44, Jun. 2013.

[111] D. Papinski and C. Kraft, "Regulation of Autophagy By Signaling Through the Atg1 / ULK1 Complex," *J. Mol. Biol.*, vol. 428, no. 9, pp. 1725–1741, 2016.

[112] Y. Kamada, T. Funakoshi, T. Shintani, K. Nagano, M. Ohsumi, and Y. Ohsumi, "Tor-mediated induction of autophagy via an Apg1 protein kinase complex," *J. Cell Biol.*, vol. 150, no. 6, pp. 1507–1513, 2000.

[113] C. H. Jung *et al.*, "ULK-Atg13-FIP200 Complexes Mediate mTOR Signaling to the Autophagy Machinery," *Mol. Biol. Cell*, vol. 20, no. 7, pp. 1992–2003, 2009.

[114] I. G. Ganley, D. H. Lam, J. Wang, X. Ding, S. Chen, and X. Jiang, "ULK1·ATG13·FIP200 complex mediates mTOR signaling and is essential for autophagy," *J. Biol. Chem.*, vol. 284, no. 18, pp. 12297–12305, 2009.

[115] N. Hosokawa *et al.*, "Nutrient-dependent mTORC1 Association with the ULK1 – Atg13 – FIP200 Complex Required for Autophagy," *Mol. Biol. Cell*, vol. 20, no. 7, pp. 1981–1991, 2009.

[116] D. Papinski *et al.*, "Early Steps in Autophagy Depend on Direct Phosphorylation of Atg9 by the Atg1 Kinase," *Mol. Cell*, vol. 53, no. 3, pp. 471–483, 2014.

[117] R. C. Russell *et al.*, "ULK1 induces autophagy by phosphorylating Beclin-1 and activating VPS34 lipid kinase," *Nat. Cell Biol.*, vol. 15, no. 7, pp. 741–750, 2013.

[118] V. Y. Nazarko and Q. Zhong, "ULK1 targets Beclin-1 in autophagy," *Nat. Cell Biol.*, vol. 15, no. 7, pp. 727–728, 2013.

[119] C. Burman and N. T. Ktistakis, "Regulation of autophagy by phosphatidylinositol 3-phosphate," *FEBS Lett.*, vol. 584, no. 7, pp. 1302–1312, 2010.

[120] K. Obara, T. Sekito, K. Niimi, and Y. Ohsumi, "The Atg18-Atg2 complex is recruited to autophagic membranes via phosphatidylinositol 3-phosphate and exerts an essential function," *J. Biol. Chem.*, vol. 283, no. 35, pp. 23972–23980, 2008.

[121] L. Ge and R. Schekman, "The ER-Golgi intermediate compartment feeds the phagophore membrane," *Autophagy*, vol. 10, no. 1, pp. 170–172, 2014.

[122] H. Yamamoto *et al.*, "Atg9 vesicles are an important membrane source during early steps of autophagosome formation.," *J. Cell Biol.*, vol. 198, no. 2, pp. 219–33, Jul. 2012.

[123] K. Shirahama-Noda, S. Kira, T. Yoshimori, and T. Noda, "TRAPPIII is responsible for vesicular transport from early endosomes to Golgi, facilitating Atg9 cycling in autophagy," *J. Cell Sci.*, vol. 126, no. 21, pp. 4963–4973, 2013.

[124] R. Gómez-Sánchez *et al.*, "Atg9 establishes Atg2-dependent contact sites between the endoplasmic reticulum and phagophores," *J. Cell Biol.*, p. jcb.201710116, 2018.

[125] T. Shpilka, H. Weidberg, S. Pietrokovski, and Z. Elazar, "Atg8: An autophagy-related ubiquitin-like

protein family," *Genome Biol.*, 2011.

[126] T. Hanada and Y. Ohsumi, "Structure-function relationship of Atg12, a ubiquitin-like modifier essential for autophagy.," *Autophagy*, 2005.

[127] H. Nakatogawa, "Two ubiquitin-like conjugation systems that mediate membrane formation during autophagy," *Essays Biochem.*, vol. 55, pp. 39–50, 2013.

[128] N. Mizushima *et al.*, "A protein conjugation system essential for autophagy," *Nature*, vol. 395, no. 6700, pp. 395–398, 1998.

[129] H. C. Dooley, M. Razi, H. E. J. Polson, S. E. Girardin, M. I. Wilson, and S. A. Tooze, "WIPI2 Links LC3 Conjugation with PI3P, Autophagosome Formation, and Pathogen Clearance by Recruiting Atg12-5-16L1," *Mol. Cell*, vol. 55, no. 2, pp. 238–252, 2014.

[130] R. Krick and M. Thumm, "Atg8 lipidation is coordinated in a PtdIns3P-dependent manner by the PROPPIN Atg21," *Autophagy*, vol. 12, no. 11, pp. 2260–2261, 2016.

[131] Y. Ichimura *et al.*, "A ubiquitin-like system mediates protein lipidation," *Nature*, vol. 408, no. 6811, pp. 488–492, 2000.

[132] I. Abdollahzadeh, M. Schwarten, T. Gensch, D. Willbold, and O. H. Weiergräber, "The Atg8 family of proteins-modulating shape and functionality of autophagic membranes," *Front. Genet.*, vol. 8, no. AUG, pp. 1–7, 2017.

[133] Y. K. Lee and J. A. Lee, "Role of the mammalian ATG8/LC3 family in autophagy: Differential and compensatory roles in the spatiotemporal regulation of autophagy," *BMB Rep.*, vol. 49, no. 8, pp. 424–430, 2016.

[134] T. Yoshimori, "An Atg4B Mutant Hampers the Lipidation of LC3 Paralogues and Causes Defects in Autophagosome Closure," *Seikagaku*, vol. 82, no. 4, pp. 327–331, 2010.

[135] K. Tabata, K. Matsunaga, A. Sakane, T. Sasaki, T. Noda, and T. Yoshimori, "Rubicon and PLEKHM1 Negatively Regulate the Endocytic/Autophagic Pathway via a Novel Rab7-binding Domain," *Mol. Biol. Cell*, vol. 21, no. 23, pp. 4162–4172, 2010.

[136] D. G. McEwan *et al.*, "PLEKHM1 regulates autophagosome-lysosome fusion through HOPS complex and LC3/GABARAP proteins," *Mol. Cell*, vol. 57, no. 1, pp. 39–54, 2015.

[137] P. Jiang *et al.*, "The HOPS complex mediates autophagosome-lysosome fusion through interaction with syntaxin 17," *Mol. Biol. Cell*, vol. 25, no. 8, pp. 1327–1337, 2014.

[138] M. Ponpuak, M. A. Mandell, T. Kimura, S. Chauhan, C. Cleyrat, and V. Deretic, "Secretory autophagy," *Curr. Opin. Cell Biol.*, vol. 35, no. Figure 1, pp. 106–116, 2015.

[139] A. Claude-Taupin, J. Jia, M. Mudd, and V. Deretic, "Autophagy's secret life: secretion instead of degradation," *Essays Biochem.*, vol. 61, no. 6, pp. 637–647, 2017.

[140] S. Chowdhury *et al.*, "Insights into autophagosome biogenesis from structural and biochemical analyses of the ATG2A-WIPI4 complex," 2018.

[141] Y. Chen and L. Yu, "Development of Research into Autophagic Lysosome Reformation," *Mol. Cells*, vol. 41, no. 1, pp. 45–49, 2018.

[142] Y. Chen and L. Yu, "Recent progress in autophagic lysosome reformation," *Traffic*, vol. 18, no. 6, pp. 358–361, 2017.

[143] S. Bernales, K. L. McDonald, and P. Walter, "Autophagy counterbalances endoplasmic reticulum expansion during the unfolded protein response.," *PLoS Biol.*, vol. 4, no. 12, pp. 2311–2324, Nov.

2006.

[144] S. Schuck, C. M. Gallagher, and P. Walter, "ER-phagy mediates selective degradation of endoplasmic reticulum independently of the core autophagy machinery.," *J. Cell Sci.*, no. July 2014, 2014.

[145] S. Matus, F. Lisbona, M. Torres, C. Leon, P. Thielen, and C. Hetz, "The Stress Rheostat: An Interplay Between the Unfolded Protein Response (UPR) and Autophagy in Neurodegeneration," *Curr. Mol. Med.*, vol. 8, no. 3, pp. 157–172, 2008.

[146] S. A. Houck *et al.*, "Quality Control Autophagy Degrades Soluble ERAD-Resistant Conformers of the Misfolded Membrane Protein GnRHR," *Mol. Cell*, vol. 54, no. 1, pp. 166–179, 2014.

[147] M. Ogata *et al.*, "Autophagy is activated for cell survival after endoplasmic reticulum stress.," *Mol. Cell. Biol.*, vol. 26, no. 24, pp. 9220–31, Dec. 2006.

[148] Y. Liu, J. S. Burgos, Y. Deng, R. Srivastava, S. H. Howell, and D. C. Bassham, "Degradation of the endoplasmic reticulum by autophagy during endoplasmic reticulum stress in Arabidopsis.," *Plant Cell*, vol. 24, no. 11, pp. 4635–51, Nov. 2012.

[149] F. Fumagalli *et al.*, "Translocon component Sec62 acts in endoplasmic reticulum turnover during stress recovery," *Nat. Cell Biol.*, vol. 18, no. 11, pp. 1173–1184, 2016.

[150] H. Wu, H. Wei, S. Arslan, L. Liu, and Q. Chen, "Free Radical Biology and Medicine Mitophagy receptors sense stress signals and couple mitochondrial dynamic machinery for mitochondrial quality control," *Free Radic. Biol. Med.*, vol. 100, pp. 199–209, 2016.

[151] S. Muñoz-Braceras, A. Mesquita, and R. Escalante, *Dictyostelium discoideum as a Model in Biomedical Research*. Berlin, Heidelberg: Springer, 2013.

[152] S. Annesley and P. Fisher, "Dictyostelium discoideum—a model for many reasons," *Mol. Cell. Biochem.*, vol. 329, no. 1, pp. 73–91, Sep. 2009.

[153] S. J. Annesley *et al.*, "Dictyostelium, a microbial model for brain disease," *Biochim. Biophys. Acta - Gen. Subj.*, vol. 1840, no. 4, pp. 1413–1432, 2014.

[154] K. Dannat, J. Tillner, T. Winckler, M. Weiss, K. Eger, and T. Dingermann, "Effects of medicinal compounds on the differentiation of the eukaryotic microorganism Dictyostelium discoideum: Can this model be used as a screening test for reproductive toxicity in humans?," *Pharmazie*, vol. 58, no. 3, pp. 204–210, 2003.

[155] X. H. Liao *et al.*, "A High-Throughput, Multi-Cell Phenotype Assay for the Identification of Novel Inhibitors of Chemotaxis/Migration," *Sci. Rep.*, vol. 6, 2016.

[156] S. Alexander and H. Alexander, "Lead genetic studies in Dictyostelium discoideum and translational studies in human cells demonstrate that sphingolipids are key regulators of sensitivity to cisplatin and other anticancer drugs," *Seminars in Cell and Developmental Biology*, vol. 22, no. 1. pp. 97–104, 2011.

[157] M. Steinert, "Pathogen?host interactions in Dictyostelium, Legionella, Mycobacterium and other pathogens," *Semin. Cell Dev. Biol.*, vol. 22, no. 1, pp. 70–76, Feb. 2011.

[158] J. D. Dunn *et al.*, "Eat prey, live: Dictyostelium discoideum as a model for cell-autonomous defenses," *Frontiers in Immunology*, vol. 8, no. JAN. 2018.

[159] W. F. Loomis, "Cell signaling during development of Dictyostelium.," *Dev. Biol.*, vol. 391, no. 1, pp. 1–16, Jul. 2014.

[160] L. Strmecki, D. M. Greene, and C. J. Pears, "Developmental decisions in Dictyostelium discoideum.," *Dev. Biol.*, vol. 284, no. 1, pp. 25–36, Aug. 2005.

[161]   P. Schaap, "Evolutionary crossroads in developmental biology: Dictyostelium discoideum.," *Development*, vol. 138, no. 3, pp. 387–96, Mar. 2011.

[162]   R. L. Chisholm and R. A. Firtel, "Insights into morphogenesis from a simple developmental system," *Nat. Rev. Mol. Cell Biol.*, vol. 5, no. 7, pp. 531–541, 2004.

[163]   A. Mesquita *et al.*, "Autophagy in Dictyostelium: Mechanisms, regulation and disease in a simple biomedical model.," *Autophagy*, vol. 13, no. 1, pp. 1–17, 2017.

[164]   E. Domínguez-Martín, E. Cardenal-Muñoz, J. King, T. Soldati, R. Coria, and R. Escalante, "Methods to Monitor and Quantify Autophagy in the Social Amoeba Dictyostelium discoideum," *Cells*, vol. 6, no. 3, p. 18, 2017.

[165]   A. Mesquita, L. C. Tábara, O. Martinez-Costa, N. Santos-Rodrigo, O. Vincent, and R. Escalante, "Dissecting the function of Atg1 complex in Dictyostelium autophagy reveals a connection with the pentose phosphate pathway enzyme transketolase," *Open Biol.*, vol. 5, no. 8, p. 150088, Aug. 2015.

[166]   J. Calvo-garrido *et al.*, "Genes and pathways , cell death and infection Autophagy in Dictyostelium," *Autophagy*, vol. 6, no. 6, pp. 686–701, 2010.

[167]   G. P. Otto, M. Y. Wu, N. Kazgan, O. R. Anderson, and R. H. Kessin, "Dictyostelium macroautophagy mutants vary in the severity of their developmental defects.," *J. Biol. Chem.*, vol. 279, no. 15, pp. 15621–9, May 2004.

[168]   J. Matthias, S. Meßling, and L. Eichinger, "The two Dictyostelium autophagy eight proteins , ATG8a and ATG8b , associate with the autophagosome in succession," *Eur. J. Cell Biol.*, vol. 95, no. 1, pp. 15–25, 2016.

[169]   G. P. Otto, M. Y. Wu, N. Kazgan, O. R. Anderson, and R. H. Kessin, "Macroautophagy is required for multicellular development of the social amoeba Dictyostelium discoideum.," *J. Biol. Chem.*, vol. 278, no. 20, pp. 17636–45, May 2003.

[170]   S. Muñoz-Braceras, R. Calvo, and R. Escalante, "TipC and the chorea-acanthocytosis protein VPS13A regulate autophagy in Dictyostelium and human HeLa cells.," *Autophagy*, vol. 11, no. 6, pp. 918–927, May 2015.

[171]   J. Calvo-Garrido, J. S. King, S. Muñoz-Braceras, and R. Escalante, "Vmp1 regulates PtdIns3P signaling during autophagosome formation in Dictyostelium discoideum," *Traffic*, vol. 11, pp. 1235–1246, Aug. 2014.

[172]   S. Carilla-Latorre, S. J. Annesley, S. Muñoz-Braceras, P. R. Fisher, and R. Escalante, "Ndufaf5 deficiency in the Dictyostelium model: new roles in autophagy and development.," *Mol. Biol. Cell*, vol. 24, no. 10, pp. 1519–28, 2013.

[173]   M. Cabral, C. Anjard, V. Malhotra, W. F. Loomis, and A. Kuspa, "Unconventional secretion of AcbA in Dictyostelium discoideum through a vesicular intermediate.," *Eukaryot. Cell*, vol. 9, no. 7, pp. 1009–17, 2010.

[174]   W. F. Whittingham and K. B. Raper, "Non-Viability of Stalk Cells in Dictyostelium.," *Proc. Natl. Acad. Sci. U. S. A.*, vol. 46, no. 5, pp. 642–9, 1960.

[175]   J.-P. Levraud, M. Adam, M.-F. Luciani, C. de Chastellier, R. L. Blanton, and P. Golstein, "Dictyostelium cell death: early emergence and demise of highly polarized paddle cells.," *J. Cell Biol.*, vol. 160, no. 7, pp. 1105–14, Mar. 2003.

[176]   B. Steiner *et al.*, "ER remodeling by the large GTPase atlastin promotes vacuolar growth of Legionella pneumophila," *EMBO Rep.*, vol. 18, no. 10, pp. 1–20, 2017.

[177] T. Morita, K. Saitoh, T. Takagi, and Y. Maeda, "Involvement of the glucose-regulated protein 94 (Dd-GRP94) in starvation response of Dictyostelium discoideum cells.," *Biochem. Biophys. Res. Commun.*, vol. 274, no. 2, pp. 323–31, Aug. 2000.

[178] J. Monnat *et al.*, "Dictyostelium discoideum protein disulfide isomerase, an endoplasmic reticulum resident enzyme lacking a KDEL-type retrieval signal.," *FEBS Lett.*, vol. 418, no. 3, pp. 357–62, Dec. 1997.

[179] J. Monnat, E. M. Neuhaus, M. S. Pop, D. M. Ferrari, B. Kramer, and T. Soldati, "Identification of a novel saturable endoplasmic reticulum localization mechanism mediated by the C-terminus of a Dictyostelium protein disulfide isomerase.," *Mol. Biol. Cell*, vol. 11, no. 10, pp. 3469–84, Oct. 2000.

[180] H. Adachi, T. Hasebe, K. Yoshinaga, T. Ohta, and K. Sutoh, "Isolation of Dictyostelium discoideum Cytokinesis Mutants by Restriction Enzyme-Mediated Integration of the Blasticidin S Resistance Marker," *Biochem. Biophys. Res. Commun.*, vol. 205, no. 3, pp. 1808–1814, 1994.

[181] D. A. Knecht, S. M. Cohen, W. F. Loomis, and H. F. Lodish, "Developmental regulation of Dictyostelium discoideum actin gene fusions carried on low-copy and high-copy transformation vectors.," *Mol. Cell. Biol.*, vol. 6, no. 11, pp. 3973–83, 1986.

[182] D. M. Veltman, G. Akar, L. Bosgraaf, and P. J. M. Van Haastert, "A new set of small, extrachromosomal expression vectors for Dictyostelium discoideum.," *Plasmid*, vol. 61, no. 2, pp. 110–8, Mar. 2009.

[183] J. Calvo-Garrido, S. Carilla-Latorre, A. Mesquita, and R. Escalante, "A proteolytic cleavage assay to monitor autophagy in dictyostelium discoideum," *Autophagy*, vol. 7, no. 9, pp. 1063–1068, 2011.

[184] J. Sambrook and D. W Russell, "Molecular Cloning: A Laboratory Manual," *Cold Spring Harb. Lab. Press. Cold Spring Harb. NY*, 2001.

[185] D. B. Flagfeldt, V. Siewers, L. Huang, and J. Nielsen, "Characterization of chromosomal integration sites for heterologous gene expression in Saccharomyces cerevisiae.," *Yeast*, vol. 26, no. 10, pp. 545–551, 2009.

[186] P. Gaudet, K. E. Pilcher, P. Fey, and R. L. Chisholm, "Transformation of Dictyostelium discoideum with plasmid DNA.," *Nat. Protoc.*, vol. 2, no. 6, pp. 1317–24, Jan. 2007.

[187] D. R. Cole Trapnell, Adam Roberts, Loyal Goff, Geo Pertea, Daehwan Kim and and L. P. Kelley, Harold Pimentel, Steven L Salzberg, John L Rinn, "Differential gene and transcript expression analysis of RNA-seq experiments with TopHat and Cufflinks," *Nat Protoc . ; 7(3) 562–578.*, vol. 7, no. 3, pp. 562–578, 2012.

[188] A. Parikh *et al.*, "Conserved developmental transcriptomes in evolutionarily divergent species.," *Genome Biol.*, vol. 11, no. 3, p. R35, 2010.

[189] D. W. Huang, B. T. Sherman, and R. A. Lempicki, "Systematic and integrative analysis of large gene lists using DAVID bioinformatics resources," *Nat. Protoc.*, vol. 4, no. 1, pp. 44–57, 2009.

[190] P. Fey, R. J. Dodson, S. Basu, and R. L. Chisholm, "One stop shop for everything Dictyostelium: DictyBase and the Dicty Stock Center in 2012," *Methods Mol. Biol.*, vol. 983, pp. 59–92, 2013.

[191] X. Huang and W. Miller, "A Time-Efficient, Linear-Space Local Similarity Algorithm," *Adv. Appl. Math.*, vol. 12, pp. 337–357, 1991.

[192] L. Duret, E. Gasteiger, and G. Perrière, "LalnView: a graphical viewer for pairwise sequence alignments," *Comput. Applic. Biosci.*, vol. 12, no. 507–510, 1996.

[193] F. Sievers *et al.*, "Fast, scalable generation of high-quality protein multiple sequence alignments

using Clustal Omega," *Mol. Syst. Biol.*, vol. 7, no. 1, pp. 539–539, 2014.

[194]   N. Hiramatsu, V. T. Joseph, and J. H. Lin, *Monitoring and Manipulating Mammalian Unfolded Protein Response*, 1st ed., vol. 491. Elsevier Inc., 2011.

[195]   M. Kwolek-Mirek and R. Zadrag-Tecza, "Comparison of methods used for assessing the viability and vitality of yeast cells," *FEMS Yeast Res.*, vol. 14, no. 7, pp. 1068–1079, 2014.

[196]   J. Nikawa, M. Akiyoshi, S. Hirata, and T. Fukuda, "Saccharomyces cerevisiae IRE2/HAC1 is involved in IRE1-mediated KAR2 expression," *Nucleic Acids Res.*, vol. 24, no. 21, 1996.

[197]   K. Kohno, "Stress-sensing mechanisms in the unfolded protein response: similarities and differences between yeast and mammals.," *J. Biochem.*, vol. 147, no. 1, pp. 27–33, Jan. 2010.

[198]   K. Arhzaouy *et al.*, "Heteromeric p97 / p97 R155C Complexes Induce Dominant Negative Changes in Wild-Type and Autophagy 9- Deficient Dictyostelium strains," *PLoS One*, vol. 7, no. 10, p. e46879, 2012.

[199]   N. R. Cohen, D. a Knecht, and H. F. Lodish, "Functional expression of rat GLUT 1 glucose transporter in Dictyostelium discoideum.," *Biochem. J.*, vol. 315, pp. 971–5, 1996.

[200]   M. Rai, Y. Xiong, and C. K. Singleton, "Disruption of the ifkA and ifkB genes results in altered cell adhesion, morphological defects and a propensity to form pre-stalk O cells during development of Dictyostelium," *Differentiation*, vol. 74, no. 9–10, pp. 583–595, 2006.

[201]   C. K. Singleton, Y. Xiong, J. H. Kirsten, and K. P. Pendleton, "eIF2α kinases regulate development through the BzpR transcription factor in Dictyostelium discoideum.," *PLoS One*, vol. 7, no. 3, p. e32500, Jan. 2012.

[202]   R. Yang, S. A. Wek, and R. C. Wek, "Glucose limitation induces GCN4 translation by activation of Gcn2 protein kinase.," *Mol. Cell. Biol.*, vol. 20, no. 8, pp. 2706–17, 2000.

[203]   R. M. Fox, C. D. Hanlon, and D. J. Andrew, "The CrebA/Creb3-like transcription factors are major and direct regulators of secretory capacity," *J. Cell Biol.*, vol. 191, no. 3, pp. 479–492, 2010.

[204]   G. Liang *et al.*, "Luman/CREB3 induces transcription of the endoplasmic reticulum (ER) stress response protein Herp through an ER stress response element.," *Mol. Cell. Biol.*, vol. 26, no. 21, pp. 7999–8010, 2006.

[205]   C. R. L. Thompson, Q. Fu, C. Buhay, R. R. Kay, and G. Shaulsky, "A bZIP/bRLZ transcription factor required for DIF signaling in Dictyostelium.," *Development*, 2004.

[206]   E. Huang, S. L. Blagg, T. Keller, M. Katoh, G. Shaulsky, and C. R. L. Thompson, "bZIP transcription factor interactions regulate DIF responses in Dictyostelium.," *Development*, vol. 133, no. 3, pp. 449–58, Feb. 2006.

[207]   Y. Yamada *et al.*, "The Dictyostelium prestalk inducer DIF-1 directs phosphorylation of a bZIP transcription factor," *Int. J. Dev. Biol.*, 2013.

[208]   E. Huang *et al.*, "BzpF is a CREB-like transcription factor that regulates spore maturation and stability in Dictyostelium," *Dev. Biol.*, vol. 358, no. 1, pp. 137–146, 2011.

[209]   W. Tirasophon, A. A. Welihinda, and R. J. Kaufman, "A stress response pathway from the endoplasmic reticulum to the nucleus requires a novel bifunctional protein kinase/endoribonuclease (Ire1p) in mammalian cells," *Genes Dev.*, vol. 12, no. 12, pp. 1812–1824, 1998.

[210]   W. Tirasophon, K. Lee, B. Callaghan, A. Welihinda, and R. J. Kaufman, "The endoribonuclease activity of mammalian IRE1 autoregulates its mRNA and is required for the unfolded protein response," *Genes Dev.*, vol. 14, no. 21, pp. 2725–2736, 2000.

[211]   A. V. Korennykh *et al.*, "The unfolded protein response signals through high-order assembly of Ire1," *Nature*, vol. 457, no. 7230, pp. 687–693, 2008.

[212]   H. Li, A. V Korennykh, S. L. Behrman, and P. Walter, "Mammalian endoplasmic reticulum stress sensor IRE1 signals by dynamic clustering.," *Proc. Natl. Acad. Sci. U. S. A.*, vol. 107, no. 37, pp. 16113–16118, 2010.

[213]   A. Mesquita, J. Calvo-garrido, S. Carilla-latorre, and R. Escalante, "Monitoring Autophagy in Dictyostelium," *Dictyostelium discoideum Protoc. Methods Mol. Biol.*, vol. 983, pp. 461–470, 2013.

[214]   A. Marchetti, E. Lelong, and P. Cosson, "A measure of endosomal pH by flow cytometry in Dictyostelium," *BMC Res. Notes*, 2009.

[215]   J. Calvo-garrido, S. Carilla-latorre, F. La, G. Egea, and R. Escalante, "Vacuole Membrane Protein 1 Is an Endoplasmic Reticulum Protein Required for Organelle Biogenesis , Protein Secretion , and Development," *Mol. Biol. Cell.*, vol. 19, no. August 2008, pp. 3442–3453, 2008.

[216]   L. C. Tabara and R. Escalante, "VMP1 establishes ER-microdomains that regulate membrane contact sites and autophagy," *PLoS One*, vol. 11, no. 11, pp. 1–20, 2016.

[217]   L.-C. Tábara, J.-J. Vicente, J. Biazik, E.-L. Eskelinen, O. Vincent, and R. Escalante, "Vacuole membrane protein 1 marks endoplasmic reticulum subdomains enriched in phospholipid synthesizing enzymes and is required for phosphoinositide distribution," *Traffic*, vol. 19, no. 8, pp. 624–638, Aug. 2018.

[218]   V. I. Korolchuk, A. Mansilla, F. M. Menzies, and D. C. Rubinsztein, "Autophagy Inhibition Compromises Degradation of Ubiquitin-Proteasome Pathway Substrates," *Mol. Cell*, vol. 33, no. 4, pp. 517–527, 2009.

[219]   I. Koyama-Honda, E. Itakura, T. K. Fujiwara, and N. Mizushima, "Temporal analysis of recruitment of mammalian ATG proteins to the autophagosome formation site," *Autophagy*, vol. 9, no. 10, pp. 1491–1499, 2013.

[220]   C. Kishi-Itakura, I. Koyama-Honda, E. Itakura, and N. Mizushima, "Ultrastructural analysis of autophagosome organization using mammalian autophagy-deficient cells," *J. Cell Sci.*, vol. 127, no. 22, pp. 4984–4984, 2014.

[221]   H. Bommiasamy *et al.*, "ATF6 induces XBP1-independent expansion of the endoplasmic reticulum," *J. Cell Sci.*, vol. 122, no. 10, pp. 1626–1636, 2009.

[222]   T. Garofalo *et al.*, "Evidence for the involvement of lipid rafts localized at the ER-mitochondria associated membranes in autophagosome formation," *Autophagy*, vol. 12, no. 6, pp. 917–935, 2016.

[223]   J. Ye *et al.*, "ER stress induces cleavage of membrane-bound ATF6 by the same proteases that process SREBPs," *Mol. Cell*, vol. 6, no. 6, pp. 1355–1364, 2000.

[224]   N. Schneider, J. M. Schwartz, J. Köhler, M. Becker, H. Schwarz, and G. Gerisch, "Golvesin-GFP fusions as distinct markers for Golgi and post-Golgi vesicles in Dictyostelium cells," *Biol. Cell*, vol. 92, no. 7, pp. 495–511, 2000.

[225]   M. a Kukuruzinska and P. W. Robbins, "Protein glycosylation in yeast: transcript heterogeneity of the ALG7 gene.," *Proc. Natl. Acad. Sci. U. S. A.*, vol. 84, no. 8, pp. 2145–9, Apr. 1987.

[226]   J. J. Credle, J. S. Finer-Moore, F. R. Papa, R. M. Stroud, and P. Walter, "On the mechanism of sensing unfolded protein in the endoplasmic reticulum.," *Proc. Natl. Acad. Sci. U. S. A.*, vol. 102, no. 52, pp. 18773–84, Dec. 2005.

[227]   C. Rubio, D. Pincus, A. Korennykh, S. Schuck, H. El-Samad, and P. Walter, "Homeostatic adaptation to endoplasmic reticulum stress depends on Ire1 kinase activity," *J. Cell Biol.*, vol. 193, no. 1, pp. 171–

184, 2011.

[228]   L. Zhang, C. Zhang, and A. Wang, "Divergence and Conservation of the Major UPR Branch IRE1-bZIP Signaling Pathway across Eukaryotes," *Sci. Rep.*, vol. 6, no. 1, p. 27362, 2016.

[229]   C. Y. Chow, X. Wang, D. Riccardi, M. F. Wolfner, and A. G. Clark, "The genetic architecture of the genome-wide transcriptional response to ER stress in the mouse," *PLoS Genet.*, vol. 11, no. 2, p. e1004924, 2015.

[230]   T. Miyazaki, H. Nakayama, Y. Nagayoshi, H. Kakeya, and S. Kohno, "Dissection of Ire1 functions reveals stress response mechanisms uniquely evolved in Candida glabrata.," *PLoS Pathog.*, vol. 9, no. 1, p. e1003160, Jan. 2013.

[231]   M. Smith and S. Wilkinson, "ER homeostasis and autophagy.," *Essays Biochem.*, vol. 61, no. 6, pp. 625–635, 2017.

[232]   Y. Nishida *et al.*, "Discovery of Atg5/Atg7-independent alternative macroautophagy," *Nature*, vol. 461, no. 7264, pp. 654–658, 2009.

[233]   S. Schuck, C. M. Gallagher, and P. Walter, "ER-phagy mediates selective degradation of endoplasmic reticulum independently of the core autophagy machinery.," *J. Cell Sci.*, vol. 127, no. Pt 18, pp. 4078–88, 2014.

[234]   A. P. Velázquez and M. Graef, "Autophagy regulation depends on ER homeostasis controlled by lipid droplets.," *Autophagy*, p. 0, May 2016.

[235]   D. Bailey and P. O'Hare, "Transmembrane bZIP transcription factors in ER stress signaling and the unfolded protein response.," *Antioxid. Redox Signal.*, vol. 9, no. 12, pp. 2305–21, 2007.

[236]   G. D. Amoutzias *et al.*, "One billion years of bZIP transcription factor evolution: Conservation and change in dimerization and DNA-binding site specificity," *Mol. Biol. Evol.*, vol. 24, no. 3, pp. 827–835, 2007.

[237]   J.-X. Liu, R. Srivastava, P. Che, and S. H. Howell, "An endoplasmic reticulum stress response in Arabidopsis is mediated by proteolytic processing and nuclear relocation of a membrane-associated transcription factor, bZIP28.," *Plant Cell*, vol. 19, no. 12, pp. 4111–9, Dec. 2007.

[238]   P. J. Seo, S. G. Kim, and C. M. Park, "Membrane-bound transcription factors in plants," *Trends Plant Sci.*, vol. 13, no. 10, pp. 550–556, 2008.

[239]   L. Eichinger *et al.*, "The genome of the social amoeba Dictyostelium discoideum," *Nature*, vol. 435, no. 7038, pp. 43–57, May 2005.

[240]   A. Radhakrishnan, L. P. Sun, P. J. Espenshade, J. L. Goldstein, and M. S. Brown, *The SREBP pathway. gene regulation through sterol sensing and gated protein trafficking*, Second Edi., vol. 3. Elsevier Inc., 2010.

[241]   A. L. Hughes, B. L. Todd, and P. J. Espenshade, "SREBP pathway responds to sterols and functions as an oxygen sensor in fission yeast," *Cell*, vol. 120, no. 6, pp. 831–842, 2005.

[242]   J.-X. Liu, R. Srivastava, P. Che, and S. H. Howell, "Salt stress responses in Arabidopsis utilize a signal transduction pathway related to endoplasmic reticulum stress signaling.," *Plant J.*, vol. 51, no. 5, pp. 897–909, 2007.

APÉNDICE I

Grupos de términos de ontología génica (GO) enriquecidos en el conjunto de genes cuya expresión cambió ante un tratamiento con tunicamicina en la cepa silvestre (WT)

Se muestran a continuación las tablas que se obtuvieron mediante un análisis con la herramienta informática DAVID (https://david.ncifcrf.gov). A partir de estos resultados se generó la **Figura 17**. Estas tablas contienen los términos GO enriquecidos en cada grupo, respectivamente para las categorías GO de Proceso Biológico, Dominio Proteico y Componente Celular. Se muestra el nivel de enriquecimiento (score) de cada grupo, así como los estadísticos (P-value, Benjamini) arrojados. También se señala el número de genes contenidos en cada grupo, su identificador, una descripción breve de cada uno, el cambió que se presentó en su abundancia, y si este cambio se generó de forma dependiente de IreA. El código de color resalta el nivel de cambio en la expresión. Los textos se encuentran en inglés.

Transcritos cuya expresión aumentó
Grupos obtenidos para la categoría Proceso Biológico

Cluster 1		Enrichment score:	1.46	
GO terms:		P value:	Benjamini:	genes/term
	response to endoplasmic reticulum stress	7.40E-03	2.30E-01	3
	protein folding	3.70E-02	5.80E-01	5
	cell redox homeostasis	1.50E-01	8.70E-01	3
Gene ID	Description	IreA depend	Log2(Fold Change)	
DDB_G0282313	heat shock protein DnaJ family protein	yes	1.3874	
DDB_G0293378	Thioredoxin domain-containing protein 5	no	1.35265	
DDB_G0283539	Calreticulin, calcium binding protein (crtA)	no	1.51079	
DDB_G0276141	protein disulfide isomerase(pdi1)	no	1.6439	
DDB_G0291434	protein disulfide isomerase(pdi2)	no	1.49158	

Cluster 2		Enrichment score:	0.93	
		P value:	Benjamini:	genes/term
GO terms:	positive regulation of proteasomal ubiquitin-dependent protein catabolic process	3.20E-02	5.90E-01	3
Gene ID	Description	IreA depend	Log2(Fold Change)	
DDB_G0292120	RING zinc finger-containing protein(cnrK)	no	1.72858	
DDB_G0270130	ubiquitin-protein ligase	yes	1.6868	
DDB_G0275171	Translation termination inhibitor protein ITT1, ubiquitin-protein ligase	no	1.79961	

Cluster 3		Enrichment score:	0.63	
		P value:	Benjamini:	genes/term
GO terms:	intracellular protein transport	8.10E-02	7.70E-01	5
	culmination involved in sorocarp development	1.60E-01	8.70E-01	4
	transport	2.00E-01	8.90E-01	10
Gene ID	Description	IreA depend	Log2(Fold Change)	
DDB_G0293416	ABC transporter B family protein(abcB1)	no	1.78039	
DDB_G0286559	ABC transporter C family protein(abcC5)	yes	1.58732	
DDB_G0292986	ABC transporter G family protein(abcG10)	yes	1.30967	
DDB_G0269206	ABC transporter G family protein(abcG21)	no	1.52133	
DDB_G0289675	ADP-ribosylarginine hydrolase(adprh)	no	1.50015	
DDB_G0278477	ARF/SAR superfamily protein(sarB)	no	3.22468	
DDB_G0269942	Vesicle-trafficking protein SEC22b,SNARE protein	no	1.82048	
DDB_G0281985	Protein transport protein SEC23,G-protein modulator	no	1.98019	
DDB_G0277797	Sec24CD ortholog, isoform C (sec24l) ,vesicle coat protein	no	1.4186	
DDB_G0293364	peptidase M8, leishmanolysin family protein(sigB)	no	1.72938	
DDB_G0277377	signal recognition particle receptor alpha subunit(srpR)	no	1.38382	

Grupos obtenidos para la categoría Dominio Proteico

Cluster 1		Enrichment score:	2.45		
			P value:	Benjamini:	genes/term
GO terms:	Alpha/beta hydrolase fold-3		3.50E-03	2.50E-01	3
Gene ID	Description		IreA depende	Log2(Fold Change)	
DDB_G0287609	alpha/beta hydrolase fold-3 domain-containing protein, lipase, vegetative-specific protein		no	1.76497	
DDB_G0290975	alpha/beta hydrolase fold-3 domain-containing protein, lipase, vegetative-specific protein		yes	1.69352	
DDB_G0291121	esterase/lipase/thioesterase domain-containing protein(cinB), vegetative-specific protein		yes	1.73016	

Cluster 2		Enrichment score:	1.58		
			P value:	Benjamini:	genes/term
GO terms:	Ubiquitin-conjugating enzyme/RWD-like		2.50E-03	2.70E-01	5
Gene ID	Description		IreA depende	Log2(Fold Change)	
DDB_G0270130	ubiquitin-protein ligase		yes	1.6868	
DDB_G0275171	Translation termination inhibitor protein ITT1, ubiquitin-protein ligase		no	1.79961	
DDB_G0281833	ligase		no	2.15756	
DDB_G0288381	unkown function		no	2.68616	
DDB_G0288697	unkown function		no	2.59869	

Cluster 3		Enrichment score:	1.58		genes/term
			P value:	Benjamini:	4
GO terms:	Ubiquitin family		1.20E-02	4.60E-01	
Gene ID	Description		IreA depende	Log2(Fold Change)	
DDB_G0289449	Polyubiquitin-F (ubqF)		yes	1.32449	
DDB_G0279721	Polyubiquitin-H (ubqH)		yes	1.80215	
DDB_G0269458	Polyubiquitin-J(ubqJ)		yes	1.92808	
DDB_G0269462	ubiquitin domain-containing protein, ribosomal protein		yes	2.22062	

Cluster 4		Enrichment score:	1.23		
GO terms:	DnaJ domain, conserved site		P value:	Benjamini:	genes/term
			2.50E-02	6.50E-01	3
Gene ID	Description		IreA depende	Log2(Fold Change)	
DDB_G0286251	DNAJ heat shock N-terminal domain-containing protein(dnajc3)		no	1.87963	
DDB_G0282313	heat shock protein DnaJ family protein		yes	1.3874	
DDB_G0281775	DnaJ homolog subfamily B member 14		no	1.35966	

Cluster 5		Enrichment score:	1.18		
			P value:	Benjamini:	genes/term
GO terms:	Thioredoxin, conserved site		8.20E-03	4.00E-01	3
Gene ID	Description		IreA depende	Log2(Fold Change)	
DDB_G0293378	Protein disulfide-isomerase TMX3		no	1.35265	
DDB_G0276141	protein disulfide isomerase(pdi1)		no	1.6439	
DDB_G0291434	protein disulfide isomerase(pdi2)		no	1.49158	

Cluster 6		Enrichment score:	0.64		
GO terms:	ABC transporter-like		P value:	Benjamini:	genes/term
			9.70E-02	8.60E-01	4
Gene ID	Description		IreA depende	Log2(Fold Change)	
DDB_G0293416	ABC transporter B family protein(abcB1)		no	1.78039	
DDB_G0286559	ABC transporter C family protein(abcC5)		yes	1.58732	
DDB_G0292986	ABC transporter G family protein(abcG10)		yes	1.30967	
DDB_G0269206	ABC transporter G family protein(abcG21)		no	1.52133	

Grupos obtenidos para la categoría de Componente Celular

Cluster 1			Enrichment score:	3.13		
						genes/term
GO terms:	endoplasmic reticulum			4.60E-11	2.70E-09	19
Gene ID	Description			IreA depend	Log2(Fold Change)	
DDB_G0278477	ARF/SAR superfamily protein(sarB)			no	3.22468	
DDB_G0270946	C-4 methyl sterol oxidase(DDB_G0270946)			no	1.57809	
DDB_G0286251	DNAJ heat shock N-terminal domain-containing protein(dnajc3)			no	1.87963	
DDB_G0284777	DUF1183 family protein(DDB_G0284777)			no	1.8708	
DDB_G0276445	Heat shock protein Hsp70 family protein, highly similar to human HSPA5(78 kDa glucose-regulated protein GRP78)			no	3.23801	
DDB_G0287617	Bax inhibitor 1 homolog			no	1.8821	
DDB_G0291436	Dehydrodolichyl diphosphate synthetase			yes	1.977	
DDB_G0293378	Thioredoxin domain-containing protein 5			no	1.35265	
DDB_G0283539	Calreticulin, calcium binding protein (crtA)			no	1.51079	
DDB_G0288833	Probable derlin-1 homolog (derl1)			no	1.59401	
DDB_G0285131	Probable derlin-2 homolog (derl2)			yes	1.36	
DDB_G0281985	Protein transport protein SEC23,G-protein modulator			no	1.98019	
DDB_G0282197	membrane bound O-acyl transferase family protein			no	1.47533	
DDB_G0278371	microsomal signal peptidase subunit(spc1)			no	2.15796	
DDB_G0290227	nuclear protein localization 4(npl4)			no	2.12259	
DDB_G0276141	protein disulfide isomerase(pdi1)			no	2.82128	
DDB_G0291434	protein disulfide isomerase(pdi2)			no	2.72951	
DDB_G0277377	signal recognition particle receptor alpha subunit(srpR)			no	2.24317	
DDB_G0278543	signal recognition particle receptor beta subunit(srpRB)			no	1.40401	

Cluster 2			Enrichment score:	0.48		
				P value:	Benjamini:	genes/term
GO terms:	ubiquitin ligase complex			9.60E-02	6.20E-01	3
Gene ID	Description			IreA depend	Log2(Fold Change)	
DDB_G0292120	RING zinc finger-containing protein(cnrK)			yes	1.72858	
DDB_G0270130	ubiquitin-protein ligase			yes	1.6868	
DDB_G0275171	Translation termination inhibitor protein ITT1, ubiquitin-protein ligase			no	1.79961	

Cluster 3			Enrichment score:	0.48		
				P value:	Benjamini:	genes/term
GO terms:	cytoplasm			4.80E-01	9.60E-01	19
Gene ID	Description			IreA depend	Log2(Fold Change)	
DDB_G0278079	3'-5' exonuclease domain-containing protein(exdl2A)			yes	1.64246	
DDB_G0267468	BRCT domain-containing protein(adprt4)			no	1.64246	
DDB_G0292120	RING zinc finger-containing protein(cnrK)			no	1.72858	
DDB_G0285725	deoxyhypusine synthase(dhps)			yes	1.69581	
DDB_G0270130	ubiquitin-protein ligase			yes	1.6868	
DDB_G0275171	Translation termination inhibitor protein ITT1, ubiquitin-protein ligase			no	1.79961	
DDB_G0278757	DIS3-like exonuclease 2			yes	1.62565	
DDB_G0282033	ribonucleoprotein			yes	1.38233	
DDB_G0282867	lyase			yes	1.76746	
DDB_G0286271	unknown function			yes	1.30219	
DDB_G0288381	unknown function			no	2.68616	
DDB_G0288697	unknown function			no	2.59869	
DDB_G0287977	Formimidoyltransferase-cyclodeaminase (ftcd), deaminase transferase			no	2.15983	
DDB_G0279289	Phosphomannomutase 1 (pmmA)			no	1.81886	
DDB_G0289449	Polyubiquitin-F(ubqF)			no	1.32449	
DDB_G0279721	Polyubiquitin-H (ubqH)			no	1.80215	
DDB_G0269458	Polyubiquitin-J (ubqJ)			no	1.92808	
DDB_G0288011	methyltransferase type 11 domain-containing protein			yes	1.28824	
DDB_G0282007	peptidase C12 family protein(uch1)			no	3.092	
DDB_G0269454	tryptophan-tRNA ligase(trpS)			no	1.91549	

Transcritos cuya expresión disminuyó
Grupos obtenidos para la categoría Proceso Biológico

Cluster 1		Enrichment score:	3.18		
		P value:		Benjamini:	genes/term
GO terms:	peptidoglycan catabolic process		2.40E-04	1.00E-02	5
	cytolysis		3.30E-04	1.10E-02	5
	cell wall macromolecule catabolic process		3.80E-03	7.80E-02	4
	defense response to bacterium		5.10E-03	9.20E-02	5
Gene ID	Description	IreA dependent	Log2(Fold Change)		
DDB_G0274181	glycoside hydrolase family 25 protein	no	-3.13683		
DDB_G0293492	glycoside hydrolase family 25 protein	no	-3.02809		
DDB_G0293566	glycoside hydrolase family 25 protein	no	-2.29178		
DDB_G0275123	Lysozyme A (alyA)	no	-3.28988		
DDB_G0275121	LysozymeC (alyC)	no	-2.88526		
DDB_G0288143	LysozymeC protein	no	-2.78539		

Cluster 2		Enrichment score:	1.95		
		P value:		Benjamini:	genes/term
GO terms:	lipid catabolic process		8.40E-03	1.20E-01	4
Gene ID	Description	IreA dependent	Log2(Fold Change)		
DDB_G0276767	phospholipase B(plbA)	no	-2.04E+00		
DDB_G0277455	phospholipase B-like protein(plbE)	no	-1.6606		
DDB_G0275125	phospholipase B-like protein(plbF)	no	-2.59093		
DDB_G0287649	phospholipase D3(pldY)	no	-3.52942		

Cluster 3		Enrichment score:	1.46		
		P value:		Benjamini:	genes/term
GO terms:	endocytosis		1.10E-03	2.70E-02	7
	phagocytosis		7.60E-03	1.20E-01	8
	phototaxis		4.60E-02	4.00E-01	4
	cell morphogenesis		5.80E-02	4.50E-01	4
	hyperosmotic response		6.20E-02	4.60E-01	5
	mitotic cytokinesis		9.60E-02	5.60E-01	6
Gene ID	Description	IreA dependent	Log2(Fold Change)		
DDB_G0280621	ADP-ribosylation factor-related(arrJ)	yes	-1.9442		
DDB_G0280633	ADP-ribosylation factor-related(arrK)	yes	-2.07811		
DDB_G0291356	G-protein-coupled receptor family 3 protein 5(grlE)	yes	-1.5342		
DDB_G0268622	Rho GTPase(rac1B)	yes	-2.77696		
DDB_G0270430	WH2 domain-containing protein(wipA)	no	-1.74977		
DDB_G0287297	endosomal membrane protein(p80)	yes	-2.75389		
DDB_G0288879	Actin(act11)	no	-1.3302		
DDB_G0274727	Actin(act19)	no	-1.6916		
DDB_G0289507	Actin (act25)	no	-1.51364		
DDB_G0289005	Actin (act4)	no	-1.45781		
DDB_G0269234	Actin (act8)	no	-1.46722		
DDB_G0275123	Lysozyme A (alyA)	no	-3.28988		
DDB_G0271916	null mutant has aberrant RaTiO of prespore to prestalk c	yes	-3.61119		
DDB_G0287363	integrin beta A-like protein(sibA)	yes	-1.61654		
DDB_G0282993	superoxide dismutase(sodC)	no	-2.01024		

Grupos obtenidos para la categoría Dominio Proteico

Cluster 1		Enrichment score:	9.69		
			P value:	Benjamini:	Genes
GO terms:	Glycoside hydrolase, superfamily		8.80E-12	2.10E-09	14
Gene ID	Description		IreA dependen	Log2(Fold Change)	
cf45-1	component of the counting factor complex(cf45-1)		no	-2.97832	
DDB_G0270074	unknown function		no	-2.75457	
DDB_G0274181	glycoside hydrolase family 25 protein		no	-3.13683	
DDB_G0281609	unknown function		no	-3.37302	
DDB_G0288289	beta-xylosidase-like protein		yes	-1.42778	
DDB_G0293428	unknown function		yes	-1.51422	
DDB_G0293492	glycoside hydrolase family 25 protein		no	-3.02809	
DDB_G0293566	glycoside hydrolase family 25 protein		no	-2.29178	
gaa	alpha-glucoside hydrolase(gaa)		no	-2.19737	
glb1	glycoside hydrolase family 35 protein(glb1)		yes	-1.55762	
gluA	beta glucosidase(gluA)		yes	-2.22741	
melA	alpha-galactosidase (melibiase)		yes	-3.04273	
nagA	glycoside hydrolase family 20 protein(nagA)		no	-2.78143	
veg111	hyaluronidase(veg111)		no	-3.4379	

Cluster 2		Enrichment score:	5.11		
			P value:	Benjamini:	Genes
GO terms:	CMP/dCMP deaminase, zinc-binding		2.10E-06	1.60E-04	6
Gene ID	Description		IreA dependen	Log2(Fold Change)	
DDB_G0272030	unknown function		no	-2.58995	
DDB_G0272442	unknown function		yes	-5.52682	
DDB_G0282171	unknown function		no	-3.08296	
DDB_G0288019	CMP/dCMP deaminase, zinc-binding domain-containing protein		yes	-2.61533	
DDB_G0292080	unknown function		no	-4.87501	
DDB_G0292096	unknown function		no	-1.44521	

Cluster 3		Enrichment score:	3.53		
GO terms:	Carboxylesterase type B, active site		P value:	Benjamini:	Genes
			2.50E-04	1.00E-02	4
Gene ID	Description		IreA dependen	Log2(Fold Change)	
DDB_G0283087	carboxylesterase, type B family protein		no	-1.33763	
DDB_G0285419	crystal protein(cryS)		yes	-2.61413	
DDB_G0283085	type-B carboxylesterase/lipase family protein D2		yes	-1.73	
DDB_G0276969	unknown function		yes	-3.68922	

Cluster 4		Enrichment score:	2.47		
GO terms:	Actin/actin-like conserved site		P value:	Benjamini:	Genes
			1.80E-03	4.30E-02	5
Gene ID	Description		IreA dependen	Log2(Fold Change)	
DDB_G0288879	Actin(act11)		no	-1.3302	
DDB_G0274727	Actin(act19)		no	-1.6916	
DDB_G0289507	Actin (act25)		no	-1.51364	
DDB_G0289005	Actin (act4)		no	-1.45781	
DDB_G0269234	Actin (act8)		no	-1.46722	

Cluster 5		Enrichment score:	2.04		
			P value:	Benjamini:	Genes
GO terms:	Saposin B		1.60E-03	4.20E-02	5
Gene ID	Description		IreA dependen	Log2(Fold Change)	
DDB_G0286653	saposin-like protein O (aplO)		no	-1.76455	
DDB_G0276479	countin3 (ctnC)		no	-5.22584	
DDB_G0284339	saposin B domain-containing protein		no	-1.65269	
DDB_G0292508	saposin B domain-containing protein		no	-3.33222	

Cluster 6		Enrichment score:	0.9		
			P value:	Benjamini:	Genes
GO terms:	P-loop containing nucleoside triphosphate hydrolases		2.50E-02	3.20E-01	8
Gene ID	Description		IreA dependen	Log2(Fold Change)	
DDB_G0274115	ABC transporter G family protein(abcG12)		no	-1.38208	
DDB_G0267432	ABC transporter G family protein(abcG15)		no	-1.43758	
DDB_G0280621	ADP-ribosylation factor-related(arrJ)		yes	-1.9442	
DDB_G0280633	ADP-ribosylation factor-related(arrK)		yes	-2.07811	
DDB_G0281559	CHR group protein(DG1080)		no	-1.77017	
DDB_G0283911	HSP20-like chaperone domain-containing protein(DDB_G0283911)		yes	-1.66108	
DDB_G0270126	Ras GTPase(rasY)		yes	-2.16568	
DDB_G0270140	Ras GTPase(rasZ)		yes	-3.38974	
DDB_G0268622	Rho GTPase(rac1B)		yes	-2.77696	
DDB_G0282365	Rho GTPase(rac1C)		no	-2.18324	
DDB_G0269176	Rho GTPase(racF1)		yes	-3.41783	
DDB_G0276967	Rho GTPase(racF2)		yes	-4.41285	
DDB_G0268504	hypothetical protein(DDB_G0268504)		yes	-2.32121	
DDB_G0275033	hypothetical protein(DDB_G0275033)		yes	-2.21441	
DDB_G0276097	hypothetical protein(DDB_G0276097)		no	-3.287	
DDB_G0292188	hypothetical protein(DDB_G0292188)		yes	-1.55995	

Grupos obtenidos para la categoría de Componente Celular

Cluster 1		Enrichment score:		16.52	
		P value:		Benjamini:	Genes
GO terms:	extracellular space/extracellular region		4.60E-25	3.20E-23	62
Gene ID	Description	IreA dependent		Log2(Fold Change)	
DDB_G0291255	Sct family protein B (29C)	no		-2.24492	
DDB_G0281663	PhoPQ-activated pathogenicity-related protein(aprA)	no		-2.23199	
DDB_G0285793	calcium-dependent cell adhesion molecule-1(cadA)	no		-1.71061	
DDB_G0269248	component of the counting factor complex(cf45-1)	no		-2.97832	
DDB_G0284363	component of the counting factor complex(cf60)	no		-1.65896	
DDB_G0276479	countin3 (ctnC)	no		-5.22584	
DDB_G0279411	cathepsin D(ctsD)	no		-1.84844	
DDB_G0293538	acid ceramidase(dcd2A)	yes		-1.61977	
DDB_G0270214	galactose-binding domain-containing protein(DD7-1)	no		-2.91803	
DDB_G0267570	unknown function	no		-4.03097	
DDB_G0268828	unknown function	yes		-1.51389	
DDB_G0268870	unknown function	yes		-2.18222	
DDB_G0269040	C-type lectin domain-containing protein(DDB_G0269040)	yes		-2.32201	
DDB_G0270074	unknown function	no		-2.75457	
DDB_G0272238	unknown function	no		-1.98769	
DDB_G0272504	unknown function	yes		-2.5456	
DDB_G0272767	unknown function	no		-1.33441	
DDB_G0274181	glycoside hydrolase family 25 protein(DDB_G0274181)	no		-3.13683	
DDB_G0278243	unknown function	no		-1.318	
DDB_G0279985	unknown function	no		-1.41385	
DDB_G0280159	unknown function	yes		-2.3614	
DDB_G0281067	unknown function	yes		-1.61058	
DDB_G0281609	unknown function	no		-3.37302	
DDB_G0281843	unknown function	no		-2.61997	
DDB_G0281861	unknown function	yes		-3.20691	
DDB_G0281967	unknown function	no		-1.93049	
DDB_G0283087	carboxylesterase, type B family protein(DDB_G0283087)	no		-1.33763	
DDB_G0283127	unknown function	no		-1.58321	
DDB_G0284671	unknown function	no		-3.80238	
DDB_G0284691	unknown function	yes		-2.32789	
DDB_G0284805	unknown function	no		-1.59825	
DDB_G0286021	unknown function	no		-1.76986	
DDB_G0287399	unknown function	no		-2.93815	
DDB_G0288143	lysozyme C family protein(DDB_G0288143)	no		-2.78539	
DDB_G0288563	unknown function	yes		-1.45953	
DDB_G0289015	unknown function	no		-3.14567	
DDB_G0289171	unknown function	no		-2.42769	
DDB_G0290387	unknown function	yes		-2.59397	
DDB_G0290409	unknown function	no		-1.79504	
DDB_G0291394	unknown function	no		-1.84534	
DDB_G0292096	unknown function	yes		-2.79784	
DDB_G0292630	unknown function	yes		-2.04381	
DDB_G0293066	unknown function	no		-5.53097	
DDB_G0293204	unknown function	yes		-1.96126	
DDB_G0293428	unknown function	yes		-1.51422	
DDB_G0293460	unknown function	no		-1.48208	
DDB_G0293492	glycoside hydrolase family 25 protein(DDB_G0293492)	no		-3.02809	
DDB_G0293566	glycoside hydrolase family 25 protein(DDB_G0293566)	no		-2.29178	
DDB_G0269790	alpha-glucoside hydrolase(gaa)	no		-2.19737	
DDB_G0290217	glycoside hydrolase family 35 protein(glb1)	yes		-1.55762	

Gene ID	Description	IreA dependent	Log2(Fold Change)	
DDB_G0292810	beta glucosidase(gluA)	yes	-2.22741	
DDB_G0286015	homologous to the Chlamydomonas reinhardtii a2gene (gmsA)	yes	-4.58878	
DDB_G0279921	glycoprotein 130(gp130)	no	-2.52731	
DDB_G0276767	phospholipase B(plbA)	no	-1.6606	
DDB_G0277455	phospholipase B-like protein(plbE)	no	-2.04289	
DDB_G0275125	phospholipase B-like protein(plbF)	no	-2.59093	
DDB_G0287649	phospholipase D3(pldY)	no	-3.52942	
DDB_G0278581	PA14 domain-containing protein(psiF)	no	-2.0081	
DDB_G0287363	integrin beta A-like protein(sibA)	yes	-1.61654	
DDB_G0287587	small aggregate formation protein(smlA)	no	-1.36256	
DDB_G0283021	superoxide dismutase(sodB)	no	-2.38531	
DDB_G0282371	hyaluronidase(veg111)	no	-3.4379	
Cluster 2		Enrichment score:	1.73	
GO terms:	plasma membrane	P value:	Benjamini:	Genes
		6.90E-04	9.50E-03	21
Gene ID	Description	IreA dependent	Log2(Fold Change)	
abcG12	ABC transporter G family protein(abcG12)	yes	-1.38208	
abcG15	ABC transporter G family protein(abcG15)	no	-1.43758	
amtA	ammonium transporter(amtA)	no	-1.35858	
cadA	calcium-dependent cell adhesion molecule-1(cadA)	no	-1.71061	
DDB_G0281967	unknown function	no	-1.93049	
DDB_G0292424	unknown function	no	-3.33222	
DDB_G0281967	unknown function	no	-1.93049	
DDB_G0292424	unknown function	no	-3.33222	
erg2	C-8 sterol isomerase(erg2)	yes	-1.97652	
gp130	glycoprotein 130(gp130)	no	-2.52731	
ponA	actin binding protein(ponA)	no	-3.12854	
ponL	ponticulin-related protein(ponL)	no	-1.37502	
rac1B	Rho GTPase(rac1B)	yes	-2.77696	
rac1C	Rho GTPase(rac1C)	no	-2.18324	
racF2	Rho GTPase(racF2)	yes	-4.41285	
rasY	Ras GTPase(rasY)	yes	-2.16568	
rasZ	Ras GTPase(rasZ)	yes	-3.38974	
rhgA	Rh-like protein/ammonium transporter(rhgA)	no	-1.32908	
sibA	integrin beta A-like protein(sibA)	yes	-1.61654	
sodB	superoxide dismutase(sodB)	no	-2.38531	
sodC	superoxide dismutase(sodC)	no	-2.01024	

Cluster 3		Enrichment score:	1.4		
GO terms:		P value:		Benjamini:	Genes
	actin filament		6.20E-04	1.10E-02	6
	cell-cell contact zone		4.50E-03	5.10E-02	5
	phagocytic vesicle		1.30E-02	1.20E-01	16
	cell pole		3.00E-02	2.10E-01	4
	cell leading edge		3.30E-02	2.00E-01	6
Gene ID	Description	IreA dependent		Log2(Fold Change)	
abpB	34 kDa actin-binding protein(abpB)	yes		-3.30548	
act11	Actin(act11)	no		-1.8574	
act19	Actin(act19)	no		-1.3302	
act25	Actin (act25)	no		-1.6916	
act4	Actin (act4)	no		-1.51364	
act8	Actin (act8)	no		-1.45781	
cadA	calcium-dependent cell adhesion molecule-1(cadA)	no		-2.07811	
DDB_G0267992	unknown function	yes		-4.03097	
DDB_G0268064	esterase/lipase/thioesterase domain-containing protein	no		-2.19302	
DDB_G0274705	unknown function	yes		-1.73455	
DDB_G0281067	unknown function	yes		-3.77692	
DDB_G0281659	unknown function	no		-2.90256	
DDB_G0283911	HSP20-like chaperone domain-containing protein	yes		-1.89906	
DDB_G0284339	saposin B domain-containing protein	no		-1.65269	
DDB_G0286653	unknown function	no		-1.49562	
DDB_G0292508	saposin B domain-containing protein	no		-3.33222	
DDB_G0293202	TRAF-type zinc finger-containing protein	yes		-5.53097	
eif5a	eukaryotic translation initiation factor 5A(eif5a)	yes		-1.73893	
fimA	actin binding protein(fimA)	no		-1.38849	
gp130	glycoprotein 130(gp130)	no		-4.58878	
guaA	GMP synthetase(guaA)	no		-1.5342	
lmpB	lysosomal integral membrane glycoprotein(lmpB)	yes		-1.66478	
maspS	aspartate-tRNA ligase(maspS)	no		-3.80754	
melA	alpha-galactosidase (melibiase)	yes		-1.70416	
mkcD	MKC subfamily protein kinase(mkcD)	yes		-3.04273	
panC	pantoate-beta-alanine ligase(panC)	no		-2.75389	
pefA	penta EF hand calcium binding protein(pefA)	no		-4.80573	
ponA	actin binding protein(ponA)	no		-3.52942	
rtoA	contains several repeats of a serine-rich motif, catalyzes the fusion of	yes		-3.91052	
smlA	small aggregate formation protein(smlA)	no		-1.63354	
sodB	superoxide dismutase(sodB)	no		-1.36256	
sodC	superoxide dismutase(sodC)	no		-2.38531	
wipA	WH2 domain-containing protein(wipA)	no		-3.4379	

Cluster 4		Enrichment score:	1.4		
GO terms:		P value:		Benjamini:	Genes
	membrane		1.50E-01	5.00E-01	71
abcG12	ABC transporter G family protein(abcG12)	no		-1.38208	
abcG15	ABC transporter G family protein(abcG15)	no		-1.43758	
abkD	ABC1 family protein kinase(abkD)	no		-1.57887	
amtA	ammonium transporter(amtA)	no		-1.35858	
cadA	calcium-dependent cell adhesion molecule-1(cadA)	no		-1.71061	
cryS	crystal protein(cryS)	yes		-2.61413	
D2	type-B carboxylesterase/lipase family protein D2 (D2)	yes		-1.73	
DD3-3	similar to tunicate proteins(DD3-3)	yes		-1.74962	
DDB_G0268026	unknown function	yes		-2.19302	
DDB_G0268862	unknown function	no		-2.71018	
DDB_G0268892	unknown function	no		-2.0129	
DDB_G0268970	unknown function	no		-1.95206	
DDB_G0269488	unknown function	no		-1.33191	
DDB_G0269850	DG1041 family protein	no		-1.68994	
DDB_G0272012	GNS1/SUR4 family protein	no		-2.17183	
DDB_G0270192	unknown function	no		-1.46599	
DDB_G0272342	unknown function	yes		-1.43968	
DDB_G0272380	unknown function	yes		-2.16328	
DDB_G0272492	unknown function	yes		-2.89264	
DDB_G0274479	unknown function	yes		-2.42444	
DDB_G0275049	short-chain dehydrogenase/reductase family protein	no		-1.69684	
DDB_G0276097	unknown function	no		-3.287	
DDB_G0276781	unknown function	yes		-1.40141	
DDB_G0276931	unknown function	yes		-1.77722	
DDB_G0277895	TM2 domain containing protein	yes		-2.19484	
DDB_G0278577	unknown function	no		-3.02385	
DDB_G0278699	unknown function	no		-1.5451	
DDB_G0278835	unknown function	no		-1.98572	
DDB_G0279985	unknown function	no		-1.41385	
DDB_G0281067	unknown function	yes		-1.61058	
DDB_G0283271	DOMON related domain-containing protein	no		-3.45257	
DDB_G0283913	heat shock protein Hsp20 domain-containing protein	yes		-1.63801	
DDB_G0284169	unknown function	yes		-1.65269	

DDB_G0284367	phosphoesterase, PA-phosphatase related-family protein	yes	-1.64383
DDB_G0284691	unknown function	yes	-2.32789
DDB_G0286021	unknown function	no	-1.76986
DDB_G0286897	unknown function	yes	-2.111
ddb_G0287003	DUF914 family protein	no	-1.72543
DDB_G0287933	unknown function	no	-2.59146
DDB_G0288435	unknown function	yes	-1.42778
DDB_G0288635	transmembrane protein	no	-1.59524
DDB_G0290177	unknown function	yes	-3.02142
DDB_G0290379	unknown function	no	-2.84026
DDB_G029040	C-type lectin domain-containing protein	no	-1.79504
DDB_G0291574	unknown function	no	-2.4019
DDB_G0292424	unknown function	no	-3.33222
DDB_G0292764	unknown function	no	-1.32283
DDB_G0293034	unknown function	no	-2.27977
DDB_G0293066	unknown function	no	-5.53097
ddb_g0295829	EGF-like domain-containing protein	yes	-2.32358
ebp	putative 3-beta-hydroxysteroid-Delta(8),Delta(7)-isomerase(ebp)	yes	-1.73893
erg2	C-8 sterol isomerase(erg2)	yes	-1.97652
gp130	glycoprotein 130(gp130)	no	-2.52731
grlE	G-protein-coupled receptor family 3 protein 5(grlE)	yes	-1.5342
lmpB	lysosomal integral membrane glycoprotein(lmpB)	yes	-1.5789
p80	endosomal membrane protein(p80)	yes	-2.75389
pefA	penta EF hand calcium binding protein(pefA)	no	-1.57102
pigX	phosphatidylinositol glycan, class X(pigX)	yes	-1.58991
ponA	actin binding protein(ponA)	no	-3.12854
ponL	ponticulin-related protein(ponL)	no	-1.37502
psiF	PA14 domain-containing protein(psiF)	no	-2.0081
rac1B	Rho GTPase(rac1B)	yes	-2.77696
rac1C	Rho GTPase(rac1C)	no	-2.18324
racF1	Rho GTPase(racF1)	yes	-3.41783
racF2	Rho GTPase(racF2)	yes	-4.41285
rasY	Ras GTPase(rasY)	yes	-2.16568
rasZ	Ras GTPase(rasZ)	yes	-3.38974
rhgA	Rh-like protein/ammonium transporter(rhgA)	no	-1.32908
sibA	integrin beta A-like protein(sibA)	yes	-1.61654
sodB	superoxide dismutase(sodB)	no	-2.38531
sodC	superoxide dismutase(sodC)	no	-2.01024

APÉNDICE II

Publicaciones generadas

IreA Controls Endoplasmic Reticulum Stress-Induced Autophagy and Survival through Homeostasis Recovery

Eunice Domínguez-Martín,[a,b] Laura Ongay-Larios,[c] Laura Kawasaki,[b] Olivier Vincent,[a] Gerardo Coello,[d] Roberto Coria,[b] Ricardo Escalante[a]

[a]Instituto de Investigaciones Biomédicas Alberto Sols, Consejo Superior de Investigaciones Científicas-Universidad Autónoma de Madrid (CSIC-UAM), Madrid, Spain

[b]Departamento de Genética Molecular, Instituto de Fisiología Celular, Universidad Nacional Autónoma de México, México City, México

[c]Unidad de Biología Molecular, Instituto de Fisiología Celular, Universidad Nacional Autónoma de México, México City, México

[d]Unidad de Cómputo, Instituto de Fisiología Celular, Universidad Nacional Autónoma de México, México City, México

ABSTRACT The unfolded protein response (UPR) is an adaptive pathway that restores cellular homeostasis after endoplasmic reticulum (ER) stress. The ER-resident kinase/RNase Ire1 is the only UPR sensor conserved during evolution. Autophagy, a lysosomal degradative pathway, also contributes to the recovery of cell homeostasis after ER stress, but the interplay between these two pathways is still poorly understood. We describe the *Dictyostelium discoideum* ER stress response and characterize its single bona fide Ire1 orthologue, IreA. We found that tunicamycin (TN) triggers a gene-expression reprogramming that increases the protein folding capacity of the ER and alleviates ER protein load. Further, IreA is required for cell survival after TN-induced ER stress and is responsible for nearly 40% of the transcriptional changes induced by TN. The response of *Dictyostelium* cells to ER stress involves the combined activation of an IreA-dependent gene expression program and the autophagy pathway. These two pathways are independently activated in response to ER stress but, interestingly, autophagy requires IreA at a later stage for proper autophagosome formation. We propose that unresolved ER stress in cells lacking IreA causes structural alterations of the ER, leading to a late-stage blockade of autophagy clearance. This unexpected functional link may critically affect eukaryotic cell survival under ER stress.

KEYWORDS *Dictyostelium*, ER stress, autophagy

The endoplasmic reticulum (ER) is a membranous network where about one-third of the synthesized proteins are folded and modified (1); ER is also critical for calcium homeostasis and lipid biosynthesis (2). Conditions that perturb the ER homeostasis interfere with proper protein folding, leading to the accumulation of unfolded proteins in the ER lumen. These conditions, referred to as ER stress, may have detrimental consequences on cellular function. Thus, a highly regulated pathway known as the unfolded protein response (UPR) has evolved to restore ER homeostasis both by reducing the ER protein load and by reprogramming gene expression to increase the ER folding capacity (3, 4) and protein degradation (5–7).

The UPR is triggered by three ER stress sensor proteins in mammalian cells, Ire1 (inositol-requiring enzyme), ATF6 (activating transcription factor 6), and PERK (protein kinase RNA-like ER kinase) (8), but only Ire1 is highly conserved between species (9). Ire1 is a type I transmembrane ER-resident protein that contains a serine-threonine kinase and an endoribonuclease domain at the cytosolic C terminus and an N-terminal luminal

Address correspondence to Roberto Coria, rcoria@ifc.unam.mx, or Ricardo Escalante, rescalante@iib.uam.es.

domain that can sense the protein-folding environment in the ER (10, 11). Under ER stress, Ire1 undergoes transautophosphorylation and activation of its endoribonuclease domain, which mediates the cleavage of a noncanonical intron contained in the mRNA of a basic leucine zipper (bZIP) transcription factor (Xbp1 in humans and Hac1 in yeast and bzip60 in plants). This splicing allows the synthesis of a functional protein, which controls the expression of chaperones, protein glycosylation enzymes, and proteases, among many other stress-response-related proteins (12–17).

Protein degradation participate in restoring cellular homeostasis after ER stress, mainly by two mechanisms: (i) the ERAD (ER-associated degradation) pathway that involves the proteasome (18, 19) and (ii) macroautophagy (19–22). Macroautophagy (here referred to as autophagy) is a conserved degradation mechanism in which intracellular double-membrane vesicles, denoted autophagosomes, capture cytosolic cellular components and organelles and then fuse with lysosomes to deliver this material for degradation (23). Basal autophagy is important for maintaining cellular homeostasis and is highly induced as a starvation survival response (24, 25). Other stimuli such as oxidative stress (26), pressure changes (27), or infection (28) can also induce autophagy.

Many ER stress-inducing drugs elicit an autophagic response (29), but the corresponding signaling pathways have been only partially elucidated. The three main UPR signaling branches seem to play differential roles in ER stress-induced autophagy. Reports addressing ER stress in mammalian cells suggest that Ire1 is required for autophagy induction, while ATF6 and PERK seem to be dispensable for this process (30). On the other hand, both PERK and Ire1 have been found to be necessary for the upregulation of some autophagic genes after ER stress (31). In plant and mammalian cells Ire1-dependent autophagy induction after ER stress seems to depend on the kinase domain of this sensor protein (30, 32). Further, in mammalian cells it has been shown that Ire1 activates autophagy after ER stress through the c-Jun N-terminal kinase (JNK) pathway (30). Nevertheless, autophagy is also induced after ER stress in organisms where the JNK pathway is not conserved, such as plants, yeasts, and algae (32–34). Therefore, if Ire1 is involved in the ER stress-dependent autophagic response in these organisms, it might be regulating other JNK-independent autophagy-inducing pathways.

The extent to which autophagy contributes to cell survival under ER stress conditions has not been clearly established. Observations from *Arabidopsis thaliana* suggest that the absence of some autophagic genes decrease plant viability after ER stress (35), although similar studies in yeasts present contradictory results (21, 36). In the present study, we sought to address these questions by studying the link between autophagy and ER stress in the model organism *Dictyostelium discoideum*, a soil-living social ameba that feeds on bacteria and yeasts. When nutrients are scarce, about 100,000 *Dictyostelium* cells aggregate and enter a developmental program that culminates in the formation of a fruiting body. Autophagy-defective mutants in *Dictyostelium* exhibit aberrant developmental phenotypes (37, 38). Since the ER stress response was not previously described in this model, we wanted to characterize the *Dictyostelium* response to ER stress and study the role of its single IRE1 orthologue gene (*ireA*). We found that a fully functional IreA is essential for ER stress survival and for the regulation of a specific gene expression program. In addition, we observed that *Dictyostelium* cells also require autophagy induction to survive ER stress. Interestingly, IreA absence does not prevent the induction of autophagy upon ER stress but rather impairs this process at a later stage, likely due to the inability of IreA-depleted cells to restore the ER homeostasis. Our results probably reveal an ancient interplay between UPR and autophagy that shapes the ER stress response in this model organism.

RESULTS

ER stress induction in *Dictyostelium*. The ER stress response had not been previously described in *Dictyostelium*, so we first studied the effect of commonly used ER stress inducers. *Dictyostelium* cells were exposed to 2 μg/ml tunicamycin (TN), 1.5 mM

dithiothreitol (DTT), or 200 mM 2-deoxy-D-glucose (2-DOG). Serial dilutions of treated cells were spotted on an SM medium plate containing a lawn of *Klebsiella aerogenes* to test cell viability. This assay was adapted to *Dictyostelium* from the commonly used spot assay to test drug sensitivity in yeasts (39, 40). After TN treatment, *Dictyostelium* cells were not able to divide and were severely impaired in their growth in association with bacteria. On the other hand, little or no effect was seen after a treatment with 2-DOG or DTT (Fig. 1A). We also observed that cell morphology was specifically altered by the TN treatment, as treated cells became rounded and more refractile (Fig. 1B) and had reduced adherence to the plastic surface. It has been previously reported that in other organisms ER stress induces the expression of ER-resident chaperones and components of the endoplasmic reticulum-associated degradation (ERAD) pathway (41, 42). There-fore, we analyzed by Western blotting the effects of different treatments on the expression of the ER-resident chaperone Grp78/BiP (which we identified to be coded by the DDB_G0276445 gene in *Dictyostelium* [Table 1]) and of the ERAD protein CdcD (homologous to human VCP/p97 and yeast Cdc48) (43), both highly conserved in *Dictyostelium*. Grp78 detection was performed with an antibody raised against the human Grp78 orthologue. This antibody recognized three bands in *Dictyostelium* protein extracts. The heaviest protein detected with this antibody corresponds to the estimated molecular mass (72 kDa) of the primary sequence of *Dictyostelium* Grp78. We consider this protein the bona fide *Dictyostelium* Grp78. The other two bands recog-nized by this antibody could correspond to chaperones of the Hsc70 family, HspB and HspE, with estimated masses of 70 and 69 kDa, respectively, which under some conditions comigrate in the gel. To further confirm the specificity of the antibody, the *Dictyostelium* Grp78/BiP gene was expressed in bacteria. Analysis of bacterial extracts with the anti-Grp78 antibody allowed detection of the *Dictyostelium* Grp78 orthologue (data not shown).

As shown in Fig. 1C and D, only TN significantly increased the expression of Grp78 (band *a*) and CdcD, while the bands corresponding to Hsc70 chaperones (band *b*) remained unchanged. TN treatment increased by ~8-fold and ~3-fold the expression of Grp78 and CdcD, respectively (Fig. 1D); in contrast, DTT and 2-DOG did not have a significant effect on the expression of both proteins.

Dictyostelium cells were subjected to increasing concentrations of TN and a dose-dependent negative effect on viability was observed in serial dilution-spot assays (Fig. 1E). An increase in expression of CdcD and the ~72-kDa protein detected by the anti-Grp78 antibody was observed for all doses tested (Fig. 1F and G). However, a significant increase in both markers was only observed after 16 h of treatment with 2 μg/ml TN (Fig. 1H and I). In conclusion, TN induces ER stress and triggers a response, whereas 2-DOG and DTT have no effect at the concentrations tested. The absence of 2-DOG effect could be due to its poor internalization rate in *Dictyostelium* cells (44). We did not characterize further the effect of DTT since it also blocks the formation of disulfide bonds of cytosolic proteins, which can lead to the formation of protein aggregates that may interfere with autophagy.

Identification and subcellular localization of the UPR sensor protein IreA in *Dictyostelium*. To identify the components of the UPR in *Dictyostelium*, the sequences of human, yeast, and *A. thaliana* UPR proteins were used as the query at the dictyBase BLAST-P program. As shown in Table 1, a putative *Dictyostelium* Ire1 orthologue (DDB_G0267650, IreA) was identified with a high level of protein sequence similarity to known Ire1 orthologues. It must be pointed out that although IfkA and IfkB were considered PERK homologues by the program, they lack the typical transmembrane domain and have already been described as orthologues of Gcn2 (45, 46). *Dictyostelium ireA* codes for a 984-residue protein that contains a signal peptide within the first 26 residues, a transmembrane domain (residues 440 to 457), a serine/threonine kinase domain (residues 575 to 851), and a kinase extension nuclease (KEN) domain (residues 854 to 984) (Fig. 2A). The sequence identity between IreA and the human, *Saccharo-myces cerevisiae*, and *A. thaliana* Ire1 orthologues is mainly restricted to the kinase and KEN domains, ranging from 20 to 70%, and these proteins share less or no sequence
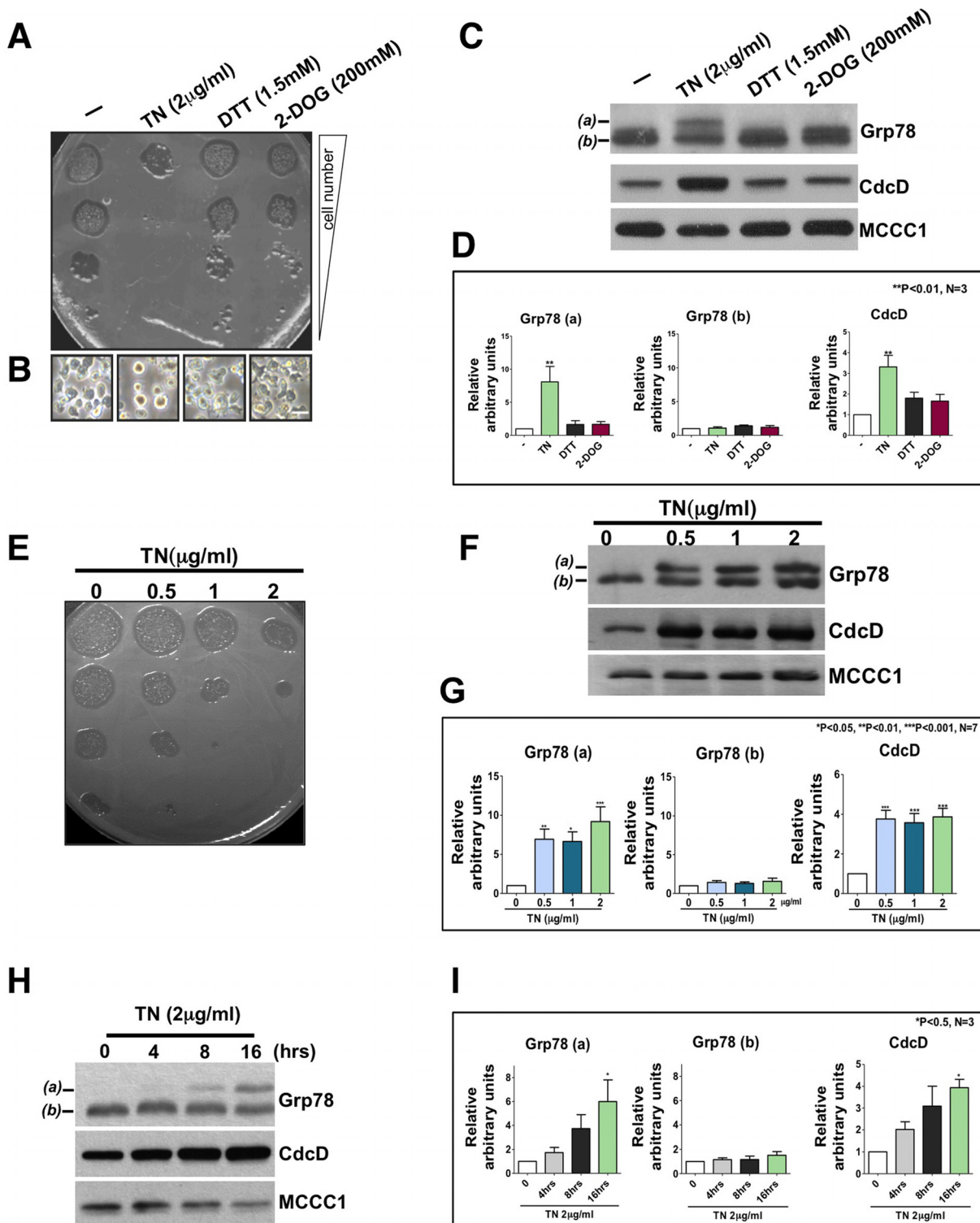
FIG 1 ER stress induction in *Dictyostelium*. (A) Cell viability of WT strain after 16 h of treatment with vehicle (DMSO), TN, DTT, or 2-DOG at the indicated concentrations. Cells were treated and spotted on SM plates containing a lawn of *K. aerogenes*, incubated at 22°C, and photographed 7 days later. (B) Phase-contrast microscopy from treated cells shown in panel A, taken right before the spot assay (scale bar, 10 μm). (C) Representative Western blot image of Grp78 and CdcD expression. (D) Densitometric quantification of Grp78 (bands a and b in panel C) and CdcD from cells treated as described in panel A. Bars represent the quotient of Grp78 or CdcD divided by MCCC1 and normalized with the DMSO treatment. Data are expressed as means ± the SD of three independent experiments. (E) Cell viability of WT strain after 16 h of treatment with different TN concentrations. Cells were treated as in panel A. (F) Representative Western blots of Grp78 and CdcD expression after different TN treatments. (G) Quantification was performed as for panel D. (H) Grp78 and CdcD expression after treatment with 2 μg/ml TN for the indicated times. Representative Western blot images are shown. (I) Quantification was performed as for panel D.

TABLE 1 BLAST analysis of *Dictyostelium* UPR orthologues

Query	UniProt identifier	Protein length(s) (spliced/unspliced [aa[a]])	*Dictyostelium* orthologue[b]	Protein length (aa)	e value
Xbp1/Hac1p	P17861 (XBP1_HUMAN)	261/376	ND		
	P41546 (HAC1_YEAST)	230/238			
	Q9C7S0 (BZP60_ARATH)	258/295			
Ire1p/Ern1	O75460 (ERN1_HUMAN)	977	IreA (DDB_G0267650)	984	4e−69
	P32361 (IRE1_YEAST)	1,115			1e−75
	Q93VJ2 (IRE1B_ARATH)	881			2e−78
BiP/Grp78/Kar2p	P11021 (GRP78_HUMAN)	654	DDB_G0276445	658	0
	P16474 (GRP78_YEAST)	682			0
	F4K007 (F4K007_ARATH)	613			0
Atf6	P18850 (ATF6A_HUMAN)	670	ND		
	Q9SG86 (BZP28_ARATH)	675	ND		
PERK	Q9NZJ5 (E2AK3_HUMAN)	1,116	IfkA (DDB_G0272837)*	2,258	4e−30
			IfKB (DDB_G0276829)*	1,358	2e−30

[a]aa, amino acids.
[b]*, IfKA and IfkB were previously described as GCN2 homologs (57, 94). ND, not detected.

similarity in the N-terminal sensor domain, located in the ER lumen (Fig. 2B). All of the Ire1 orthologues share a global sequence identity of about 30% (Fig. 2C).

To determine whether IreA, like its orthologues in other organisms (47), is an ER-resident protein in *Dictyostelium*, the predicted IreA coding sequence fused to green fluorescent protein (GFP) was introduced in *Dictyostelium* wild-type (WT) AX4 cells.
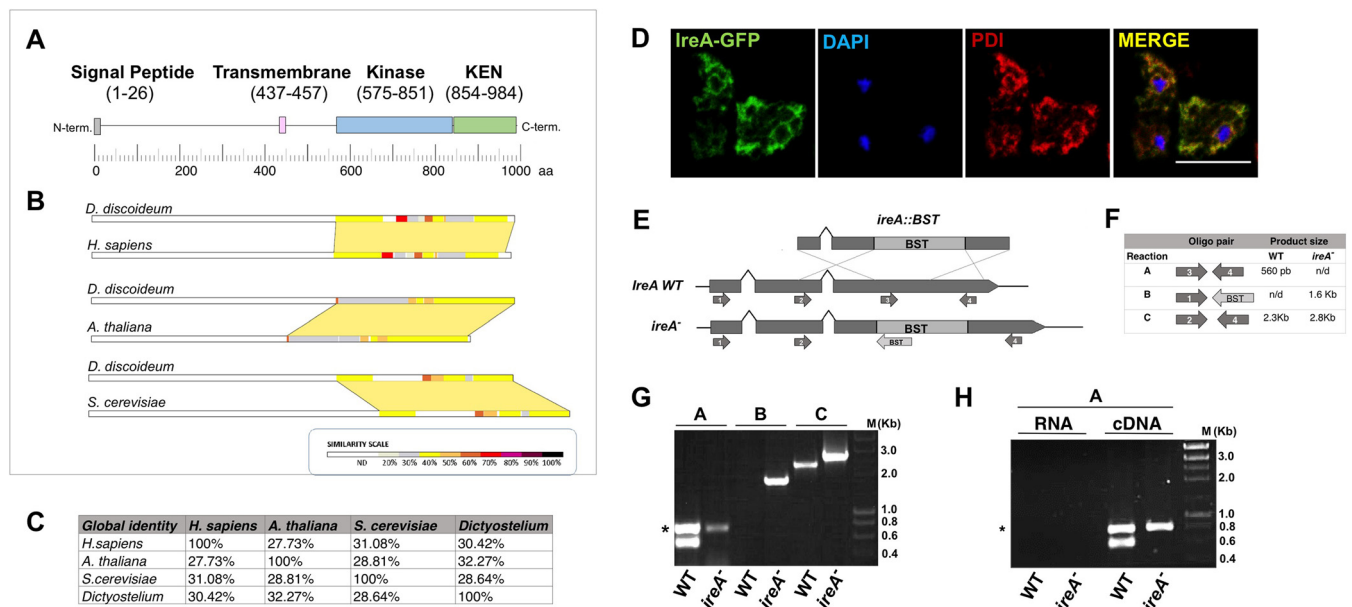
FIG 2 Sequence analysis of *Dictyostelium* IreA protein and its subcellular localization. (A) Diagram of the IreA predicted protein structure. The signal peptide (residues 1 to 26), the transmembrane region (residues 437 to 457), the kinase domain (residues 575 to 851), and kinase extension nuclease (KEN) domain (residues 854 to 984) are highlighted. (B) Pairwise alignments between *Dictyostelium* IreA and the *H. sapiens*, *A. thaliana*, and *S. cerevisiae* orthologues. Protein sequences of Ire1 orthologues were analyzed with SIM alignment tool, and results were visualized with LALNVIEW. (C) Percent identity between Ire1 orthologues obtained from a multiple alignment analysis. (D) Confocal microscopy of WT cells expressing an IreA-GFP hybrid protein, prepared for immunofluorescence detection of PDI (labeled with a secondary antibody conjugated to Alexa Fluor red 546) and DAPI-stained nuclei (scale bar, 10 μm). (E) Diagrams of the WT *ireA* locus, the *ireA*::BST construct, and the generated *ireA*− BST-interrupted locus. Gray boxes represent coding sequences; lines between boxes are introns. Arrows represent primers used for PCR amplification. A 998-bp deletion was generated in the *ireA* chromosomal locus by homologous recombination of a blasticidin (BST) resistance cassette. The insertion of BST in the *ireA* locus was corroborated by PCR with the indicated oligonucleotides. (F) Table presenting the expected sizes of the PCR amplification products that would be obtained with the respective oligonucleotide pairs depicted in panel E. (G and H) PCR products obtained using DNA (G) or cDNA (H) as the template. RNA was used as a negative control for DNA contamination. The asterisk denotes a control PCR amplification of an unrelated gene. M, molecular size marker.

Transformed cells were selected, fixed, and used for colocalization studies with the ER marker protein disulfide isomerase (PDI). IreA-GFP presented a reticulate pattern that clearly colocalized with PDI (Fig. 2D).

IreA-depleted cells cannot cope with ER stress. To study the function of IreA in *Dictyostelium*, the corresponding gene was deleted by inserting a blasticidin resistance cassette (BST) by homologous recombination (Fig. 2E). Several independent clones were obtained, and BST integration at the *ireA* locus was confirmed by genomic PCR (Fig. 2E to G). The lack of expression of a complete mRNA was also confirmed by reverse transcription-PCR (Fig. 2F and H). The *ireA*⁻ mutant strains had no evident growth defects on liquid medium (HL5) or in association with bacteria. When development was analyzed, the only noticeable phenotype of this mutant was a slight delay in the culmination of some structures due to an extended period as migrating slugs (Fig. 3A). Nevertheless, normal-looking fruiting bodies were eventually formed.

We next sought to determine whether IreA is required for ER stress survival. For this, we analyzed the morphology of treated cells by microscopy after a 16-h TN treatment and observed that both WT and *ireA*⁻ cells became rounded. Nevertheless, *ireA*⁻ cells were much more affected, and some lysed cells were evident in the sample (Fig. 3B). Then, we evaluated whether *ireA*⁻ cells could restore growth in association with bacteria after 4, 8, and 16 h of treatment with 2 μg/ml TN and found that *ireA*⁻ cells grew poorly after all treatments (Fig. 3C).

Expression of the Grp78 chaperone was significantly decreased in the *ireA*⁻ mutant in the presence of TN, dropping 4- to 5-fold with respect to its expression in the WT strain (Fig. 3D and E). Expression of CdcD showed exactly the same behavior as Grp78. This result indicates that the overexpression of both Grp78 and CdcD upon TN treatment is dependent on the presence of IreA. Together, these results indicate that *ireA*⁻ cells are highly sensitive to TN and that IreA is required to cope with ER stress.

IreA kinase and RNase activities are both required for the ER stress response. We next examined the role of the putative IreA kinase and KEN domains in the *Dictyostelium* ER stress response by expressing WT and mutated forms of the IreA protein in the *ireA*-deficient strain and by determining the level of complementation of its TN-sensitive phenotype. A kinase-inactive mutant was generated by replacing a conserved lysine residue with asparagine (*ireA*^{K603N}) at the predicted ATP-binding site. The RNase-deficient mutant was generated by the substitution of a conserved asparagine in the KEN domain for alanine (*ireA*^{N927A}) (Fig. 4A). Both mutations have been proved to inactivate efficiently the kinase and RNase activities of Ire1 in other organisms (48, 49). The genes encoding the WT and mutant proteins tagged with GFP were introduced into the *ireA*⁻ strain to determine their expression and cellular localization. As seen in Fig. 4B, the mutant proteins, as well as the wild-type protein, were distributed in a reticulated pattern characteristic of cortical and perinuclear ER and colocalized with the ER marker PDI. This indicates that both IreA mutant forms were expressed and inserted in the ER. We next sought to determine whether these mutant alleles could revert the ER stress response deficiency of the *ireA*⁻ mutant. We found that the expression of both mutant genes did not allow the growth of the *ireA*⁻ mutant after incubation with 2 μg/ml TN (Fig. 4C). The mutant proteins were also unable to induce expression of Grp78 and CdcD after the TN treatment (Fig. 4D and E). Overall, these results indicate that the ER stress response and the regulation of the expression of Grp78 and CdcD depend on both the kinase and the RNase activities of IreA.

It has been observed that yeast and human Ire1 form high-order oligomers during ER stress conditions (50). To assess whether *Dictyostelium* IreA can associate and form oligomers under stress and to evaluate whether the kinase and RNase activities are required in this process, we analyzed cells expressing the WT and mutant proteins tagged with GFP by live confocal imaging. TN treatment induced IreA association (cluster formation seen as tiny puncta) in approximately 30% of the cells in the *ireA*⁻ strain expressing the IreA WT construct (Fig. 4F and G). This proportion remained constant until 8 h of treatment with TN (Fig. 4G). Interestingly, although mutant forms
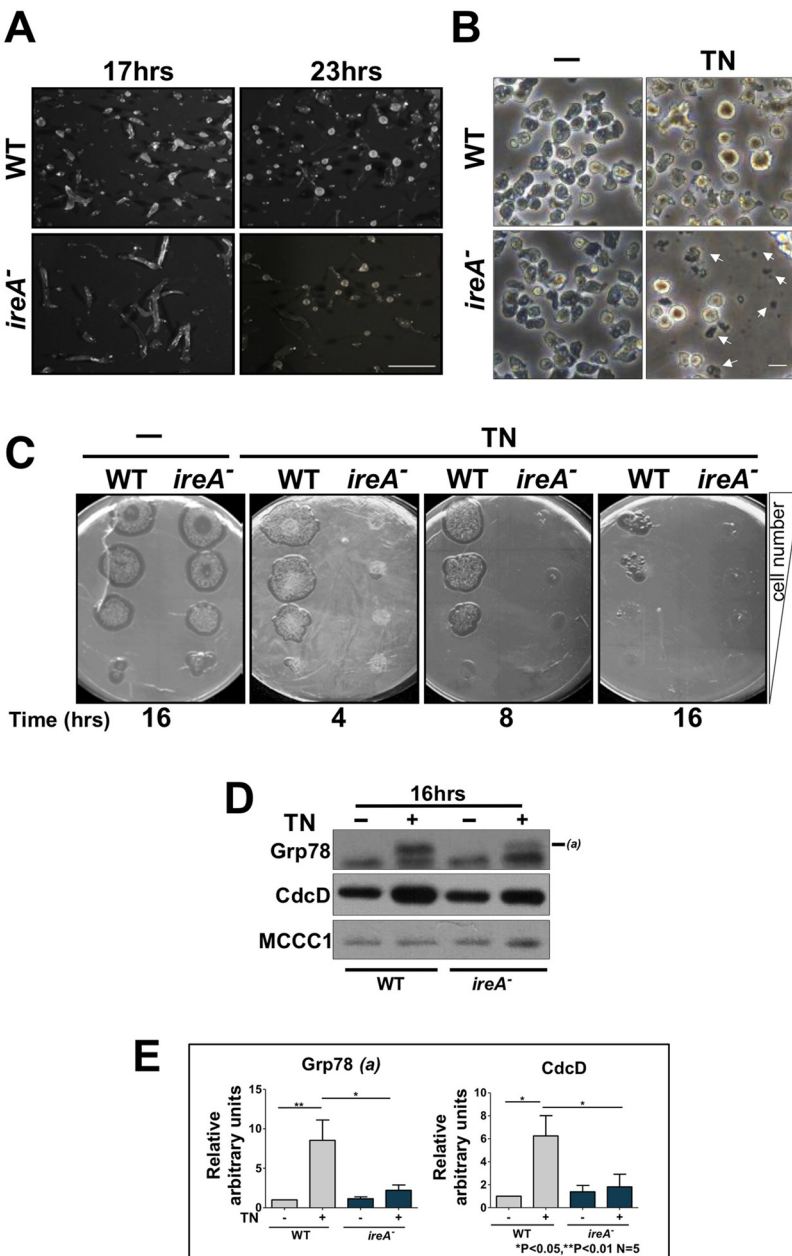
FIG 3 Effects of *ireA* inactivation on development and ER stress response. (A) Photographs of WT and *ireA⁻* strains showing different development stages (scale bar, 1 mm). Cells were deposited over nitrocellulose filters without nutrients and allowed to develop for the indicated times. (B) Light microscopy pictures of WT and *ireA⁻* cells treated for 16 h with vehicle (DMSO) or TN (2 μg/ml). Arrows point to lysed cells and debris (scale bar, 10 μm). (C) Serial dilution spot assay of WT and *ireA⁻* cells treated for the indicated times with vehicle (DMSO) or TN (2 μg/ml). (D and E) Representative Western blot (D) and densitometric quantification of Grp78 (*a*) and CdcC expression in WT and *ireA⁻* cells after 16 h of treatment with TN (2 μg/ml) (E). Densitometry was performed as described for Fig. 1D. Values are means ± the SD of five independent assays. Statistical significant differences are indicated by asterisks.

of IreA could oligomerize, the proportion of cells with clusters was significantly different from that observed in the WT. Around 15% of the cells expressing the kinase-inactive IreA mutant (*ireA^{K603N}*) presented cluster formation, while almost 100% of the RNase-inactive mutant (*ireA^{N927A}*) cells contained clusters (Fig. 4F and G). This indicates that the point mutations that inactivate either the kinase or the RNase activities do not affect IreA association but do alter the regulation and abundance of cluster structures.
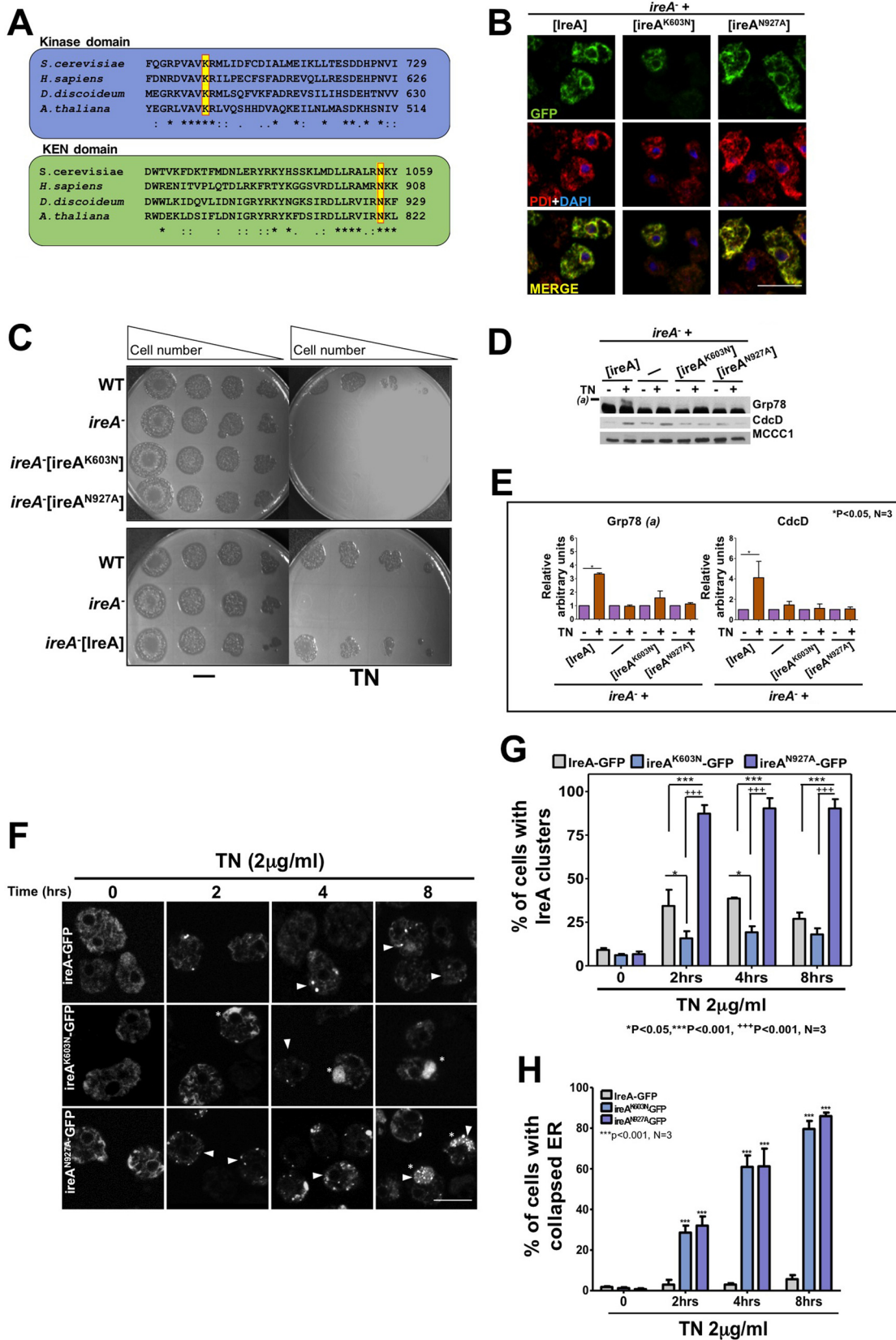
FIG 4 Effects of IreA kinase and KEN point mutations on ER stress response. (A) Alignment of the kinase and RNase domains of *S. cerevisiae*, *H. sapiens*, *D. discoideum*, and *A. thaliana* Ire1 orthologues. The conserved residues that were mutated on *D. discoideum* IreA are highlighted. K603 and N927 (relative to *D. discoideum*) were mutated to N and A, respectively. (B) Confocal microscopy of

(Continued on next page)

It has been observed that the morphology of the ER is altered during stressful conditions (21) and that ER cisternae can collapse in Ire1-defficient cells (51). Similar effects were observed in *Dictyostelium* cells after a TN treatment, and we thus determined ER damage during TN treatment in cells expressing either the WT or mutant IreA constructs. Some cells under TN treatment showed a large collapsed ER structure instead of a well-spread tubular ER (Fig. 4F). We quantified the percentage of cells with this aberrant ER by live confocal microscopy. The proportion of cells with collapsed ER increased significantly in cells expressing IreA-mutant versions (Fig. 4H) compared to that of the WT in a time-dependent manner. After 8 h of TN treatment, most cells expressing IreA mutant forms presented a collapsed ER, while the cells expressing the WT version maintained a normal ER morphology. Taken together, these results suggest that in order to maintain the integrity of the ER during stress conditions, the cells require both the kinase and RNase activities of IreA and that this process is independent on the capacity to form oligomeric IreA structures.

IreA participates in a TN-induced transcriptional response. In *S. cerevisiae* and other organisms, the ER stress response triggers a gene expression program regulated by Ire1 through the activation of a b-zip transcription factor (7), whereas in some species the ER stress does not induce a transcriptional reprogramming; instead, the response relies on the regulation of mRNAs stability (52). To gain insight into the transcriptional changes that TN treatment elicit in *Dictyostelium* cells and to assess whether IreA is implicated in this response, we performed deep RNA sequencing of poly(A) RNA extracted from WT and *ireA*⁻ cells treated with 2 μg/ml of this drug or with the vehicle (dimethyl sulfoxide [DMSO]). In WT cells, we observed that 433 transcripts were differentially regulated after a TN treatment. Within this group, 166 transcripts were upregulated ($\log_2$ fold change $\geq$ 1.3) (Fig. 5A; see also Archive S1 in the supplemental material), whereas 267 were downregulated ($\log_2$ fold change $\leq$ −1.3) (Fig. 5B; see also Archive S1 in the supplemental material). From these data, we estimated that the transcript levels of nearly 3.5% of *Dictyostelium* genes were altered after a TN treatment. The participation of IreA in the transcriptional response elicited by TN was evaluated by obtaining the set of genes whose expression change depended on IreA. We found that 76 of the 166 genes that were upregulated and 92 of the 267 genes that were downregulated by a TN treatment in the WT strain were IreA dependent (Fig. 5A and E; see also Archive S2 in the supplemental material).

To determine which processes might be affected after a TN treatment, we categorized the up- and downregulated sets of genes using the DAVID gene ontology (GO) enrichment clustering tool (53, 54). For this analysis, we used the default parameters of the program and selected the categories "biological process," "protein domain," and "cellular component." The clusters resulting from the enrichment analysis are briefly displayed in Fig. 5, and the complete results are available in Archives S3 and S4 in the supplemental material. This clustering analysis revealed that the upregulated set of genes is associated with the ER stress response (Fig. 5C) and is significantly enriched in terms related to protein degradation processes ("protein ubiquitination," "ubiquitin,"

FIG 4 Legend (Continued)

ireA⁻ cells expressing WT IreA and its mutated versions (K603N and N927A) tagged with GFP. Cells were fixed and stained with DAPI, and PDI was immunodetected as in Fig. 2D (scale bar, 10 μm). (C) Serial dilution spot assay of *ireA*⁻ cells expressing, an IreA-GFP, IreA[K603N]-GFP, or IreA[N927A]–GFP construct. Cells were treated for 16 h with vehicle (DMSO) or TN (2 μg/ml), spotted over a lawn of *K. aerogenes*, and photographed 5 to 7 days later. (D and E) Representative Western blot and (D) densitometric quantification of Grp78 [(*a*)] and CdcD expression after a DMSO or TN (2 μg/ml) treatment of *ireA*⁻ cells expressing either IreA-GFP, IreA[K603N]-GFP, or IreA[N927A]–GFP (E). Densitometry was performed as described for Fig. 1D. Values are the means ± the SD of three independent assays. Asterisks indicate statistically significant differences. (F) One-stack confocal microscopy images of the localization and clustering (formation of puncta) of IreA-GFP, IreA[K603N]-GFP, and IreA[N927A]–GFP. *ireA*⁻ cells expressing the fusion proteins were treated with TN (2 μg/ml) for the indicated times. *In vivo* confocal images were taken every 2 h (scale bar, 10 μm). Arrowheads indicate cells containing IreA clusters, and asterisks indicate cells presenting collapsed ER. (G) Percentage of cells containing IreA clusters. Values represent the means ± the SD of three independent experiments. Statistically significant differences are denoted by an asterisk [between WT and mutant IreA(s)] and by a "+" sign (between *ireA*[K603N] and *ireA*[N927A]). (H) Percentage of *ireA*⁻ cells presenting collapsed ER. Cells with collapsed ER (see panel F) were counted, and the mean percentages ± the SD of three independent experiments were graphed. Statistically significant differences relative to the DMSO treatment are indicated.
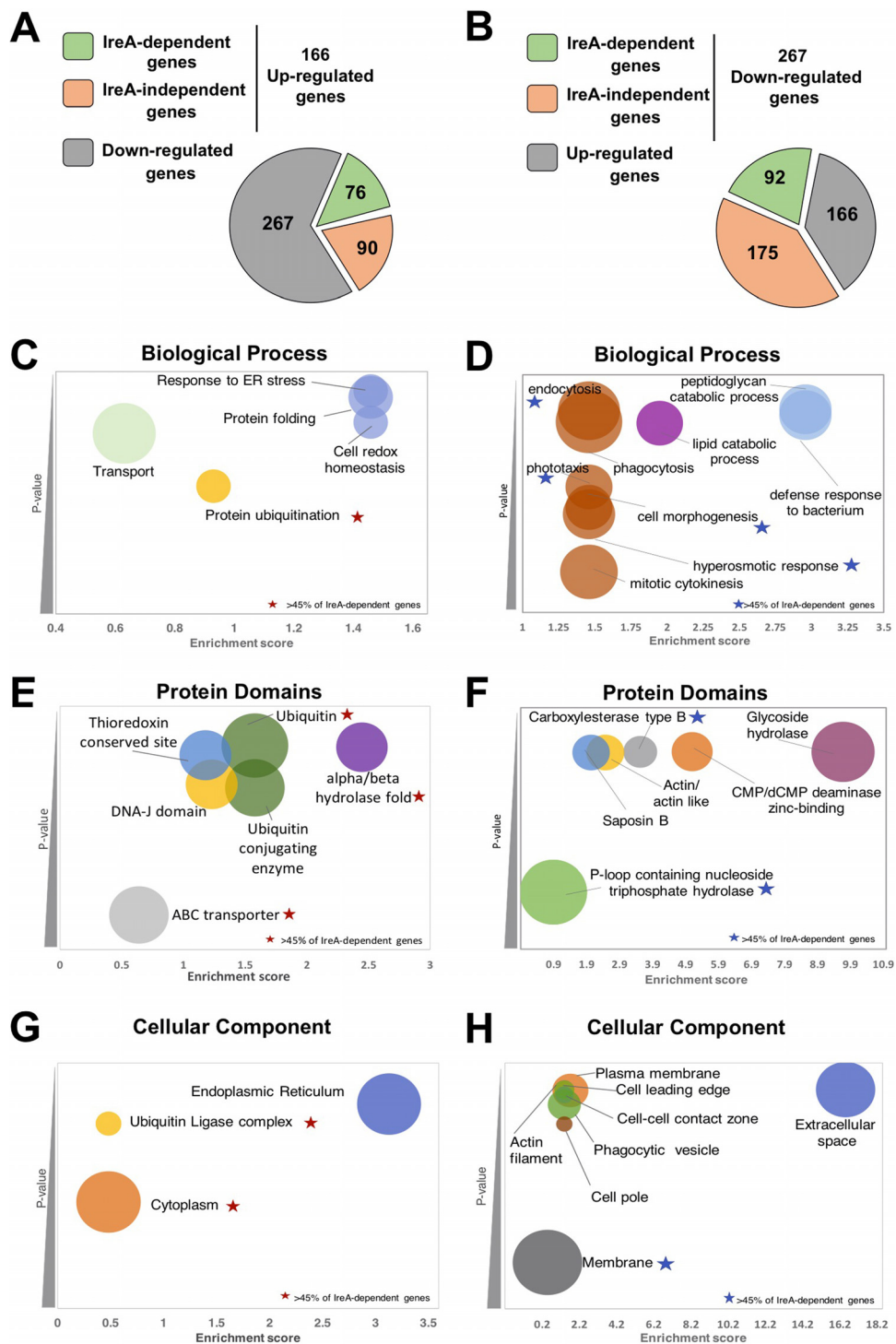
FIG 5 Identification of IreA-dependent and IreA-independent regulated genes upon TN treatment. RNA-seq was used to detect gene expression changes in WT and *ireA⁻* strains treated or not treated with TN (2 μg/ml). Only genes with a log₂ fold change of ≥1.3 were included. (A and B) Upregulated (A) and downregulated (B) genes after TN treatment. Both upregulated and downregulated gene groups were analyzed with the DAVID gene ontology enrichment tool. (C to H) Genes were clustered into three categories for both upregulated genes (C, E, and G) and downregulated genes (D, F, and H): biological process (C and D), protein domains (E and F), and cellular component (G and H). The GO terms of the enriched clusters are presented in accordance with the obtained enrichment score and *P* value (≥0.5), and the color code highlights GO terms that belong to the same cluster. The size of the bubble corresponds to the number of genes in each cluster. GO clusters where at least 45% of the genes were IreA dependent are indicated by stars.

"ubiquitin conjugating enzyme," and "alpha/beta hydrolase fold") and to protein folding ("DNA-J domain" and "thioredoxin containing site") (Fig. 5C, E and G; see also Archive S3 in the supplemental material). Also, from these results it can be inferred that TN could be upregulating transport-related processes (Fig. 5C and E).

In contrast, the GO cluster results of the downregulated set of genes were completely different (Fig. 5D, F, and H; see also Archive S4 in the supplemental material). "Carbohydrate metabolism" was the most enriched biological term for this set of genes, and "glycoside hydrolase" was the most enriched term in the protein domain category (Fig. 5D and F). These data suggest that *Dictyostelium* cells may experience an imbalance in the carbohydrate metabolism after a TN treatment, possibly caused by the effect of this antibiotic on protein glycosylation. Interestingly, the downregulated set is enriched in lipid metabolism terms (Fig. 5D; see also Archive S5 in the supplemental material). Since many of the proteins associated with lipid metabolism are targeted to the ER, this group of transcripts might be downregulated to alleviate ER protein load. Nevertheless, another group of genes associated with lipid metabolism is upregulated (see Archive S5 in the supplemental material), reflecting that lipid homeostasis might be adapted to cope with ER stress. The term "extracellular space" was significantly enriched in the downregulated set of genes (Fig. 5H), suggesting an effect on secreted proteins. In addition, many of the downregulated transcripts code for membrane proteins or proteins involved in processes that require membrane remodeling, such as endocytosis, phagocytosis, and hyperosmotic stress (Fig. 5D and H). These data suggest that in *Dictyostelium* one of the functions of the UPR may be to downregulate the expression of proteins that are targeted to the secretory pathway or that should be inserted into the membrane, possibly to alleviate the ER protein load.

From the set of genes that are upregulated after a TN treatment, we observed that the clusters related to protein degradation processes (such as protein ubiquitination, ubiquitin ligase complex, ubiquitin, and alpha/beta hydrolase fold) contains a higher percentage (more than 45%) of IreA-dependent genes (Fig. 5C, E, and G; see also Archive S1 in the supplemental material). This suggests that the IreA-dependent response might contribute significantly to increase the degradative capacity of the cell, mainly through ubiquitin-related processes. IreA may also be required to increase drug resistance, since it was required for the upregulation of two transcripts that code for multidrug resistance ABC transporters (*abcC5* and *abcG10*) (see Archive S3 in the supplemental material). In addition, almost all clusters related to biological processes that were obtained from the analysis of the downregulated set of the genes contained more than 45% of IreA-dependent genes (Fig 5D, F, and H), and most of them code for membrane proteins (Fig. 5H), suggesting that IreA might alleviate the ER protein load by decreasing the abundance of transcripts that code for membrane-localized proteins.

We observed that under nonstressful conditions, IreA regulates the transcription of only 25 genes (see Archive S6 in the supplemental material). In addition, the transcript level of a large subset of genes (1,988) was altered specifically in the *ireA*⁻ mutant strain after a TN treatment. Since the absence of IreA during ER stress compromises cell viability and may have profound consequences in multiple cellular processes, these transcriptional changes might reflect a strong compensatory response related with cell survival and/or cell death-related pathways.

Altogether, these data strongly suggest that ER stress triggers a complex transcriptional response that modulates the levels of a diverse set of transcripts, increasing the expression of proteins involved in protein folding and degradation while decreasing the expression of proteins that may burden the ER capacity. Also, the fact that nearly half of the transcriptional response is mediated by IreA suggests that IreA might regulate the activity of an unknown transcription factor under ER stress conditions. Our data also suggest the existence of an IreA-independent pathway responsible for the regulation of the remaining transcriptional response observed in an *ireA*⁻ mutant.

Autophagy contributes to cell survival under ER stress. Since autophagy in *Dictyostelium* is activated by a variety of stress conditions such as starvation and
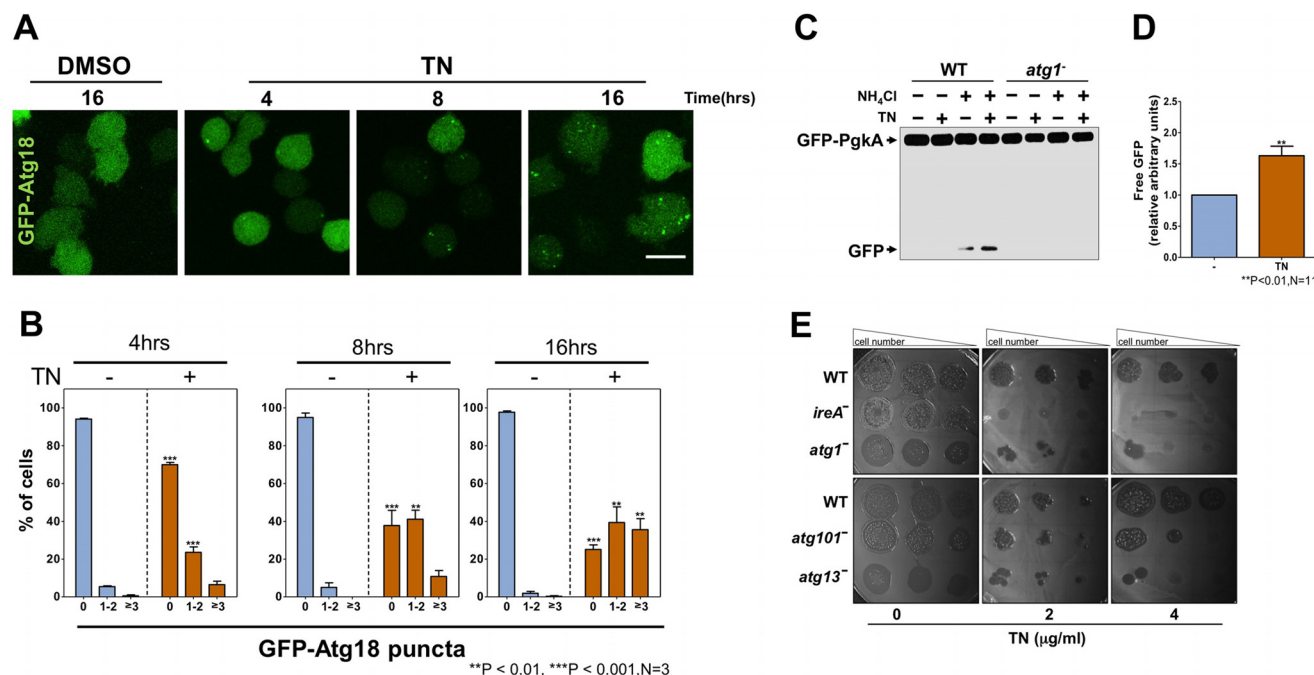
FIG 6 Tunicamycin induces autophagy. (A) Autophagy was determined as punctum formation in cells expressing GFP-Atg18 (maximum intensity z-projection representative picture). WT cells were treated with vehicle (DMSO) or TN (2 μg/ml) for the indicated times and visualized by confocal microscopy (scale bar, 10 μm). (B) Percentages of cells containing 0, 1 or 2, or $\geq$3 GFP-Atg18 puncta. Values are means $\pm$ the SD of three independent experiments. Asterisks indicate statistically significant differences. (C) Representative Western blot of an NH$_4$Cl-induced GFP-PgkA cleavage assay. WT and atg1$^-$ cells overexpressing the GFP-PgkA were treated for 8 h with TN (2 μg/ml) or vehicle (DMSO). During the last 2 h of treatment, the cells were incubated in the presence or absence of NH$_4$Cl as described in Materials and Methods. (D) Quantification of accumulated free GFP in WT cells as determined by densitometry. GFP was normalized against GFP-PgkA and refers to DMSO-treated cells. The means $\pm$ the SD of 11 independent experiments were graphed. Asterisks denote significance. (E) Visualization of cell viability through a serial dilution spot assay. The indicated strains were treated for 16 h with TN or DMSO and spotted on a lawn of K. aerogenes. Plates were incubated at 22°C and photographed 5 to 7 days later.

mechanical stress (55), we next sought to characterize the autophagic response to ER stress by measuring autophagy induction in cells exposed to a TN treatment. Quantification of GFP-Atg18-positive puncta has been previously reported to be an accurate method to evaluate autophagy induction in *Dictyostelium* (56).

WT cells expressing GFP-Atg18 were treated for 4, 8, and 16 h with TN and analyzed *in vivo* by confocal microscopy (Fig. 6A). We observed that the TN treatment caused a significant increase in the autophagosome-containing cell population in a time-dependent manner (Fig. 6A and B), since the proportion of cells containing multiple GFP-Atg18 puncta increased with longer exposure to TN (Fig. 6B). We next sought to determine whether the increase in autophagosome formation induced by TN was associated with a higher degradative capacity. To answer this question, we measured the accumulation of free GFP derived from the cleavage of the cytosolic fusion protein PgkA-GFP in the presence of a nonsaturating NH$_4$Cl concentration. This protocol has been established to evaluate protein degradation associated with autophagy (57, 58). We found that TN treatment caused a significant increase in the accumulation of free GFP (Fig. 6C and D). This accumulation was detected after the addition of NH$_4$Cl only in the WT but not in the atg1$^-$ strain, indicating that GFP-PgkA degradation is associated with the autophagy pathway.

We tested whether the autophagy pathway is required for a normal cellular response to TN. For this, we tested mutants of Atg1, Atg13, and Atg101 that block autophagy. The three proteins are constituents of the Atg1 complex but display different autophagy phenotypes. Atg1 and Atg13 are essential for autophagy induction, so knockout mutant strains present a complete autophagy blockage, whereas Atg101, which might play only a regulatory role, exhibits reduced levels of autophagy (59). All mutants were sensitive to TN treatment, although their sensitivity was not as

strong as that of the *ireA*⁻ strain (Fig. 6E). As expected, both *atg1*⁻ and *atg13*⁻ strains appeared to be more sensitive to TN treatment than the *atg101*⁻ strain. These results indicate that autophagy is part of the cellular response to TN and is required to trigger a complete response to ER stress.

IreA is dispensable for autophagy induction but is required for efficient autophagy. The autophagic response of *ireA*⁻ to TN was evaluated using the GFP-Atg18 marker as described above. Unexpectedly, the percentage of cells that contained GFP-Atg18 puncta after a TN treatment was higher in the *ireA*⁻ strain than in the WT strain (Fig. 7A and B). This increase is evident in the number of cells with three or more GFP-Atg18 puncta, which is even higher than that observed under starvation conditions in both strains. However, TN-induced GFP-Atg18 puncta in *ireA*⁻ cells appeared larger compared to the tiny puncta observed in WT cells after the same treatment or even in *ireA*⁻ cells under starvation conditions (Fig. 7A). Large puncta may result from the accumulation of abnormal autophagosomes unable to degrade their cargo, as observed previously in the *Dictyostelium* autophagic *vmp1*⁻ mutant (60). To clarify this possibility, the *ireA*⁻ mutant was exposed to TN, and the autophagy flux was evaluated using the GFP-PgkA proteolytic assay described above (Fig. 7C and D). Under these conditions, the level of free GFP accumulated in the *ireA*⁻ cells was significantly lower than in the WT cells. In contrast, the level of free GFP in the absence of stress did not differ significantly between WT and *ireA*⁻ strains, indicating that the autophagy degradation defect of *ireA*⁻ cells occurs specifically under ER stress conditions. Similar experiments were performed in *ireA*⁻ cells expressing the K603N or N927A mutant forms to determine the requirement of the kinase and KEN domains in the TN-induced autophagic response (Fig. 8A and B). Compared to the WT strain, *ireA*⁻ mutant strains presented a significantly reduced amount of accumulated free-GFP, indicating that both IreA domains are required for productive TN-induced autophagy. Immunoblot detection of the IreA mutant forms was performed with an anti-GFP antibody to evaluate whether the IreA forms were degraded after the consecutive TN and NH₄Cl treatments. As can be observed in overexposed membrane (Fig. 8C), under this treatment free GFP was not significantly generated by these constructs compared to cells expressing the GFP-PgkA construct, and therefore the detected free GFP reflects only the autophagic degradation of the cytosolic GFP-PgkA.

It has been reported that *Dictyostelium* autophagy-deficient cells accumulate ubiquitin-positive aggregates and that the ineffective degradation of these protein aggregates can be used as a reliable marker of autophagy inhibition (61, 62). These ubiquitin-positive protein aggregates can be visualized by confocal microscopy using immunofluorescence techniques (62). As shown in Fig. 9, *ireA*⁻ cells expressing the autophagic marker GFP-Atg18 exhibited large ubiquitin-positive aggregates after a TN treatment; such aggregates were absent in WT cells, further supporting that the autophagy flux after TN treatment is impaired in the absence of IreA. Interestingly, some the ubiquitin-containing aggregates are closed to enlarged GFP-Atg18 puncta. Together, all these results suggest that under ER stress, *ireA*⁻ cells are unable to degrade autophagic cargoes, even though autophagy induction is not altered.

***ireA*⁻ cells present abnormal autophagic structures and a collapsed endoplasmic reticulum after ER stress.** It has been observed that during autophagy induction, Atg18 (WIPI-1) localizes transiently at autophagosome initiation sites in *Dictyostelium* and human cells (27, 63). Mutant cells with defective autophagosome closure present abnormal Atg18 recruitment patterns (60, 64). The autophagosome assembly can be followed by detection of GFP-tagged Atg18 with live time-lapse confocal microscopy. WT and *ireA*⁻ cells expressing this marker were treated with TN for 7 h, and then the cells were monitored for 900 s (Fig. 10A; see also Movies S1 and S2 in the supplemental material). A specific GFP-Atg18 puncta was selected and followed on the *z*-axis until it was no longer visible. In WT cells, GFP-Atg18 could only be visualized for short periods of time ranging from 30 to 80 s, as previously described (27). In contrast, the GFP-Atg18-positive elongated structures in *ireA*⁻ cells were very static and persisted during the entire time course of this experiment (900 s). These data, together with the
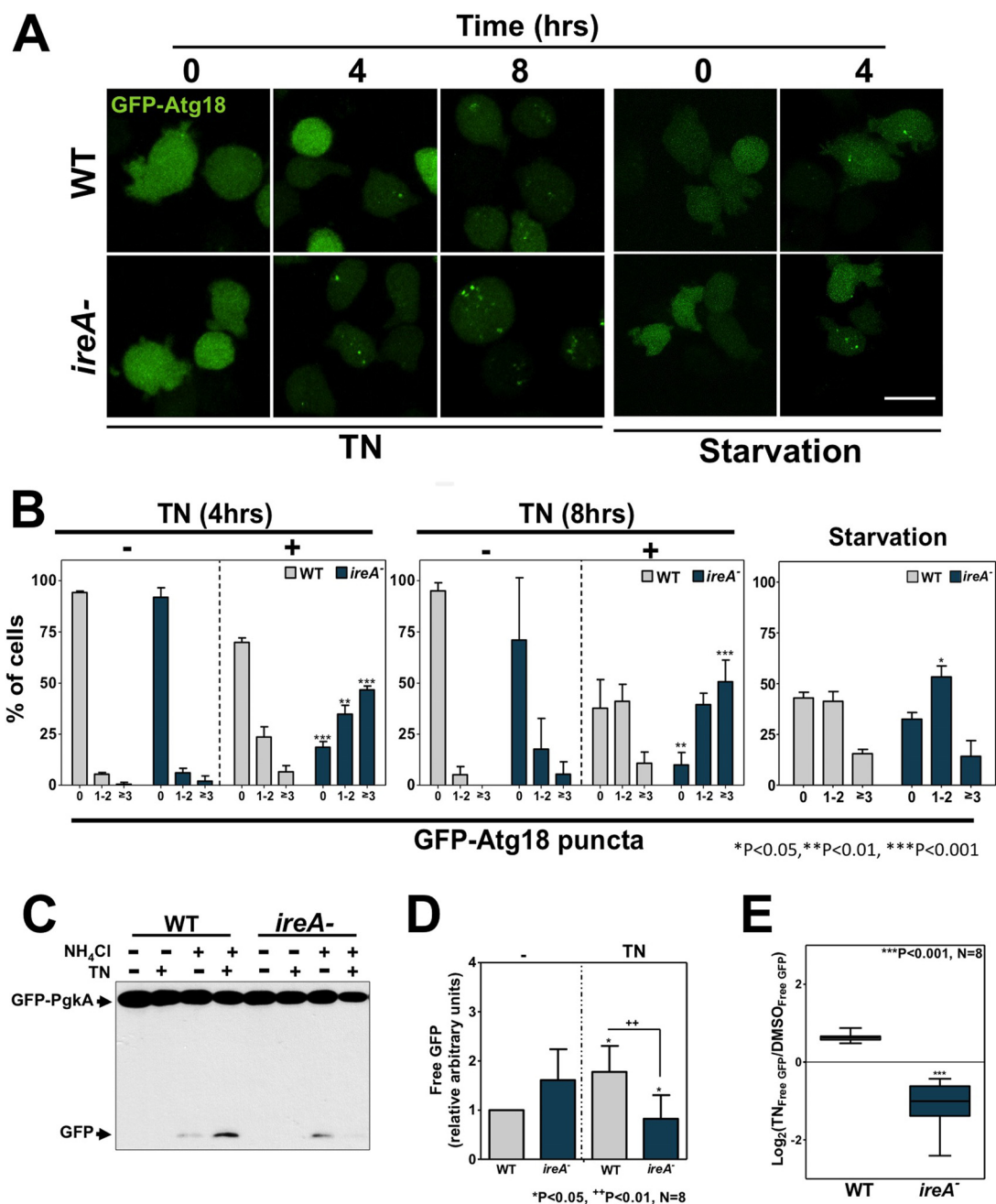
FIG 7 The absence of IreA alters ER stress-induced autophagy. (A) Autophagy was determined as punctum formation in cells expressing GFP-Atg18 (maximum intensity z-projection representative picture). WT and $ireA^-$ cells were treated with 2 μg/ml TN or incubated in starvation buffer for the indicated times. Cells were visualized *in vivo* by confocal microscopy (scale bar, 10 μm). (B) Percentages of cells containing 0, 1 or 2, or $\geq$3 GFP-Atg18 puncta. Values are means $\pm$ the SD of three independent experiments. Asterisks denote statistically significant differences. (C) Representative Western blot of a NH$_4$Cl-induced GFP-PgkA cleavage assay. WT and $ireA^-$ cells overexpressing the GFP-PgkA were treated for 8 h with 2 μg/ml TN. During the last 2 h of treatment, cells were incubated in the presence or absence of NH$_4$Cl as described in Materials and Methods. (D) Quantification of accumulated free GFP in WT and $ireA^-$ cells determined by densitometry. Mean values $\pm$ the SD of eight independent experiments were graphed. GFP was normalized against GFP-PgkA and refers to untreated cells. Asterisks indicate statistically significant differences. (E) Means $\pm$ the SD of the log$_2$ (TN$_{free\ GFP}$/DMSO$_{free\ GFP}$) from the data in panel D.

observations of the decreased degradation capacity of $ireA^-$ cells upon a TN treatment, suggest that the lack of IreA impairs the regulation of autophagosome assembly.

It has been reported that ER stress causes expansion of the ER membrane (21), and our expression data suggest that after TN treatment the ER membrane composition may be adapted to cope with ER stress in *Dictyostelium* cells. In addition, we observed
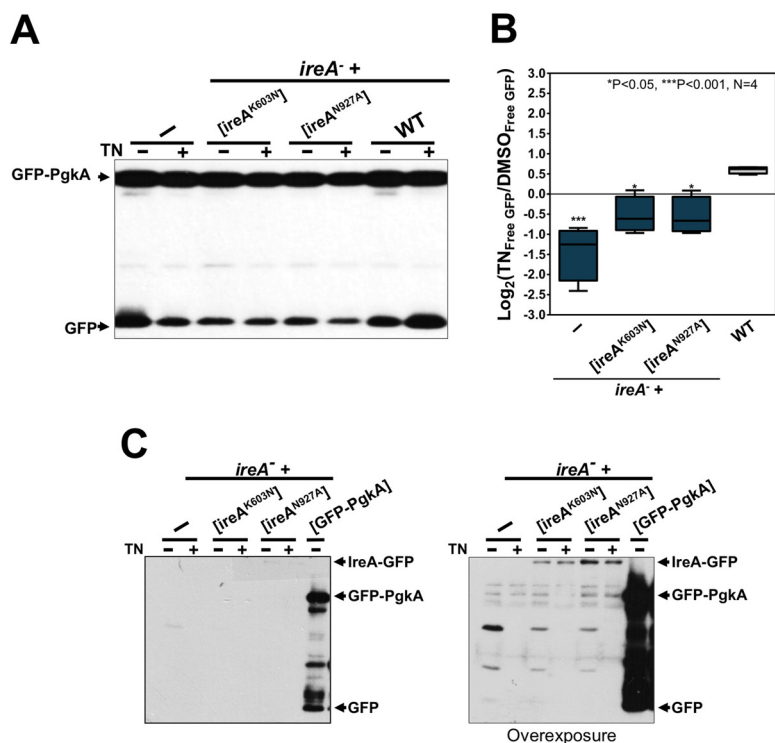
FIG 8 Expression of inactive IreA forms cannot rescue autophagy blockage caused by IreA disruption. (A) NH$_4$Cl-induced GFP-PgkA cleavage assay. A representative Western blot is shown. WT and *ireA*$^-$ cells expressing the indicated constructs were not treated or treated for 8 h with 2 μg/ml TN. During the last 2 h of treatment, cells were incubated in the presence of NH$_4$Cl as described in Materials and Methods. (B) Means ± the SD of the log$_2$(TN$_{free\ GFP}$/DMSO$_{free\ GFP}$) derived from densitometries of the gel in panel A. Free GFP accumulation was normalized against GFP-PgkA and referred to GFP accumulation in the WT strain treated with vehicle alone (DMSO). Values represent the mean of four independent experiments. Significant differences are indicated by asterisks. (C) *ireA*$^-$ cells expressing the GFP-tagged K603N or N927A IreA constructs were treated with DMSO or TN and incubated with NH$_4$Cl.

that ER morphology maintenance upon ER stress depends on a fully functional IreA. Considering that the ER membrane serves as a platform for autophagosome formation in *Dictyostelium* and mammalian cells (27, 61, 65), we hypothesized that the aberrant autophagic structures in *ireA*$^-$ cells may arise from ER dysfunction. To address this possibility, we analyzed ER morphology by immunodetection of PDI in cells expressing the GFP-Atg18 protein. We found that IreA-deficient cells under TN treatment lost the normal structure and distribution of the ER cisternae, which appeared collapsed in large perinuclear structures (Fig. 10B; see also Movie S3 in the supplemental material). In contrast to the WT strain, the aberrant ER of the *ireA*$^-$ mutant presented conspicuous and elongated GFP-Atg18 structures (Fig. 10B and C). These observations support the idea that autophagosome assembly at the ER is impaired in the *ireA*$^-$ cells as a consequence of its inability to restore ER homeostasis upon TN treatment.

DISCUSSION

In this work we present the first characterization of the *Dictyostelium* ER stress response and the UPR pathway. We identified IreA as an essential UPR regulator and studied its connection and relationship with autophagy. *Dictyostelium* contains a single IreA gene, which facilitates the analysis of the role of this sensor in comparison to other organisms such as humans (66) or *A. thaliana* (12), which contain two orthologues. Furthermore, the ER in *Dictyostelium* seems to present more structural similarities with high-order eukaryotes than with yeasts, as can be inferred from microscopy observations from this and other reports (67, 68), making it a good model system for ER-related processes.

Our genome-wide expression data analysis shows that *Dictyostelium* UPR regulates
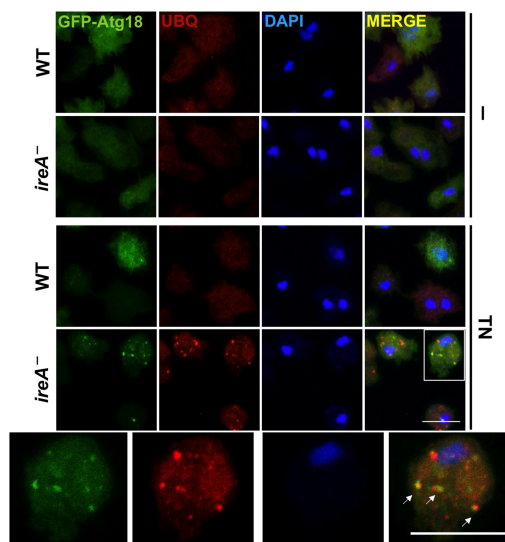
FIG 9 *ireA⁻* cells accumulate aberrant ubiquitin aggregates after TN treatment. Confocal microscopy images of WT and *ireA⁻* cells expressing GFP-Atg18 are shown. Cells were fixed and labeled for immunofluorescence detection with an anti-human ubiquitin antibody (red) after 8 h treatment with 2 μg/ml TN or vehicle alone. Nuclei were stained with DAPI. Arrows indicate GFP-Atg18 and ubiquitin colocalization. Scale bars, 10 μm.

the levels of specific mRNAs upon ER stress, and we concluded that, as described in yeast and mammalian cells (7, 69), *Dictyostelium* adapts to ER stress conditions by increasing the expression of proteins involved in protein folding and degradation processes. Also, a decrease in the ER protein load is achieved by downregulating the expression of genes that are targeted to membranes and to the secretory pathway, among others. Both parts of this transcriptional reprogramming partially depend on IreA, which may activate a transcriptional factor, as described in other organisms (66), since its RNase activity results essential for cell survival and for proper IreA-clustering kinetics after a TN treatment. However, bioinformatics analyses failed to identify an orthologue of the bZIP HAC1/XBP1 transcription factor encoded by the *Dictyostelium* genome. This does not rule out the possible existence of such protein in *Dictyostelium*, since these transcription factors show scarce amino acid similarities between species (70).

In *Schizosaccharomyces pombe* and *Candida glabrata* no homologues of a canonical HAC1/XBP1 have been identified, and the Ire1 RNase activity has been shown to be involved in the degradation of mRNAs in a process known as regulated Ire1-dependent decay of mRNA (RIDD) (52, 71). This process is also part of the UPR in other organisms, such as *Drosophila* and humans (4), and in *Dictyostelium* a similar mechanism could be responsible for the IreA-dependent downregulation of some mRNAs after TN treatment. In addition, the fact that *S. pombe* Ire1 can increase the BiP-mRNA stability directly by processing its 3′ untranslated region (52) opens new possibilities for a direct role of Ire1 in the positive regulation of mRNA stability. This function of Ire1 could be conserved in other organisms in which a canonical HAC1/XBP1 homologue has not been identified, such as *Dictyostelium*.

Almost half of the transcriptional response to the TN treatment in *Dictyostelium* cells is independent of IreA, thus supporting the existence of other ER stress transducers. In animal and plant cells, the UPR is mediated, in addition to Ire1, by ATF6 homologues (72). These ER-resident transmembrane bZIP transcription factors are liberated from the ER under ER stress conditions and translocate to the nucleus to contribute to the transcriptional activation of protein-folding-associated genes, such as the Grp78 gene (72, 73), although we could not identify by BLAST analysis any ATF6 orthologue gene in the *Dictyostelium* genome. In animal cells, ER stress-induced transcriptional regula-
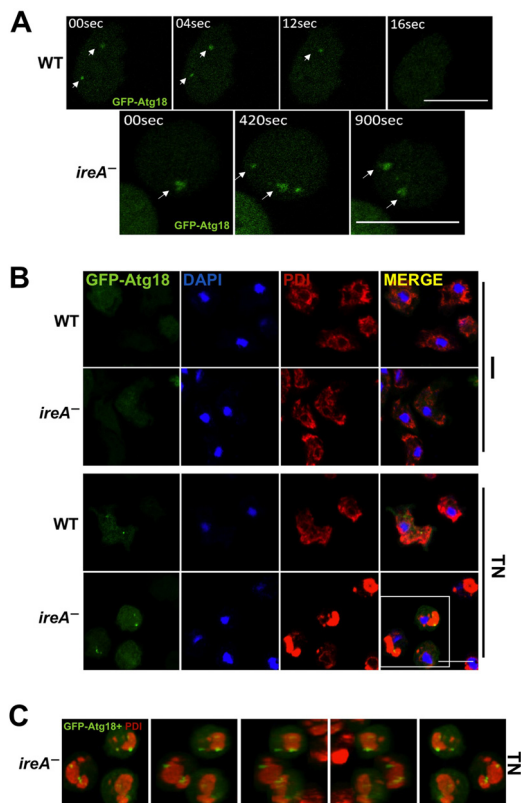
FIG 10 *ireA*⁻ cells exhibit long-lived GFP-Atg18 aberrant structures upon ER stress. (A) Time-lapse confocal images of WT and *ireA*⁻ cells expressing GFP-Atg18 after a 7-h treatment with 2 μg/ml TN. Arrows indicate the same GFP-Atg18 structure in the different time exposures. The corresponding video lapses are included as Movies S1 and S2 in the supplemental material. (B) Confocal microscopy images of WT and *ireA*⁻ cells expressing GFP-Atg18 and prepared for immunodetection of the ER marker PDI (red). Cells were treated for 8 h with 2 μg/ml TN or with vehicle alone. Nuclei were stained with DAPI. (C) Rotational views of a three-dimensional (3D) reconstruction of *ireA*⁻ TN-treated cells. A complete 3D reconstruction is provided in Movie S3 in the supplemental material. Scale bars (A and B), 10 μm.

tion is mediated also by the ER membrane-resident eukaryotic translation initiation factor 2α (eIF2α) kinase PERK; nevertheless, orthologues of this protein have not been identified in fungi or plants (74). BLAST analysis identifies two eIF2α kinases encoded by the *Dictyostelium* genome. However, these proteins have been described as functionally related to yeast Gcn2p, another eIF2α kinase involved in amino acid metabolism (45, 75).

The assembly of Ire oligomers correlates with Ire1 activation and persists only until the adaptation state is reached (50, 76). From our data on oligomer formation it can be inferred that IreA may get activated after a short time of TN treatment (2 h), and adaption under persistent ER stress might take place after longer periods (8 h). In yeast, it has been observed that inactivation of both Ire1 kinase and RNase domains cause persistent Ire1 clustering upon ER stress, indicating that Ire1 activity is required to regulate its activation-inactivation switch during the adaptation process (77). Consistently, IreA must be fully active to properly regulate its clustering behavior during sustained ER stress in *Dictyostelium*.

It has been widely described that ER stress-inducing treatments trigger autophagy. Our data support these observations and, together with the reports from yeasts (21, 33), mammals (30, 78), insects (79, 80), and plants (32, 34), show that this process is highly conserved between species. Despite the TN-induced autophagy in *Dictyostelium* and the sensitivity of autophagy-defective mutants to ER stress, we did not detect any change in the expression of *atg* genes in our whole-genome expression analysis. Since *Dictyostelium* cells possess a highly active autophagy machinery during vegetative
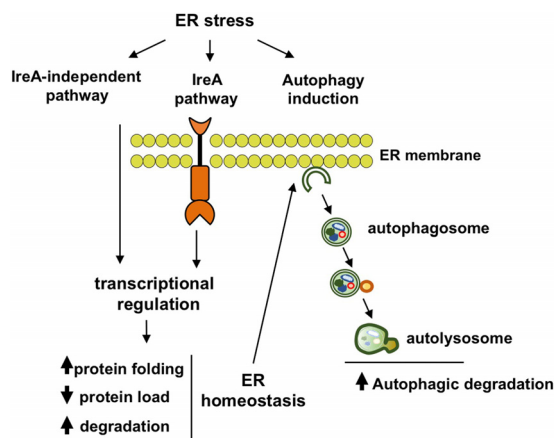
FIG 11 Graphical model of the *Dictyostelium* response to ER stress. IreA and other unknown sensors detect the ER stress stimulus. In turn, they restore ER stability by triggering a transcriptional response that increases the protein folding and degradation capacity of the cell while decreasing the protein load at the ER. Autophagy is also induced in an IreA-independent manner as a response to ER stress and contributes to increase the cellular degradation capacity of cells. ER homeostasis recovery by IreA-dependent and -independent pathways is essential in order to achieve a functional increase in autophagy-associated degradation.

growth (62), an increase in the expression of these genes may not be required. However, we found that the transcript levels of the gene encoding sqstm1 (p62) (61), a protein involved in the degradation of ubiquitinated protein aggregates by autophagy (81), are highly induced. This, together with the observation that the expression of the ERAD retrotranslocation protein CdcD (VCP/p96 orthologue) is also highly induced, suggest that autophagy in *Dictyostelium* may in part participate in the degradation of cytosolic ubiquitinated aggregates that arise from protein retrotranslocation. Autophagy might also be clearing ER-derived nonfunctional membranes, a recovery mechanism that has been observed in stressed yeast (21).

This is the first work evaluating the induction of autophagy upon ER stress in an organism with a complete depletion of Ire1 activity. The autophagy phenotype of single knockouts of both Ire1 plant homologues was analyzed in a previous report (28), and similar analyses were performed in mammalian cells using small interference RNAs (30), a technique that might not completely deplete the expression of the target protein. Yorimitsu et al. (31) reported that in yeasts Ire1-depleted cells under ER stress may show an autophagy blockage, but no experimental data were presented. We observed that autophagy is induced in IreA-depleted cells after a TN treatment, since there is an increase in GFP-Atg18 puncta. However, these structures are persistent, abnormal, and trapped at the ER after TN treatment. In addition, the accumulation of ubiquitinated aggregates and the reduced degradation of GFP-PgkA observed in the *ireA*⁻ strain strongly suggest that these GFP-Atg18-positive structures are unable to degrade cargoes during ER stress. This characteristic is similar to that observed in VMP1-depleted cells in *Dictyostelium* (61). VMP1 is an ER-resident protein involved in the maintenance of ER structure, autophagy, and the regulation of membrane contact sites between the ER and other organelles (68, 82). These phenotypic similarities suggest that abnormalities in the ER might impair the formation of functional omegasomes, the ER-derived structures required for autophagosome formation (83), thereby leading to a blockage in autophagy-dependent degradation.

Our data support a model in which ER stress activates IreA-dependent and -independent pathways (Fig. 11). These pathways cooperate to restore ER homeostasis by reducing the ER protein load and by increasing the protein folding and degradation capacities of the cell. Autophagy is also induced after ER stress in an IreA-independent manner, but complete autophagosome assembly can only proceed if ER homeostasis and the ER structure have been restored. Our findings highlight the delicate balance between

autophagy and ER homeostasis and pinpoint IreA as an important component of this functional relationship.

MATERIALS AND METHODS

***Dictyostelium* cell growth, transformation, and development.** All of the strains used in this study were derived from *D. discoideum* strain AX4. Cells were grown at 22°C in a standard microbiology incubator. Axenic growth was performed in HL5 medium (Formedium, catalog no. HLB0102) supplemented with 1% glucose and penicillin-streptomycin (10,000 U/ml penicillin and 10,000 mg/ml streptomycin; Gibco). For growth in association with bacteria, *K. aerogenes* (Ka strain) was spread onto SM agar plates (1% glucose [Sigma], 1% peptone [Difco], 0.1% yeast extract, 4 mM $MgSO_4$, 13 mM KH_2PO_4, 3 mM K_2HPO_4, and 2% agar). Starvation was induced in PDF buffer (20 mM KCl, 9 mM K_2HPO_4, 13 mM KH_2PO_4, 1 mM $CaCl_2$, 1 mM $MgSO_4$ [pH 6.4]). For drug treatments, stock solutions were prepared, and working solutions at the desired concentrations were prepared by diluting fresh stock aliquots each time in HL5 at the indicated concentrations. Tunicamycin (Enzo Life Sciences) was prepared in DMSO. DTT (Thermo Fisher Scientific) and 2-DOG (Sigma) were diluted in water. All treatments were performed on axenically growing cells at exponential phase.

For transformation, 5×10^6 cells were washed with H50 buffer (4.76 g/liter HEPES, 3.73 g/liter KCl, 0.58 g/liter NaCl, 0.12 g/liter $MgSO_4$, 0.42 g/liter $NaHCO_3$, 0.156 g/liter NaH_2PO_4 [pH 7]) and electroporated with 2 to 10 μg of linear or plasmid DNA. The detailed procedure and the antibiotic concentrations used for selection are described elsewhere (84).

The *ireA* mutant strain was generated by homologous recombination. Cells were transformed with a 2,773-bp PCR product obtained from the pGEM-[*ireA::BST*] construct (see "Plasmid constructs" below). After selection with blasticidin, the transformants were plated on SM plates with *K. aerogenes* for clonal isolation. Homologous recombination was evaluated by colony PCR. For this, DNA was extracted with Master Amp DNA extraction solution (Epicentre) and tested with the indicated oligonucleotides (see Fig. 2 and Results). Other strains used in this study (*atg1⁻*, *atg13⁻*, and *atg101⁻* strains) have been described previously (59). For the development assays 5×10^7 cells growing axenically in HL5 were collected, centrifuged at 1,000 rpm for 5 min, washed two times, and then resuspended in PDF buffer before depositing them in nitrocellulose filters (Millipore, catalog no. HABP04700) soaked in PDF buffer.

Serial dilution spot assays. Exponentially growing cells were adjusted at 10^6 cells/ml density and then subjected to the indicated treatments at the specified concentrations and times. After the treatment, 10-fold serial dilutions were prepared, and 4 μl of each dilution was spotted over a lawn of *K. aerogenes* previously plated on SM agar plates. Depending on the experiment, pictures were taken after 5 to 7 days of incubation at 22°C. All spot assays were performed at least three times.

Plasmid constructs. The *ireA* gene was amplified from genomic DNA, cloned into the pGEM-T Easy vector (Promega), and used as the template for all other constructs. All the IreA-GFP fusion constructs were expressed in *Dictyostelium* using the extrachromosomal pDM323 plasmid (85). PCR products were inserted between the BglII and SpeI sites of this plasmid. Point mutations were introduced by PCR using as the template the complete pGEM-T-[*ireA*] plasmid according to a previously described protocol (86). All constructs were completely sequenced. The pBluescript II containing the blasticidin resistance cassette cloned between EcoRI and HindIII (pBSII-[BST]) (87), was used to generate the *ireA::BST* construction. To generate the pGEM-T-Easy-[*ireA::BST*] construct, the SmaI/KpnI fragment of pBSII-[BST] was introduced between the EcoRV and KpnI sites of the pGEM-T-Easy-[*ireA*] vector. Then, to generate the *ireA::BST* knockout strain, the construct was amplified by PCR with *ireA*-specific oligonucleotides, and *Dictyostelium* AX4 WT cells were electroporated with 5 μg of purified PCR product (see above). Insertion of the BST cassette interrupted the *ireA* gene and caused a 998-bp deletion in the locus (see Fig. 2 and Results). pSJSK489 plasmid expressing GFP-Atg18 was kindly provided by J. King. pDM358 expressing the PgkA-GFP fusion was generated as described previously (56).

RNA extraction and deep RNA sequencing. Cells were adjusted to a density of 10^6 cells/ml and treated for 16 h with 2 μg/ml TN or DMSO in HL5. Cells were separated by centrifugation from this medium and washed with PDF buffer. RNA was extracted according to a standard TRIzol protocol (Sigma). cDNA libraries were prepared from total RNA using a TruSeq sample preparation v2 kit (Illumina), according to the manufacturer's recommendations. Briefly, poly(A) containing mRNA was purified from 1 μg using poly(T) oligonucleotide-attached magnetic beads [oligo(dT) magnetic beads]. Once purified, the mRNA was fragmented using divalent cations under high temperature. After fragmentation, first-strand cDNA was synthesized using reverse transcriptase and random primers, and then a second strand was generated using DNA polymerase I and RNase H. cDNA fragments were end repaired, and a single "A" base was added (to the 3' end of the blunt fragment); barcoded (indexed) adapters were then ligated to each sample. The products were purified and enriched with a 15-cycle PCR to obtain the final cDNA libraries.

Libraries were validated using an Agilent tape station system. Samples were normalized and pooled for sequencing on an Illumina MiSeq. Libraries at a 9 pM concentration were run using a 150-bp single-read protocol. An RNA deep sequencing (RNA-seq) experiment was performed with two biological replicates. This assay was performed at the sequencing service of the molecular biology facility of the Instituto de Fisiología Celular (IFC), UNAM, Mexico.

RNA-seq data assembly was performed using TopHat and Cufflinks (88), and the set of significantly differentially expressed genes was obtained using the two biological replicates (raw data can be found at NCBI GEO database under accession number GSE104409). The obtained list was further filtered in order to contain only genes that were represented by ~1 mRNA per cell in one of the two compared conditions. In accordance to Parikh et al. (89), using our conditions 1 mRNA would be represented by 15

normalized read counts. The genes that presented a $\log_2$ fold change of ≥ 1.3 or ≤ -1.3 between the tested conditions (see Archive S1 in the supplemental material) were further analyzed and classified in enriched gene ontology categories with the DAVID functional annotation tool (53, 54), using the biological process (GOTERM_BP_DIRECT), cellular component (GOTERM_CC_DIRECT), and protein domains (INTERPRO) categories, with default settings.

Bioinformatic analysis. *Dictyostelium* sequences were obtained from the dictyBase (90), and BLAST searches were also performed using the tool provided in this database. Protein sequences from other organisms were obtained from the UniProt database (91). The SIM alignment tool (92) was used for local protein alignments, and results were visualized with LALNVIEW (93). Multiple alignments were performed with CLUSTAL OMEGA (57). The assembly of the data obtained from the deep RNA sequencing of poly(A) RNA was performed using the TopHat and Cufflinks open source software as described previously (88). Ontology enrichment analyses were performed with the PANTHER (94) and DAVID (53, 54) web tools.

Microscopy. Exponentially growing cells were adjusted to 10^6 cells/ml, treated as specified, and transferred to Ibidi m-Slide 8-well slides. The cells were then directly observed *in vivo* (for cells expressing fluorescently tagged proteins) or fixed for immunofluorescence detection. For this procedure, cells were fixed for 15 min after the desired treatment with 2% paraformaldehyde dissolved in phosphate-buffered saline or PDF buffer. Primary antibody incubation was performed overnight at 4°C. Antibody to *Dictyostelium* PDI was kindly provided by Pierre Cosson, and anti-human ubiquitin (P4D1) 3936 was purchased from Cell Signaling (used at 1:1,000 and 1:500 dilutions, respectively). For fluorescence detection, preparations were incubated 30 min at room temperature with a secondary antibody conjugated to Alexa Fluor red 546. Nuclei were stained with DAPI (4′,6′-diamidino-2-phenylindole). Confocal images were acquired with an inverted Zeiss spectral LSM710 microscope. To evaluate cell morphology, cells were deposited on standard microscope slides and analyzed with an inverted phase-contrast microscope. Cells developing in nitrocellulose filters were visualized with a Nikon SMZ800 microscope.

Western blotting. After the specified treatments, the cells were washed with PDF buffer and resuspended in lysis buffer (10 mM Tris-HCl [pH 7.5], 150 mM NaCl, 0.5 mM EDTA, 0.5% NP-40, 0.05% SDS) supplemented with a fresh protease inhibitor cocktail (Sigma), followed by incubation for 30 min on ice. The total protein concentration was assayed from cleared protein extracts using a BCA commercial kit (Thermo Fisher Scientific). Total cell extracts were subjected to SDS-PAGE separation and transferred to polyvinylidene difluoride membranes (Millipore). Immunoblot detection was performed with the following specified antibodies: anti-GFP (Sigma-Aldrich, G1544), anti-Grp78 (Santa Cruz Biotechnology, sc-1050, goat anti-human GRP78 [N-20], discontinued), or anti-cdcD (Vcp/P97; rabbit anti-*Dictyostelium* CdcD, kindly provided by Ludwig Eichinger [43]). MCCC1 was used as an internal load control and was detected by using streptavidin conjugated to horseradish peroxidase as described elsewhere (95). Densitometric analysis of Western blot images was performed with ImageJ software. These measurements were used to determine arbitrary protein level values. MCCC1 or GFP-PgkA was used for normalization.

Autophagy assays. Cells expressing GFP-Atg18 were analyzed by live confocal microscopy imaging, and punctum-containing cells were quantified manually with ImageJ software by analyzing maximum z-projections and comparing them with individual stacks.

Autophagy capacity was evaluated using a modification of the previously described proteolytic assay (56, 58). PgkA-GFP-expressing cells were adjusted to 10^6 cells/ml and then treated for 8 h with 2 μg/ml TN or vehicle (DMSO). During the last 2 h of treatment, two 1-h pulses of 150 mM NH_4Cl were applied. The cells were then collected, lysed, and prepared for Western blot analysis as described above. The accumulation of free GFP was quantified by densitometry and normalized against GFP-PgkA.

Statistical analyses. Mean values, standard deviations (SD), and significance were graphed and analyzed from at least three independent experiments using GraphPad Prism 5. Statistical significance was tested with either a Student t test, a one-way analysis of variance (ANOVA) with Dunnett's posttest, or a two-way ANOVA with a Bonferroni posttest depending on the number of variables for the experiment.

Accession number(s). The raw RNA-seq data analyzed during the present study are available from the NCBI GEO database under accession number GSE104409.

SUPPLEMENTAL MATERIAL

Supplemental material for this article may be found at https://doi.org/10.1128/MCB .00054-18.

SUPPLEMENTAL FILE 1, AVI file, 1.4 MB.
SUPPLEMENTAL FILE 2, AVI file, 2.4 MB.
SUPPLEMENTAL FILE 3, AVI file, 1.6 MB.
SUPPLEMENTAL FILE 4, XLS file, 0.2 MB.
SUPPLEMENTAL FILE 5, XLS file, 0.1 MB.
SUPPLEMENTAL FILE 6, XLS file, 0.1 MB.
SUPPLEMENTAL FILE 7, XLS file, 0.1 MB.
SUPPLEMENTAL FILE 8, XLS file, 0.1 MB.
SUPPLEMENTAL FILE 9, XLS file, 0.1 MB.

ACKNOWLEDGMENTS

REFERENCES

1. Snapp E. 2005. Endoplasmic reticulum biogenesis: proliferation and differentiation, p 63–95. Landes Bioscience/Kluwer Academic/Plenum Publishers, New York, NY.

2. Fagone P, Jackowski S. 2009. Membrane phospholipid synthesis and endoplasmic reticulum function. J Lipid Res 50(Suppl):S311–S316. https://doi.org/10.1194/jlr.R800049-JLR200.

3. Scheuner D, Song B, McEwen E, Liu C, Laybutt R, Gillespie P, Saunders T, Bonner-Weir S, Kaufman RJ. 2001. Translational control is required for the unfolded protein response and *in vivo* glucose homeostasis. Mol Cell 7:1165–1176. https://doi.org/10.1016/S1097-2765(01)00265-9.

4. Maurel M, Chevet E, Tavernier J, Gerlo S. 2014. Getting RIDD of RNA: IRE1 in cell fate regulation. Trends Biochem Sci 39:245–254. https://doi.org/10.1016/j.tibs.2014.02.008.

5. Lee A, Iwakoshi N, Glimcher L. 2003. XBP-1 regulates a subset of endoplasmic reticulum resident chaperone genes in the unfolded protein response. Mol Cell Biol 23:7448–7459. https://doi.org/10.1128/MCB.23.21.7448-7459.2003.

6. Sriburi R, Jackowski S, Mori K, Brewer JW. 2004. XBP1: a link between the unfolded protein response, lipid biosynthesis, and biogenesis of the endoplasmic reticulum. J Cell Biol 167:35–41. https://doi.org/10.1083/jcb.200406136.

7. Travers KJ, Patil CK, Wodicka L, Lockhart DJ, Weissman JS, Walter P. 2000. Functional and genomic analyses reveal an essential coordination between the unfolded protein response and ER-associated degradation. Cell 101:249–258. https://doi.org/10.1016/S0092-8674(00)80835-1.

8. Ron D, Walter P. 2007. Signal integration in the endoplasmic reticulum unfolded protein response. Nat Rev Cell Biol 8:519–529. https://doi.org/10.1038/nrm2199.

9. Chen Y, Brandizzi F. 2013. IRE1: ER stress sensor and cell fate executor. Trends Cell Biol 23:547–555. https://doi.org/10.1016/j.tcb.2013.06.005.

10. Gardner BM, Walter P. 2011. Unfolded proteins are Ire1-activating ligands that directly induce the unfolded protein response. Science 333:1891–1894. https://doi.org/10.1126/science.1209126.

11. Kimata Y, Kimata YI, Shimizu Y, Abe H, Farcasanu IC, Takeuchi M. 2003. Genetic evidence for a role of BiP/Kar2 that regulates Ire1 in response to accumulation of unfolded proteins. Mol Biol Cell 14:2559–2569.

12. Nagashima Y, Mishiba K, Suzuki E, Shimada Y, Iwata Y, Koizumi N. 2011. *Arabidopsis* IRE1 catalyses unconventional splicing of bZIP60 mRNA to produce the active transcription factor. Sci Rep 1:29. https://doi.org/10.1038/srep00029.

13. Kawahara T, Yanagi H, Yura T, Mori K. 1997. Endoplasmic reticulum stress-induced mRNA splicing permits synthesis of transcription factor Hac1p/Ern4p that activates the unfolded protein response. Mol Biol Cell 8:1845–1862. https://doi.org/10.1091/mbc.8.10.1845.

14. Bowring C, Llewellyn D. Differences in HAC1 mRNA processing and translation between yeast and mammalian cells indicate divergence of the eukaryotic ER stress response. Biochem Biophys Res Commun 287:789–800.

15. Iwata Y, Koizumi N. 2005. An *Arabidopsis* transcription factor, AtbZIP60, regulates the endoplasmic reticulum stress response in a manner unique to plants. Proc Natl Acad Sci U S A 102:5280–5285. https://doi.org/10.1073/pnas.0408941102.

16. Cox JS, Walter P. 1996. A novel mechanism for regulating activity of a transcription factor that controls the unfolded protein response. Cell 87:391–404. https://doi.org/10.1016/S0092-8674(00)81360-4.

17. Martinez IM, Chrispeels MJ. 2003. Genomic analysis of the unfolded protein response in *Arabidopsis* shows its connection to important cellular processes. Plant Cell 15:561–576. https://doi.org/10.1105/tpc.007609.

18. Ruggiano A, Foresti O, Carvalho P. 2014. Quality control: ER-associated degradation: protein quality control and beyond. J Cell Biol 204:869–879. https://doi.org/10.1083/jcb.201312042.

19. Tsai B, Ye Y, Rapoport Ta. 2002. Retro-translocation of proteins from the endoplasmic reticulum into the cytosol. Nat Rev Mol Cell Biol 3:246–255. https://doi.org/10.1038/nrm780.

20. Yorimitsu T, Klionsky DJ. 2007. Eating the endoplasmic reticulum: quality control by autophagy. Trends Cell Biol 17:279–285. https://doi.org/10.1016/j.tcb.2007.04.005.

21. Bernales S, McDonald KL, Walter P. 2006. Autophagy counterbalances endoplasmic reticulum expansion during the unfolded protein response. PLoS Biol 4:e423. https://doi.org/10.1371/journal.pbio.0040423.

22. Cheng Y. 2011. Survival and death of endoplasmic-reticulum-stressed cells: role of autophagy. World J Biol Chem 2:226–231. https://doi.org/10.4331/wjbc.v2.i10.226.

23. Klionsky DJ, Emr SD. 2000. Autophagy as a regulated pathway of cellular degradation. Science 290:1717–1721. https://doi.org/10.1126/science.290.5497.1717.

24. Kroemer G, Mariño G, Levine B. 2010. Autophagy and the integrated stress response. Mol Cell 40:280–293. https://doi.org/10.1016/j.molcel.2010.09.023.

25. Russell RC, Yuan H-X, Guan K-L. 2014. Autophagy regulation by nutrient signaling. Cell Res 24:42–57. https://doi.org/10.1038/cr.2013.166.

26. Filomeni G, Zio DD, Cecconi F, De Zio D, Cecconi F. 2015. Oxidative stress and autophagy: the clash between damage and metabolic needs. Cell Death Differ 22:377–388. https://doi.org/10.1038/cdd.2014.150.

27. King JS, Veltman DM, Insall RH. 2011. The induction of autophagy by mechanical stress. Autophagy 7:1490–1499. https://doi.org/10.4161/auto.7.12.17924.

28. Desai M, Fang R, Sun J. 2015. The role of autophagy in microbial infection and immunity. Immunotargets Ther 4:13–27. https://doi.org/10.2147/ITT.S76720.

29. Suh DH, Kim M-K, Kim HS, Chung HH. 2012. Unfolded protein response to autophagy as a promising druggable target for anticancer therapy. Ann N Y Acad Sci 1271:20–32. https://doi.org/10.1111/j.1749-6632.2012.06739.x.

30. Ogata M, Hino S-I, Saito A, Morikawa K, Kondo S, Kanemoto S, Murakami T, Taniguchi M, Tanii I, Yoshinaga K, Shiosaka S, Hammarback Ja Urano F, Imaizumi K. 2006. Autophagy is activated for cell survival after endoplasmic reticulum stress. Mol Cell Biol 26:9220–9231. https://doi.org/10.1128/MCB.01453-06.

31. Deegan S, Koryga I, Glynn SA, Gupta S, Gorman AM, Samali A. 2014. A close connection between the PERK and IRE arms of the UPR and the transcriptional regulation of autophagy. Biochem Biophys Res Commun 456:305–311. https://doi.org/10.1016/j.bbrc.2014.11.076.

32. Liu Y, Burgos JS, Deng Y, Srivastava R, Howell SH, Bassham DC. 2012. Degradation of the endoplasmic reticulum by autophagy during endoplasmic reticulum stress in *Arabidopsis*. Plant Cell 24:4635–4651. https://doi.org/10.1105/tpc.112.101535.

33. Yorimitsu T, Nair U, Yang Z, Klionsky DJ. 2006. Endoplasmic reticulum stress triggers autophagy. J Biol Chem 281:30299–30304. https://doi.org/10.1074/jbc.M607007200.

34. Perez-Martin M, Perez-Perez ME, Lemaire SD, Crespo JL. 2014. Oxidative stress contributes to autophagy induction in response to endoplasmic reticulum stress in *Chlamydomonas*. Plant Physiol 166:997–1008. https://doi.org/10.1104/pp.114.243659.

35. Yang X, Srivastava R, Howell SH, Bassham DC. 2016. Activation of autophagy by unfolded proteins during endoplasmic reticulum stress. Plant J 85:83–95. https://doi.org/10.1111/tpj.13091.

36. Schuck S, Gallagher CM, Walter P. 2014. ER-phagy mediates selective degradation of endoplasmic reticulum independently of the core autophagy machinery. J Cell Sci 127(Pt 18):4078–4088. https://doi.org/10.1242/jcs.154716.

37. Mesquita A, Cardenal-Munoz E, Dominguez E, Munoz-Braceras S, Nunez-Corcuera B, Phillips BA, Tabara LC, Xiong Q, Coria R, Eichinger L, Golstein P, King JS, Soldati T, Vincent O, Escalante R. 2017. Autophagy in *Dictyostelium*: mechanisms, regulation and disease in a simple biomedical model. Autophagy 13:24–40. https://doi.org/10.1080/15548627.2016.1226737.

38. Calvo-garrido J, Carilla-latorre S, Kubohara Y, Santos-rodrigo N, Mesquita A, Soldati T, Golstein P, Escalante R. 2010. Genes and pathways, cell death and infection autophagy in *Dictyostelium*. Autophagy 6:686–701. https://doi.org/10.4161/auto.6.6.12513.

39. Back S, Schröder M, Lee K, Zhang K, Kaufman RJ. 2005. ER stress signaling by regulated splicing: IRE1/HAC1/XBP1. Methods 35:395–416. https://doi.org/10.1016/j.ymeth.2005.03.001.

40. Kwolek-Mirek M, Zadrag-Tecza R. 2014. Comparison of methods used for assessing the viability and vitality of yeast cells. FEMS Yeast Res 14:1068–1079.

41. Nikawa J, Akiyoshi M, Hirata S, Fukuda T. 1996. *Saccharomyces cerevisiae* IRE2/HAC1 is involved in IRE1-mediated KAR2 expression. Nucleic Acids Res 24:4222–4226.

42. Wolf DH, Stolz A. 2012. The Cdc48 machine in endoplasmic reticulum associated protein degradation. Biochim Biophys Acta 1823:117–124. https://doi.org/10.1016/j.bbamcr.2011.09.002.

43. Arhzaouy K, Strucksberg KH, Tung SM, Tangavelou K, Stumpf M, Faix J, Schroder R, Clemen CS, Eichinger L. 2012. Heteromeric p97/p97(R155C) complexes induce dominant negative changes in wild-type and autophagy 9-deficient *Dictyostelium* strains. PLoS One 7:e46879. https://doi.org/10.1371/journal.pone.0046879.

44. Cohen NR, Knecht DA, Lodish HF. 1996. Functional expression of rat GLUT1 glucose transporter in *Dictyostelium discoideum*. Biochem J 315:971–975. https://doi.org/10.1042/bj3150971.

45. Rai M, Xiong Y, Singleton CK. 2006. Disruption of the ifkA and ifkB genes results in altered cell adhesion, morphological defects and a propensity to form pre-stalk O cells during development of *Dictyostelium*. Differentiation 74:583–595. https://doi.org/10.1111/j.1432-0436.2006.00085.x.

46. Singleton CK, Xiong Y, Kirsten JH, Pendleton KP. 2012. eIF2α kinases regulate development through the BzpR transcription factor in *Dictyostelium discoideum*. PLoS One 7:e32500. https://doi.org/10.1371/journal.pone.0032500.

47. Shamu C, Cox J, Walter P. 1994. The unfolded-protein-response pathway in yeast. Trends Cell Biol 4:56–60. https://doi.org/10.1016/0962-8924(94)90011-6.

48. Tirasophon W, Welihinda A, Kaufman R. 1998. A stress response pathway from the endoplasmic reticulum to the nucleus requires a novel bifunctional protein kinase/endoribonuclease (Ire1p) in mammalian cells. Genes Dev 12:1812–1824. https://doi.org/10.1101/gad.12.12.1812.

49. Tirasophon W, Lee K, Callaghan B, Welihinda A, Kaufman RJ. 2000. The endoribonuclease activity of mammalian IRE1 autoregulates its mRNA and is required for the unfolded protein response. Genes Dev 14:2725–2736. https://doi.org/10.1101/gad.839400.

50. Li H, Korennykh AV, Behrman SL, Walter P. 2010. Mammalian endoplasmic reticulum stress sensor IRE1 signals by dynamic clustering. Proc Natl Acad Sci U S A 107:16113–16118. https://doi.org/10.1073/pnas.1010580107.

51. Xu Z, Chikka MR, Xia H, Ready DF. 2016. Ire1 supports normal ER differentiation in developing *Drosophila* photoreceptors. J cell science 44:921–929. https://doi.org/10.1242/jcs.180406.

52. Kimmig P, Diaz M, Zheng J, Williams CC, Lang A, Aragón T, Li H, Walter P. 2012. The unfolded protein response in fission yeast modulates stability of select mRNAs to maintain protein homeostasis. Elife 1:e00048. https://doi.org/10.7554/eLife.00048.

53. Huang da W, Sherman BT, Lempicki RA. 2009. Systematic and integrative analysis of large gene lists using DAVID bioinformatics resources. Nat Protoc 4:44–57. https://doi.org/10.1038/nprot.2008.211.

54. Huang da W, Sherman BT, Lempicki RA. 2009. Bioinformatics enrichment tools: paths toward the comprehensive functional analysis of large gene lists. Nucleic Acids Res 37:1–13. https://doi.org/10.1093/nar/gkn923.

55. Mesquita A, Cardenal-Muñoz E, Dominguez E, Muñoz-Braceras S, Nuñez-Corcuera B, Phillips BA, Tábara LC, Xiong Q, Coria R, Eichinger L, Golstein P, King JS, Soldati T, Vincent O, Escalante R. 2016. Autophagy in *Dictyostelium*: mechanisms, regulation, and disease in a simple biomedical model. Autophagy 13:1–17.

56. Mesquita A, Calvo-Garrido J, Carilla-Latorre S, Escalante R. 2013. Monitoring autophagy in *Dictyostelium*. Methods Mol Biol 983:461–470. https://doi.org/10.1007/978-1-62703-302-2_26.

57. Sievers F, Wilm A, Dineen D, Gibson TJ, Karplus K, Li W, Lopez R, McWilliam H, Remmert M, Soding J, Thompson JD, Higgins DG. 2014. Fast, scalable generation of high-quality protein multiple sequence alignments using Clustal Omega. Mol Syst Biol 7:539–539. https://doi.org/10.1038/msb.2011.75.

58. Calvo-Garrido J, Carilla-Latorre S, Mesquita A, Escalante R. 2011. A proteolytic cleavage assay to monitor autophagy in *Dictyostelium discoideum*. Autophagy 7:1063–1068. https://doi.org/10.4161/auto.7.9.16629.

59. Mesquita A, Tabara LC, Martinez-Costa O, Santos-Rodrigo N, Vincent O, Escalante R. 2015. Dissecting the function of Atg1 complex in *Dictyostelium* autophagy reveals a connection with the pentose phosphate pathway enzyme transketolase. Open Biol 5:150088. https://doi.org/10.1098/rsob.150088.

60. Calvo-Garrido J, King JS, Munoz-Braceras S, Escalante R. 2014. Vmp1 regulates PtdIns3P signaling during autophagosome formation in *Dictyostelium discoideum*. Traffic 15:1235–1246. https://doi.org/10.1111/tra.12210.

61. Calvo-Garrido J, Escalante R. 2010. Autophagy dysfunction and ubiquitin-positive protein aggregates in *Dictyostelium* cells lacking Vmp1. Autophagy 6:100–109. https://doi.org/10.4161/auto.6.1.10697.

62. Dominguez-Martin E, Cardenal-Munoz E, King JS, Soldati T, Coria R, Escalante R. 2017. Methods to monitor and quantify autophagy in the social amoeba *Dictyostelium discoideum*. Cells 6:E18. https://doi.org/10.3390/cells6030018.

63. Koyama-Honda I, Itakura E, Fujiwara TK, Mizushima N. 2013. Temporal analysis of recruitment of mammalian ATG proteins to the autophagosome formation site. Autophagy 9:1491–1499. https://doi.org/10.4161/auto.25529.

64. Kishi-Itakura C, Koyama-Honda I, Itakura E, Mizushima N. 2014. Ultrastructural analysis of autophagosome organization using mammalian autophagy-deficient cells. J Cell Sci 127:4089–4102. https://doi.org/10.1242/jcs.156034.

65. Simonsen A, Stenmark H. 2008. Self-eating from an ER-associated cup. J Cell Biol 182:621–622. https://doi.org/10.1083/jcb.200807061.

66. Yoshida H, Matsui T, Yamamoto A, Okada T, Mori K. 2001. XBP1 mRNA is induced by ATF6 and spliced by IRE1 in response to ER stress to produce a highly active transcription factor. Cell 107:881–891. https://doi.org/10.1016/S0092-8674(01)00611-0.

67. Monnat J, Neuhaus EM, Pop MS, Ferrari DM, Kramer B, Soldati T. 2000. Identification of a novel saturable endoplasmic reticulum localization mechanism mediated by the C terminus of a *Dictyostelium* protein disulfide isomerase. Mol Biol Cell 11:3469–3484. https://doi.org/10.1091/mbc.11.10.3469.

68. Calvo-Garrido J, Carilla-Latorre S, La F, Egea G, Escalante R. 2008. Vacuole membrane protein 1 is an endoplasmic reticulum protein required for organelle biogenesis, protein secretion, and development. Mol Biol Cell 19:3442–3453. https://doi.org/10.1091/mbc.E08-01-0075.

69. Chow CY, Wang X, Riccardi D, Wolfner MF, Clark AG. 2015. The genetic architecture of the genome-wide transcriptional response to ER stress in the mouse. PLoS Genet 11:e1004924. https://doi.org/10.1371/journal.pgen.1004924.

70. Hooks KB, Griffiths-Jones S. 2011. Conserved RNA structures in the non-canonical Hac1/Xbp1 intron. RNA Biol 8:552–556. https://doi.org/10.4161/rna.8.4.15396.

71. Miyazaki T, Nakayama H, Nagayoshi Y, Kakeya H, Kohno S. 2013. Dissection of Ire1 functions reveals stress response mechanisms uniquely

evolved in *Candida glabrata*. PLoS Pathog 9:e1003160. https://doi.org/10.1371/journal.ppat.1003160.

72. Haze K, Yoshida H, Yanagi H, Yura T, Mori K. 1999. Mammalian transcription factor ATF6 is synthesized as a transmembrane protein and activated by proteolysis in response to endoplasmic reticulum stress. Mol Biol Cell 10:3787–3799. https://doi.org/10.1091/mbc.10.11.3787.

73. Baumeister P, Luo S, Skarnes W, Sui G, Seto E, Shi Y, Lee A. 2005. Endoplasmic reticulum stress induction of the Grp78/BiP promoter: activating mechanisms mediated by YY1 and its interactive chromatin modifiers. Mol Cell Biol 25:4529–4540. https://doi.org/10.1128/MCB.25.11.4529-4540.2005.

74. Hollien J. 2013. Evolution of the unfolded protein response. Biochim Biophys Acta 1833:2458–2463. https://doi.org/10.1016/j.bbamcr.2013.01.016.

75. Singleton CK, Xiong Y, Kirsten JH, Pendleton KP. 2012. eIF2α kinases regulate development through the BzpR transcription factor in *Dictyostelium discoideum*. PLoS One 7:e32500. https://doi.org/10.1371/journal.pone.0032500.

76. Aragon T, van Anken E, Pincus D, Serafimova IM, Korennykh AV, Rubio CA, Walter P. 2009. Messenger RNA targeting to endoplasmic reticulum stress signaling sites. Nature 457:736–740. https://doi.org/10.1038/nature07641.

77. Rubio C, Pincus D, Korennykh A, Schuck S, El-Samad H, Walter P. 2011. Homeostatic adaptation to endoplasmic reticulum stress depends on Ire1 kinase activity. J Cell Biol 193:171–184. https://doi.org/10.1083/jcb.201007077.

78. Ding WX, Ni HM, Gao W, Hou YF, Melan MA, Chen X, Stolz DB, Shao ZM, Yin XM. 2007. Differential effects of endoplasmic reticulum stress-induced autophagy on cell survival. J Biol Chem 282:4702–4710. https://doi.org/10.1074/jbc.M609267200.

79. Fouillet A, Levet C, Virgone A, Robin M, Dourlen P, Rieusset J, Belaidi E, Ovize M, Touret M, Nataf S, Mollereau B. 2012. ER stress inhibits neuronal death by promoting autophagy. Autophagy 8:915–926. https://doi.org/10.4161/auto.19716.

80. Velentzas PD, Velentzas AD, Mpakou VE, Antonelou MH, Margaritis LH, Papassideri IS, Stravopodis DJ. 2013. Detrimental effects of proteasome inhibition activity in *Drosophila melanogaster*: implication of ER stress, autophagy, and apoptosis. Cell Biol Toxicol 29:13–37. https://doi.org/10.1007/s10565-012-9235-9.

81. Pankiv S, Clausen TH, Lamark T, Brech A, Bruun JA, Outzen H, Øvervatn A, Bjørkøy G, Johansen T. 2007. p62/SQSTM1 binds directly to Atg8/LC3 to facilitate degradation of ubiquitinated protein aggregates by autophagy. J Biol Chem 282:24131–24145. https://doi.org/10.1074/jbc.M702824200.

82. Tabara LC, Escalante R. 2016. VMP1 establishes ER-microdomains that regulate membrane contact sites and autophagy. PLoS One 11:e0166499. https://doi.org/10.1371/journal.pone.0166499.

83. Axe EL, Walker SA, Manifava M, Chandra P, Roderick HL, Habermann A, Griffiths G, Ktistakis NT. 2008. Autophagosome formation from membrane compartments enriched in phosphatidylinositol 3-phosphate and dynamically connected to the endoplasmic reticulum. J Cell Biol 182:685–701. https://doi.org/10.1083/jcb.200803137.

84. Gaudet P, Pilcher KE, Fey P, Chisholm RL. 2007. Transformation of *Dictyostelium discoideum* with plasmid DNA. Nat Protoc 2:1317–1324. https://doi.org/10.1038/nprot.2007.179.

85. Veltman DM, Akar G, Bosgraaf L, Van Haastert PJ. 2009. A new set of small, extrachromosomal expression vectors for *Dictyostelium discoideum*. Plasmid 61:110–118. https://doi.org/10.1016/j.plasmid.2008.11.003.

86. Kunkel TA. 1985. Rapid and efficient site-specific mutagenesis without phenotypic selection. Proc Natl Acad Sci U S A 82:488–492. https://doi.org/10.1073/pnas.82.2.488.

87. Adachi H, Hasebe T, Yoshinaga K, Ohta T, Sutoh K. 1994. Isolation of *Dictyostelium discoideum* cytokinesis mutants by restriction enzyme-mediated integration of the blasticidin S resistance marker. Biochem Biophys Res Commun 205:1808–1814. https://doi.org/10.1006/bbrc.1994.2880.

88. Trapnell C, Roberts A, Goff L, Pertea G, Kim D, Kelley DR, Pimentel H, Salzberg SL, Rinn JL, Pachter L. 2012. Differential gene and transcript expression analysis of RNA-seq experiments with TopHat and Cufflinks. Nat Protoc 7:562–578. https://doi.org/10.1038/nprot.2012.016.

89. Parikh A, Miranda ER, Katoh-Kurasawa M, Fuller D, Rot G, Zagar L, Curk T, Sucgang R, Chen R, Zupan B, Loomis WF, Kuspa A, Shaulsky G. 2010. Conserved developmental transcriptomes in evolutionarily divergent species. Genome Biol 11:R35. https://doi.org/10.1186/gb-2010-11-3-r35.

90. Fey P, Dodson RJ, Basu S, Chisholm RL. 2013. One stop shop for everything *Dictyostelium*: dictyBase and the Dicty Stock Center in 2012. Methods Mol Biol 983:59–92. https://doi.org/10.1007/978-1-62703-302-2_4.

91. Consortium TU. 2008. The universal protein resource (UniProt). Nucleic Acids Res 36:D190–D195. https://doi.org/10.1093/nar/gkm895.

92. Huang X, Miller W. 1991. A time-efficient, linear-space local similarity algorithm. Adv Appl Math 12:337–357. https://doi.org/10.1016/0196-8858(91)90017-D.

93. Duret L, Gasteiger E, Perriere G. 1996. LALNVIEW: a graphical viewer for pairwise sequence alignments. Comput Appl Biosci 12:507–510.

94. Mi H, Muruganujan A, Thomas PD. 2013. PANTHER in 2013: modeling the evolution of gene function, and other gene attributes, in the context of phylogenetic trees. Nucleic Acids Res 41(Database Issue):D377–D386. https://doi.org/10.1093/nar/gks1118.

95. Davidson AJ, King JS, Insall RH. 2013. The use of streptavidin conjugates as immunoblot loading controls and mitochondrial markers for use with *Dictyostelium discoideum*. Biotechniques 55:39–41. https://doi.org/10.2144/000114054.

Methods to Monitor and Quantify Autophagy in the Social Amoeba *Dictyostelium discoideum*

Eunice Domínguez-Martín [1,2], Elena Cardenal-Muñoz [3] ⓘ, Jason S. King [4], Thierry Soldati [3] ⓘ, Roberto Coria [2] and Ricardo Escalante [1,*]

[1] Instituto de Investigaciones Biomédicas "Alberto Sols" (CSIC-UAM), Arturo Duperier 4, 28029 Madrid, Spain; edominguez@iib.uam.es

[2] Departamento de Genética Molecular, Instituto de Fisiología Celular, Universidad Nacional Autónoma de México, 04510 Ciudad de México, Mexico; rcoria@ifc.unam.mx

[3] Département de Biochimie, Faculté des Sciences, Université de Genève, Sciences II, CH-1211-Genève-4, Switzerland; Elena.Cardenal@unige.ch (E.C.-M.); Thierry.Soldati@unige.ch (T.S.)

[4] Department of Biomedical Sciences and Bateson Centre, University of Sheffield, Sheffield S10 2TN, UK; jason.king@sheffield.ac.uk

[*] Correspondence: rescalante@iib.uam.es; Tel.: +34-915-854-467; Fax: +34-915-854-401

Abstract: Autophagy is a eukaryotic catabolic pathway that degrades and recycles cellular components to maintain homeostasis. It can target protein aggregates, superfluous biomolecular complexes, dysfunctional and damaged organelles, as well as pathogenic intracellular microbes. Autophagy is a dynamic process in which the different stages from initiation to final degradation of cargo are finely regulated. Therefore, the study of this process requires the use of a palette of techniques, which are continuously evolving and whose interpretation is not trivial. Here, we present the social amoeba *Dictyostelium discoideum* as a relevant model to study autophagy. Several methods have been developed based on the tracking and observation of autophagosomes by microscopy, analysis of changes in expression of autophagy genes and proteins, and examination of the autophagic flux with various techniques. In this review, we discuss the pros and cons of the currently available techniques to assess autophagy in this organism.

Keywords: autophagy; *Dictyostelium*; flux assays; autophagic markers; cleavage assays

1. Introducing *Dictyostelium* as a Model for Autophagy Research

Intracellular degradation processes are ubiquitous to all organisms and essential to maintain cellular homeostasis. One of the major degradative pathways in eukaryotes is macroautophagy (hereafter referred to as autophagy), a dynamic process that captures and delivers diverse cellular material, including cytoplasm, organelles, and protein aggregates, to the lysosomes. Although basal levels of autophagy might be sufficient for homeostasis under normal growth conditions, a variety of stresses induce a strong up-regulation of this pathway, such as starvation [1], mechanical deformations [2], oxidative and endoplasmic reticulum (ER) stresses [3], and infection [4], among others. In order to reach the degradation stage, the cargo must be sequestered from the cytosol by de novo formation of a double-membrane cisterna, the phagophore. In yeast, this occurs only at one site near the vacuole, known as the phagophore assembly site (PAS). In other eukaryotes, including *Dictyostelium discoideum* and human cells, this occurs at multiple sites on the ER, and the initial structure formed is referred to as the omegasome. The phagophore expands using membranes from many sources, such as the ER, Golgi, endosomes, mitochondria, and plasma membrane [5,6], eventually closing and generating a completed vesicle, the autophagosome.

Although the study of autophagy dates back to the early 1960s, when C. de Duve coined the term [7], it is still a growing research field, mainly due to its complexity and importance in many physiological and pathological aspects of human health and disease [8]. A large number of proteins that participate in and regulate the autophagic process have been defined (termed Atg proteins). Many of these studies have been performed in model organisms, mainly yeast, as recognized recently by the Nobel prize awarded to Yoshinori Ohsumi for his discoveries on the autophagic machinery [9,10].

One of the organisms that has recently contributed to this area is *Dictyostelium*, a soil amoeba that was isolated and described by Kenneth Raper in 1935. Since then, it has become a well-established model in cell and developmental biology [11,12]. Importantly, *Dictyostelium* has conserved genes involved in processes that were lost during the specialization of fungi, such as phagocytosis, macropinocytosis, chemotaxis, and motility. So, in many ways (including autophagosome formation), *Dictyostelium* is more similar to metazoans than yeasts are [13], justifying the use of *Dictyostelium* as a model for human diseases and even for drug screening [14–20]. For example, research on *Dictyostelium* has contributed to the unraveling of the signaling pathways implicated in the poorly defined therapeutic effects of valproic acid and lithium [18]. Additionally, *Dictyostelium* has proven to be a good model organism to address questions regarding the etiology of some human diseases; for instance, orthologues of the genes implicated in neurological disorders such as neuronal ceroid lipofuscinosis [21], chorea-acanthocytosis [22], Alzheimer's disease [23], and lissencephaly [24] (among others) have been studied in *Dictyostelium*, shedding light on the cellular biology underlying these conditions. Further, as many innate immunity mechanisms used by animal phagocytes are conserved in *Dictyostelium*, studies using this amoeba as a model organism have expanded the knowledge on the molecular mechanisms of infection and pathogen–host interactions [20,25].

Dictyostelium has an unusual life cycle that alternates between unicellular and multicellular phases. As a unicellular amoeba, *Dictyostelium* feeds on bacteria and yeasts and multiplies by fission about every 8 h. However, when nutrients are scarce, vegetative growing cells enter a developmental program that begins with the secretion of diverse molecules for intercellular communication. One of these, cyclic adenosine monophosphate (cAMP), functions as a chemoattractant, resulting in cell aggregation. Collectives of about 100,000 cells then differentiate to form a multicellular slug that finally culminates in a fruiting body, a structure composed of a stalk of dead cells supporting a sorocarp filled with spores that will disperse and germinate under favorable environmental conditions (Figure 1A) (a comprehensive review on *Dictyostelium* development can be found in [26]). Interestingly, *Dictyostelium* defends itself against pathogens both as a single cell and as a multicellular organism. Inside the slug, a subset of specialized phagocytic cells called Sentinel cells function as a primitive innate immune system and patrol the facultative multicellular organism to scavenge and kill invading microbes by phagocytosis or using extracellular DNA traps [27,28].

During development, *Dictyostelium* cells rely on autophagy to obtain the energy and metabolites required for aggregation and differentiation [29]. However, besides this recycling function, autophagy also functionally participates in the developmental program. For example, autophagy is required for the vacuolization that accompanies differentiation and death of the stalk cells [30], and is required for the unconventional secretion of AcbA—the precursor of SDF-2, a protein involved in spore formation [31]. Consequently, a blockade in autophagy results in abnormal development.

Since the first *Dictyostelium* autophagy mutants were described [29,32], it became clear that the severity of the phenotypes correlates with the level of autophagy inhibition [33]. These phenotypes range from a complete lack of aggregation to incomplete development, characterized by the formation of multi-tipped structures and aberrant fruiting bodies, which has facilitated the isolation and characterization of many autophagy mutants (Figure 1B). Comprehensive reviews on autophagy in *Dictyostelium* can be found in [34,35]. It must be noted that the severity of the multi-tipped phenotype depends on the genetic background of the laboratory strain used. For example, while mutants of Atg16 in the AX4-background produce large, abnormal mounds with many finger-like tips [22], a similar mutant in AX2 forms smaller mounds with only three tips [36]. In both cases, however, as development

progresses, the multi-tipped structures from both strains form highly abnormal fruiting bodies and few viable spores.
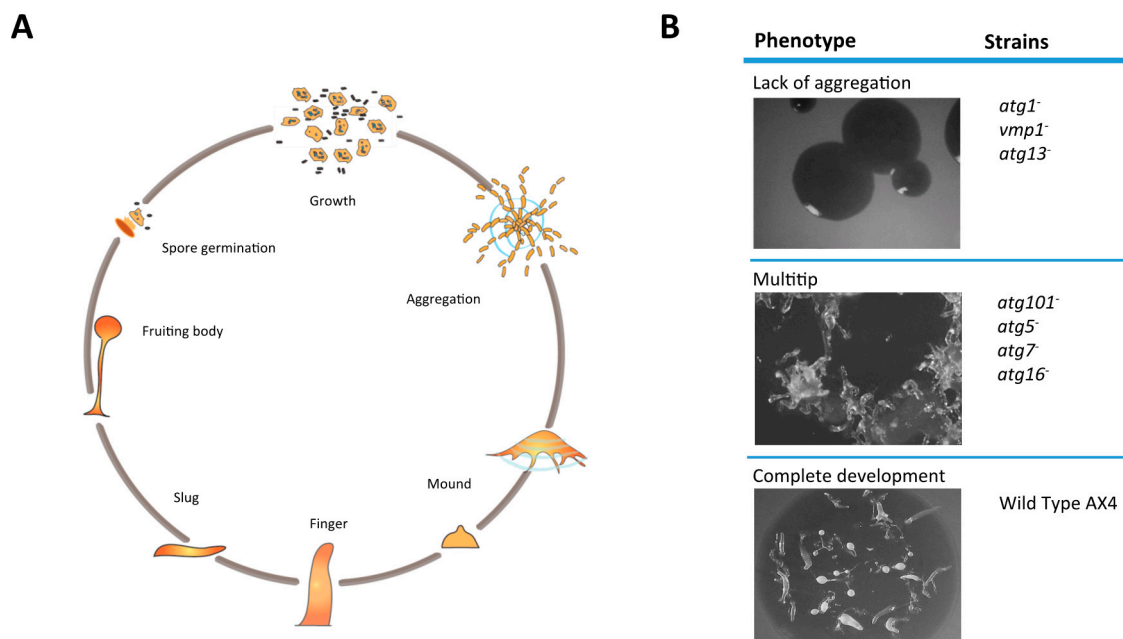

Figure 1. *Dictyostelium* as a model for autophagy. *Dictyostelium discoideum* is a social amoeba that enters a developmental program during starvation. (**A**) Scheme of the *Dictyostelium* developmental cycle. Individual amoebas aggregate to form mounds of cells that undergo different stages of development that culminate with the formation of a fruiting body containing spores. (**B**) The lack of autophagy in *Dictyostelium* leads to developmental arrest either at the aggregation stage or at the mound stage. In the latter, the formation of multiple tips is characteristic of some of the strains.

2. Strategies to Induce Autophagy in *Dictyostelium*

Starvation is the most common stimulus used to activate *Dictyostelium* autophagy in the laboratory. Like in other organisms, autophagy can be triggered by a complete starvation, which is accomplished by incubating the cells in a phosphate buffer, or by depleting lysine and arginine—two essential amino acids—and nitrogen sources from otherwise complete medium. Note that the two conditions vary in their impact on cell physiology, whilst the depletion of specific amino acids simply causes growth arrest and a loss of viability over time, a complete lack of nutrients additionally activates the developmental program. Usually, after about 15 min of either of the above treatments, the average number of autophagosomes increases from about 1 to around 2.5 per cell [2,37].

Mechanical stress also activates autophagy in *Dictyostelium* similarly to other eukaryotic cells. This can be accomplished by overlaying the cells with a thin agarose sheet [2]. In addition, it has been shown that the exposure to the *Staphylococcus aureus* lipopolysaccharide or the damage to the phagosomal membrane caused by *Mycobacterium marinum* infection induce an autophagic response [38,39].

In yeast and mammalian cells, rapamycin (RAP) is often used as an autophagy activator, which acts by allosterically inhibiting the mechanistic target of rapamycin complex 1 (mTORC1), which directly phosphorylates Atg1 and connects nutrient availability to autophagy induction. The effect of RAP on autophagy activation is therefore very rapid in most cell types (from minutes to a few hours), but it may not inhibit TOR completely. Other inhibitors such as Torin1, PP242, KU-0063794, PI-103, and NVP-BEZ235 target the catalytic domain of TOR and are more potent inhibitors, although they target both TORC1 and TORC2. In *Dictyostelium*, short-term RAP treatment does not seem to induce autophagy (Figure 2), despite reports showing that the functional TORC1 complex is sensitive

to RAP inhibition [40]. Either the level of inhibition of TORC1 is insufficient to activate autophagy, or *Dictyostelium* has evolved other pathways to transmit the signal of nutrient availability to the autophagy machinery. However, long-term RAP treatment (24 h) has been reported to activate autophagy in *Dictyostelium* [41]. As these long treatments may have additional indirect effects, it is not clear whether the observed induction is the result of secondary cell damage instead of a direct signaling pathway. Further studies are required to unambiguously determine whether in *Dictyostelium* TORC1 directly signals to the Atg1 complex to regulate autophagy, as described in other organisms.

In contrast, the drug AR-12 (OSU-03012) has recently been shown to induce the autophagic flux in *Dictyostelium* [39]. A two-hour treatment with this drug—which induces autophagosome formation in mammals by various mechanisms, such as the inhibition of the 3-phosphoinositide-dependent protein kinase 1 (PDK1), the induction of ER stress, and the accumulation of reactive oxygen species (ROS) [42,43]—is enough to increase the number of autophagosomes and the rate of degradation of the GFP cleaved from GFP-Atg8 in *Dictyostelium* [39].
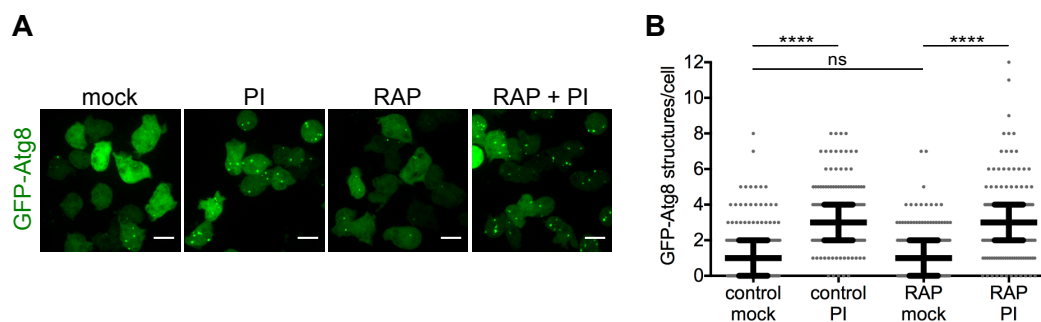
Figure 2. A short-term rapamycin (RAP) treatment does not induce autophagic flux in *Dictyostelium*. *Dictyostelium* Ax2(Ka) cells expressing green fluorescent protein (GFP)-Atg8 were treated or mock-treated with RAP at 500 nM for 2 h. One hour before the end of the treatment, cells were incubated or not with a protease inhibitor cocktail (PI, Roche 11873580001) at 2.5×. (**A**) Representative maximum projections of live cells under the treatments described above. Scale bars, 10 μm; (**B**) Median and interquartile ranges of the number of GFP-Atg8 structures per cell during the mentioned treatments. Each dot represents one cell; 162–168 cells per condition were counted. The values of λ that define the Poisson distribution of each data set and differences between them were calculated as described before [34] (**** $p \leq 0.0001$; ns, $p > 0.05$). No significant differences were observed by quantification of the percentage of cells with GFP-Atg8 dots under RAP treatment (not shown).

3. Microscopy Techniques

3.1. Transmission Electron Microscopy (TEM)

TEM has been a key technique in the study of autophagy since its discovery. The first autophagic structures in *Dictyostelium* were observed using this method [44]. Additionally, the first studies that identified orthologous *atg* genes in this amoeba relied on TEM to evaluate autophagosome formation [29]. More recently, thanks to an improved fixation protocol, the double-membrane autophagic structures can be visualized with an unprecedented level of detail (Figure 3) [39,45]. However, due to the low number of autophagosomes, it is rather difficult to identify them in thin EM sections. Consequently, this technique remains essential to analyze the ultrastructure of abnormal autophagic organelles and the lack of bona fide autophagosomes [46], but is not adequate to quantitatively monitor the generation and fate of autophagic bodies.

Figure 3. Visualization of autophagosomes in *Dictyostelium* by TEM. Electron micrographs of a *Dictyostelium* Ax2(Ka) cell treated with the autophagy inducer drug AR-12 at 2.5 μM for 2 h and with PI at 2.5× for 1 h. For imaging, cells were fixed for 1 h with 2% glutaraldehyde and stained for 30 min with a 2% osmium/0.1 M imidazole solution. Fixed cells were pelleted, washed in phosphate-buffered saline (PBS), and further processed, as previously described [38]. The red arrow marks the enlarged panel showing two autophagosomes; the green arrow marks the enlargement where a fusion event between a late endosome and an autophagosome can be observed. Scale bar, 2 μm.

3.2. Fluorescence Microscopy

Quantitative studies of the number of autophagic structures can be achieved by confocal microscopy of cells expressing a fusion of the green fluorescent protein (GFP) with Atg8 (microtubule-associated protein 1A/1B-light chain 3 (LC3) in mammals), which labels all stages of autophagosome formation, or Atg18 (WD-repeat protein interacting with phosphoinositides (WIPI) in mammals), which only marks the expanding phagophore [47]. When autophagy is induced, Atg8 is conjugated to phosphatidylethanolamine (PE) and is incorporated into the membrane of the expanding phagophore, where it remains until the autophagic body is degraded (Figure 4A). This marker has also been used extensively in *Dictyostelium* to monitor autophagosome formation and to study the dynamics of autophagosomes [2,37,39]. Using GFP-Atg8, it has been possible to perform in vivo time-lapse studies that followed the whole process from the formation to the closure of the autophagosome, and to establish the timing of this process. As autophagosomes move quickly, they are difficult to track for long periods of time, and thus it is advantageous to slightly compress the cells by overlaying them with a thin agarose sheet [2,39]. In addition, since GFP-Atg8 translocates to autophagosomal membranes during autophagy induction, one can monitor both the decrease in the fluorescence intensity of the cytosolic fraction and the concomitant increase in the number of GFP-Atg8 structures [2,39]. It is worth noting, however, that *Dictyostelium* possesses two Atg8 orthologues, which appear to play partly non-redundant roles in autophagosome formation, with different dynamics of recruitment [48,49].

Atg18 and its mammalian orthologues are essential for autophagosome biogenesis and recruited to the membranes of nascent and elongating autophagosomes via their phosphatidylinositol 3-phosphate (PtdIns(3)P) binding domain [50]. Therefore, GFP fusions of Atg18 allow the tracking of PtdIns(3)P-enriched membranes during autophagosome formation, and in contrast to Atg8, is lost immediately following closure. GFP-Atg18 has emerged as a robust marker after some difficulties using GFP-Atg8 were noticed. GFP-Atg8 has been observed to aggregate and localize to large punctate structures in *Dictyostelium* cells lacking autophagy, thereby causing aberrations [2,51], making this marker unsuitable for quantitative analysis in some experiments. In contrast, GFP-Atg18 does not aggregate, and its puncta can also be tracked and quantified. The small GFP-Atg18 puncta seem to expand into cup-like structures, resembling mammalian omegasomes [2,39]. Because Atg18 is released from mature autophagosomes in both *Dictyostelium* and mammalian cells, it only indicates the rate of autophagosome formation, and is not representative of the total number of autophagosomes in a cell. Therefore, to obtain a complete picture, it is advisable to monitor and quantitate both Atg8- and Atg18-positive structures. Additionally, as antibodies against the two Atg8 *Dictyostelium* orthologues have been generated, the endogenous proteins can be evaluated using immunohistochemistry [48,52].
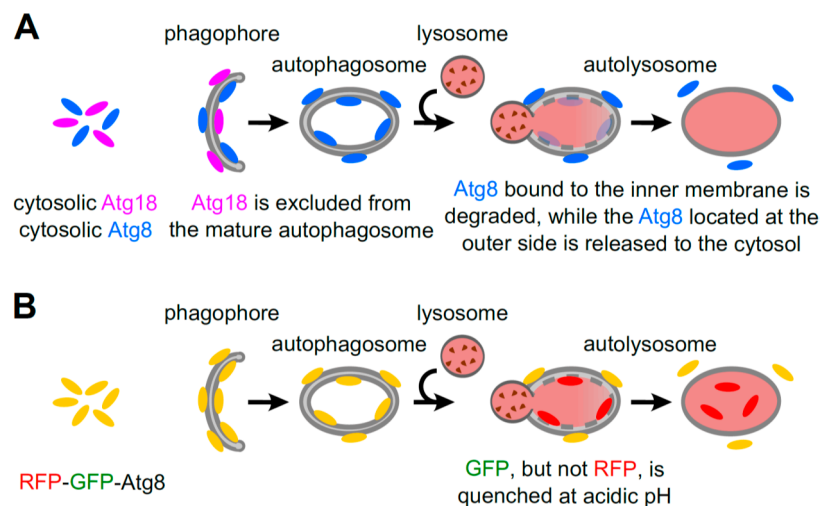
Figure 4. Atg18 and Atg8 as autophagic markers. (**A**) Atg18 is necessary for autophagosome formation, but it is released from mature autophagosomes. The cytosolic Atg8 protein is conjugated to phosphatidylethanolamine (PE) upon induction of autophagy, and is stably integrated into both the outer and the inner membranes of the phagophore. Therefore, the Atg8 fraction residing inside the autophagosome is degraded, together with other autophagic cargos, after lysosomal fusion; (**B**) red fluorescent protein (RFP)-GFP-Atg8 binds the autophagosomal membranes when autophagy is induced. Inside the autolysosomes, GFP is quenched due to the low pH, but RFP remains fluorescent. The increase in yellow and red Atg8 indicates induction of the autophagic flux, while the increase only in yellow Atg8 structures implies autophagic flux blockage.

4. Measurement of Gene and Protein Expression Levels

Although autophagy is essential for *Dictyostelium* development, the regulation of the expression of autophagy genes during development has not been studied in detail. The first descriptions were obtained using Northern blots to monitor the expression of *atg1*, *atg8*, *atg5*, *atg9*, and *atg12*, which all increase in mRNA level at early times during development [29]. An alternative, non-radioactive method is quantitative reverse transcription polymerase chain reaction qRT-PCR [39]. In addition, the steady-state protein levels of the two *Dictyostelium* Atg8 orthologues were recently analyzed by western blot, and were shown to have different expression patterns during development [48]. Unfortunately, while in mammalian cells it is possible to separate and quantify the cytoplasmic and autophagosome-associated lipidated forms of Atg8 (LC3 I/II), in *Dictyostelium* only a single form can be observed, and consequently Atg8 western blotting results must be interpreted carefully. It is possible that the fast-migrating lipidated form is under the detection level. Consequently, this technique can only shed light on the total amount of Atg8, and thus an increase in Atg8 levels can be interpreted as a rise in autophagy induction or as an autophagy blockage [36].

Gene and protein expression analyses can be useful as initial approaches to evaluate mutants or novel autophagy inducers, but cannot provide enough evidence of the real cellular autophagic activity, and so must be accompanied by other assays.

5. Autophagic Flux Assays

To perform a complete autophagy evaluation, it is important to analyze not only autophagosome formation, but also whether the cargos are being degraded. As discussed above, GFP-Atg8 puncta reflect only the steady-state levels of autophagosomes; therefore, the presence of higher number of puncta may be due either to an increase in autophagosome induction or to an autophagy blockage at a subsequent stage. In order to circumvent this problem, a number of autophagic flux assays have been developed in *Dictyostelium*.

5.1. Protein Cleavage Assays

In many organisms, the autophagic flux is assayed by following the breakdown of a nominal cytoplasmic protein fused to the relatively hydrolase-resistant GFP. In *Dictyostelium*, this technique has been developed using either transketolase (Tkt) or phosphoglycerate kinase (PgkA) fused to GFP as cargoes [37,53]. As *Dictyostelium* possesses extremely acidic lysosomes with a pH of 3.5 or below [54], the use of non-saturating concentrations of the lysosomotropic agent NH4Cl is essential to visualize the free GFP fragments that accumulate from autophagic degradation (Figure 5). It is important to point out that the NH4Cl concentration required to visualize the GFP fragments is very high, inducing an elevated autophagic response per se that hinders the use of this assay to evaluate the effect of autophagy-inducing agents, although cells can be treated with other drugs prior to NH4Cl treatment [55]. In addition, NH4Cl also induces osmotic swelling of endosomes and lysosomes, which severely impairs microscopy observations. Nevertheless, this cleavage assay has proven to be very effective to evaluate the degradation capacity of both autophagy-deficient and over-activated strains [22,33,56]. This technique is very sensitive to changes in the metabolic status of the cells, so each experiment must be carefully controlled. For example, cells should have similar growth history, avoiding overconfluency. In addition, comparisons should always be performed within the same parental strain, since differences in the lysosomal pH and the autophagic capacity between the commonly used laboratory strains may occur. In this case, and when evaluating strains that present moderate phenotypes, it is advisable to optimize the NH4Cl concentration and/or compare the autophagic flux at different concentrations of NH4Cl within the same experiment.
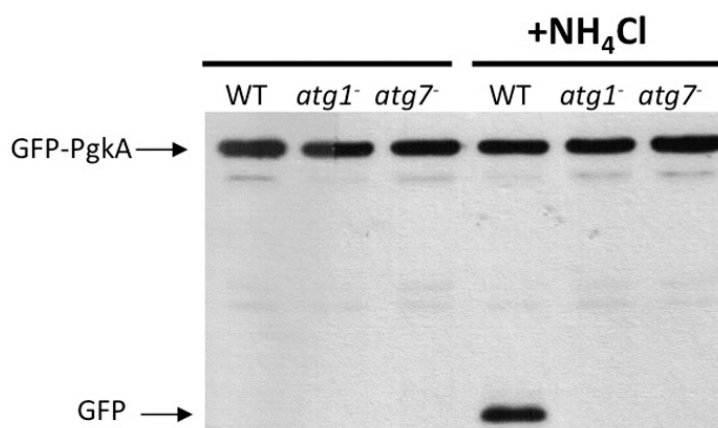
Figure 5. Protein cleavage assay. AX4 wild-type (WT), *atg1⁻*, or *atg7⁻* cells constitutively expressing GFP-PgkA (phosphoglycerate kinase) were subjected to two 150 mM pulses of NH4Cl, each of 2 h, as previously described (see text). Total cell extracts were analyzed by western blot using an anti-GFP antibody. Free GFP cannot be detected in autophagy-deficient strains.

An alternative technique, based on the breakdown of GFP-Atg8, does not require the use of NH4Cl. When the flux is completely blocked by, for instance, impairment of the lysosomal activity with a protease inhibitor treatment, the accumulation of GFP-Atg8 can be observed by western-blot while the free GFP disappears. On the other hand, when GFP-Atg8 is actively degraded, free GFP accumulates because of its relative resistance to degradation by lysosomal hydrolases. As this technique does not require the use of NH4Cl, it can be used to monitor autophagic changes upon drug or infection treatments [39]. Changes in the levels of free GFP are indicative of changes in the autophagic flux. However, interpretation of the results must take into account that both an induction or a blockage of autophagy may decrease the levels of free GFP, and additional flux assays are required to discriminate these possibilities [39]. In addition, it must also be considered that a small amount of free GFP is generated in an autophagy-independent manner as it occurs in the *atg1* mutant, which

has been shown by other methods to have a complete block in autophagosome formation [32,39] (RE, personal communication).

5.2. Quantification of Fluorescently-Tagged Proteins

Imaging GFP-Atg8-expressing cells and counting GFP-Atg8 dots can also serve as a proxy readout for the autophagic flux if combined with inhibitors of degradation. In *Dictyostelium*, lysosomal inhibition can be achieved by treating the cells with a cocktail of protease inhibitors (Figure 2) or with the V-ATPase inhibitor concanamycin B [39]. Both the induction of autophagosome formation and the blockage of the autophagic flux lead to an increase in the number of GFP-Atg8 structures in the cell. Thus, when autophagy is induced, a higher number of GFP-Atg8 dots is expected when blocking the autophagic flux by the mentioned inhibitors. However, if the autophagic flux is already blocked, no change in the number of GFP-Atg8 structures will occur.

5.3. RFP-GFP-Atg8 Puncta Monitoring

Another kind of autophagic flux assay is based on the differential stability of green and red fluorescent proteins (GFP and RFP, respectively) in acidic environments. At a pH of 5 or below (which is found in lysosomes), the fluorescence of GFP is completely quenched, whilst RFP fluorescence is retained. For these assays, a fusion of Atg8 to a tandem GFP-RFP tag is expressed, and the autophagic flux is examined by monitoring the relative fluorescence of both tags with confocal microscopy. When green–red merged images of cells are analyzed, yellow puncta represent early autophagosomes, while red-only puncta (lacking green fluorescence) indicate acidic autolysosomes. Thus, when the autophagic flux is augmented, more of both yellow and red puncta are expected. However, when there is a blockage in lysosomal fusion or acidification, yellow puncta will accumulate (Figure 4B).

The GFP-RFP-Atg8 construct has been evaluated in *Dictyostelium* [53], and it was observed that the use of NH_4Cl is required to reveal the presence of autolysosomes (red-only puncta) in the strain AX4, likely because the extremely low lysosomal pH in this organism even quenches the fluorescence of RFP (Figure 6). In AX2, however, it has been reported that this technique can be applied without the need of NH_4Cl, as red-only puncta are present under starvation [57].
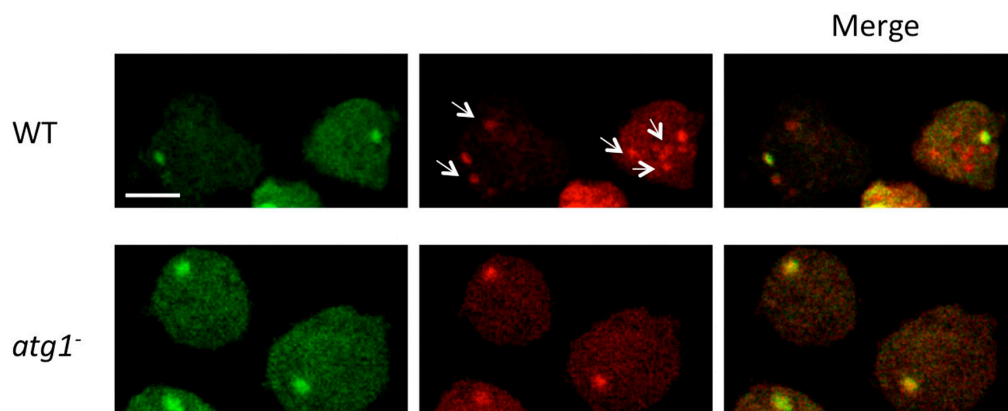
Figure 6. Wild-type (WT) (AX4) and *atg1⁻* cells expressing the marker RFP-GFP-Atg8 were incubated for four hours with two pulses of 100 mM NH_4Cl and visualized by confocal microscopy. The arrows show the presence of red-only puncta in WT that presumably represent autophagolysosomes. Cells lacking Atg1 typically show a large aggregate and no red-only puncta. Scale bar 5 μm.

6. Determination of Ubiquitin Aggregates

Autophagic dysfunction often leads to an abnormal increase of ubiquitinated protein aggregates. This is because either autophagy participates in the clearance of ubiquitinated proteins, or because in its absence the autophagy targets remain long enough to get ubiquitinated [58]. In either case, the

increase in ubiquitin aggregates in autophagy-deficient strains has been exploited to evaluate the autophagic capacity of cells.

　　Ubiquitinated protein aggregates can be detected either by analyzing the Triton-insoluble fraction of total cellular lysates by western blot, or directly by the observation of immunohistochemically labeled cells by microscopy (Figure 7). In *Dictyostelium*, this technique revealed that in autophagy-deficient mutants the accumulation of ubiquitin aggregates correlates with impairment of the autophagic flux [36,37,51]. This method is thus useful to indirectly visualize impairments in autophagy, but quantitative analyses are difficult and should be complemented with other techniques. Note that defective proteasomal degradation can also cause an increase in ubiquitinated proteins.
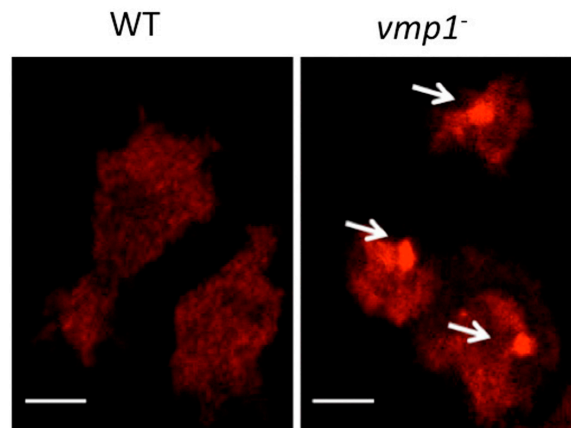
Figure 7. Detection of ubiquitinated protein aggregates by confocal microscopy. WT (AX4) and *vmp1⁻* cells were fixed and prepared for immunocytochemistry detection of ubiquitin (red), and analyzed by confocal microscopy. Autophagy-deficient *vmp1⁻* cells are not able to degrade proteins by autophagy and accumulate large ubiquitinated aggregates (denoted by white arrows). Scale bars 5 μm.

7. Concluding Remarks

　　We have presented the current available strategies to assess autophagic activity in *Dictyostelium*. It is important to emphasize that—as in any other organism and cell type—there is no single perfect method to determine autophagic activity. The use of different strategies—even with overlapping approaches—should therefore be considered to accurately monitor autophagy in *Dictyostelium*. Additionally, due to the high conservation of this process, new methods can surely be adapted from other species to the study of autophagy in this model organism.

Conflicts of Interest: The authors declare no conflict of interest.

References

1.　Onodera, J.; Ohsumi, Y. Autophagy is required for maintenance of amino acid levels and protein synthesis under nitrogen starvation. *J. Biol. Chem.* **2005**, *280*, 31582–31586. [CrossRef] [PubMed]

2.　King, J.S.; Veltman, D.M.; Insall, R.H. The induction of autophagy by mechanical stress. *Autophagy* **2011**, *7*, 1490–1499. [CrossRef] [PubMed]

3.　Yorimitsu, T.; Nair, U.; Yang, Z.; Klionsky, D.J. Endoplasmic reticulum stress triggers autophagy. *J. Biol. Chem.* **2006**, *281*, 30299–30304. [CrossRef] [PubMed]

4.　Miller, C.; Celli, J. Avoidance and Subversion of Eukaryotic Homeostatic Autophagy Mechanisms by Bacterial Pathogens. *J. Mol. Biol.* **2016**, *428*, 3387–3398. [CrossRef] [PubMed]

5.　Lamb, C.A.; Yoshimori, T.; Tooze, S.A. The autophagosome: Origins unknown, biogenesis complex. *Nat. Rev. Mol. Cell Biol.* **2013**, *14*, 759–774. [CrossRef] [PubMed]

6. Shibutani, S.T.; Yoshimori, T. A current perspective of autophagosome biogenesis. *Cell Res.* **2014**, *24*, 58–68. [CrossRef] [PubMed]

7. De Duve, C. Ciba Foundation Symposium. In *Lysosome*; De Reuck, A., Cameron, M.P., Eds.; Little Brown and Company: Boston, MA, USA, 1963.

8. Schneider, J.L.; Cuervo, A.M. Autophagy and human disease: Emerging themes. *Curr. Opin. Genet. Dev.* **2014**, *26*, 16–23. [CrossRef] [PubMed]

9. Levine, B.; Klionsky, D.J. Autophagy wins the 2016 Nobel Prize in Physiology or Medicine: Breakthroughs in baker's yeast fuel advances in biomedical research. *Proc. Natl. Acad. Sci. USA* **2017**, *114*, 201–205. [CrossRef] [PubMed]

10. Tsukada, M.; Ohsumi, Y. Isolation and characterization of autophagy-defective mutants of *Saccharomyces cerevisiae*. *FEBS Lett.* **1993**, *333*, 169–174. [CrossRef]

11. Romeralo, M.; Escalante, R.; Baldauf, S.L. Evolution and diversity of dictyostelid social amoebae. *Protist* **2012**, *163*, 327–343. [CrossRef] [PubMed]

12. Annesley, S.J.; Fisher, P.R. Dictyostelium discoideum—A model for many reasons. *Mol. Cell. Biochem.* **2009**, *329*, 73–91. [CrossRef] [PubMed]

13. King, J.S. Autophagy across the eukaryotes: Is *S. cerevisiae* the odd one out? *Autophagy* **2012**, *8*, 1159–1162. [CrossRef] [PubMed]

14. Muñoz-Braceras, S.; Mesquita, A.; Escalante, R. Dictyostelium discoideum as a model in biomedical research. In *Dictyostelids. Evolution, Genomics and Cell Biology*; Romeralo, M., Baldauf, S., Escalante, R., Eds.; Springer: Berlin/Heiderberg, Germany, 2013; pp. 1–34.

15. Alexander, S.; Alexander, H. Lead genetic studies in Dictyostelium discoideum and translational studies in human cells demonstrate that sphingolipids are key regulators of sensitivity to cisplatin and other anticancer drugs. *Semin. Cell Dev. Biol.* **2011**, *22*, 97–104. [CrossRef] [PubMed]

16. Cai, H.; Devreotes, P.N. Moving in the right direction: How eukaryotic cells migrate along chemical gradients. *Semin. Cell Dev. Biol.* **2011**, *22*, 834–841. [CrossRef] [PubMed]

17. Francione, L.M.; Annesley, S.J.; Carilla-Latorre, S.; Escalante, R.; Fisher, P.R. The Dictyostelium model for mitochondrial disease. *Semin. Cell Dev. Biol.* **2011**, *22*, 120–130. [CrossRef] [PubMed]

18. Ludtmann, M.H.; Boeckeler, K.; Williams, R.S. Molecular pharmacology in a simple model system: Implicating MAP kinase and phosphoinositide signalling in bipolar disorder. *Semin. Cell Dev. Biol.* **2011**, *22*, 105–113. [CrossRef] [PubMed]

19. Maniak, M. Dictyostelium as a model for human lysosomal and trafficking diseases. *Semin. Cell Dev. Biol.* **2011**, *22*, 114–119. [CrossRef] [PubMed]

20. Steinert, M. Pathogen-host interactions in Dictyostelium, Legionella, Mycobacterium and other pathogens. *Semin. Cell Dev. Biol.* **2011**, *22*, 70–76. [CrossRef] [PubMed]

21. Huber, R.J. Using the social amoeba Dictyostelium to study the functions of proteins linked to neuronal ceroid lipofuscinosis. *J. Biomed. Sci.* **2016**, *23*, 83. [CrossRef] [PubMed]

22. Munoz-Braceras, S.; Calvo, R.; Escalante, R. TipC and the chorea-acanthocytosis protein VPS13A regulate autophagy in Dictyostelium and human HeLa cells. *Autophagy* **2015**, *11*, 918–927. [CrossRef] [PubMed]

23. McMains, V.C.; Myre, M.; Kreppel, L.; Kimmel, A.R. Dictyostelium possesses highly diverged presenilin/gamma-secretase that regulates growth and cell-fate specification and can accurately process human APP: A system for functional studies of the presenilin/gamma-secretase complex. *Dis. Model Mech.* **2010**, *3*, 581–594. [CrossRef] [PubMed]

24. Meyer, I.; Kuhnert, O.; Graf, R. Functional analyses of lissencephaly-related proteins in Dictyostelium. *Semin. Cell Dev. Biol.* **2011**, *22*, 89–96. [CrossRef] [PubMed]

25. Lima, W.C.; Lelong, E.; Cosson, P. What can Dictyostelium bring to the study of Pseudomonas infections? *Semin. Cell Dev. Biol.* **2011**, *22*, 77–81. [CrossRef] [PubMed]

26. Schaap, P. Evolutionary crossroads in developmental biology: Dictyostelium discoideum. *Development* **2011**, *138*, 387–396. [CrossRef] [PubMed]

27. Zhang, X.; Zhuchenko, O.; Kuspa, A.; Soldati, T. Social amoebae trap and kill bacteria by casting DNA nets. *Nat. Commun.* **2016**, *7*, 10938. [CrossRef] [PubMed]

28. Zhang, X.; Soldati, T. Of Amoebae and Men: Extracellular DNA Traps as an Ancient Cell-Intrinsic Defense Mechanism. *Front. Immunol.* **2016**, *7*, 269. [CrossRef] [PubMed]

29. Otto, G.P.; Wu, M.Y.; Kazgan, N.; Anderson, O.R.; Kessin, R.H. Macroautophagy is required for multicellular development of the social amoeba Dictyostelium discoideum. *J. Biol. Chem.* **2003**, *278*, 17636–17645. [CrossRef] [PubMed]

30. Uchikawa, T.; Yamamoto, A.; Inouye, K. Origin and function of the stalk-cell vacuole in Dictyostelium. *Dev. Biol.* **2011**, *352*, 48–57. [CrossRef] [PubMed]

31. Duran, J.M.; Anjard, C.; Stefan, C.; Loomis, W.F.; Malhotra, V. Unconventional secretion of Acb1 is mediated by autophagosomes. *J. Cell. Biol.* **2010**, *188*, 527–536. [CrossRef] [PubMed]

32. Otto, G.P.; Wu, M.Y.; Kazgan, N.; Anderson, O.R.; Kessin, R.H. Dictyostelium macroautophagy mutants vary in the severity of their developmental defects. *J. Biol. Chem.* **2004**, *279*, 15621–15629. [CrossRef] [PubMed]

33. Mesquita, A.; Tabara, L.C.; Martinez-Costa, O.; Santos-Rodrigo, N.; Vincent, O.; Escalante, R. Dissecting the function of Atg1 complex in Dictyostelium autophagy reveals a connection with the pentose phosphate pathway enzyme transketolase. *Open Biol.* **2015**, *5*. [CrossRef] [PubMed]

34. Mesquita, A.; Cardenal-Munoz, E.; Dominguez, E.; Munoz-Braceras, S.; Nunez-Corcuera, B.; Phillips, B.A.; Tabara, L.C.; Xiong, Q.; Coria, R.; Eichinger, L.; et al. Autophagy in Dictyostelium: Mechanisms, regulation and disease in a simple biomedical model. *Autophagy* **2016**, *13*, 24–40. [CrossRef] [PubMed]

35. Calvo-Garrido, J.; Carilla-Latorre, S.; Kubohara, Y.; Santos-Rodrigo, N.; Mesquita, A.; Soldati, T.; Golstein, P.; Escalante, R. Autophagy in Dictyostelium: Genes and pathways, cell death and infection. *Autophagy* **2010**, *6*, 686–701. [CrossRef] [PubMed]

36. Xiong, Q.; Unal, C.; Matthias, J.; Steinert, M.; Eichinger, L. The phenotypes of ATG9, ATG16 and ATG9/16 knock-out mutants imply autophagy-dependent and–independent functions. *Open Biol.* **2015**, *5*, 150008. [CrossRef] [PubMed]

37. Mesquita, A.; Calvo-Garrido, J.; Carilla-Latorre, S.; Escalante, R. Monitoring autophagy in Dictyostelium. *Methods Mol. Biol.* **2013**, *983*, 461–470. [CrossRef] [PubMed]

38. Pflaum, K.; Gerdes, K.; Yovo, K.; Callahan, J.; Snyder, M.L. Lipopolysaccharide induction of autophagy is associated with enhanced bactericidal activity in Dictyostelium discoideum. *Biochem. Biophys. Res. Commun.* **2012**, *422*, 417–422. [CrossRef] [PubMed]

39. Cardenal-Munoz, E.; Arafah, S.; Lopez-Jimenez, A.T.; Kicka, S.; Falaise, A.; Bach, F.; Schaad, O.; King, J.S.; Hagedorn, M.; Soldati, T. Mycobacterium marinum antagonistically induces an autophagic response while repressing the autophagic flux in a TORC1-and ESX-1-dependent manner. *PLoS Pathog.* **2017**, *13*, e1006344. [CrossRef] [PubMed]

40. Rosel, D.; Khurana, T.; Majithia, A.; Huang, X.; Bhandari, R.; Kimmel, A.R. TOR complex 2 (TORC2) in Dictyostelium suppresses phagocytic nutrient capture independently of TORC1-mediated nutrient sensing. *J. Cell Sci.* **2012**, *125*, 37–48. [CrossRef] [PubMed]

41. Swer, P.B.; Lohia, R.; Saran, S. Analysis of rapamycin induced autophagy in Dictyostelium discoideum. *Indian J. Exp. Biol.* **2014**, *52*, 295–304. [PubMed]

42. Gao, M.; Yeh, P.Y.; Lu, Y.S.; Hsu, C.H.; Chen, K.F.; Lee, W.C.; Feng, W.C.; Chen, C.S.; Kuo, M.L.; Cheng, A.L. OSU-03012, a novel celecoxib derivative, induces reactive oxygen species-related autophagy in hepatocellular carcinoma. *Cancer Res.* **2008**, *68*, 9348–9357. [CrossRef] [PubMed]

43. Park, M.A.; Yacoub, A.; Rahmani, M.; Zhang, G.; Hart, L.; Hagan, M.P.; Calderwood, S.K.; Sherman, M.Y.; Koumenis, C.; Spiegel, S.; et al. OSU-03012 stimulates PKR-like endoplasmic reticulum-dependent increases in 70-kDa heat shock protein expression, attenuating its lethal actions in transformed cells. *Mol. Pharmacol.* **2008**, *73*, 1168–1184. [CrossRef] [PubMed]

44. de Chastellier, C.; Ryter, A. Changes on the cell surface and of the digestive apparatus of Dictyostelium discoideum during the starvation period triggering aggregation. *J. Cell Biol.* **1977**, *75*, 218–236. [CrossRef] [PubMed]

45. Barisch, C.; Paschke, P.; Hagedorn, M.; Maniak, M.; Soldati, T. Lipid droplet dynamics at early stages of Mycobacterium marinum infection in Dictyostelium. *Cell. Microbiol.* **2015**, *17*, 1332–1349. [CrossRef] [PubMed]

46. Calvo-Garrido, J.; Carilla-Latorre, S.; Lazaro-Dieguez, F.; Egea, G.; Escalante, R. Vacuole membrane protein 1 is an endoplasmic reticulum protein required for organelle biogenesis, protein secretion, and development. *Mol. Biol. Cell* **2008**, *19*, 3442–3453. [CrossRef] [PubMed]

47. Klionsky, D.J.; Abdelmohsen, K.; Abe, A.; Abedin, M.J.; Abeliovich, H.; Acevedo Arozena, A.; Adachi, H.; Adams, C.M.; Adams, P.D.; Adeli, K.; et al. Guidelines for the use and interpretation of assays for monitoring autophagy (3rd edition). *Autophagy* **2016**, *12*, 1–222. [CrossRef] [PubMed]

48. Matthias, J.; Messling, S.; Eichinger, L. The two *Dictyostelium* autophagy eight proteins, ATG8a and ATG8b, associate with the autophagosome in succession. *Eur. J. Cell Biol.* **2016**, *95*, 15–25. [CrossRef] [PubMed]

49. Messling, S.; Matthias, J.; Xiong, Q.; Fischer, S.; Eichinger, L. The two *Dictyostelium discoideum* autophagy 8 proteins have distinct autophagic functions. *Eur. J. Cell Biol.* **2017**. [CrossRef] [PubMed]

50. Proikas-Cezanne, T.; Takacs, Z.; Donnes, P.; Kohlbacher, O. WIPI proteins: Essential PtdIns3P effectors at the nascent autophagosome. *J. Cell Sci.* **2015**, *128*, 207–217. [CrossRef] [PubMed]

51. Calvo-Garrido, J.; Escalante, R. Autophagy dysfunction and ubiquitin-positive protein aggregates in Dictyostelium cells lacking Vmp1. *Autophagy* **2010**, *6*, 100–109. [CrossRef] [PubMed]

52. Gerstenmaier, L.; Pilla, R.; Herrmann, L.; Herrmann, H.; Prado, M.; Villafano, G.J.; Kolonko, M.; Reimer, R.; Soldati, T.; King, J.S.; et al. The autophagic machinery ensures nonlytic transmission of mycobacteria. *Proc. Natl. Acad. Sci. USA* **2015**, *112*, E687–E692. [CrossRef] [PubMed]

53. Calvo-Garrido, J.; Carilla-Latorre, S.; Mesquita, A.; Escalante, R. A proteolytic cleavage assay to monitor autophagy in *Dictyostelium discoideum*. *Autophagy* **2011**, *7*, 1063–1068. [CrossRef] [PubMed]

54. Marchetti, A.; Lelong, E.; Cosson, P. A measure of endosomal pH by flow cytometry in *Dictyostelium*. *BMC Res. Notes* **2009**, *2*, 7. [CrossRef] [PubMed]

55. Ostrowski, P.P.; Fairn, G.D.; Grinstein, S.; Johnson, D.E. Cresyl violet: A superior fluorescent lysosomal marker. *Traffic* **2016**, *17*, 1313–1321. [CrossRef] [PubMed]

56. Carilla-Latorre, S.; Annesley, S.J.; Munoz-Braceras, S.; Fisher, P.R.; Escalante, R. Ndufaf5 deficiency in the *Dictyostelium* model: New roles in autophagy and development. *Mol. Biol. Cell* **2013**, *24*, 1519–1528. [CrossRef] [PubMed]

57. Lohia, R.; Jain, P.; Jain, M.; Burma, P.K.; Shrivastava, A.; Saran, S. Dictyostelium discoideum Sir2D modulates cell-type specific gene expression and is involved in autophagy. *Int. J. Dev. Biol.* **2017**, *61*, 95–104. [CrossRef] [PubMed]

58. Korolchuk, V.I.; Mansilla, A.; Menzies, F.M.; Rubinsztein, D.C. Autophagy inhibition compromises degradation of ubiquitin-proteasome pathway substrates. *Mol. Cell* **2009**, *33*, 517–527. [CrossRef] [PubMed]

Unfolding the Endoplasmic Reticulum of a Social Amoeba: *Dictyostelium discoideum* as a New Model for the Study of Endoplasmic Reticulum Stress

Eunice Domínguez-Martín [1,2] , **Mariana Hernández-Elvira** [2], **Olivier Vincent** [1], **Roberto Coria** [2,*] **and Ricardo Escalante** [1,*]

[1] Instituto de Investigaciones Biomédicas "Alberto Sols" (CSIC-UAM), Arturo Duperier 4, 28029 Madrid, Spain; edominguez@iib.uam.es (E.D.-M.); ovincent@iib.uam.es (O.V.)

[2] Departamento de Genética Molecular, Instituto de Fisiología Celular, Universidad Nacional Autónoma de México, 04510 Ciudad de México, México; melvira@email.ifc.unam.mx (M.H.-E)

[*] Correspondence: rcoria@ifc.unam.mx (R.C.); rescalante@iib.uam.es (R.E.);
Tel.: +52-55-56-22-56-52 (R.C.); +34-915-854-467 (R.E.); Fax: +34-915-854-401 (R.E.)

Abstract: The endoplasmic reticulum (ER) is a membranous network with an intricate dynamic architecture necessary for various essential cellular processes. Nearly one third of the proteins trafficking through the secretory pathway are folded and matured in the ER. Additionally, it acts as calcium storage, and it is a main source for lipid biosynthesis. The ER is highly connected with other organelles through regions of membrane apposition that allow organelle remodeling, as well as lipid and calcium traffic. Cells are under constant changes due to metabolic requirements and environmental conditions that challenge the ER network's maintenance. The unfolded protein response (UPR) is a signaling pathway that restores homeostasis of this intracellular compartment upon ER stress conditions by reducing the load of proteins, and by increasing the processes of protein folding and degradation. Significant progress on the study of the mechanisms that restore ER homeostasis was achieved using model organisms such as yeast, *Arabidopsis*, and mammalian cells. In this review, we address the current knowledge on ER architecture and ER stress response in *Dictyostelium discoideum*. This social amoeba alternates between unicellular and multicellular phases and is recognized as a valuable biomedical model organism and an alternative to yeast, particularly for the presence of traits conserved in animal cells that were lost in fungi.

Keywords: *Dictyostelium*; endoplasmic reticulum; endoplasmic reticulum stress; unfolded protein response; inositol-requiring enzyme 1 (IRE1)

1. *Dictyostelium* as a Model Organism for Experimental Biology Research

Owing to its simplicity and easy genetic manipulability, some microbial organisms prove to be powerful biology-research tools; for instance, *Saccharomyces cerevisiae* is one of the most widely studied eukaryotic organisms. Much of the current knowledge in biochemistry, and molecular and cellular biology arose from research performed with this yeast. However, since this fungal organism has some specific genetic, cellular, and metabolic traits that are not widely conserved, other eukaryotic microbial organisms emerged to address cellular processes that diverged greatly in yeast cells. One of these organisms is *Dictyostelium discoideum*, a social soil-dwelling protist, taxonomically classified in the Amoebozoa phylum, the sister group to animals and fungi [1]. Despite its phylogenetic classification, *Dictyostelium* displays cellular processes that are conserved in animal cells, but that are absent in fungal or plant cells, such as phagocytosis and chemotaxis. Interestingly, it also has traits that are conserved in

fungi and plants, but were lost in animal cells, such as phosphorelay signaling systems, and cellulose production [2,3].

Dictyostelium has a life cycle that alternates between unicellular and multicellular phases, depending on nutrient availability (Figure 1). As unicellular amoebas, they obtain nutrients from phagocytizing yeast or bacteria, and they multiply via fission about every 8 h. Remarkably, under starvation, *Dictyostelium* cells stop mitotic division, and start an intercellular signaling communication process mediated by the secretion of various molecules. One of them, the cyclic adenosine monophosphate (cAMP), acts as a chemoattractant that triggers the polarization, migration, and aggregation of groups of about 10^5 cells from the species *Dictyostelium discoideum*. These aggregates of apparently homogeneous cells enter a developmental program that generates a multicellular organism with distinct cell types. After various developmental stages, including one as a multicellular motile slug, the *Dictyostelium* differentiation program culminates in the formation of a fruiting body composed of a sorogen filled with spores, which is supported by a cellulose stalk made of dead cells (a detailed review of this process was addressed in Reference [4]).
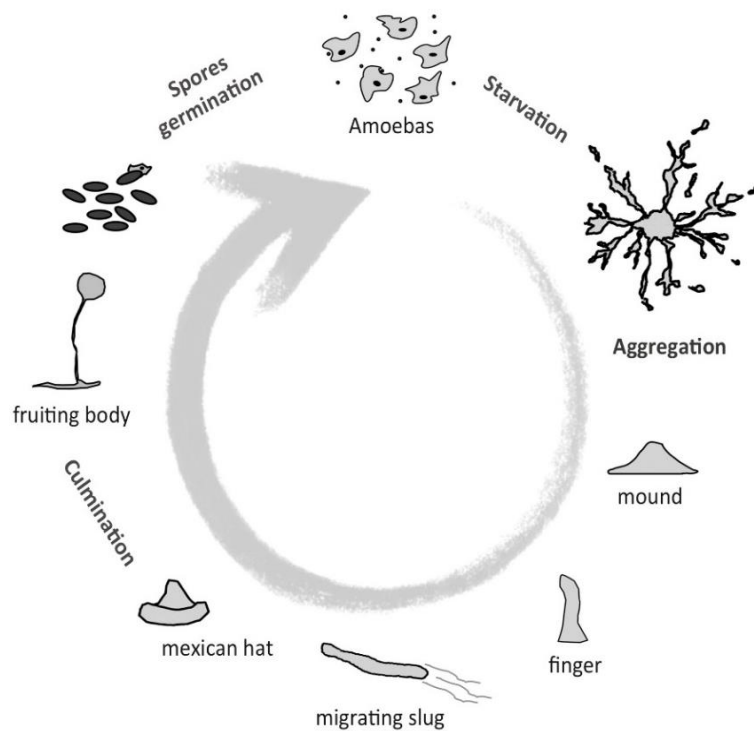
Figure 1. Diagram of the *Dictyostelium* life cycle. Individual amoebas feed on yeast and bacteria, and multiply via fission. When nutrients are scarce, cells aggregate and undergo a developmental program, comprised of distinct stages that culminate in the formation of a fruiting body, which is composed of a stalk, and a sorogen filled with spores. Under suitable environmental conditions, the spores germinate.

Since its first isolation and description more than 80 years ago, a growing number of studies used *Dictyostelium discoideum* to unravel diverse biological questions [2,3]. The genome of this haploid organism is fully sequenced [5], and many different techniques were developed allowing the study of a wide range of topics including infection and drug testing [6]. In addition, *Dictyostelium* was used in basic studies of cell and developmental signaling, among them, the pathways involved in endoplasmic reticulum (ER) homeostasis, maintenance, and regulation [7]. Conditions that interfere with ER homeostasis contribute to the pathogenesis of human chronic disorders including diabetes and some neurodegenerative syndromes, such as Alzheimer's, Parkinson's, and Huntington's diseases [8,9]. *Dictyostelium* emerged as an advantageous model for the study of signaling pathways involved in neurodegeneration (reviews on this topic were addressed in References [10–12]). In addition,

this amoeba is an interesting model for the study of pathways involved in neurological disorders associated with protein aggregation, since it efficiently regulates the accumulation of prion-like protein aggregates [13,14].

2. The Endoplasmic Reticulum of a Social Amoeba

The ER is the largest eukaryotic organelle. This complex membranous network is the place where essential functions such as protein folding and modification, lipid synthesis, and calcium (Ca^{2+}) storage are fulfilled. In the following sections, a general comparative description of the current knowledge on the *Dictyostelium* ER structure and function is presented. Table 1 contains a summary of all the *Dictyostelium* ER proteins that were discussed throughout this text.

2.1. A Membranous Network with an Intricate Structure

Two domains that maintain luminal continuity can be identified in the ER, the nuclear envelope (NE) and the peripheral ER, each with a particular structure and specific characteristics. In the NE, two stacked membranes of low curvature form the inner and outer nuclear membrane (INM and ONM), whereas the peripheral ER spreads across the cytosol, shaped by a network of interconnected tubules and flat sheet-like regions [15,16]. In mammalian cells, an array of constricted tubule clusters, enriched with three-way junctions, forms the peripheral ER matrices. This set of structures is relatively flat, and has a heterogeneous composition and topology [16]. In addition, there are some specialized ER regions formed through flattened membranes, which can be found shaping the nuclear envelope, in the perinuclear region or close to the plasma membrane [17–19]. A tubular network that expands from the NE and these matrices forms a system that connects all the ER domains. The tubules' surface is highly curved, which facilitates surface-dependent functions such as lipid synthesis, and signaling between the ER and other organelles [15].

The *Dictyostelium* ER can be visualized by expressing inositol-requiring enzyme A (IreA) tagged with a fluorescent protein. IreA is an ER-resident protein that participates in the unfolded protein response (UPR) pathway (see Section 3.1—The IreA Branch). The *Dictyostelium* ER can be divided into an NE region and a peripheral zone, consisting of a network of tubules and sheet-like regions, which spread throughout the cell (Figure 2). Domains with sheet-like appearance are distributed mainly in peripheral cell zones, and in close proximity to the NE, while tubules are spread throughout the cell, and can be observed as more defined structures in medial cell sections.
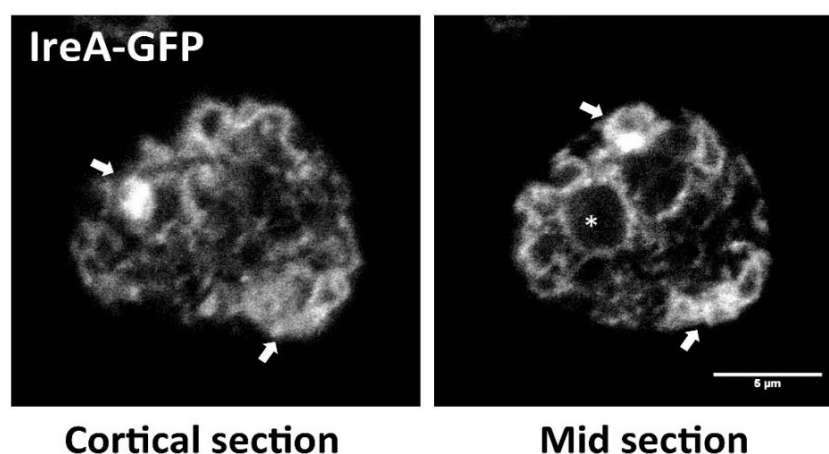
Figure 2. The *Dictyostelium* endoplasmic reticulum (ER). In vivo confocal microscopy pictures showing a cortical section and a mid-section of a wild-type (WT) cell expressing the ER marker, Inositol requiring enzyme A (IreA) fused to the GFP. The asterisk pinpoints the nucleus, surrounded by the perinuclear ER. Arrows highlight zones where sheet-like regions are evident. Tubules can be distinguished across the entire cell area. (Scale bar represents 5 μm).

Table 1. List of the endoplasmic reticulum (ER) protein orthologs mentioned throughout this text.

Function/Features	*Dictyostelium* [a]	*Human* [a]	*Saccharomyces cerevisiae* [a]	*Arabidopsis thaliana* [a]
ER structure				
Transmembrane protein that promotes membrane curvature, and participates in maintenance of tubular ER morphology	Reticulon-like group C (Rtnlc)/ Q54CA6	Reticulons-1 to 4 (RTN1 to RTN4)/ Q16799, O75298, O95197, Q9JK11	Reticulon-like proteins 1 (RTN1) and 2 (RTN2)/ A0A250W951, Q12443	Reticulon-like proteins B1 to 18, and 21 to 23 (RTNLB1 to 18 and RTNLB21 to 23)/ Q9SUR3, Q9SUT9, Q9SH59, Q9FFS0, O82352, Q6DBN4, Q9M145, Q9SS37, Q9LJQ5, Q6NPD8, Q9LT71, Q9M392, O64837, A2RVT6, Q9ZU43, Q8GYH6, Q6DR04, Q8LDS3, Q56X72, Q8GWH5, P0C941
Dynamin-like GTPase that mediates homotypic ER fusion	Sey1/ Q54W90	Atlastin-1 (ATL1)/ Q8WXF7	Sey1/ Q99287	Root hair defective 3 (RHD3) and root hair defective 3 homolog 2 (RHD3-2)/ P93042, Q9FKE9
ER contact sites				
Components of the mitochondria encounter sites (ERMES), which are involved in the tether between the ER and the mitochondria to promote inter-organellar calcium and phospholipid exchange	Maintenance of mitochondrial morphology-1 (Mmm1)/ Q54MI5	ND	Maintenance of mitochondrial morphology protein 1 (Mmm1)/ P41800	ND
	Mitochondrial distribution and morphology-10 (Mdm10)/ Q54XQ5	ND	Mitochondrial distribution and morphology 10 (Mdm10)/ P18409	ND
	Mitochondrial distribution and morphology 34 (Mdm34)/ Q869R5	ND	Mitochondrial distribution and morphology protein 34 (Mdm34)/ P53083	ND
Transmembrane protein required to regulate ER contact sites, essential for autophagy and proper ER homeostasis	Vacuole membrane protein 1 (Vmp1)/ Q54NL4	Vacuole membrane protein 1 (VMP1)/ Q96GC9	ND	Vacuole membrane proteins 1 (KMS1) and 2 (KMS2)/ Q5XF36, F4I8Q7

Table 1. *Cont.*

Function/Features	*Dictyostelium* [a]	*Human* [a]	*Saccharomyces cerevisiae* [a]	*Arabidopsis thaliana* [a]
Lipid metabolism				
Protein that associates to the lipid droplet surface	Perilipin (PlnA)/ Q54WC4	Perilipin proteins 1 to 5 (PLIN1 to 5)/ O60240, Q99541, O60664, Q96Q06, Q00G26	ND	ND
Catalyze the conversion of acyl coenzyme A (CoA) and 1,2-diacylglycerol to CoA and triacylglycerol.	Diacylglycerol *O*-acyltransferases 1 (Dgat1) and 2 (Dgat2)/ Q55BH9, Q54GC1	Diacylglycerol *O*-acyltransferases 1 (DGAT1), 2-acylglycerol *O*-acyltransferase 1 (MOGAT1)/ O75907, Q96PD6	Sterol *O*-acyltransferases 1 (Are1) and 2 (Are2)/ P25628, P53629	Diacylglycerol *O*-acyltransferase 1 (DGAT1)/ Q9SLD2
Protein folding and modification Subunits of the oligosaccharyl transferase complex, which catalyzes asparagine-linked glycosylation of newly synthesized proteins in the ER lumen	Oligosaccharyl transferase-1 (Ost1)/ Q54C27	Dolichyl-diphosphooligosaccharide-protein glycosyltransferase subunit 1 (RPN1)/ P04843	Dolichyl-diphosphooligosaccharide-protein glycosyltransferase subunit 1 (Ost1)/ P41543	Dolichyl-diphosphooligosaccharide-protein glycosyltransferase subunits 1A (OST1A) and 1B (OST1B)/ Q9SFX3, Q9ZUA0
	Oligosaccharyl transferase-2 (Ost2)/ Q54FB6	Dolichyl-diphosphooligosaccharide-protein glycosyltransferase subunit (DAD1)/ P61803	Dolichyl-diphosphooligosaccharide-protein glycosyltransferase subunit (OST2)/ P46964	Dolichyl-diphosphooligosaccharide-protein glycosyltransferase subunits 1 (DAD1) and 2 (DAD2)/ Q39080, O22622
	Oligosaccharyl transferase-3 (Ost3)/ Q54N33	ND	Dolichyl-diphosphooligosaccharide-protein glycosyltransferase subunit 3 (Ost3)/ P48439	Dolichyl-diphosphooligosaccharide-protein glycosyltransferase subunits 3A (OST3A) and 3B (OST3B)/ F4I8X8, Q9SYB5
	Oligosaccharyl transferase-4 (Ost4)/ Q54V54	Dolichyl-diphosphooligosaccharide-protein glycosyltransferase subunit 4 (OST4)/ P0C6T2	Dolichyl-diphosphooligosaccharide-protein glycosyltransferase subunit 4 (Ost4)/ Q99380	ND

Table 1. *Cont.*

Function/Features	*Dictyostelium* [a]	*Human* [a]	*Saccharomyces cerevisiae* [a]	*Arabidopsis thaliana* [a]
	Oligosaccharyl transferase complex subunit C (Ostc)/ Q54X66	Oligosaccharyltransferase complex subunit OSTC (OSTC)/ Q9NRP0	ND	Oligosaccharyl transferase complex/magnesium transporter family protein (At4g29870)/ Q9SZQ8
	Wheat germ agglutinin-binding protein (Wbp1)/ Q54E62	Dolichyl-diphosphooligosa ccharide-protein glycosyltransferase 48 kDa subunit (DDOST)/ P39656	Dolichyl-diphosphooligosa ccharide-protein glycosyltransferase subunit (Wbp1)/ P33767	Dolichyl-diphosphooligosa ccharide-protein glycosyltransferase 48 kDa subunit (OST48)/ Q944K2
	Suppressor of a *WBP1* mutation (Swp1)/ Q54HG9	Dolichyl-diphosphooligosa ccharide-protein glycosyltransferase subunit 2 (RPN2)/ P04844	Dolichyl-diphosphooligosa ccharide-protein glycosyltransferase subunit (Swp1)/ Q02795	Dolichyl-diphosphooligosa ccharide-protein glycosyltransferase subunit 2 (RPN2)/ Q93Z16
	Staurosporine and temperature sensitivity (Stt3)/ Q54NM9	Dolichyl-diphosphooligosa ccharide-protein glycosyltransferase subunits A (STT3A) and B (STT3B)/ P46977, Q8TCJ2	Dolichyl-diphosphooligosa ccharide-protein glycosyltransferase subunit (Stt3)/ P39007	Dolichyl-diphosphooligosaccharide-protein glycosyltransferase subunits A (STT3A) and B (STT3B)/ Q93ZY3, Q9FX21
Heat shock protein 70 (Hsp70)-family chaperone	78 kDa Glucose-regulated protein (Grp78)/ Q8T869	Binding immunoglobulin protein/78 kDa glucose-regulated protein (BiP/Grp78)/ P11021	Binding immunoglobulin protein (BiP/Kar2)/ P16474	Binding immunoglobulin protein 2 (BIP2)/ F4K007
Hsp90-family chaperone	94 kDa Glucose-regulated protein (Dd-grp94)/ Q9NKX1	Endoplasmin (GRP94)/ P14625	ATP-dependent molecular chaperone (Hsp82)/ P02829	Endoplasmin homolog (HSP90-7)/ Q9STX5
Calcium-binding proteins with chaperone activity	Calreticulin (CrtA)/ Q23858	Calreticulin (CALR)/ P27797	ND	Calreticulin-1 (CRT1) and 2 (CRT2)/ O04151, Q388587
	Calnexin (CnxA)/ Q55BA8	Calnexin (CANX)/ P27824	Calnexin homolog (Cne1)/ P27825	Calnexin homolog 1 (CNX1) and 2 (CNX2)/ P29402, Q38798

Table 1. *Cont.*

Function/Features	Dictyostelium [a]	Human [a]	Saccharomyces cerevisiae [a]	Arabidopsis thaliana [a]
ER luminal protein that catalyzes the formation and remodeling of protein disulfide bonds	Protein disulfide isomerases 1 (Pdi1) and 2 (Pdi2)/ Q86IA3, Q54EN4	Protein disulfide isomerases (P4HB), A4 (PDIA4), A3 (PDIA3), and A6 (PDIA6)/ P07237, P13667, P30101, Q15084	Protein disulfide isomerase (Pdi1)/ P17967	Protein disulfide isomerase-like proteins 1-1 (PDIL1-1), 1-2 (PDIL1-2), 2-2 (PDIL2-2), and 2-3 (PDIL2-3)/ Q9XI01, Q9SRG3, O22263, O48773
Unfolded Protein Response				
ER transmembrane serine and threonine kinase with ribonuclease activity that senses ER stress	Inositol-requiring enzyme A (IreA)/ Q55GJ2	Inositol-requiring enzyme proteins 1α (IRE1 α or ERN1) and 1β (IRE1β or ERN2)/ O75460, Q76MJ5	Inositol-requiring enzyme 1 (Ire1)/ P32361	Inositol-requiring enzyme proteins 1a (IRE1a) and 1b (IRE1b)/ Q93VJ2,
Calcium channel Ion channel participates in calcium release from the ER, and is activated by inositol trisphosphate	Inositol 1,4,5-trisphosphate receptor (IplA)/ Q9NA13	Inositol 1,4,5-trisphosphate receptors type 1 (ITPR1), type 2 (ITPR2), and type 3 (ITPR3)/ Q14643, Q14571, Q14573	ND	ND

[a] Protein orthologs/ UNIPROT identifiers. ND, no homology detected.

In mammalian cells, the curvature of the tubules is maintained by a highly conserved integral membrane family of proteins, referred to as reticulons (RTNs) [20]. RTN proteins contain a reticulon homology domain (RHD) at their C-terminus which is formed by two long hairpin transmembrane domains, separated by a hydrophilic linker [21]. These hairpins are inserted in the cytoplasmic leaflet of the ER membrane to provoke membrane bending. RTNs can also oligomerize in order to determine the diameter of the tubules [20–22].

Studies on how the *Dictyostelium* ER structure is maintained are still scarce; however, a homolog of the reticulon family was phylogenetically identified (annotated as *rtnlc*/DDB_G0293088) [23]. Owing to the presence in *Dictyostelium* of single orthologs of some of the proteins involved in the maintenance of ER architecture, it represents an advantageous model for combined genetic studies on ER dynamics and structure. For instance, reticulons were implicated in neurodegenerative disorders [24], but the study of this protein family in mammalian cells is challenging since they contain a large number of isoforms.

2.2. The ER Is a Dynamic Structure Continuously Rearranged

The ER is a highly dynamic network; its architecture is modified according to specific cellular demands or processes, such as changes in cellular morphology, cell migration, mitosis, and upon stressful conditions. For instance, specialized secretory cells require an increase in the number of sheet-like structures to synthesize large amounts of proteins, while adrenal, liver, and muscle cells require an ER network predominantly formed by tubules [25].

The synthesis of new tubules in the ER, together with the maintenance of its network and dynamics, depends greatly on the association of the ER with the cytoskeleton [26–28], while the maintenance of the reticulated network requires continuous events of contact and fusion between tubules. ER fusion events are mediated by atlastin (ATL) proteins, a dynamin-related family of GTPases that mediate homotypic membrane fusion [29,30]. During the fusion events, two GTP-bound ATLs, localized at opposing membranes, transdimerize, and GTP hydrolysis induces a conformational change that pulls the ER membrane close enough to fuse [31,32]. Plants and yeasts possess functional homolog GTPases of ATLs [33,34].

Recently, the role of the *Dictyostelium* ATL homolog Synthetic enhancement of *YOP1* (Sey1) was evaluated during infection with the intracellular bacteria *Legionella pneumophila* (*L. pneumophila*) [35]. This pathogen exploits a conserved replication mechanism in mammalian macrophages and in *Dictyostelium* cells, based on the construction of a special ER-derived compartment known as a *Legionella*-containing vacuole (LCV). Interestingly, in *Dictyostelium* cells, Sey1 modulates *L. pneumophila* replication, possibly by mediating homotypic membrane fusion at later steps of LCV maturation.

2.3. A Well-Connected Membranous System

The ER interacts dynamically with other membranes, such as the plasma membrane, and has contacts with other organelles such as mitochondria, the Golgi body, and endosomes, among others. These interactions, known as membrane contact sites (MCSs), allow the transport of ER-synthesized lipids and Ca^{2+} to other organelles. In addition, MCSs are involved in organelle biogenesis, distribution, inheritance, and maintenance (a more extensive review on ER contact sites can be found in Reference [36]).

In yeasts, the mitochondria–ER membrane contacts (MERCs) are tethered by the ER–mitochondria encounter structure (ERMES), which organizes the contact between the ER and the mitochondrial outer membrane. Similarly, the mitochondrial contact site and cristae organizing system (MICOS) enables the contact between the mitochondrial inner and outer membranes. Together, both systems are referred to as the ER–mitochondria organizing network (ERMIONE). In addition, there is an heteromeric hexamer known as the ER membrane protein complex that participates in diverse ER processes, and in the tethering of MERCs, where it is presumably involved in phosphatidylserine traffic (a review with an evolutionarily analysis on the topic was given in Reference [37]).

In yeasts, the ERMES system comprises an ER transmembrane protein, maintenance of mitochondrial morphology-1 (Mmm1p), and a cytosolic protein, mitochondrial distribution and morphology 12 protein (Mdm12p), which form a complex with two outer mitochondrial membrane proteins, Mdm34p and Mdm10p [38]. Strikingly, orthologs of this complex are absent in mammalian cells, but proteins such as mitofusins, phosphofurin acid cluster sorting protein 2 (PACS2), the mitochondrial voltage-dependent anion channel (VDAC), and the vacuole membrane protein 1 (VMP1), among others, were implicated in the regulation of this contact site; however, a conclusive outlook on how MERCs are tethered in these organisms remains elusive [39,40].

In *Dictyostelium*, the architecture of the ER contact sites with other membranes has not been described. However, the ER–mitochondria contact sites may be regulated by a homolog of the fungal ERMES, since an ortholog of the Mdm12p ERMES protein was recently identified in this amoeba, and was purified for structural analysis [41]. In addition, ortholog genes of *mmm1* (DDB_G0285921), *mdm10* (DDB_G0278805), and *mdm34* (DDB_G0274475) were predicted and are annotated in the *Dictyostelium* genome database [42].

Interestingly, the *Dictyostelium* genome encodes a VMP1 ortholog. This ER transmembrane resident protein is conserved in plants and animals, but it is absent in yeast. *Dictyostelium vmp1* knock-out mutant cells show severe ER and Golgi structural alterations, together with a set of pleiotropic phenotypes, ranging from autophagy defects to deficient osmoregulation [43,44]. The phenotypes of *vmp1⁻* cells may be a consequence of the severe imbalance in ER homeostasis. Studies using this amoeba were crucial in unraveling the role of this still poorly understood ER protein and paved the way for further studies on other ER proteins that are conserved in *Dictyostelium*, but not in yeast cells.

2.4. The Main Source of Lipid Synthesis

The ER and the Golgi body are the major sites of membrane lipid synthesis in eukaryotic cells. Lipid synthesis occurs in specialized ER regions rich in tubules, and in vesicles that are adjacent to the Golgi body, called the ER–Golgi intermediate compartment (ERGIC) [45]. Once lipids reach the ERGIC, they are transported to their final destination through contact with other organelles, or via vesicle transport [46].

Dictyostelium total lipids are partitioned into approximately 60% phospholipids and 40% neutral lipids [47]. The membranes of this amoeba display a composition similar to that observed in mammalian cells, where phosphatidylserine, choline, and ethanolamine are the major constituents [47]; therefore, it can represent a comparative model for the study of ER lipid-associated processes. Of note, *Dictyostelium* contains several unsaturated fatty acid species, with stigmastenol as the major steroid [47,48], and ether inositol phospholipids [49]. As in other organisms, *Dictyostelium* maintains lipid homeostasis by packing excess lipids as inert neutral species sheltered in vesicles that emerge from the ER, which are referred to as lipid droplets (LDs). Upon addition of palmitic acid and cholesterol, *Dictyostelium* cells accumulate LDs which contain triacylglycerol (TAG) and steryl esters in an approximate ratio of 1:15, similar to the ratio observed in mammalian adipocytes [50]. These vesicles contain about 72 proteins, including perilipin, which is implicated in protecting LDs from lipolysis. Perilipin which is conserved in mammals, but absent in yeast and *Caenorhabditis* [51], has a homologous gene in *Dictyostelium*, *plnA*.

Analogously to mammalian organisms, *Dictyostelium* cells contain two acyl coenzyme A (CoA) diacyl-glycerol acyltransferases (DGATs) that participate in the synthesis of TAG. One of these enzymes, Dgat1, localizes to the ER membrane, and provides most of the TAG synthesis activity. As with human DGAT1, this enzyme participates in the synthesis of other lipids such as waxes and ether lipids. The other DGAT enzyme coded for in the *Dictyostelium* genome localizes at lipid droplets (LDs), and has a minor role in total cellular TAG synthesis [52].

2.5. A Perfect Compartment to Fold and Modify Proteins

The ER lumen contains a unique glycosylation machinery, and a particular environment enriched with Ca^{2+}, with a high oxidizing potential and a high viscosity. All these conditions make up a perfect situation for the synthesis, folding, and modification of integral and secreted proteins.

In order to achieve their functional state, proteins undergo various processes in the ER lumen; these include N-linked glycosylation, disulfide bond formation, folding cycles, and oligomerization.

N-linked glycosylation is a co-translational modification that consists of the addition of an oligosaccharide tree to the asparagine (Asn) residues contained in the Asn-X-serine/threonine motif of proteins. This reaction is triggered by the oligosaccharyl transferase (OST) enzyme, and it is essential for the recruitment of carbohydrate-binding factors in the ER lumen that stimulate protein folding. It serves to increase protein stability by masking hydrophobic stretches or proteolytic cleavage sites, and avoiding back-translocation [53]. Although the *Dictyostelium* OST enzyme is unstudied, it was inferred through comparative studies that it is formed by at least seven subunits, and that it shares similarity with its plant and fly homologs [54].

ER luminal chaperones help the newly synthesized proteins to reach their active conformation by promoting their folding, and by preventing aggregation. There are two groups of ER chaperones: the heat shock proteins (HSP), a protein family that can also be found in all cellular compartments, and the carbohydrate-binding chaperones (CBC), which are specifically located in the ER [55,56].

The ER is mainly enriched with members of the HSP70 and HSP90 families. These proteins recognize specific domains in glycosylated proteins, or exposed hydrophobic segments in the non-glycosylated ones, thus protecting intermediate folded precursors from aggregation by shielding these regions from intermolecular hydrophobic interactions. There is an ER resident HSP70 chaperone, called GRP78/binding immunoglobulin protein (BiP) in metazoans, or Kar2p in yeast, which participates in a broad number of processes besides protein folding [57]. Additionally, the calnexin and calreticulin proteins are two of the main CBCs. These chaperones interact with the glycan moiety to achieve protein maturation and quality control [55].

Orthologs of the broad spectrum of ER-resident folding proteins were identified and described in *Dictyostelium*, among them, the calcium-regulated chaperones—calreticulin and calnexin [58], the HSP70 chaperone—78 kDa glucose-regulated protein (Grp78) [7], and Dd-grp94, a member of the HSP90 family [59].

During the various stages of its life cycle, the *Dictyostelium* ER adapts to continuously changing metabolic demands. As vegetative amoebas, they obtain nutrients primarily via phagocytosis. Through this process, the ER transiently contacts the phagosome during the uptake process. This contact requires calreticulin and calnexin, which participate in Ca^{2+} storage [58]. These observations suggest that the ER participates during phagosome formation, possibly as a membrane source and as a regulator of Ca^{2+} homeostasis.

Two other non-chaperone protein families participate in the ER protein-folding process: the peptidyl-prolyl isomerases (PPIs), which catalyze cis/trans isomerization of peptide bonds, and the protein disulfide isomerases (PDIs) [56,60], a protein family that participates in the formation of disulfide bonds between inter- and intra-chain cysteine residues, a covalent linkage which provides stability to proteins. The formation and disruption of disulfide bonds can also act as a regulatory mechanism for protein activity control. PDI oxidoreductases exchange disulfide bonds with their substrates, which results either in the reduction of its active site and the oxidation of two adjacent cysteines in the substrate to form a disulfide bond, or in the opposite reaction. In yeasts, PDI is kept oxidized through an electron flow pathway catalyzed by the ER oxidase protein 1 (Ero1) [61].

The *Dictyostelium* genome codes for two members of the PDI family (*pdi1* and *pdi2*). Remarkably, PDI (*pdi1*) lacks the canonical C-terminus retrieval signal motif for ER localization composed by the amino acids HDEL, and instead, requires a sequence in its last 57 C-terminal amino acids [62]. This motif allows the retention of PDIs at the ER when overexpressed in yeast cells, indicating that this ER-retention mechanism might be conserved in evolution [63].

3. Endoplasmic Reticulum Stress and the Unfolded Protein Response in a Social Amoeba

To support ER protein homeostasis, the cell must achieve equilibrium between the protein load and the concentration of the ER folding machinery. Conditions that alter this equilibrium may cause defects in protein folding and modification, thus leading to the accumulation of misfolded proteins in the ER lumen, a condition termed as ER stress (ERS) [64].

Dictyostelium development is regulated via a variety of secreted extracellular signals; it was observed that about 2.6% of the 12,257 proteins predicted to be encoded in its genome are secreted during this process [65]. In addition to the fluctuating metabolic demands of its life cycle, *Dictyostelium* cells encounter various stressful conditions derived from the complex ecosystem it inhabits, some of which cause ER homeostasis imbalances. For instance, this amoeba might share a habitat with the *Streptomyces* species, which evolved competitive survival mechanisms based on the production of antibiotics.

Recently, it was demonstrated that tunicamycin (TN), a fatty acyl nucleoside antibiotic produced by *Streptomyces lysosuperificus* and *Streptomyces chartreusis,* which interferes with N-glycosylation, induces ERS in *Dictyostelium* [7]. In *Dictyostelium*, this antibiotic effectively inhibits protein glycosylation [66]. The TN effects on *Dictyostelium* development were first determined in the early 1980s. Since then, TN was widely used to evaluate the role of N-glycosylated cell-adhesion proteins during the aggregation process. This antibiotic was found to inhibit cellular growth, and to impair development [66–73]. In addition, TN blocks cell fusion during *Dictyostelium* sexual development, mainly due to its effects on glycoprotein production [74]. Interestingly, TN can partially suppress the developmental phenotypes, but not allorecognition impairment, as presented by null-mutants of Transmembrane IPT/IG/E-set repeat protein (TgrB1) and TgrC1, two immunoglobulin-like proteins required for kin discrimination and cell type differentiation during *Dictyostelium* development [72].

After TN treatment, *Dictyostelium* cells undergo evident morphological changes by adopting a spherical shape [7]. Likewise, upon hyperosmotic stress, *Dictyostelium* cells suffer morphological changes due to a cytoskeletal reorganization [75]. Interestingly, a similar rounded morphology was also described for a subpopulation of stress- and detergent-resistant *Dictyostelium* cells, in which the expression of some lipid-metabolism genes were modified [76].

To cope with ERS, eukaryotic cells evolved a conserved system referred to as the unfolded protein response (UPR), which restores ER homeostasis through the activation of a complex transcriptional program that changes the expression of genes encoding proteins associated with the synthesis of membranes, and for chaperones and degradative enzymes [77]. In addition, the UPR decreases the protein load at the ER through the selective degradation of messenger RNAs (mRNAs) that are targeted to this compartment, and by decreasing the translation rates [78,79]. In metazoans, the UPR is activated in parallel by three ER transmembrane sensors: the inositol-requiring enzyme 1 (IRE1), the protein kinase RNA-like ER kinase (PERK), and the activating transcription factor 6 (ATF6) (Figure 3). Each of these branches senses the folding environment in the ER lumen and activates several transcription factors upon ERS.

After ERS, *Dictyostelium* cells trigger an adaptive transcriptional response, which diminishes the ER protein load, increases ER protein folding, and favours the cellular degradation processes [7]. Interestingly, ERS induces transcriptional changes in some genes that code for proteins of the actin cytoskeleton, and some genes involved in lipid metabolism [7], which suggests that the round cellular morphology caused by ERS might be the consequence of membrane and cytoskeletal rearrangements. Adopting a round morphology devoid of pseudopodia might be advantageous to *Dictyostelium* cells, by aiding in the lipid-balance maintenance in the plasma membrane, and by decreasing energy requirements.
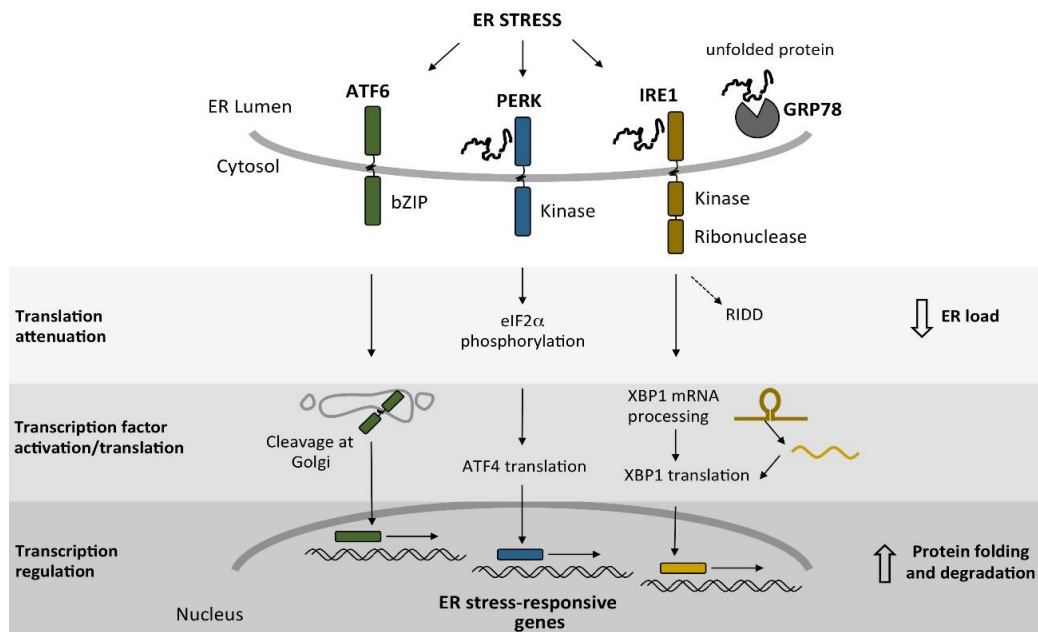
Figure 3. Signaling pathways involved in the unfolded protein response (UPR). In mammalian cells, three signaling branches that depend on the ER transmembrane sensor proteins—activating transcription factor 6 (ATF6), protein kinase RNA-like ER kinase (PERK), and inositol-requiring enzyme 1 (IRE1)—are activated upon ER stress (ERS). PERK and IRE1 can sense ERS by interacting directly with unfolded proteins through their luminal sensor domain. In addition, ATF6, PERK, and IRE1 detect an increase in unfolded proteins when they lose their association with the ER chaperone GRP78/binding immunoglobulin protein (BiP). When these transducers detect ERS, a recovery response is activated. This response mainly regulates two events: the reduction of ER protein load, and an increase in the protein-folding and degradation capacity of the cell. The former is accomplished via translation inhibition, triggered by the PERK-mediated phosphorylation of the eukaryotic initiation factor 2α (eIF2α), and by the degradation of certain messenger RNAs (mRNAs) in the regulated IRE1-dependent decay (RIDD). The second event regulates the activation or translation of transcription factors that, when transported to the nucleus, reprogram transcription to increase the expression of ER homeostatic genes, thus promoting protein folding and modification of the ER.

3.1. The IreA Branch

As in other organisms, the transcriptional response to ERS in *Dictyostelium* is mediated by the IRE1 pathway, which is, until now, the only UPR signaling branch identified in this amoeba. In plants, yeasts, and mammals, this pathway is constituted by the type I ER-resident transmembrane protein, IRE1, and a basic zipper leucine transcription factor known as the X-box binding protein 1 (XBP1) in mammalian cells, HAC1 in yeast, and bZIP60 in plants.

IRE1, the most conserved UPR transducer, contains an amino N-terminal ER luminal stress-sensor domain, and a carboxy C-terminal cytoplasmic region that harbors a kinase and a kinase extension nuclease (KEN) domain [80]. IRE1 plays a prominent role in the UPR of plants and animals, and it is the only sensor in *Saccharomyces cerevisiae* [81]. Mammalian cells contain two IRE1 isoforms, IRE1α, which is ubiquitously expressed, and IRE1β, which is exclusively expressed in the intestinal and lung epithelia [82,83]. *Arabidopsis thaliana* also has two IRE1 orthologs (IRE1A and IRE1B) that display differential expression patterns [84].

When the cell is under ERS conditions, IRE1 is activated via a conformational change triggered by direct interaction with unfolded proteins through its sensor domain and/or by the release of the chaperone GRP78/Kar2p from the same domain. This leads to the formation of high-order IRE1 oligomers, and their transautophosphorylation [85–87]. Once activated, IRE1 processes the mRNA of a

transcription factor through an unconventional splicing event that eliminates an intron. The processed mRNA is translated into a bZIP that upregulates the transcription of genes encoding ER-resident chaperones and modification enzymes, among others [88]. Although the protein sequence of this transcription factor is poorly conserved between species, the IRE1 cleavage site and the stem-loop structure of the unconventional intron are widely preserved [89–91].

In mammalian cells, IRE1 is able to regulate its protein levels via the degradation of its own mRNA. The IRE1 N-terminus can bind to the 5′ end of its own mRNA while the nascent protein is translated and attached to the ribosome. After the release of the nascent protein, IRE1 can dimerize, and activates its RNAse domain to degrade the mRNA [92]. The yeast Ire1p kinase domain participates in the downregulation of the pathway through an autophosphorylation process that requires a 28-amino-acid region in its kinase domain; this hyperphosphorylation destabilizes Ire1p oligomers [93].

The *Dictyostelium* genome encodes a single IRE1 sensor ortholog, IreA, an ER-localized protein with a single predicted transmembrane domain [7]. IreA comprises two regions, one localized in the ER lumen, which is poorly conserved and likely functions as the ER environment sensor, and the other region that is predicted to be at the cytosolic face of the ER and contains a serine/threonine kinase and a KEN domain (Figure 4A). Both kinase and ribonuclease domains are required in *Dictyostelium* cells to survive ER stress, and both must be fully active to regulate IreA oligomer-formation dynamics during sustained ERS [7]. Upon ER stress, IreA forms transient high-order oligomers (Figure 4B). Oligomerization in the yeast Ire1p is required for the recruitment of unprocessed *HAC1* mRNA [94], and to trigger Ire1p RNAse activation [95]. However, in *Dictyostelium*, the possible transcription factor is yet unidentified.
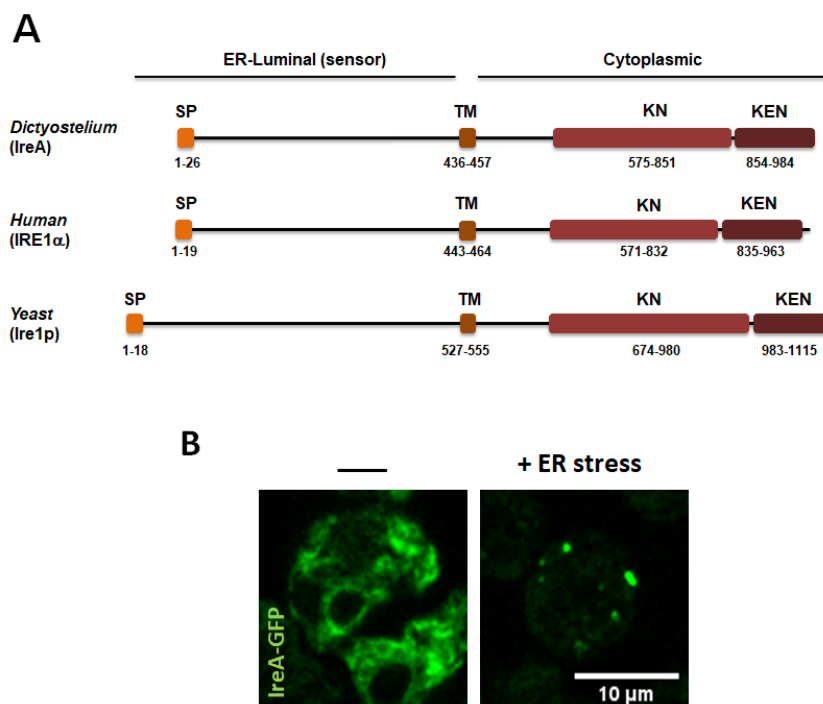
Figure 4. (**A**) Diagram of the structural domains of *Dictyostelium* IreA, compared with its *Saccharomyces cerevisiae* and human orthologs. SP (signal peptide), TM (transmembrane domain), KN (kinase domain), and KEN (kinase extension nuclease domain). Proteins were drawn to scale. Numbers indicate amino acid coordinates. Protein domains were obtained from www.uniprot.org. (**B**) Live-cell confocal microscopy of *ireA*⁻ cells expressing the IreA-GFP construct after 4 h, in the absence or in the presence of an ER-stress inducer. The IreA-GFP signal forms large puncta (possibly high-order oligomers). (Scale bar corresponds to 10 μm).

In animal cells, IRE1 regulates transcript abundance in a branched fashion, since it splices the XBP1 transcript, but also degrades mRNAs through its RNAse domain via a mechanism named regulated IRE1-dependent decay (RIDD) [78,79,96]. The RIDD pathway decreases the ER protein load of secreted and transmembrane proteins, and can activate apoptosis by degrading anti-apoptotic pre-mRNAs [97]. Interestingly, the yeasts *Schizosaccharomyces pombe* and *Candida glabrata* possess the RIDD pathway, but lack any XBP1/HAC1-like transcription factors [90,91], and thus, their UPR-dependent transcriptional changes are solely regulated by RIDD in a single-component pathway [91,98]. In *Dictyostelium*, a considerable number of transcripts are downregulated in an IreA-dependent manner, thus suggesting the existence of a RIDD pathway. However, the ERS response also increases the abundance of specific transcripts, suggesting the existence of an IreA-dependent transcription factor; however, an XBP1 ortholog is yet unidentified [7]. Therefore, the *Dictyostelium* ERS response pathway may resemble that of the IRE1-branched animal mechanism.

3.2. IreA-Independent UPR Pathways in Dictyostelium

In contrast to the yeast UPR, in which the entire transcriptional response depends on the IRE1 pathway, in *Dictyostelium,* the response is only partially dependent on IreA [7], which suggests that, as in plants and animals, additional input signaling pathways must exist in this amoeba. The IreA-dependent transcriptional reprogramming primarily triggers an increase in the degradative capacity of the cell, and a decrease in protein load at the ER. As in yeast, the *Dictyostelium* IRE1 pathway regulates the expression of genes that participate in degradative processes, such as ubiquitin and ubiquitin ligases, together with ester-bond hydrolases and peptidases [7]. However, the expression of only a few ER chaperones depends on IreA, suggesting that, as in animal cells, IRE1-independent pathways may be implicated in the regulation of these components.

In animal cells, there are two UPR pathways that account for additional inputs, besides IRE1, to regulate the UPR (Figure 3). One of them is regulated by ATF6, a type II transmembrane ER-resident protein that bears a bZIP transcription factor domain in its cytosolic N-terminal portion. This UPR component is present in metazoan cells, and functional homologs were identified in plants (bZIP28 and bZIP17) [99,100]. Upon ERS, ATF6 is translocated from the ER to the Golgi body, where its transcription factor domain is released via a proteolytic cleavage triggered by the site-1 and site-2 proteases (S1P and S2P) [101,102]. The ATF6-dependent transcriptional reprogramming is required to induce the expression of genes that code for chaperones and degradative enzymes, and of genes involved in ER-membrane remodeling [103]. ATF6 signaling participates in senescence-associated ER expansion [104], and variants of this gene underlie the pathogenesis of inherited retinal and cone photoreceptor disorders [105,106].

In addition, in animals, the UPR is regulated by PERK, a transmembrane kinase that regulates protein translation through phosphorylating the eukaryotic initiation factor 2α (eIF2α) [107]. In plants, the presence of PERK orthologs is unreported.

Identification of ATF6 and PERK orthologs in *Dictyostelium* was unsuccessful; nevertheless, the existence of homolog components of these pathways cannot be ruled out. ATF6 belongs to the bZIP transcription factor family, and *Dictyostelium* contains a large number of these transcription factors. It was suggested that bZIPs evolved from a single common ancestor, which expanded and diversified greatly during evolution [108]. The current opisthokont bZIP transcription factors emerged from three ancestral groups that appeared during the evolution of this phylogenetic branch. One of these ancestral groups gave rise to the ATF6/HAC1 set of transcription factors, which is absent in other phylogenetic branches, such as the Amoebozoa or Plantae [108]. However, ER transmembrane bZIP transcription factors, which are activated upon ERS by a mechanism analogous to the one that regulates ATF6 and XBP1, were identified in plants [99,109]. *Dictyostelium* transcription factors may have diverged largely, so further characterization of the potential 19 bZIP transcription factors coded for in its genome may unravel the presence of ATF6 and XBP1 functional homologs.

4. ER Stress and the Autophagy Pathway in *Dictyostelium*

Degradative pathways also participate in homeostasis recovery upon ERS. Protein degradation is mainly achieved through two mechanisms. One is the ER-associated degradation (ERAD), which is accomplished by the proteasome, and thus, requires protein retro-translocation from the ER to the cytoplasm [110,111]. The other is autophagy, which delivers cytoplasmic material to the lysosome through double-membrane vesicles, known as autophagosomes [112]. If cells are not able to recover from ERS, the UPR represses the adaptive response, and triggers cell death [113].

In mammalian and plant cells, IRE1 activity is not only devoted to mRNA processing. In addition to the activation of its RNAse domain, IRE1 kinase can regulate other signaling pathways that orchestrate a more complex response. In animal cells, upon persistent ER stress, IRE1 can activate the Jun N-terminal kinase (JNK) by interacting with the adaptor protein TNF-receptor associated factor 2 (TRAF2) [114]. Depending on the severity of the stress, this signaling leads either to autophagy induction or to apoptosis activation [97,115]. Similarly, in plants, it was observed that the IRE1 kinase domain is required for the induction of autophagy upon ERS [116]. However, the JNK pathway is absent in *Dictyostelium*, and in other organisms outside the animal kingdom, such as plants or fungi [117,118]. The JNKs belong to the high osmolarity glycerol (HOG1)-like mitogen-activated protein kinase (MAPK) family, a group that emerged through duplication from a common ancestor that gave rise in fungi to a single HOG1 kinase. In contrast to p38, the other animal MAPK of this group, JNK genes underwent rapid evolution [118]. Thus, the IRE1-mediated JNK signaling, triggered by ERS in animal cells, might be a specialized trait of this phylogenetic group that emerged later during animal evolution.

Recently, we determined that autophagy is required for cell survival in response to ER stress in *Dictyostelium* cells [7]. However, in contrast with the animal and plant scenario, we found that IreA is not required for this autophagy induction. This suggests the presence of IRE1-independent pathways that may sense ERS and induce autophagy as a survival response. However, the IreA-mediated recovery of ER homeostasis was required to achieve a fully functional autophagy-dependent degradation, thus highlighting the functional connection of the ER with autophagosome biogenesis [7].

Dictytostelium cells not only lack JNK signaling pathways, but also caspase-dependent apoptotic cell death. However, there is a pathway of programmed cell death that is displayed by these amoebas with the characteristics of autophagic cell death (ACD) [119]. ACD is a death process characterized by cytoplasm vacuolization without chromatin condensation as in apoptosis, or organelle swelling as in necrosis [120]. It was described that ACD participates in cell death during *Drosophila* development [121], in hypersensitive cell death in plants [122], and in mammalian cell death under certain conditions [123]. Still, the nature and specific mechanisms that regulate ACD remain poorly defined.

In *Dictyostelium*, stalk cells die through ACD during fruiting-body formation [124,125]. Interestingly, research using this amoeba uncovered a novel link between the ER and ACD regulation, since it was observed that this type of cell death depends on the ER Ca^{2+}-channel inositol 1,4,5-trisphosphate receptor (IP3R). Presumably, it is required to increase the cytosolic concentration of Ca^{2+} [126]. Since changes in calcium homeostasis at the ER might imbalance several cellular functions (for example, ER protein-folding and chaperone functions), studies on the participation of the UPR pathways in ACD regulation in this amoeba might unravel novel links between both pathways. It can also be inferred that, due to the absence of caspase-dependent apoptosis in *Dictyostelium,* the UPR may only be devoted to survival responses; thus, the study of the cellular effects of sustained ER stress in *Dictyostelium* may shed light on conserved survival responses that are hindered in animal cells by apoptotic signaling.

5. Assessing ER Stress in *Dictyostelium*

The onset of a stress response is usually evaluated by analyzing changes in the expression of marker genes. In *Dictyostelium*, ERS induces an increase in the abundance of several transcripts [7], whose levels can be analyzed to determine whether or not a defined treatment or growth condition

leads to ERS. In Table 2, we present a selected list of IreA-dependent and independent genes, whose expression showed significant changes upon a TN treatment, and that can be useful as ERS markers. In addition, the changes in the expression of proteins such as cell division cycle protein D (CdcD), a conserved ATPase that participates in protein retro-translocation from the ER [127], can be evaluated via western blotting. It can also be determined whether a certain stimulus activates an IreA-dependent response, by following IreA clustering behavior in a time-lapse confocal microscopy assay of IreA-GFP-expressing cells that were exposed to the stimulus under study (Figure 4B).

Table 2. List of selected genes that showed a significant transcript increase upon a 16 h tunicamycin treatment, and that are suggested for evaluation as ER stress markers (list extracted from Domínguez-Martín, E. et al., 2018 [7]).

Gene ID	Name	Description	IreA-Dependent
DDB_G0276445	Grp78	Heat shock protein Hsp70 family protein.	no
DDB_G0274199	DDB_G0274199	Putative metallophosphoesterase.	no
DDB_G0278477	sarB	ADP ribosylation factors/ Secretion-associated and Ras-related (ARF/SAR) superfamily protein. GTP-binding protein Sar1B involved in vesicular transport between the endoplasmic reticulum and the Golgi body.	no
DDB_G0283867	*cprC*	Cysteine proteinase 3.	no
DDB_G0278371	*spc1*	Ortholog of the conserved microsomal signal peptidase 12 kDa subunit; the signal peptidase complex is a membrane-bound endo-proteinase that removes signal peptides from nascent proteins as they are translocated into the lumen of the endoplasmic reticulum.	no
DDB_G0281833	DDB_G0281833	Ubiquitin-conjugating enzyme E2.	no
DDB_G0283113	*eriA*	RNA exonuclease.	no
DDB_G0290227	*npl4*	Ortholog of nuclear protein localization 4 (NPL4), which, together with ubiquitin fusion degradation protein 1 (Ufd1) and cell division cycle protein D (CdcD), is involved in recognition of polyubiquitinated proteins, and their presentation to the 26S proteasome for degradation.	no
DDB_G0287685	*cinC*	Elongation factor 2. Translocates the peptidyl-tRNA from the aminoacyl site to the peptidyl site on the ribosome during protein synthesis; induced by cycloheximide; knockdown has significantly reduced ability for protein synthesis.	yes
DDB_G0269462	DDB_G0269462	Large protein containing two ubiquitin domains.	yes
DDB_G0291121	*cinB*	Esterase/lipase/thioesterase domain-containing protein.	yes
DDB_G0285131	derl2	Derlin-2. component of endoplasmic reticulum-associated degradation (ERAD) for misfolded luminal proteins.	yes
DDB_G0270272	uae1	Ubiquitin activating enzyme E1.	yes

Changes in ER morphology upon ERS can be followed using immunofluorescence staining. Specific antibodies against *Dictyostelium* ER-resident proteins, such as calnexin and PDI [62,128], are available. As depicted in Figure 5, ER morphology defects in ERS-sensitive strains, such as the *ireA*⁻ mutant, can be easily detected with this technique.

The sensitivity of mutant strains to ER stressors, such as TN, can be evaluated via serial dilution spotting assays, as described previously [7] (Figure 6). This assay is performed by spotting serial dilutions of cells that were previously treated with various concentrations of the ERS inducer and/or for various treatment times, over agar plates with bacteria (Figure 6A). It is recommended to evaluate cell morphology before spotting cells (Figure 6B). After removal of the stressor, cells that survived the treatment can reinstate growth in association with bacteria. The inability of a certain strain to restore growth after treatment with ERS inducers reflects its sensitivity to this condition (Figure 6C). Currently, the only reported ER stress-sensitive strain is the *ireA*⁻ mutant, which can be included as a control in this sort of assay [7].
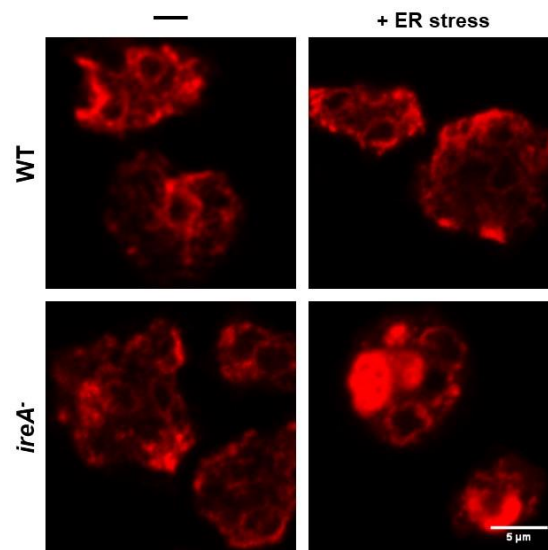
Figure 5. WT and *ireA⁻* cells, after an ER stress treatment or mock, were fixed and prepared for the detection of the ER-resident protein disulfide isomerase (PDI) via an immunofluorescence assay and were visualized using confocal microscopy. An ER stress treatment severely impaired the ER morphology of the sensitive *ireA⁻* cells. (Scale bar corresponds to 5 μm).
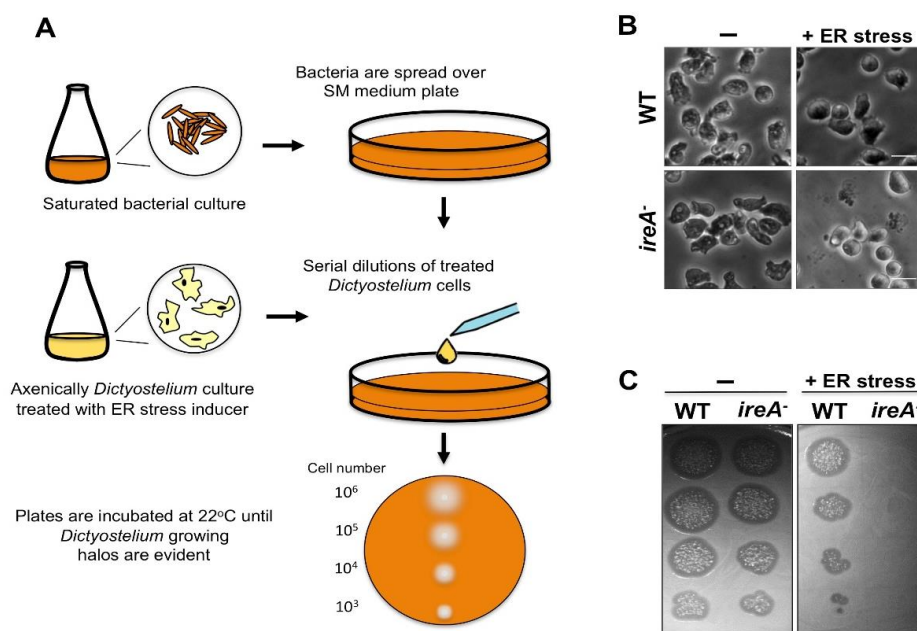

Figure 6. (**A**) Descriptive diagram of a serial dilution spotting assay used to test if a certain strain is sensitive to an ER stress inducer. A culture of bacterial cells (*Dictyostelium* is usually fed with *Klebsiella aerogenes* or *Escherichia coli*) is grown to saturation, and an aliquot is spread over an SM agar plate. Axenically growing *Dictyostelium* strains in the mid-logarithmic growth phase (with a density of around 1×10^6 cells/mL) are prepared and treated for the desired times with the ER stress inducer. After the treatment, *Dictyostelium* cells are collected, and serial dilutions are prepared and spotted on the SM agar plates. Plates are incubated at 22 °C until lysis plaques emerge due to the presence of growing amoebas feeding on bacteria. (**B**) Light microscopy pictures of WT and ER stress-sensitive *ireA⁻* cells treated with a stress inducer. Morphological changes and cell lysis can be analyzed before the spotting assay. Notice the presence of round cells and the cell debris in the *ireA⁻* strain after the treatment. (**C**) Picture of a spotting assay where a WT and an ER stress-sensitive strain (*ireA⁻* cells) were tested with mock or ER stress inducer treatment.

6. Concluding Remarks

Dictyostelium proved to be an advantageous model in cell biology, and more recently, it emerged as a valuable organism for the study of ER-associated processes, such as the pathways involved in the ER stress response. These pathways show intriguing similarities, but also some differences between *Dictyostelium* and other organisms, expanding our knowledge of this conserved pathway across evolution. In addition, *Dictyostelium* poses an interesting model to unravel the role of proteins with unknown functions that are conserved in animals, but absent in yeast, and whose study may lead to a deeper understanding of how the complex regulation of the ER network is attained.

References

1. Sheikh, S.; Thulin, M.; Cavender, J.C.; Escalante, R.; Kawakami, S.; Lado, C.; Landolt, J.C.; Nanjundiah, V.; Queller, D.C.; Strassmann, J.E.; et al. A New Classification of the Dictyostelids. *Protist* **2018**, *169*, 1–28. [CrossRef] [PubMed]

2. Annesley, S.; Fisher, P. Dictyostelium discoideum—A model for many reasons. *Mol. Cell. Biochem.* **2009**, *329*, 73–91. [CrossRef] [PubMed]

3. Muñoz-Braceras, S.; Mesquita, A.; Escalante, R. Dictyostelium discoideum as a model in biomedical research. In *Dictyostelids. Evolution, Genomics and Cell Biology*; Romeralo, M., Baldauf, S., Escalante, R., Eds.; Springer: Berlin/Heiderberg, Germany, 2013; pp. 1–34. ISBN 978-3-642-38486-8.

4. Loomis, W.F. Cell signaling during development of Dictyostelium. *Dev. Biol.* **2014**, *391*, 1–16. [CrossRef] [PubMed]

5. Eichinger, L.; Pachebat, J.A.; Glockner, G.; Rajandream, M.-A.; Sucgang, R.; Berriman, M.; Song, J.; Olsen, R.; Szafranski, K.; Xu, Q.; et al. The genome of the social amoeba Dictyostelium discoideum. *Nature* **2005**, *435*, 43–57. [CrossRef] [PubMed]

6. Williams, J.G. Dictyostelium finds new roles to model. *Genetics* **2010**, *185*, 717–726. [CrossRef] [PubMed]

7. Domínguez-Martín, E.; Ongay-Larios, L.; Kawasaki, L.; Vincent, O.; Coello, G.; Coria, R.; Escalante, R. IreA controls endoplasmic reticulum stress-induced autophagy and survival through homeostasis recovery. *Mol. Cell. Biol.* **2018**, MCB.00054-18. [CrossRef]

8. Roussel, B.D.; Kruppa, A.J.; Miranda, E.; Crowther, D.C.; Lomas, D.A.; Marciniak, J.S. Endoplasmic reticulum dysfunction in neurological disease. *Lancet Neurol.* **2013**, *12*, 105–118. [CrossRef]

9. Ozcan, L.; Tabas, I. Role of Endoplasmic Reticulum Stress in Metabolic Disease and Other Disorders. *Annu. Rev. Med.* **2012**, *63*, 317–328. [CrossRef] [PubMed]

10. Annesley, S.J.; Chen, S.; Francione, L.M.; Sanislav, O.; Chavan, A.J.; Farah, C.; De Piazza, S.W.; Storey, C. L.; Ilievska, J.; Fernando, S.G.; et al. Dictyostelium, a microbial model for brain disease. *Biochim. Biophys. Acta Gen. Subj.* **2014**, *1840*, 1413–1432. [CrossRef] [PubMed]

11. Huber, R.J. Using the social amoeba Dictyostelium to study the functions of proteins linked to neuronal ceroid lipofuscinosis. *J. Biomed. Sci.* **2016**, *23*, 83. [CrossRef] [PubMed]

12. Myre, M.A.; Huber, R.J.; Day, D.H.O. *Functional Analysis of Proteins Involved in Neurodegeneration Using the Model Organism Dictyostelium: Alzheimer's, Huntington's, and Batten Disease*; Elsevier Inc.: New York, NY, USA, 2018; ISBN 9780128040782.

13. Malinovska, L.; Palm, S.; Gibson, K.; Verbavatz, J.-M.; Alberti, S. *Dictyostelium discoideum* has a highly Q/N-rich proteome and shows an unusual resilience to protein aggregation. *Proc. Natl. Acad. Sci. USA* **2015**, *112*, E2620–E2629. [CrossRef] [PubMed]

14. Santarriaga, S.; Petersen, A.; Ndukwe, K.; Brandt, A.; Gerges, N.; Scaglione, J.B.; Scaglione, K.M. The social amoeba *Dictyostelium discoideum* is highly resistant to polyglutamine aggregation. *J. Biol. Chem.* **2015**, *290*, 25571–25578. [CrossRef] [PubMed]

15. Westrate, L.M.; Lee, J.E.; Prinz, W.A.; Voeltz, G.K. Form Follows Function: The Importance of Endoplasmic Reticulum Shape. *Annu. Rev. Biochem.* **2015**, *84*, 791–811. [CrossRef] [PubMed]

16. Nixon-Abell, J.; Obara, C.J.; Weigel, A.V.; Li, D.; Legant, W.R.; Xu, C.S.; Pasolli, H.A.; Harvey, K.; Hess, H.F.; Betzig, E.; et al. Increased spatiotemporal resolution reveals highly dynamic dense tubular matrices in the peripheral ER. *Science* **2016**, *354*, aaf3928. [CrossRef] [PubMed]

17. Fernández-Busnadiego, R.; Saheki, Y.; de Camilli, P. Three-dimensional architecture of extended synaptotagmin-mediated endoplasmic reticulum—Plasma membrane contact sites. *Proc. Natl. Acad. Sci. USA* **2015**, *112*, E2004–E2013. [CrossRef] [PubMed]

18. Hetzer, M.W. The nuclear envelope. *Cold Spring Harb. Perspect. Biol.* **2010**. [CrossRef] [PubMed]

19. Terasaki, M.; Shemesh, T.; Kasthuri, N.; Klemm, R.W.; Schalek, R.; Hayworth, K.J.; Hand, A.R.; Yankova, M.; Huber, G.; Lichtman, J.W.; et al. Stacked endoplasmic reticulum sheets are connected by helicoidal membrane motifs. *Cell* **2013**, *154*, 285–296. [CrossRef] [PubMed]

20. Zurek, N.; Sparks, L.; Voeltz, G. Reticulon short hairpin transmembrane domains are used to shape ER tubules. *Traffic* **2011**, *12*, 28–41. [CrossRef] [PubMed]

21. di Sano, F.; Bernardoni, P.; Piacentini, M. The reticulons: Guardians of the structure and function of the endoplasmic reticulum. *Exp. Cell Res.* **2012**, *318*, 1201–1207. [CrossRef] [PubMed]

22. Shibata, Y.; Voss, C.; Rist, J.M.; Hu, J.; Rapoport, T.A.; Prinz, W.A.; Voeltz, G.K. The reticulon and Dp1/Yop1p proteins form immobile oligomers in the tubular endoplasmic reticulum. *J. Biol. Chem.* **2008**, *283*, 18892–18904. [CrossRef] [PubMed]

23. Oertle, T.; Klinger, M.; Stuermer, C.A.O.; Schwab, M.E. A reticular rhapsody: Phylogenic evolution and nomenclature of the RTN/Nogo gene family. *FASEB J.* **2003**, *17*, 1238–1247. [CrossRef] [PubMed]

24. Chiurchiù, V.; Maccarrone, M.; Orlacchio, A. The role of reticulons in neurodegenerative diseases. *NeuroMol. Med.* **2014**, *16*, 3–15. [CrossRef] [PubMed]

25. Schwarz, D.S.; Blower, M.D. The endoplasmic reticulum: Structure, function and response to cellular signaling. *Cell. Mol. Life Sci.* **2016**, *73*, 79–94. [CrossRef] [PubMed]

26. Bola, B.; Allan, V. How and why does the endoplasmic reticulum move? *Biochem. Soc. Trans.* **2009**, *37 Pt 5*, 961–965. [CrossRef] [PubMed]

27. Fehrenbacher, K.L.; Davis, D.; Wu, M.; Boldogh, I.; Pon, L.A. Endoplasmic reticulum dynamics, inheritance, and cytoskeletal interactions in budding yeast. *Mol. Biol. Cell* **2002**, *13*, 854–865. [CrossRef] [PubMed]

28. Boevink, P.; Oparka, K.; Cruz, S.S.; Martin, B.; Betteridge, A.; Hawes, C. Stacks on tracks: The plant Golgi apparatus traffics on an actin/ER network. *Plant J.* **1998**, *15*, 441–447. [CrossRef] [PubMed]

29. Liu, T.Y.; Bian, X.; Sun, S.; Hu, X.; Klemm, R.W.; Prinz, W.A.; Rapoport, T.A.; Hu, J. Lipid interaction of the C terminus and association of the transmembrane segments facilitate atlastin-mediated homotypic endoplasmic reticulum fusion. *Proc. Natl. Acad. Sci. USA* **2012**, *109*, E2146–E2154. [CrossRef] [PubMed]

30. McNew, J.A.; Sondermann, H.; Lee, T.; Stern, M.; Brandizzi, F. GTP-Dependent Membrane Fusion. *Annu. Rev. Cell Dev. Biol.* **2013**, *29*, 529–550. [CrossRef] [PubMed]

31. Bian, X.; Klemm, R.W.; Liu, T.Y.; Zhang, M.; Sun, S.; Sui, X.; Liu, X.; Rapoport, T.A.; Hu, J. Structures of the atlastin GTPase provide insight into homotypic fusion of endoplasmic reticulum membranes. *Proc. Natl. Acad. Sci. USA* **2011**, *108*, 3976–3981. [CrossRef] [PubMed]

32. Byrnes, L.J.; Sondermann, H. Structural basis for the nucleotide-dependent dimerization of the large G protein atlastin-1/SPG3A. *Proc. Natl. Acad. Sci. USA* **2011**, *108*, 2216–2221. [CrossRef] [PubMed]

33. Wang, H.; Lockwood, S.K.; Hoeltzel, M.F.; Schiefelbein, J.W. The Root Hair Defective3 gene encodes an evolutionarily conserved protein with GTP-binding motifs and is required for regulated cell enlargement in Arabidopsis. *Genes Dev.* **1997**, *11*, 799–811. [CrossRef] [PubMed]

34. Hu, J.; Shibata, Y.; Zhu, P.P.; Voss, C.; Rismanchi, N.; Prinz, W.A.; Rapoport, T.A.; Blackstone, C. A Class of Dynamin-like GTPases Involved in the Generation of the Tubular ER Network. *Cell* **2009**, *138*, 549–561. [CrossRef] [PubMed]

35. Steiner, B.; Swart, A.L.; Welin, A.; Weber, S.; Personnic, N.; Kaech, A.; Freyre, C.; Ziegler, U.; Klemm, R. W.; Hilbi, H. ER remodeling by the large GTPase atlastin promotes vacuolar growth of Legionella pneumophila. *EMBO Rep.* **2017**, *18*, 1–20. [CrossRef] [PubMed]

36. Phillips, M.J.; Voeltz, G.K. Structure and function of ER membrane contact sites with other organelles. *Nat. Rev. Mol. Cell Biol.* **2016**, *17*, 69–82. [CrossRef] [PubMed]

37. Wideman, J.G.; Muñoz-Gómez, S.A. The evolution of ERMIONE in mitochondrial biogenesis and lipid homeostasis: An evolutionary view from comparative cell biology. *Biochim. Biophys. Acta Mol. Cell Biol. Lipids* **2016**, *1861*, 900–912. [CrossRef] [PubMed]

38. Kornmann, B.; Currie, E.; Collins, S.R.; Schuldiner, M.; Nunnari, J.; Weissman, J.S.; Walter, P. An ER-mitochondria tethering complex revealed by a synthetic biology screen. *Science* **2009**, *325*, 477–481. [CrossRef] [PubMed]

39. Tabara, L.C.; Escalante, R. VMP1 establishes ER-microdomains that regulate membrane contact sites and autophagy. *PLoS ONE* **2016**, *11*, 18892–18904. [CrossRef] [PubMed]

40. Herrera-Cruz, M.S.; Simmen, T. Of yeast, mice and men: MAMs come in two flavors. *Biol. Direct* **2017**, *12*, 1–21. [CrossRef] [PubMed]

41. AhYoung, A.P.; Lu, B.; Cascio, D.; Egea, P.F. Crystal structure of Mdm12 and combinatorial reconstitution of Mdm12/Mmm1 ERMES complexes for structural studies. *Biochem. Biophys. Res. Commun.* **2017**, *488*, 129–135. [CrossRef] [PubMed]

42. Fey, P.; Gaudet, P.; Pilcher, K.E.; Franke, J.; Chisholm, R.L. dictyBase and the Dicty Stock Center. *Methods Mol. Biol.* **2006**, *346*, 51–74. [PubMed]

43. Calvo-garrido, J.; Carilla-latorre, S.; La, F.; Egea, G.; Escalante, R. Vacuole Membrane Protein 1 Is an Endoplasmic Reticulum Protein Required for Organelle Biogenesis, Protein Secretion, and Development. *Mol. Biol. Cell.* **2008**, *19*, 3442–3453. [CrossRef] [PubMed]

44. Calvo-Garrido, J.; King, J.S.; Muñoz-Braceras, S.; Escalante, R. Vmp1 regulates PtdIns3P signaling during autophagosome formation in Dictyostelium discoideum. *Traffic* **2014**, *11*, 1235–1246. [CrossRef] [PubMed]

45. Fagone, P.; Jackowski, S. Membrane phospholipid synthesis and endoplasmic reticulum function. *J. Lipid Res.* **2009**, *50*, S311–S316. [CrossRef] [PubMed]

46. Appenzeller-Herzog, C. The ER-Golgi intermediate compartment (ERGIC): In search of its identity and function. *J. Cell Sci.* **2006**, *119*, 2173–2183. [CrossRef] [PubMed]

47. Davidoff, F.; Korn, E.D. Fatty acid and phospholipid composition of the cellular slime mold, Dictyostelium discoideum. *J. Biol. Chem.* **1963**, *238*, 3199–3209. [PubMed]

48. Weeks, G.; Herring, F.G. The lipid composition and membrane fluidity of Dictyostelium discoideum plasma membranes at various stages during differentiation. *J. Lipid Res.* **1980**, *21*, 681–686. [PubMed]

49. Clark, J.; Kay, R.R.; Kielkowska, A.; Niewczas, I.; Fets, L.; Oxley, D.; Stephens, L.R.; Hawkins, P.T. Dictyostelium uses ether-linked inositol phospholipids for intracellular signalling. *EMBO J.* **2014**, *33*, 2188–2200. [CrossRef] [PubMed]

50. Du, X.; Barisch, C.; Paschke, P.; Herrfurth, C.; Bertinetti, O.; Pawolleck, N.; Otto, H.; Rühling, H.; Feussner, I.; Herberg, F.W.; et al. Dictyostelium lipid droplets host novel proteins. *Eukaryot. Cell* **2013**, *12*, 1517–1529. [CrossRef] [PubMed]

51. Lu, X.; Gruia-Gray, J.; Copeland, N.G.; Gilbert, D.J.; Jenkins, N.A.; Londos, C.; Kimmel, A.R. The murine perilipin gene: The lipid droplet-associated perilipins derive from tissue-specific, mRNA splice variants and define a gene family of ancient origin. *Mamm. Gen.* **2001**, *12*, 741–749. [CrossRef]

52. Du, X.; Herrfurth, C.; Gottlieb, T.; Kawelke, S.; Feussner, K.; Rühling, H.; Feussner, I.; Maniak, M. Dictyostelium discoideum Dgat2 can substitute for the essential function of Dgat1 in triglyceride production but not in ether lipid synthesis. *Eukaryot. Cell* **2014**, *13*, 517–526. [CrossRef] [PubMed]

53. Xu, C.; Ng, T.W.D. Glycosylation-directed quality control of protein folding. *Nat. Rev. Mol. Cell Biol.* **2015**, *16*, 742–752. [CrossRef] [PubMed]

54. Kelleher, D.J.; Gilmore, R. An evolving view of the eukaryotic oligosaccharyltransferase. *Glycobiology* **2006**, *16*, 47R–62R. [CrossRef] [PubMed]

55. Braakman, I.; Hebert, D.N. Protein folding in the endoplasmic reticulum. *Cold Spring Harb. Perspect. Biol.* **2013**, *5*, a013201. [CrossRef] [PubMed]

56. Halperin, L.; Jung, J.; Michalak, M. The many functions of the endoplasmic reticulum chaperones and folding enzymes. *IUBMB Life* **2014**, *66*, 318–326. [CrossRef] [PubMed]

57. Gidalevitz, T.; Stevens, F.; Argon, Y. Orchestration of secretory protein folding by ER chaperones. *Biochim. Biophys. Acta Mol. Cell Res.* **2013**, *1833*, 2410–2424. [CrossRef] [PubMed]

58. Müller-Taubenberger, A.; Lupas, N.; Li, H.; Ecke, M.; Simmeth, E.; Gerisch, G. Calreticulin and calnexin in the endoplasmic reticulum are important for phagocytosis. *EMBO J.* **2001**, *20*, 6772–6782. [CrossRef] [PubMed]

59. Morita, T.; Saitoh, K.; Takagi, T.; Maeda, Y. Involvement of the glucose-regulated protein 94 (Dd-GRP94) in starvation response of Dictyostelium discoideum cells. *Biochem. Biophys. Res. Commun.* **2016**, *274*, 323–331. [CrossRef] [PubMed]

60. Braakman, I.; Bulleid, N.J. Protein Folding and Modification in the Mammalian Endoplasmic Reticulum. *Annu. Rev. Biochem.* **2011**, *80*, 71–99. [CrossRef] [PubMed]

61. Bulleid, N.J. Disulfide Bond Formation in the Mammalian Endoplasmic Reticulum. *Cold Spring Harb. Perspect. Biol.* **2012**, *4*, a013219. [CrossRef] [PubMed]

62. Monnat, J.; Hacker, U.; Geissler, H.; Rauchenberger, R.; Neuhaus, E.M.; Maniak, M.; Soldati, T. Dictyostelium discoideum protein disulfide isomerase, an endoplasmic reticulum resident enzyme lacking a KDEL-type retrieval signal. *FEBS Lett.* **1997**, *418*, 357–362. [CrossRef]

63. Monnat, J.; Neuhaus, E.M.; Pop, M.S.; Ferrari, D.M.; Kramer, B.; Soldati, T. Identification of a Novel Saturable Endoplasmic Reticulum Localization Mechanism Mediated by the C-Terminus of a *Dictyostelium* Protein Disulfide Isomerase. *Mol. Biol. Cell* **2000**, *11*, 3469–3484. [CrossRef] [PubMed]

64. Oslowski, C.M.; Urano, F. *Measuring ER Stress and the Unfolded Protein Response Using Mammalian Tissue Culture System*, 1st ed.; Elsevier Inc.: New York, NY, USA, 2011; Volume 490.

65. Bakthavatsalam, D.; Gomer, R.H. The secreted proteome profile of developing Dictyostelium discoideum cells. *Proteomics* **2010**, *10*, 2556–2559. [CrossRef] [PubMed]

66. Lam, T.Y.; Siu, C.-H. Inhibition of cell differentiation and cell cohesion by tunicamycin in Dictyostelium discoideum. *Dev. Biol.* **1982**, *92*, 398–407. [CrossRef]

67. Yamada, H.; Takatsuki, A.; Hirano, T.; Miyazaki, T.; Tamura, G. Effects of Tunicamycin on Cell Adhesion and Biosynthesis of of Glycoproteins in Aggregation-Competent Cells of Dictyostelium discoideum. *J Biochem.* **1982**, *92*, 399–406. [CrossRef] [PubMed]

68. Ochiai, H.; Stadler, J.; Westphal, M.; Wagle, G.; Merkl, R.; Gerisch, G. Monoclonal antibodies against contact sites A of Dictyostelium discoideum: Detection of modifications of the glycoprotein in tunicamycin-treated cells. *EMBO J.* **1982**, *1*, 1011–1016. [PubMed]

69. Hirano, T.; Yamada, H.; Miyazaki, T. Inhibition of cell adhesion in Dictyostelium discoideum by tunicamycin is prevented by leupeptin. *J. Biochem.* **1983**, *93*, 1249–1257. [CrossRef] [PubMed]

70. McDonald, C.J.; Sampson, J. The effects of inhibition of protein glycosylation on the aggregation of Dictyostelium discoideum. *J. Embryol. Exp. Morphol.* **1983**, *78*, 229–248. [PubMed]

71. Sadeghi, H.; Klein, C. Inhibition of N-linked glycosylation in Dictyostetium discoideum: Effects of aggregate formation. *Differentiation* **1988**, *38*, 99–103. [CrossRef] [PubMed]

72. Frank, L.C.-L.; Chen, G.; Nicole, W.A.; Shaulsky, G. Altered N-glycosylation modulates TgrB1/TgrC1-mediated development but not allorecognition in Dictyostelium. *J. Cell Sci.* **2015**, *128*, 3990–3996. [CrossRef]

73. Huber, R.J.; Myre, M.A.; Cotman, S.L. Aberrant adhesion impacts early development in a Dictyostelium model for juvenile neuronal ceroid lipofuscinosis. *Cell Adhes. Migr.* **2017**, *11*, 399–418. [CrossRef] [PubMed]

74. Browning, D.D.; O'Day, D.H. Concanavalin A and wheat germ agglutinin binding glycoproteins associated with cell fusion and zygote differentiation in Dictyostelium discoideum: Effects of calcium ions and tunicamycin on glycoprotein profiles. *Biochem. Cell Biol.* **1991**, *69*, 282–290. [CrossRef] [PubMed]

75. Kuwayama, H.; Ecke, M.; Gerisch, G.; VanHaastert, P.J.M. Protection against osmotic stress by cDGMP-mediated myosin phosphorylation. *Science* **1996**, *271*, 207–209. [CrossRef] [PubMed]

76. Serafimidis, I.; Bloomfield, G.; Skelton, J.; Ivens, A.; Kay, R.R. A new environmentally resistant cell type from Dictyostelium. *Microbiology* **2007**, *153*, 619–630. [CrossRef] [PubMed]

77. Travers, K.J.; Patil, C.K.; Wodicka, L.; Lockhart, D.J.; Weissman, J.S.; Walter, P. Functional and genomic analyses reveal an essential coordination between the unfolded protein response and ER-associated degradation. *Cell* **2000**, *101*, 249–258. [CrossRef]

78. Hollien, J.; Weissman, J.S. Decay of Endoplasmic Reticulum-Localized mRNAs During the Unfolded Protein Response. *Science* **2006**, *313*, 104–107. [CrossRef] [PubMed]

79. Hollien, J.; Lin, J.H.; Li, H.; Stevens, N.; Walter, P.; Weissman, J.S. Regulated Ire1-dependent decay of messenger RNAs in mammalian cells. *J. Cell Biol.* **2009**, *186*, 323–331. [CrossRef] [PubMed]

80. Lee, K.P.K.; Dey, M.; Neculai, D.; Cao, C.; Dever, T.E.; Sicheri, F. Structure of the Dual Enzyme Ire1 Reveals the Basis for Catalysis and Regulation in Nonconventional RNA Splicing. *Cell* **2008**, *132*, 89–100. [CrossRef] [PubMed]

81. Shamu, C.; Cox, J.; Walter, P. The unfolded-protein-response pathway in yeast. *Trends Cell Biol.* **1994**, *4*, 56–60. [CrossRef]

82. Bertolotti, A.; Wang, X.Z.; Novoa, I.; Jungreis, R.; Schlessinger, K.; Cho, J.H.; West, A.B.; Ron, D. Increased sensitivity to dextran sodium sulfate colitis in IRE1β-deficient mice. *J. Clin. Investig.* **2001**, *107*, 585–593. [CrossRef] [PubMed]

83. Martino, M.B.; Jones, L.; Brighton, B.; Ehre, C.; Abdulah, L.; Davis, C.W.; Ron, D.; O'Neal, W.K.; Ribeiro, C.M.P. The ER stress transducer IRE1β is required for airway epithelial mucin production. *Mucosal Immunol.* **2013**, *6*, 639–654. [CrossRef] [PubMed]

84. Fanata, W.I.D.; Lee, S.Y.; Lee, K.O. The unfolded protein response in plants: A fundamental adaptive cellular response to internal and external stresses. *Proteomics. J.* **2013**, *93*, 356–368. [CrossRef] [PubMed]

85. Okamura, K.; Kimata, Y.; Higashio, H.; Tsuru, A.; Kohno, K. Dissociation of Kar2p/BiP from an ER Sensory Molecule, Ire1p, Triggers the Unfolded Protein Response in Yeast. *Biochem. Biophys. Res. Commun.* **2000**, *279*, 445–450. [CrossRef] [PubMed]

86. Kimata, Y.; Ishiwata-Kimata, Y.; Ito, T.; Hirata, A.; Suzuki, T.; Oikawa, D.; Takeuchi, M.; Kohno, K. Two regulatory steps of ER-stress sensor Ire1 involving its cluster formation and interaction with unfolded proteins. *J. Cell Biol.* **2007**, *179*, 75–86. [CrossRef] [PubMed]

87. Gardner, B.M.; Walter, P. Unfolded proteins are Ire1-activating ligands that directly induce the unfolded protein response. *Science* **2011**, *333*, 1891–1894. [CrossRef] [PubMed]

88. Bowring, C.E.; Llewellyn, D.H. Differences in HAC1 mRNA processing and translation between yeast and mammalian cells indicate divergence of the eukaryotic ER stress response. *Biochem. Biophys. Res. Commun.* **2001**, *287*, 789–800. [CrossRef] [PubMed]

89. Hooks, K.B.; Griffiths-Jones, S. Conserved RNA structures in the non-canonical Hac1/Xbp1 intron. *RNA Biol.* **2011**, *8*, 552–556. [CrossRef] [PubMed]

90. Wu, H.; Ng, B.S.H.; Thibault, G. Endoplasmic reticulum stress response in yeast and humans. *Biosci. Rep.* **2014**, *34*, 321–330. [CrossRef] [PubMed]

91. Kimmig, P.; Diaz, M.; Zheng, J.; Williams, C.C.; Lang, A.; Aragón, T.; Li, H.; Walter, P. The unfolded protein response in fission yeast modulates stability of select mRNAs to maintain protein homeostasis. *Elife* **2012**, *1*, e00048. [CrossRef] [PubMed]

92. Tirasophon, W.; Lee, K.; Callaghan, B.; Welihinda, A.; Kaufman, R.J. The endoribonuclease activity of mammalian IRE1 autoregulates its mRNA and is required for the unfolded protein response. *Genes Dev.* **2000**, *14*, 2725–2736. [CrossRef] [PubMed]

93. Rubio, C.; Pincus, D.; Korennykh, A.; Schuck, S.; El-Samad, H.; Walter, P. Homeostatic adaptation to endoplasmic reticulum stress depends on Ire1 kinase activity. *J. Cell Biol.* **2011**, *193*, 171–184. [CrossRef] [PubMed]

94. van Anken, E.; Pincus, D.; Coyle, S.; Aragón, T.; Osman, C.; Lari, F.; Gómez Puerta, S.; Korennykh, A.V.; Walter, P. Specificity in endoplasmic reticulum-stress signaling in yeast entails a step-wise engagement of *HAC1* mRNA to clusters of the stress sensor Ire1. *Elife* **2014**, *3*, 1–17. [CrossRef] [PubMed]

95. Aragón, T.; van Anken, E.; Pincus, D.; Serafimova, I.M.; Korennykh, A.V.; Rubio, C.A.; Walter, P. Messenger RNA targeting to endoplasmic reticulum stress signalling sites. *Nature* **2009**, *457*, 736–740. [CrossRef] [PubMed]

96. Coelho, D.S.; Cairrão, F.; Zeng, X.; Pires, E.; Coelho, A.V.; Ron, D.; Ryoo, H.D.; Domingos, P.M. Xbp1-Independent Ire1 Signaling Is Required for Photoreceptor Differentiation and Rhabdomere Morphogenesis in Drosophila. *Cell Rep.* **2013**, *5*, 791–801. [CrossRef] [PubMed]

97. Chen, Y.; Brandizzi, F. IRE1: ER stress sensor and cell fate executor. *Trends Cell Biol.* **2013**, *23*, 547–555. [CrossRef] [PubMed]

98. Miyazaki, T.; Nakayama, H.; Nagayoshi, Y.; Kakeya, H.; Kohno, S. Dissection of Ire1 functions reveals stress response mechanisms uniquely evolved in Candida glabrata. *PLoS Pathog.* **2013**, *9*, e1003160. [CrossRef] [PubMed]

99. Liu, J.-X.; Srivastava, R.; Che, P.; Howell, S.H. An endoplasmic reticulum stress response in Arabidopsis is mediated by proteolytic processing and nuclear relocation of a membrane-associated transcription factor, bZIP28. *Plant Cell* **2007**, *19*, 4111–4119. [CrossRef] [PubMed]

100. Che, P.; Bussell, J.D.; Zhou, W.; Estavillo, G.M.; Pogson, B.J.; Smith, S.M. Signaling from the endoplasmic reticulum activates brassinosteroid signaling and promotes acclimation to stress in Arabidopsis. *Sci. Signal.* **2010**, *3*, ra69. [CrossRef] [PubMed]

101. Chen, X.; Shen, J.; Prywes, R. The luminal domain of ATF6 senses endoplasmic reticulum (ER) stress and causes translocation of ATF6 from the er to the Golgi. *J. Biol. Chem.* **2002**, *277*, 13045–13052. [CrossRef] [PubMed]

102. Yamamoto, K.; Yoshida, H.; Kokame, K.; Kaufman, R.J.; Mori, K. Differential contributions of ATF6 and XBP1 to the activation of endoplasmic reticulum stress-responsive cis-acting elements ERSE, UPRE and ERSE-II. *J. Biochem.* **2004**, *136*, 343–350. [CrossRef] [PubMed]

103. Okada, T.; Yoshida, H.; Akazawa, R.; Negishi, M.; Mori, K. Distinct roles of activating transcription factor 6 (ATF6) and double-stranded RNA-activated protein kinase-like endoplasmic reticulum kinase (PERK) in transcription during the mammalian unfolded protein response. *Biochem. J.* **2002**, *366 Pt 2*, 585–594. [CrossRef] [PubMed]

104. Druelle, C.; Drullion, C.; Deslé, J.; Martin, N.; Saas, L.; Cormenier, J.; Malaquin, N.; Huot, L.; Slomianny, C.; Bouali, F.; et al. ATF6α regulates morphological changes associated with senescence in human fibroblasts. *Oncotarget* **2016**, *7*, 67699–67715. [CrossRef] [PubMed]

105. Skorczyk-Werner, A.; Chiang, W.C.; Wawrocka, A.; Wicher, K.; Jarmuz-Szymczak, M.; Kostrzewska-Poczekaj, M.; Jamsheer, A.; Płoski, R.; Rydzanicz, M.; Pojda-Wilczek, D.; et al. Autosomal recessive cone-rod dystrophy can be caused by mutations in the ATF6 gene. *Eur. J. Hum. Genet.* **2017**, *25*, 1210–1216. [CrossRef] [PubMed]

106. Chiang, W.-C.; Chan, P.; Wissinger, B.; Vincent, A.; Skorczyk-Werner, A.; Krawczyński, M.R.; Kaufman, R.J.; Tsang, S.H.; Héon, E.; Kohl, S.; et al. Achromatopsia mutations target sequential steps of ATF6 activation. *Proc. Natl. Acad. Sci. USA* **2017**, *114*, 400–405. [CrossRef] [PubMed]

107. Marciniak, S.J.; Garcia-Bonilla, L.; Hu, J.; Harding, H.P.; Ron, D. Activation-dependent substrate recruitment by the eukaryotic translation initiation factor 2 kinase PERK. *J. Cell Biol.* **2006**, *172*, 201–209. [CrossRef] [PubMed]

108. Jindrich, K.; Degnan, B.M. The diversification of the basic leucine zipper family in eukaryotes correlates with the evolution of multicellularity Genome evolution and evolutionary systems biology. *BMC EBiol.* **2016**, *16*, 1–12.

109. Nagashima, Y.; Mishiba, K.; Suzuki, E.; Shimada, Y.; Iwata, Y.; Koizumi, N. Arabidopsis IRE1 catalyses unconventional splicing of bZIP60 mRNA to produce the active transcription factor. *Sci. Rep.* **2011**, *1*, 29. [CrossRef] [PubMed]

110. Ruggiano, A.; Foresti, O.; Carvalho, P. ER-associated degradation: Protein quality control and beyond. *J. Cell Biol.* **2014**, *204*, 869–879. [CrossRef] [PubMed]

111. Tsai, B.; Ye, Y.; Rapoport, T.A. Retro-translocation of proteins from the endoplasmic reticulum into the cytosol. *Nat. Rev. Mol. Cell Biol.* **2002**, *3*, 246–255. [CrossRef] [PubMed]

112. Klionsky, D.J.; Emr, S.D. Autophagy as a regulated pathway of cellular degradation. *Science* **2000**, *290*, 1717–1721. [CrossRef] [PubMed]

113. Walter, P.; Ron, D. The unfolded protein response: From stress pathway to homeostatic regulation. *Science* **2011**, *334*, 1081–1086. [CrossRef] [PubMed]

114. Urano, F.; Wang, X.-Z.; Bertolotti, A.; Zhang, Y.; Chung, P.; Harding, H.P.; Ron, D. Coupling of Stress in the Endoplasmic Reticulum to Activation of JNK Protein Kinases by Transmembrane Protein Kinase IRE1. *Science* **2000**, *287*, 664–666. [CrossRef] [PubMed]

115. Ogata, M.; Hino, S.; Saito, A.; Morikawa, K.; Kondo, S.; Kanemoto, S.; Murakami, T.; Taniguchi, M.; Tanii, I.; Yoshinaga, K.; et al. Autophagy is activated for cell survival after endoplasmic reticulum stress. *Mol. Cell. Biol.* **2006**, *26*, 9220–9231. [CrossRef] [PubMed]

116. Liu, Y.; Burgos, J.S.; Deng, Y.; Srivastava, R.; Howell, S.H.; Bassham, D.C. Degradation of the endoplasmic reticulum by autophagy during endoplasmic reticulum stress in Arabidopsis. *Plant Cell* **2012**, *24*, 4635–4651. [CrossRef] [PubMed]

117. Goldberg, J.M.; Manning, G.; Liu, A.; Fey, P.; Pilcher, K.E.; Xu, Y.; Smith, J.L. The dictyostelium kinome—Analysis of the protein kinases from a simple model organism. *PLoS Genet.* **2006**, *2*, e38. [CrossRef] [PubMed]

118. Caffrey, D.R.; O'Neill, L.A.; Shields, D.C. The evolution of the MAP kinase pathways: Coduplication of interacting proteins leads to new signaling cascades. *J. Mol. Evol.* **1999**, *49*, 567–582. [CrossRef] [PubMed]

119. Giusti, C.; Tresse, E.; Luciani, M.F.; Golstein, P. Autophagic cell death: Analysis in Dictyostelium. *Biochim. Biophys. Acta Mol. Cell Res.* **2009**, *1793*, 1422–1431. [CrossRef] [PubMed]

120. Kroemer, G.; Galluzzi, L.; Vandenabeele, P.; Abrams, J.; Alnemri, E.S.; Baehrecke, E.H.; Blagosklonny, M.V.; El-Deiry, W.S.; Golstein, P.; Green, D.R.; et al. Classification of cell death: Recommendations of the Nomenclature Committee on Cell Death 2009. *Cell Death Differ.* **2009**, *16*, 3–11. [CrossRef] [PubMed]

121. Baehrecke, E.H. Autophagic programmed cell death in Drosophila. *Cell Death Differ.* **2003**, *10*, 940–945. [CrossRef] [PubMed]

122. Hofius, D.; Schultz-Larsen, T.; Joensen, J.; Tsitsigiannis, D.I.; Petersen, N.H.T.; Mattsson, O.; Jørgensen, L. B.; Jones, J.D.G.; Mundy, J.; Petersen, M. Autophagic Components Contribute to Hypersensitive Cell Death in Arabidopsis. *Cell* **2009**, *137*, 773–783. [CrossRef] [PubMed]

123. Liu, Y.; Levine, B. Autosis and autophagic cell death: The dark side of autophagy. *Cell Death and Differentiation* **2015**, *22*, 367–376. [CrossRef] [PubMed]

124. Whittingham, W.F.; Raper, K.B. Non-Viability of Stalk Cells in Dictyostelium. *Proc. Natl. Acad. Sci. USA* **1960**, *46*, 642–649. [CrossRef] [PubMed]

125. Levraud, J.-P.; Adam, M.; Luciani, M.-F.; de Chastellier, C.; Blanton, R.L.; Golstein, P. Dictyostelium cell death: Early emergence and demise of highly polarized paddle cells. *J. Cell Biol.* **2003**, *160*, 1105–1114. [CrossRef] [PubMed]

126. Lam, D.; Golstein, P. A specific pathway inducing autophagic cell death is marked by an IP3R mutation. *Autophagy* **2008**, *8627*, 349–350. [CrossRef]

127. Wolf, D.H.; Stolz, A. The Cdc48 machine in endoplasmic reticulum associated protein degradation. *Biochim. Biophys. Acta Mol. Cell Res.* **2012**, *1823*, 117–124. [CrossRef] [PubMed]

128. Müller-Taubenberger, A. Application of fluorescent protein tags as reporters in live-cell imaging studies. *Meth. Mol. Biol.* **2006**, *346*, 229–246.
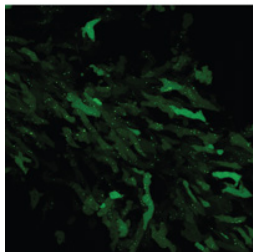
Autophagy in Dictyostelium: Mechanisms, regulation and disease in a simple biomedical model

Ana Mesquita, Elena Cardenal-Muñoz, Eunice Dominguez, Sandra Muñoz-Braceras, Beatriz Nuñez-Corcuera, Ben A. Phillips, Luis C. Tábara, Qiuhong Xiong, Roberto Coria, Ludwig Eichinger, Pierre Golstein, Jason S. King, Thierry Soldati, Olivier Vincent & Ricardo Escalante

View supplementary material ⧉	Published online: 07 Oct 2016.
Submit your article to this journal ⧉	Article views: 322
View related articles ⧉	View Crossmark data ⧉

Taylor & Francis
Taylor & Francis Group

REVIEW

Autophagy in *Dictyostelium*: Mechanisms, regulation and disease in a simple biomedical model

Ana Mesquita[a,b], Elena Cardenal-Muñoz[c], Eunice Dominguez[a,d], Sandra Muñoz-Braceras[a], Beatriz Nuñez-Corcuera[a], Ben A. Phillips[e], Luis C. Tábara[a], Qiuhong Xiong[f], Roberto Coria[d], Ludwig Eichinger[f], Pierre Golstein[g], Jason S. King[e], Thierry Soldati[c], Olivier Vincent[a], and Ricardo Escalante[a]

[a]Instituto de Investigaciones Biomédicas "Alberto Sols" (CSIC-UAM), Madrid, Spain; [b]University of Cincinnati College of Medicine, Cincinnati, OH, USA; [c]Départment de Biochimie, Faculté des Sciences, Université de Genève, Switzerland; [d]Departamento de Genética Molecular, Instituto de Fisiología Celular, Universidad Nacional Autónoma de México, Mexico City, México; [e]Department of Biomedical Sciences, University of Sheffield, UK; [f]Center for Biochemistry, Medical Faculty, University of Cologne, Cologne, Germany; [g]Centre d'Immunologie de Marseille-Luminy, Aix Marseille Université UM2, Inserm, U1104, CNRS UMR7280, Marseille, France

ABSTRACT

Autophagy is a fast-moving field with an enormous impact on human health and disease. Understanding the complexity of the mechanism and regulation of this process often benefits from the use of simple experimental models such as the social amoeba *Dictyostelium discoideum*. Since the publication of the first review describing the potential of *D. discoideum* in autophagy, significant advances have been made that demonstrate both the experimental advantages and interest in using this model. Since our previous review, research in *D. discoideum* has shed light on the mechanisms that regulate autophagosome formation and contributed significantly to the study of autophagy-related pathologies. Here, we review these advances, as well as the current techniques to monitor autophagy in *D. discoideum*. The comprehensive bioinformatics search of autophagic proteins that was a substantial part of the previous review has not been revisited here except for those aspects that challenged previous predictions such as the composition of the Atg1 complex. In recent years our understanding of, and ability to investigate, autophagy in *D. discoideum* has evolved significantly and will surely enable and accelerate future research using this model.

Introducing D. discoideum, *a simple model for autophagy with striking similarities to animal cells*

Dictyostelium discoideum is a protist that belongs to the Amoebozoa, a sister group of animals and fungi. They are known as social amoebae since the motile cells are able to aggregate and form a simple multicellular organism. Under starvation, groups of approximately 100,000 cells form a mound that goes through different stages of development to give rise to a fruiting body, in which vacuolated dead cells form a stalk that supports the spores (Fig. 1). Vegetative *D. discoideum* cells are more similar to animal cells than fungi or plant cells in many respects. For example, they lack rigid cell walls that might restrict movement, allowing the cells to perform typical animal-like processes such as phagocytosis, macropinocytosis, pseudopod-based cell motility and chemotaxis. The parallels with animal cells extends to the evolutionary conservation of many genes that have been lost during fungal evolution.[1]

The similarity to animal cells makes *D. discoideum* a suitable model to address the study of genes or processes relevant to human disease. These include the study of pathogen infections,[2] cell motility-related pathologies,[3] mitochondrial diseases,[4] the study of the mechanism of action of certain drugs,[5] cancer,[6] neurodegenerative disorders[7] and lysosomal-related disorders[8] among others. *D. discoideum* also provides useful ways to study the mechanisms and the physiological roles of autophagy.[9] As in in other organisms, autophagy is required for *D. discoideum* to survive starvation, for the turnover of proteins, to remove protein aggregates and is also fundamental during infection by intracellular pathogens. The first description of autophagic vacuoles in *D. discoideum* (defined at that time simply as "bodies containing partially degraded cytoplasmic material") comes from transmission electron microscopy (TEM) studies of germinating spores in 1969,[10] shortly after Christian de Duve coined the term autophagy.[11] We have come a long way from these initial morphological observations and now begin to understand the significance and the mechanisms of this crucial cellular process in the context of a whole organism.

During starvation, autophagy is responsible for the liberation of nutrients to maintain viability. Therefore, defects in autophagy drastically reduce the ability of cells to survive prolonged periods of nutrient deprivation. Typically, wild-type
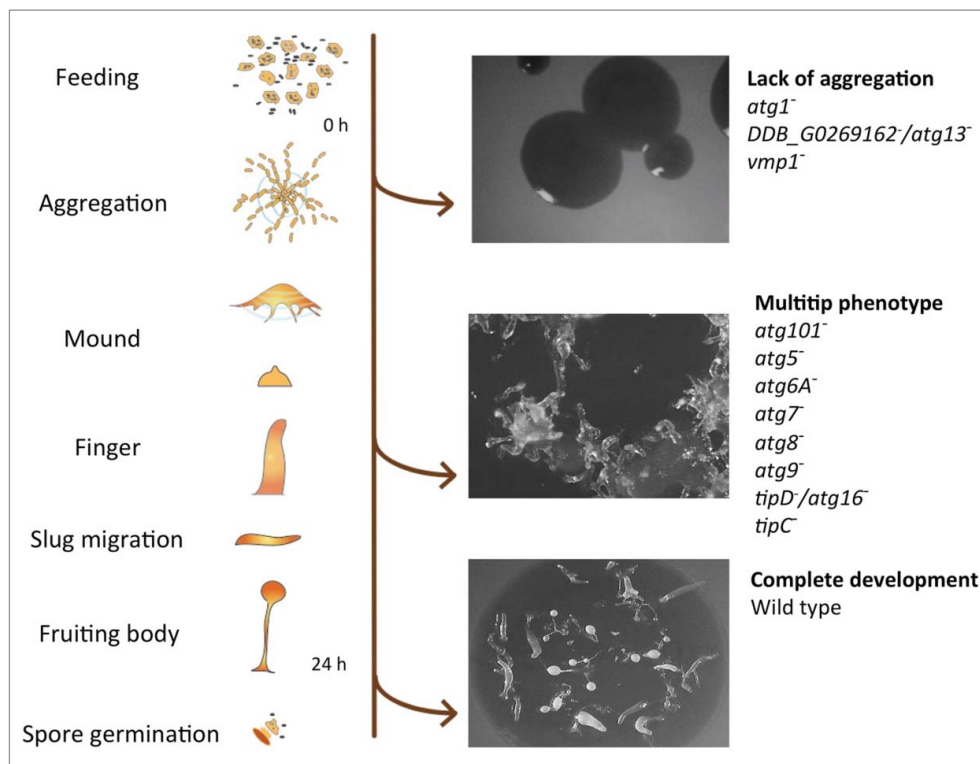

Figure 1. *D. discoideum's* life cycle and representative phenotypes associated with the lack of autophagy. Mutant strains have been described for the genes depicted at the right side (see details in the main text). The pictures correspond from top to bottom to the strains *DDB_G0269162⁻/atg13⁻*, *tipC⁻* and wild-type AX4.

D. discoideum cells survive for more than 10 d under amino acid starvation, whereas autophagy-deficient mutants start losing viability after just 24 h.[12,13] During starvation, autophagy is also responsible for a reduction in both cell volume and total protein.[12,13] The *D. discoideum* developmental program takes place in the absence of nutrients; therefore, the intracellular degradation and recycling of the cell's own material by autophagy becomes essential as a source of energy and simple metabolites required for the biosynthetic pathways taking place during development. Thus, it is not surprising that autophagic dysfunction leads to abnormal development, which facilitates the identification of autophagy mutants in the laboratory. The severity of the phenotype ranges from complete lack of aggregation to the formation of multi-tipped mounds, which are unable to form normal stalks and viable spores (Fig. 1).[13] It is unclear how much of the defects in development are simply the result of imbalanced nutrient homeostasis or whether more specific signaling events are involved. However, the signaling peptide SDF-2 (spore differentiation factor 2) is essential for spore formation, and its precursor protein, AcbA, is secreted by an unconventional mechanism that requires autophagy.[14] Moreover, terminal stalk differentiation also seems to require autophagy for the formation of the vacuoles that accompany stalk cell differentiation.[15] Nonrecyling roles for autophagy are therefore important for the terminal differentiation of both spores and stalk cells.

Three forms of autophagy have been described that differ in the mechanism by which the cargo is delivered to the lysosome. Chaperone-mediated autophagy,[16] microautophagy,[17] and macroautophagy. Macroautophagy (denoted here as autophagy for simplicity) is the best known, the most conserved autophagic pathway and the only one described in *D. discoideum* so far.

Although autophagy was initially thought to simply be a mechanism to recycle nutrients by nonselective self-degradation (so called bulk autophagy), the enormous importance of selective autophagy is now becoming clear. The selective process is devoted to the specific degradation of abnormal protein aggregates (aggrephagy), organelles (mitophagy, pexophagy, ribophagy, reticulophagy, nucleophagy) or pathogens (xenophagy). Impaired selective autophagy is therefore thought to underlie the etiology of numerous diseases.[18]

The hallmark of autophagy is the formation of intracellular double-membrane vesicles (autophagosomes), which eventually fuse with lysosomes, leading to degradation of the cargo and the inner membrane. The basic molecular machinery that controls autophagy was initially discovered in *Saccharomyces cerevisiae*, in which the proteins involved were named Atg, for autophagy-related. These proteins form different complexes that are required for the induction, elongation and completion of the autophagic process. This has been extensively reviewed in the past few years.[19-21] Most of these proteins and complexes can be recognized in *D. discoideum* by sequence homology as summarized in Fig. 2. A more detailed description of the putative *D. discoideum* Atg protein homologs was included in a previous review.[9] The generation and analysis of a number of mutants from each complex have subsequently confirmed the functional conservation of the autophagic machinery in *D. discoideum* (the available mutants and their phenotypes are depicted in Fig. 1). Lack of aggregation is the phenotype observed for *atg1⁻*,[22] *DDB_G0269162⁻/atg13⁻*,[23] and *vmp1⁻*.[24] Formation of multiple tips in mounds is the phenotype observed in *atg101⁻*,[23] *atg5⁻*,[13] *atg6A⁻*,[22] *atg7⁻*,[13] *atg8⁻*,[22] *atg9⁻*,[25] *tipD⁻/atg16⁻*[26-28] and *tipC⁻*.[27] Importantly, additional non-Atg proteins have been found to be involved in
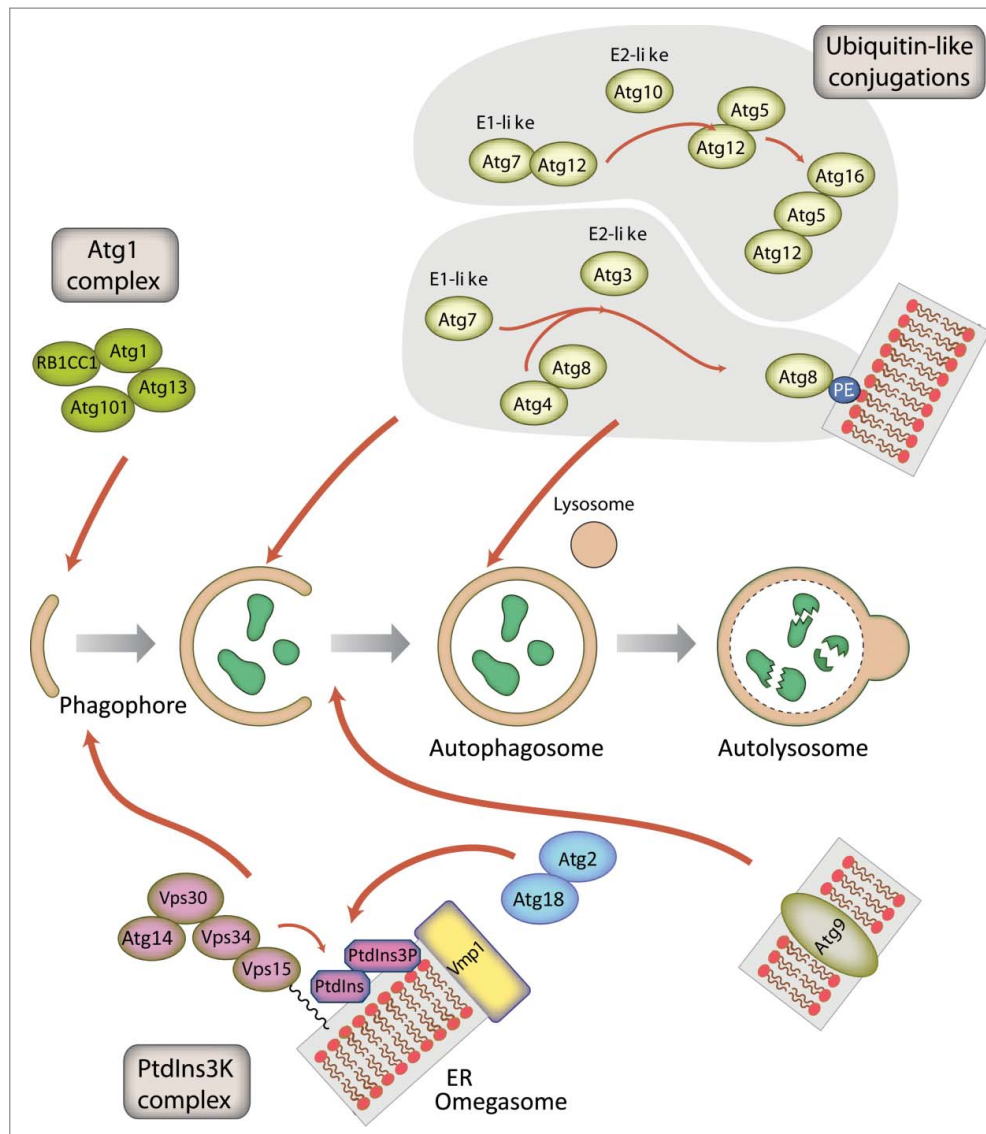
Figure 2. Schematic representation of autophagosome formation and the proteins involved in *D. discoideum*. The autophagic proteins were identified by sequence homology with those described in yeast and mammalian cells. The predicted complexes have been organized using the information available from the yeast *S. cerevisiae*, mammalian cells and *D. discoideum*. The inductive stage depends on the serine/threonine Atg1 kinase complex and the class III PtdIns3K complex. The latter complex generates the signaling lipid PtdIns3P, which is essential for the recruitment of Atg18 and Atg2. The elongation of the phagophore membrane requires 2 ubiquitin-like (Ubl) conjugation systems (upper right). In the first conjugation reaction Atg12 is covalently bound to Atg5. Atg12–Atg5 interacts with Atg16 and localizes to the phagophore membrane, from which it regulates the second conjugation reaction that attaches the protein Atg8 (known as LC3 in mammals) to phosphatidylethanolamine (PE) of the expanding phagophore membrane. Atg8 initially localizes to both sides of the phagophore and remains inside the completed autophagosome until fusion with the lysosome occurs; Atg8 on the cytosolic side of the autophagosome is cleaved from PE by Atg4 and recycled, whereas Atg8–PE of the lumenal leaflet of the bilayer is degraded. Atg9-containing vesicles supply membrane for phagophore expansion. Recent advances have clarified the composition of the Atg1 complex and the role of Vmp1 as a key protein in the origin of the autophagosomes from the ER.

Dictyostelium autophagy such as the ER transmembrane protein Vmp1 (vacuole membrane protein 1), which demonstrates the usefulness of *Dictyostelium* as an alternative simple genetic system to study autophagy.

Methods and tools to study autophagy in D. discoideum

Over recent years the number of tools available to study autophagy in *D. discoideum* has expanded greatly. TEM remains the gold standard for identifying the double-membrane autophagic structures, but it is difficult and time-consuming to obtain quantitative data. In particular, as each *D. discoideum* cell only contains approximately 5 autophagosomes under conditions of amino acid starvation,[29] very few are present in each of the thin sections required for TEM.[13] However, with recent advances in 3D electron microscopy it should now be possible to reconstruct complete amoeba, although quantification of autophagosomes has yet to be demonstrated. In contrast, light microscopy has been extensively used, allowing rapid quantification of large numbers of cells, and dynamic information to be captured.

It is often experimentally desirable to induce autophagy in a defined manner. Typically in mammalian cell cultures autophagy is induced using either starvation e.g. Hank's balanced salt solution or drug treatment, e.g., rapamycin, which inhibits MTORC1 (mechanistic target of rapamycin [serine/threonine

kinase] complex 1) function. In *D. discoideum*, complete starvation can be induced using non-nutrient buffers but this initiates development, complicating interpretation. To avoid this, it is preferable to use a defined medium such as SIH medium lacking arginine and lysine (available from ForMedium for use in SILAC). Within 5 min this gives a comparable induction of autophagy to complete starvation, without cells entering development.[29] Although *D. discoideum* has a functional rapamycin-sensitive TORC1 complex,[30] short-term rapamycin treatment is unable to activate autophagy.

Several markers have been used to study autophagy in *D. discoideum*. In mammalian systems the most commonly used markers are MAP1LC3/LC3 (microtubule associated protein 1 light chain 3) family proteins, the ubiquitin-like (Ubl) orthologs of yeast Atg8 that associate with autophagic entities from initiation until recycling.[31] *D. discoideum* possess 2 Atg8 paralogs (Atg8a and b), which are both good markers of autophagosomes although they play partially nonredundant roles (discussed below).[32] Another useful marker is Atg18, the ortholog of mammalian WIPI2. Atg18 localizes to omegasome-anchored phagophores (the precursors to autophagosomes) at initiation events but, in contrast to Atg8, dissociates immediately after autophagosome formation is completed.[29,33,34] Atg18 is therefore specific for the formation of new autophagosomes.

Immunolabeling of endogenous autophagy proteins allows a variety of markers to be observed, and several good antibodies against *D. discoideum* Atg8 have been generated.[32,35] While these antibodies are useful for many experiments, fixed samples lack dynamic information. It is therefore often useful to perform live-cell imaging and track markers in real-time to dissect the different phases of autophagosome formation. GFP-Atg8 fusions permit visualization from initiation through expansion, closure and fusion with the lysosome, whereupon the GFP fluorescence becomes quenched. Movement in the Z-axis, however, makes following individual autophagosomes over time challenging. To reduce this problem, sheets of agarose can be placed upon the cells to compress them, reducing cell height and improving image quality. This approach allows individual autophagosomes to be followed from an initial punctum, to a cup and then a complete circular autophagosome (Fig. 3 and Movie S1). The timing of each phase can be quantified from such movies, as well as the time it takes for the GFP fluorescence to be quenched, giving an indirect combined measure of acidification and proteolysis. This is a powerful method to directly quantify autophagosome dynamics, but does not represent basal autophagy levels, as the compression itself potently induces autophagosome initiation.[29]

An additional way to differentiate autolysosomes (the product of autophagosomes fusing with lysosomes) is by fusing Atg8 to both GFP and RFP in tandem.[36] As RFP is less sensitive to quenching by low pH, only the red signal can be observed in mammalian autolysosomes, whereas phagophores and autophagosomes emit both green and red fluorescence. Unfortunately, *D. discoideum* lysosomes have a much lower pH than their mammalian counterparts (3.5 compared to 4.5-5.0), which is sufficient to quench both GFP and RFP. Treatment with lysosomotropic agents such as ammonium chloride (NH_4Cl), however, can be used to partially elevate lysosomal pH, and reveal autolysosomes, with the caveat that this
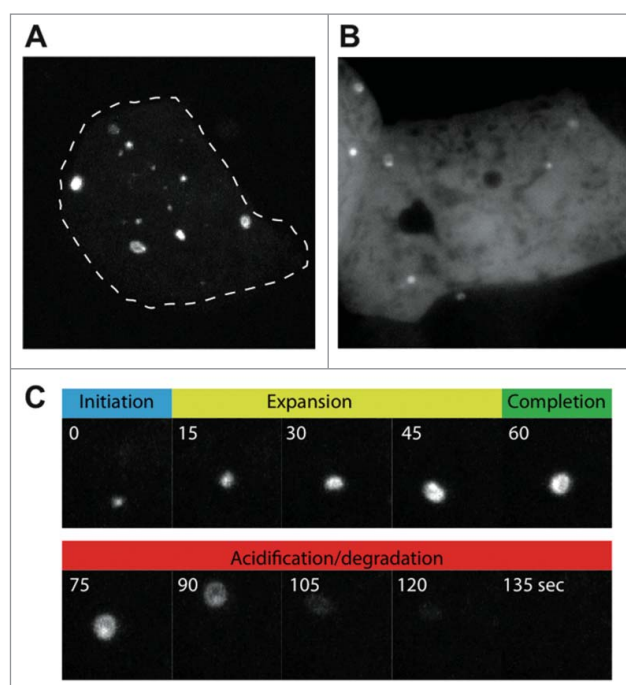

Figure 3. Live-cell imaging of autophagosome formation in *D. discoideum*, using (A) GFP-Atg8a, and (B) GFP-Atg18. Images were obtained under compression to improve clarity, and to allow individual autophagosomes to be followed over time. (C) Shows the different stages of autophagosome formation from the cell in (A) marked by GFP-Atg8a. The autophagosome shown in (C) has been marked by an arrow in Movie S1.

treatment itself will induce autophagy and lead to osmotically distended compartments with dilute content.[37,38]

Autophagic flux refers to the net amount of material that is captured and degraded by this pathway over time. This is an important but complex and dynamic measurement and is not a simple reflection of the number of autophagosomes. Currently, the best method to measure flux is based on observing the autophagic cleavage of GFP from its fusion with cytosolic proteins.[38] Although GFP fluorescence is rapidly quenched within acidic lysosomes, the GFP protein itself is relatively resistant to lysosomal proteolysis. When GFP is fused to cytosolic proteins, captured and delivered to lysosomes by autophagy, GFP fragments accumulate while the rest of the fusion protein is degraded.[39] GFP cleavage fragments can therefore be quantified by western blot analysis of whole cell lysates probed with anti-GFP antibodies. As *D. discoideum* are professional phagocytes, they possess an extremely efficient proteolytic machinery and free GFP is barely detectable due to rapid degradation. Therefore NH_4Cl treatment is again required to inhibit proteolysis sufficiently for cleaved GFP fragments to accumulate.[37,38] Band intensities for GFP-marker and free-GFP can then be quantified to give a measure of autophagic flux. It is again important to note that the concentrations of NH_4Cl required are very high (0.2-0.3 M), and likely to induce autophagy themselves. Nonetheless, this system provides a good measure of maximum autophagic capacity, and is useful to demonstrate gross effects of mutations on the pathway.[37,38]

The array of techniques available, coupled with orthologs of most mammalian autophagy genes, makes *D. discoideum* a robust model for the study of autophagy. While a system for studying autophagic flux in noninduced conditions is yet to be

established, significant progress has been made and *D. discoideum* provides many useful means in which to study this pathway.

Phagophore nucleation: The Atg1 complex in D. discoideum *is closely related to the mammalian ULK1 complex*

The Atg1/ULK1 protein kinase complex works at the initiation step in both selective and nonselective autophagy.[40] In mammals, ULK1 phosphorylates BECN1 to activate the PIK3C3/VPS34 lipid kinase,[41] and phosphorylation of the transmembrane protein Atg9 by its budding yeast homolog Atg1 plays a key role in the recruitment of Atg18 and Atg8 to the phagophore assembly site (PAS).[42] Initial studies of nonselective autophagy in yeast identified the different components of the Atg1 complex: the Atg1 protein kinase itself, the regulatory subunit Atg13 and the Atg17-Atg31-Atg29 scaffolding subcomplex.[43] Selective autophagy processes, such as the cytoplasm-to-vacuole targeting (Cvt) pathway, involve a different scaffold protein, Atg11 (Fig. 4). Although not absolutely required in nonselective autophagy, Atg11 interacts with Atg29[44] and, thus, it is still unclear whether Atg11 and the Atg17-Atg31-Atg29 subcomplex form mutually exclusive complexes with Atg1. Dephosphorylation of the TOR kinase substrate Atg13 upon nutrient starvation promotes Atg1 complex assembly in nonselective autophagy.[45] In contrast, under nutrient-rich conditions, selective autophagy receptor-bound targets activate Atg1 via the scaffold protein Atg11.[46] Autophagy receptors have been identified in mitophagy (Atg32), pexophagy (Atg36), nucleophagy (Atg39), reticulophagy (Atg40) and the Cvt pathway (Atg19 and Atg34).[47]

The ULK1 protein complex in mammals differs from the budding yeast Atg1 complex in several aspects. This complex consists of the ULK1 protein kinase and 3 proteins, ATG13, ATG101 and the scaffold protein RB1CC1/FIP200 (Fig. 4). ATG101, which is absent in budding yeast, binds to and stabilizes Atg13.[48,49] The crystal structure of the Atg13-Atg101 complex revealed that the HORMA domains present in these 2 proteins heterodimerize.[50,51] In budding yeast, Atg13 contains a 3-strand β-sheet insertion in the HORMA domain that stabilizes this protein in the absence of ATG101. The scaffold protein RB1CC1 is the functional counterpart of both Atg17 and Atg11 in yeast, and results from phylogenetic analysis suggest that Atg17 arose via gene duplication of Atg11 and loss of the C-terminal region.[52] This gene duplication event and functional specialization appears to be essentially restricted to fungi. In mammals, the HTT (huntingtin) protein also shares structural similarity to yeast Atg11 and, like RB1CC1, functions as a scaffold protein in the ULK1 complex.[53]

The Atg1 complex in *D. discoideum* is evolutionarily closer to the mammalian ULK1 complex than its budding yeast counterpart. In addition to the Atg1 protein kinase,[54] Atg13 and Atg101 homologs have been identified[23] and interaction studies have shown that Atg13, like its mammalian homolog, binds to both Atg1 and Atg101 (Fig. 4). The likely RB1CC1/Atg11 homolog in *D. discoideum* is DDB_G0285767.[52] A putative Atg17 homolog has also been reported but functional studies argue against a role in autophagy,[23] thus supporting the idea that Atg17 proteins are restricted to fungi. Similarities between mammals and *D. discoideum* are not limited to the core components of the complex, as shown by the conservation of the mammalian selective autophagy receptor and Atg8-binding protein Sqstm1/p62 in *D. discoideum*.[23,55] Interestingly, *D. discoideum* Atg1 kinase also interacts with the pentose phosphate pathway (PPP) enzyme transketolase (Tkt).[23] Although no direct phosphorylation has been reported, the activity of TKT is altered in strains lacking or overexpressing Atg1, suggesting a possible crosstalk between autophagy and the PPP. Interestingly, a recent report shows that another component of the PPP, the ribose-5-phosphate isomerase (RpiA), regulate autophagy in HeLa cells.[56]

The origin of the autophagosomal membrane, function of Vmp1 and regulation of PtdIns3P

The origin and elongation of the phagophore membrane are still the subject of intense research. In mammalian cells the ER, establishing close contacts with other organelles such as mitochondria and lipid droplets, forms a specialized cradle-like
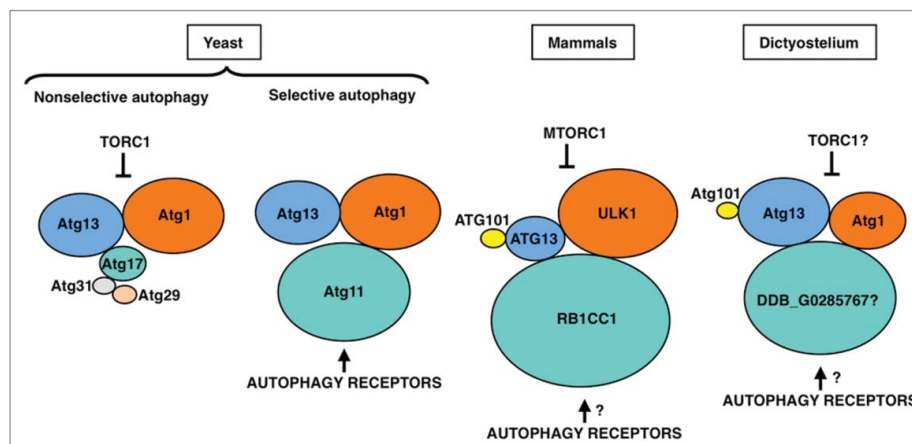

Figure 4. The Atg1/ULK1 complex in yeast, mammalian cells and *D. discoideum*. Proteins are colored according to their conservation, and protein size is proportional to the molecular weight. The inhibition of the Atg1/ULK1 kinase activity by TORC1, and its activation through binding of the autophagy receptors to the Atg11 subunit, are indicated.

structure known as the omegasome.[57] This structure is enriched in the signaling lipid PtdIns3P, generated by the class III phosphatidylinositol 3-kinase (PtdIns3K) PIK3C3/VPS34. It is thought that the phagophore expands by fusing with vesicles that originate from different cellular compartments. Some of these vesicles contain the transmembrane protein ATG9 and emanate from the Golgi and recycling endosomes,[58,59] whereas others can originate from the ER-Golgi intermediate compartment (ERGIC).[60-62]

D. discoideum autophagosomes form simultaneously in different locations of the ER[29] and are thus, in this respect, more similar to those in mammalian cells than yeast, in which autophagosomes originate from the PAS, a single spot near the vacuole. It has been proposed that *S. cerevisiae* has become highly specialized during evolution. As a result, some processes such as autophagy have diverged from a more universally conserved mechanism, which has remained unaltered in other organisms such as *D. discoideum*.[63] A valuable example of these differences is the presence in *D. discoideum* of the conserved protein Vmp1 that is required for correct formation of the omegasome, but absent in *S. cerevisiae* and other fungi.

The phenotype of Vmp1-deficient cells differs from that of cells lacking classical Atg proteins because it affects a wide array of processes apparently not connected to autophagy as described in *D. discoideum* and *Chlamydomonas reinhardtii*.[24,64] Autophagic flux is blocked in Vmp1-deficient *D. discoideum* but PtdIns3P production and subsequent recruitment of the autophagy machinery to the ER still occurs. Indeed, PtdIns3P is abnormally high in the mutants and correlates with the accumulation of enlarged omegasomes and LC3-containing structures in *D. discoideum*,[65] *C. elegans*[66] and mammalian cells.[67] Taken together, these studies suggest that Vmp1 might be required for the correct structure of the omegasome and/or

the capacity of the phagophore to elongate and become a functional autophagosome. Since Vmp1 is an ER-resident protein it is tempting to speculate that Vmp1 generates an ER microenvironment that orchestrates the autophagic machinery to allow the correct expansion of the phagophore rather than the recruitment of Atg proteins (Fig. 5).

Another interesting phenotype of the Vmp1 mutant is the defect in macropinocytosis, a mechanism of nutrient uptake that allows *D. discoideum* to grow in liquid media. The abnormal accumulation of PtdIns3P in the mutant impairs macropinocytosis indirectly and prevents growth in liquid media. This conclusion is based on experiments that preclude the accumulation of PtdIns3P. Atg1 is upstream of the PtdIns3K and therefore a double mutant in Vmp1 and Atg1 lacks this abnormal signaling.[65] Remarkably, macropinocytosis and cell growth in liquid media is recovered in the double mutant, suggesting that additional nonautophagy-related defects may occur as a result of an abnormal regulation of PtdIns3P signaling at the omegasome.[65] It will be interesting to determine if such a phenomenon also occurs in mammalian cells.

The 2 ubiquitin-like (Ubl) conjugation systems are highly conserved in D. discoideum

The proteins involved in the 2 Ubl conjugation systems are highly conserved from yeast to mammalian cells and very likely function in an analogous manner in all eukaryotes including *D. discoideum*.[9] However, while yeast harbors only one isoform for each of the 8 different proteins of the 2 Ubl conjugation systems there are 2 paralogs for ATG16 (ATG16L1, L2), 4 for ATG4 (ATG4A, B, C, D) and 7 for ATG8/LC3 in mammals.[9,68,69] In particular, the large number of ATG8/LC3 paralogs in humans and mice complicates
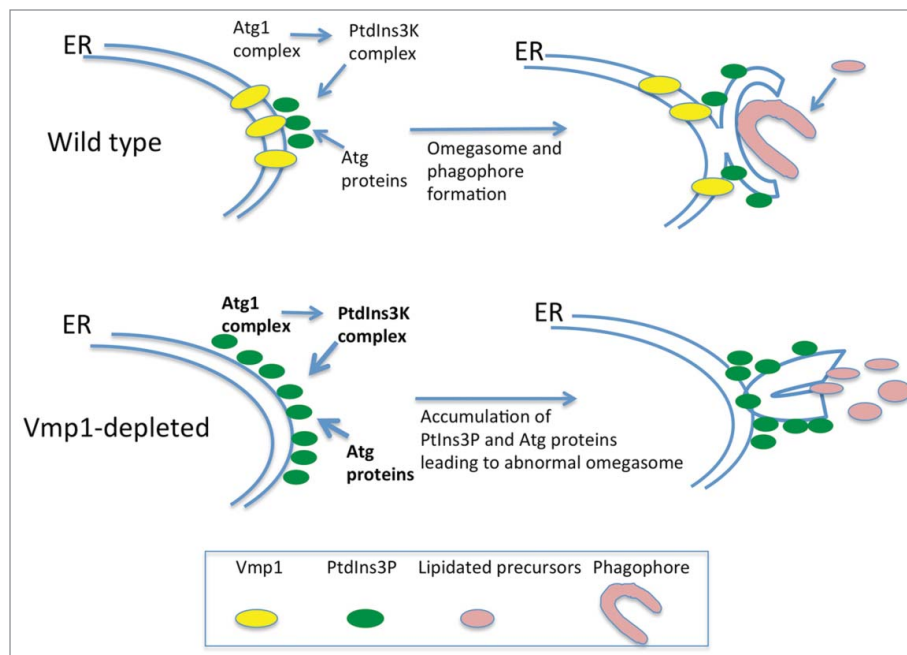

Figure 5. Vmp1 is essential for correct PtdIns3P signaling and omegasome formation in *D. discoideum* and mammalian cells. Vmp1 accumulates in subdomains of the ER where the autophagic machinery is recruited. PtdIns3P is formed at these domains to regulate omegasome formation and phagophore elongation. In the absence of Vmp1, PtdIns3P is aberrantly generated leading to persistent recruitment of autophagy proteins and unproductive autophagosome formation.

functional studies in these organisms. These proteins are grouped into the MAP1LC3 (microtubule associated protein 1 light chain 3) subfamily with 4 members (LC3A, B, B2 and C), and the GABARAP (GABA type A receptor-associated protein) subfamily with 3 members (GABARAP, GABARAPL1 and GABARAPL2/GATE16) protein.[68] The GABARAPL2 protein is approximately equally distant from the LC3 and the GABARAP subfamilies (Fig. 6) and the precise functions of the individual proteins are largely unresolved.[70] In contrast, fungi possess only a single *ATG8* gene, while plants, insects, nematodes and amoebozoa, like *D. discoideum*, usually have 2 genes for Atg8.

Phylogenetic analysis showed that *D. discoideum* Atg8a and *Acanthamoeba castellanii* Atg8 are situated in the same evolutionary branch as the orthologs from fungi and plants. In contrast, the 2 Atg8b proteins from *D. discoideum* and *A. castellanii* appear evolutionarily more closely related to the LC3 subfamily from animals (Fig. 6). Live cell imaging of *D. discoideum* cells expressing RFP-Atg8a and GFP-Atg8b showed that Atg8b associates with autophagosomes before ATG8a.[32] In mammals, LC3 subfamily members are involved in the elongation of the phagophore, whereas the GABARAP subfamily seem to be essential for a later stage in maturation.[71,72] Thus, Atg8b is likely the functional ortholog of the mammalian LC3 subfamily, which is also supported by the grouping in the

evolutionary tree (Fig. 6), and Atg8a the ortholog of the GABARAP subfamily.[32] It appears therefore, that duplication of Atg8 early in eukaryotic evolution allowed specialization of the paralogs during autophagosome maturation. Expansion of the respective subfamilies in mammals likely led to the acquisition of further specialized functions in more complex animals.[70] Similarly, the Atg4 paralogs and the Atg16 paralog in the 2 Ubl conjugation systems may enable the fine-tuning of the activation of the different Atg8/LC3 family members.

Atg9 studies in D. discoideum reveal new functions

The multimembrane spanning Atg9 protein is the only known integral membrane protein of the core autophagic machinery and thought to be involved in the delivery of membrane lipids to the growing autophagosome.[73] Atg9 orthologs exist in all eukaryotic species so far examined and the protein is essential for autophagy. For example, in *Drosophila melanogaster*, Atg9 depletion reduces both the number and size of autophagosomes, and blocks the fusion of autophagosomes with lysosomes.[74] Modulation of Atg9 levels in yeast strains directly correlates with the frequency of autophagosome formation and autophagic activity.[75]

The PAS in yeast originates from Atg9-positive clusters, called Atg9 peripheral sites.[76] The origin of these clusters,
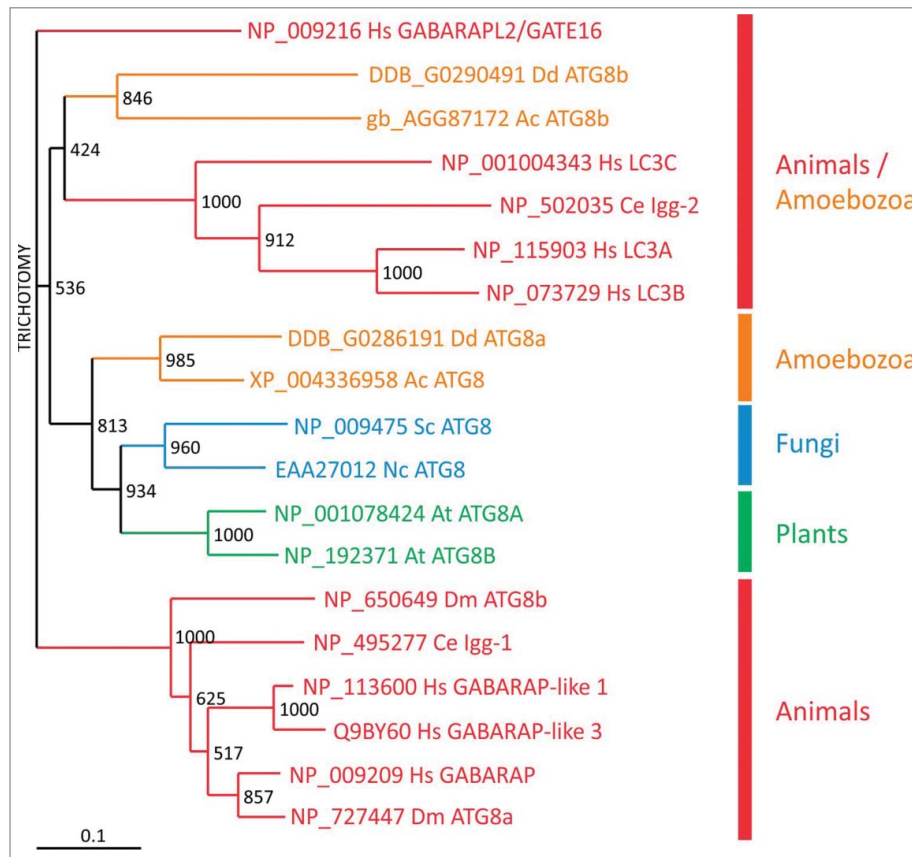

Figure 6. Evolutionary relationship of Atg8/LC3 family members. Phylogenetic analysis of Atg8/LC3 family proteins from animals (red), amoebozoa (orange), fungi (blue) and plants (green). A CLUSTALX alignment was used to create a phylogenetic tree with the TreeView program. The scale bar indicates amino acid substitutions per site. Bootstrap values are provided at the node of each branch. GenBank, SwissProt or dictyBase (http://dictybase.org/) accession numbers are provided on the right of the tree. Hs, *Homo sapiens*; Dm, *Drosophila melanogaster*; Ce, *Caenorhabditis elegans*; At, *Arabidopsis thaliana*; Nc, *Neurospora crassa*; Sc, *Saccharomyces cerevisiae*; Ac, *Acanthamoeba castellanii*; Dd, *D. discoideum*. LC3, microtubule-associated protein 1 light chain 3; GABARAP, GABA type A receptor-associated protein; GABARAPL2/GATE16, GABA type A receptor associated protein like 2; lgg: LC3, GABARAP and GATE-16 family.

however, has remained poorly understood. They localize in proximity to the mitochondrial membrane[77] and may represent vesicles derived from mitochondrial-ER contact sites. Alternatively, based on partial colocalization between Atg9 and the late Golgi protein marker Sec7, the Atg9 peripheral sites could emerge as a new organelle through the delivery of newly synthesized Atg9 to these sites via the secretory pathway.[76] Upon delivery of the lipids, Atg9 is no longer required and may be retrieved to the peripheral sites by an as yet unknown mechanism.

In mammals, there are 2 ATG9 paralogs, namely ATG9A/ATG9L1 and ATG9B/ATG9L2. ATG9A (ATG9 hereafter) is ubiquitously expressed in human adult tissues, whereas ATG9B is only expressed in placenta and pituitary gland.[78] Mammalian ATG9 is localized at the ER, the trans-Golgi network and early, late and recycling endosomes.[79,80] Recently, it was shown that in *D. melanogaster* and in human cells the Atg1/ULK1 protein kinase phosphorylates a MYLK/myosin light chain kinase, which in turn activates MYL/myosin II regulatory light chain. This is followed by myosin II activation, which apparently drives transport of ATG9-containing membranes to the phagophore.[81] *D. discoideum* Atg9 does not colocalize with mitochondria, the ER or lysosomes; however, there is a partial colocalization with the Golgi apparatus and many Atg9-GFP-containing vesicles localize along microtubules and accumulate around the microtubule organizing center.[25] Disruption of *Atg9* results in a pleiotropic phenotypes with severe impairments in development, slug migration, vegetative growth, phagocytosis, clearance of *Legionella pneumophila* and proteasomal activity.[25] A similar pleiotropic phenotype is observed in *tipD⁻/atg16⁻* cells.[26]

Unexpectedly, some of the defects of the *atg9* knockout mutant can be partially or fully restored by expression of wild-type or point-mutated CdcD/p97, an evolutionarily highly conserved member of the AAA-ATPase family.[82] VCP/p97, the mammalian homologue, is a key player in ER-associated protein degradation, in the ubiquitin-proteasome system for protein degradation system, in aggresome formation and also in autophagosome maturation.[83-85] Heterozygous mutations in the human *VCP/p97* gene cause autosomal-dominant inclusion body myopathy with early onset Paget disease of bone and frontotemporal dementia and further neurological disorders;[86,87] however, the molecular basis of the pathogenesis remains unknown. VCP is essential for autophagosome maturation in mouse embryonic fibroblasts and, moreover, disease-causing VCP point mutations impair autophagy.[88]

Interestingly, *atg9⁻*, *tipD⁻/atg16⁻* and *atg9⁻ tipD⁻/atg16⁻* double mutant *D. discoideum* cells have a severe and counterintuitive defect in proteasomal activity. Since the amounts of proteasomal subunits are not altered in knockouts of *atg9* or *tipD/atg16*, this result suggests that intact autophagy is required for optimal proteasomal activity.[26,82] Furthermore, this phenotype is fully or partially suppressed by overexpression of wild-type or point-mutated *cdcD/p97* in *atg9⁻* cells. This result provides evidence that in *D. discoideum* CdcD/p97 and Atg9 are functionally directly or indirectly linked and supports the existence of a delicate balance between the 2 major protein degradation pathways, proteasomal degradation and autophagy. Disruption of this balance causes severe impairment of essential cellular

functions in lower eukaryotes such as *D. discoideum* but ultimately may cause late-onset complex diseases in humans. How exactly the ubiquitin-proteasome system and autophagy are interconnected needs to be unraveled in the future.

Autophagy and disease: New leads from the social amoeba in human genetic disorders

Autophagic dysfunction may lead to defects in protein and organelle homeostasis associated with numerous human diseases.[89] A very relevant example is the connection of autophagy with major neurodegenerative diseases (including Alzheimer, Parkinson and Huntington diseases), often associated with the accumulation of abnormal protein aggregates or nonfunctional organelles. Autophagy dysfunction in *D. discoideum* often leads to the accumulation of large ubiquitinated protein aggregates.[55] Ubiquitin is a small regulatory protein that can be covalently linked to proteins to target them for proteasomal or autophagic degradation. These protein aggregates can be observed by both immunofluorescence microscopy using anti-ubiquitin antibodies and by western blot. As these aggregates are insoluble in 1% Triton X-100, they can rapidly be separated from whole cell lysates by centrifugation, separated by SDS-PAGE and detected using commercially available anti-ubiquitin antibodies. Ubiquitinated proteins are dramatically increased in the Triton-insoluble fraction of autophagy-deficient mutants.[55] The size and number of these aggregates correlates well with the severity of the phenotypes of the different autophagy mutants.[55] Interestingly, the protein aggregates formed in the Vmp1 mutant also accumulate the receptor protein Sqstm1,[55] which is involved in the clearance of several ubiquitinated cargos in mammalian cells and has been implicated in aggregation disorders and infectious diseases.[90]

Packing proteins into aggregates, if properly degraded by autophagy, could function as a regulated cellular mechanism to handle abnormal proteins that otherwise would be toxic. However, several studies in *D. discoideum* suggest that the protein aggregation phenotype might be deleterious for cell function. Overexpression of the actin-binding protein VasP fused to an endosomal targeting signal leads to the formation of huge actin aggregates reminiscent of Hirano bodies,[91] structures that are often present in neurodegenerative diseases. These actin aggregates sequester a number of actin binding and endosomal proteins promoting their disappearance from their normal location in the cytoplasm[91] leading to cytoskeletal defects. These findings open the possibility that protein sequestration might also contribute to neuronal malfunction in these pathologies. Hirano body-like aggregates can also be induced in *D. discoideum* by the overexpression of a truncated form of a 34-kDa actin-binding protein.[92] Another report showed that both autophagy and the proteasome pathway contribute to the degradation of Hirano bodies in *D. discoideum*.[91] The autophagosome marker protein GFP-Atg8 colocalizes with Hirano bodies in wild-type *D. discoideum* cells, but not in cells deficient in the autophagic proteins Atg5 or Atg1.[93] Interestingly, Hirano bodies can be released by exocytosis following autophagy, which could explain the presence of these aggregates in both intracellular and extracellular spaces in the brain.[93]

Another example using *D. discoideum* to study autophagy-related pathologies was the discovery of a possible connection of the rare disease Chorea-acanthocytosis (ChAc) with autophagy. ChAc is a neurodegenerative disease associated with abnormally shaped erythrocytes known as acanthocytes, leading to disability and premature death. ChAc is caused by loss-of-function mutations in *VPS13A*, most of which lead to a decrease or absence of the VPS13A protein (also known as Chorein).[94,95] The molecular function of this protein is not known and the literature provides fragmented and nonconclusive results. Proposed functions for VPS13A include membrane trafficking, membrane morphogenesis, phagocytosis and actin cytoskeleton regulation.[96-99] There are 3 additional VPS13 proteins in humans (VPS13B,C and D)[100] and mutations in 2 of them, VPS13B and C, lead to Cohen syndrome and Parkinson disease, respectively.[101,102] *D. discoideum* has 6 VPS13-related proteins, which are more similar to human VPS13A and C than to VPS13B or D. One of these proteins was initially named TipC since the phenotype of an insertional mutant was the formation of multiple tips in large mounds, a typical phenotype of autophagy mutants as pointed out above.[28] Several years later this mutant was revisited and the presence of a strong autophagy blockade was confirmed.[27] Subsequently, additional studies of the autophagic pathway in VPS13A-depleted human HeLa cells confirmed that autophagy could play a role in the etiology of this devastating disease.[27]

Defects in either the retromer or WASH (WAS protein family homolog) complexes also lead to endosomal trafficking and autophagy defects associated with human diseases. The WASH complex regulates the formation of actin filaments on endosomes, driving multiple endocytic protein sorting and recycling events,[103] and mutations in the gene encoding KIAA0196/strumpellin, a component of the WASH complex, cause a form of autosomal dominant hereditary spastic paraplegia.[104] Furthermore, an aspartate to asparagine substitution (D620N) in VPS35, a component of the retromer sorting complex that recruits WASH to endosomes, results in autosomal dominant familial Parkinson disease.[105] *D. discoideum* have all components of the WASH complex, and mutants in WASH also have a defect in autophagy. However, while defects either in the retromer or WASH lead to an early inhibition of autophagosome formation due to defective trafficking of ATG9-containing vesicles and deficient BECN1 activation in mammals,[105,106] *D. discoideum* WASH null cells do not have defects in the induction of autophagosome formation.[12] The observed blockade in autophagy is due to impaired recycling of vacuolar-type H⁺-translocating ATPase (V-ATPase) subunits and lysosomal hydrolases that leads to a late defect in lysosome recycling that blocks degradation of the cargo.[12]

Mitochondrial diseases are complex degenerative disorders caused by mutations in mitochondrial proteins encoded in the nuclear or mitochondrial genome. *D. discoideum* has been used to study the cytopathology involved in mitochondrial disease, specially those involving alterations in pathways that affect AMP-activated protein kinase (AMPK), the kinase required to sense cellular energy levels and regulate autophagy through MTOR, ULK1 and BECN1.[4,107,108] Unexpected connections with autophagy are observed in *D. discoideum* cells deficient in components of the NADH:ubiquinone oxidoreductase or complex I, the first complex of the respiratory chain. Mutants affecting complex I assembly factors Ndufaf5 and MidA/Ndufaf7 have a strong activation of bulk autophagy,[109,110] but not mitophagy, which, in the case of MidA could be mediated by a chronic activation of AMPK. Given the importance of autophagy in cellular homeostasis, this connection might have relevance in human pathology and subsequently a similar phenomenon has been observed in skin fibroblast cultures derived from patients with mitochondrial disease.[111,112]

Autophagy and bacterial infectious diseases in D. discoideum

Autophagy also represents an efficient mechanism for eukaryotic cells to capture and kill invading pathogens. The killing of intracellular pathogens by autophagy, termed "xenophagy," is therefore emerging as a major regulator of both cytosolic and vacuolar pathogens. Many bacterial pathogens are able to manipulate, either by inhibition or induction, the host xenophagic response to take advantage of autophagy for their own benefits.[113] Since *D. discoideum* lives in the soil and feeds on bacteria and yeasts, it likely developed mechanisms to discriminate between food and pathogenic organisms early during evolution. Due to its easy experimental manipulation, *D. discoideum* has become a useful model to study host-pathogen interactions and xenophagy[9] and in the past 5 y has been used to study interactions of the host autophagic machinery with pathogenic microbes such as *Salmonella enterica* serovar Typhimurium (*S. enterica*), *L. pneumophila*, Francisella *noatunensis, Staphylococcus aureus* and *Mycobacterium marinum*.[26,35,114-118] Furthermore, *D. discoideum* has also been used to identify and dissect the mechanisms of action of drugs with potential utility in medical therapy against pathogens.[119-122]

M. marinum infects mainly fish and frogs, but it can also produce skin lesions in humans. Due to safety reasons and to the faster growth rate than its close relative *M. tuberculosis*,[123] *M. marinum* represents an easier tool to research mycobacterial pathogenesis. In mammalian cells and zebrafish, *M. marinum* induces an autophagic response that includes upregulation of some autophagy-related genes and LC3 recruitment to the mycobacteria-containing vacuole (MCV).[124-128] This recognition by the autophagy machinery requires the activity of the mycobacterial pore-forming toxin ESAT-6, and engagement of the host autophagy-related proteins SQSTM1, MYD88 (myeloid differentiation primary response 88), DRAM1 (DNA damage regulated autophagy modulator protein 1) and TMEM173/STING (transmembrane protein 173).[124,125,129,130] ESAT-6 is secreted by the type VII secretion system ESX-1, and induces permeabilization of the MCV membrane, exposing *M. marinum* to the cytosol.[131] As a consequence, the ESX-1-dependent membrane damage allows the host autophagy machinery to recognize bacterial products including DNA, and to induce an autophagic response dependent on the cytosolic DNA-sensing TMEM173/STING pathway.[125,129] However, apart from its indirect role in MCV permeabilization, ESX-1 seems to be dispensable for ubiquitination of *M. marinum* in macrophages.[130]

It has been recently shown that, in *D. discoideum*, the autophagy machinery is not only recruited to cytosolic *M. marinum*, but it also targets the bacteria escaping out of

hosts cell by the nonlytic mechanism called "ejection."[35,132] During this process, ubiquitin, Atg8, Sqstm1 and Atg18 localize at the distal pole of the ejecting bacteria, with a proposed function in sealing the plasma membrane wound.[35] This recruitment of autophagy to the ejecting bacteria seems to be independent on ESX-1, as well as on other *M. marinum* virulence factors. However, host Atg1, Atg5, Atg6A and Atg7 are all required for Atg8 association with the ejecting bacterium suggesting that this process may be entirely driven by the host. Furthermore, even though Atg1 is not necessary for ejectosome formation, it is essential for the tight membrane sealing during ejection, avoiding cytosolic leakage and, thereby, death upon bacterial egress.[35]

Interestingly, disruption of *Sqstm1*, encoding the only selective autophagy receptor protein described so far in *D. discoideum*, seems to have no effect on Atg8 recruitment to *M. marinum*. Gerstenmaier and collaborators thus suggest that other receptor proteins must exist in this amoeba.[35] Ubiquitin-binding CUE-domain containing proteins have been recently described to act as autophagy recepptors for protein aggregates in yeast and humans. Consistent with the evolutionary conservation of these proteins, 2 *D. discoideum* CUE domain-

containing proteins, CnrD and DDB_G0274365/CueA also localize to MCVs (Drs. J. King and T. Soldati, unpublished results). In addition to the domain for ubiquitin binding, these proteins present LIR motifs in their sequences (Fig. 7), making them ideal selective autophagy receptor candidates.

The WASH complex is also necessary for *M. marinum* ejection and is possibly involved in *D. discoideum* xenophagy.[118] During infection, WASH-induced actin polymerization prevents MCV acidification by promoting recycling of the V-ATPase, rendering the compartment more permissive to infection.[118] This correlates with previous results in mammalian cells, in which *M. marinum* modifies the composition of its MCV by depleting the V-ATPase and the lysosomal protease CTSD (cathepsin D), as also observed during infection of *D. discoideum*.[124,133]

D. discoideum has also been recently established as a model host for another fish pathogen, *F. noatunensis*.[116] This Gram-negative bacterium exploits autophagy in human and murine macrophages.[134,135] In *D. discoideum*, the mRNA levels of *atg8* and *sqstm1* slightly increase during *F. noatunensis* infection, and Atg8, Sqstm1 and ubiquitin are recruited to the compartment containing this bacterium, suggesting an induction of
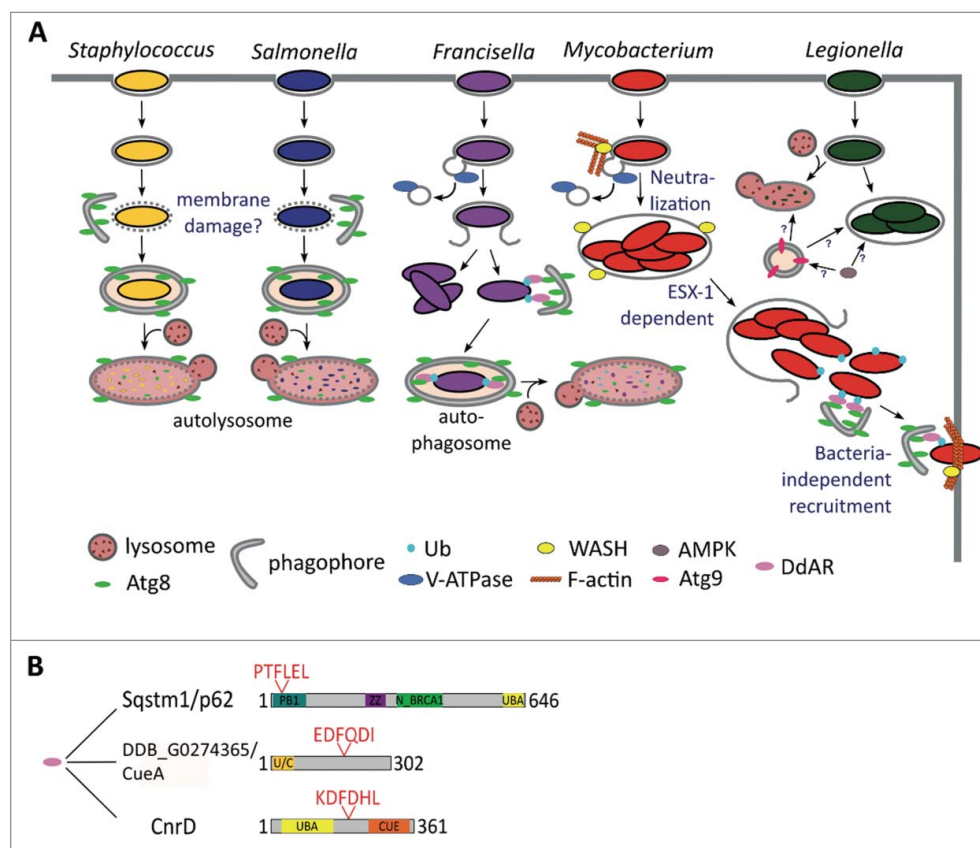

Figure 7. Xenophagy in *D. discoideum*. (A) The autophagosomal marker Atg8 is recruited to the compartment harboring both *S. aureus* and *S. enterica*, which might be a response to the putative membrane damage produced by these bacteria. As a consequence, the bacteria are engulfed in phagophores and killed in autolysosomes, where the lumenal leaflet Atg8 is digested. After uptake by *D. discoideum*, *F. noatunensis* escapes phagosomal maturation and resides in a compartment lacking the V-ATPase. The majority of *F. noatunensis* replicates in the cytosol, while a small proportion of bacteria succumb to autophagy; *M. marinum* also prevents phagosomal acidification by the V-ATPase via WASH-induced actin polymerization. After proliferation inside the MCV, *M. marinum* is released to the cytosol, where it recruits the autophagy machinery, but does not seem to be fully engulfed in autophagosomes (unpublished observations). Finally, *M. marinum* is ejected through the *D. discoideum* plasma membrane in an autophagy-dependent manner; Atg9 controls *L. pneumophila* infection, whereas the autophagy activator kinase AMPK enhances its proliferation. Therefore, the function of autophagy during *L. pneumophila* in *D. discoideum* remains unclear. (B) Domain and motif organization of the already characterized *D. discoideum* autophagy receptor (DdAR) Sqstm1 and the 2 additional putative adaptors CnrD and DDB_G0274365/CueA. PB1, Phox and Bem1 domain; ZZ, zinc finger, ZZ-type; N_BRCA1, Next to BRCA1, central domain; UBA, ubiquitin-associated domain; CUE, ubiquitin system component Cue; U/C, UBA and CUE domains. Protein domains and LIR motifs were predicted with the web prediciton resources InterPro (http://www.ebi.ac.uk/interpro) and iLIR, respectively.

autophagy. Furthermore, autophagy controls intracellular proliferation of *F. noatunensis*, since deletion of *atg1* in *D. discoideum* increases the bacterial burden after 24 h of infection.[116]

In contrast to growth of *F. noatunensis, L. pneumophila* shows similar proliferation kinetics when infecting wild-type and *atg1⁻*, *atg5⁻*, *atg6A⁻*, *atg7⁻* and *atg8⁻ D. discoideum* cells. Likewise, this intracellular pathogen of amoebae and macrophages, rarely recruits Atg8, suggesting that xenophagy is not involved in amoebal immunity against *L. pneumophila*.[136] Whether *L. pneumophila* actively escapes autophagic capture in *D. discoideum* by uncoupling Atg8 from the phagophore membrane, via action of the RavZ toxin, as it does in human cells,[137] remains to be studied. Interestingly, Atg9 might be involved in controlling *L. pneumophila*, because its expression rises after 24 h of infection, and bacterial clearance decreases in *atg9⁻* cells. Uptake of this bacterium is also decreased in *atg9⁻*, *tipD⁻/atg16⁻* and *atg9⁻ tipD⁻/atg16⁻* double-mutant *D. discoideum* cells.[25,26] However, the mechanism is unclear, because, contrary to *atg9*, the expression of TipD/Atg16 and Atg8a is downregulated after infection with *L. pneumophila*.[25] Interestingly, the intracellular proliferation of *L. pneumophila* in *D. discoideum* increases in cells overexpressing the catalytic subunit of AMPK. Since AMPK regulates ATG9 localization via the activation of ULK1 in mammalian cells,[138] the different *L. pneumophila* proliferation rates observed during infection of *atg1⁻*, *atg9⁻* and AMPK-overexpressing cells may indicate autophagy-independent functions for Atg9 and TipD/Atg16 as suggested by Xiong and collaborators.[26]

Finally, it is controversial whether *S. enterica*, one of the Gram-negative bacteria more commonly used in laboratories to study the host innate immune responses at the molecular level,[139] is pathogenic or not for *D. discoideum*. *S. enterica* survives and proliferates inside very diverse human cell types,[140] but both its survival and death inside amoebae have been reported.[114,141,142] Sillo and collaborators proposed that the discrepancies observed might be due to the use of the antibiotic gentamicin, normally employed in *S. enterica* infection protocols for mammalian cells. Gentamicin is likely to be taken up in large quantities by macropinocytosis during *D. discoideum* infection, thus affecting intracellular bacteria.[114] Regardless, early during infection of *D. discoideum*, Atg8 is recruited to the compartment harboring *S. enterica*,[142] and concomitant cleavage of GFP-Atg8 suggests an enhanced autophagic response.[115] Together with the fact that *atg1⁻*, *atg6A⁻* and *atg7⁻* cells are more permissive for *S. enterica* growth,[142] this observation implies a rapid autophagy-dependent killing of these bacteria by *D. discoideum* cells.

Autophagy has also been implicated during infection of lipopolysaccharide-treated *D. discoideum* cells with *S. aureus*.[115] The fate of this Gram-positive bacterium inside amoebae is affected by autophagy, since its uptake is reduced in *atg9⁻* cells.[25,115] Treatment with lipopolysaccharide, which also induces bacteria clearance in an Atg1- and Atg9-dependent manner, further increases the localization of Atg8 to the vacuoles containing *S. aureus*.[115] Because *S. aureus* localizes to LC3-labeled compartments and subverts the autophagy pathway in mammalian cells,[143-145] manipulating autophagy with protease inhibitors or compounds blocking autolysosome formation is

needed to confirm the induction or blockade of autophagy by these bacteria.[146]

In conclusion, different bacterial species differentially subvert autophagy in *D. discoideum*, as occurs in mammalian cells. The *D. discoideum* autophagy machinery is recruited to *S. aureus*, *S. enterica*, *F. noatunensis* and *M. marinum* at different stages during infection (Fig. 7). This recruitment is normally induced by the damage or rupture of the bacteria-containing compartments and, as a consequence, the bacteria are killed in autolysosomes. However, both *F. noatunensis* and *M. marinum* are able to prevent phagosomal acidification by the V-ATPase, therefore, bypassing xenophagy.

Autophagy and cell death pathways in D. discoideum

In addition to caspase-mediated apoptosis in animal cells, an increasing number of nonapoptotic cell death types are being reported within and outside the animal kingdom. In these multiple different cell death types there might be common, conserved cell death core elements that can be analyzed through studying cell death in alternative model organisms[147] such *D. discoideum*.

The *D. discoideum* fruiting body includes a stalk made of vacuolized, cellulose-walled dead cells.[148] This developmental cell death can be mimicked in vitro in monolayer conditions[149-151] that include a stereotyped sequence of events[9,150] such as vacuolization and cellulose encasing (Fig. 8). The induction of this process requires 2 exogenous signals. The first signal, starvation and cAMP, sensitizes the cells. Only cells which have received this first signal can be induced to die by a second signal, classically the polyketide DIF-1.[152] In starved cells subjected to DIF-1, autophagy determines the type of cell
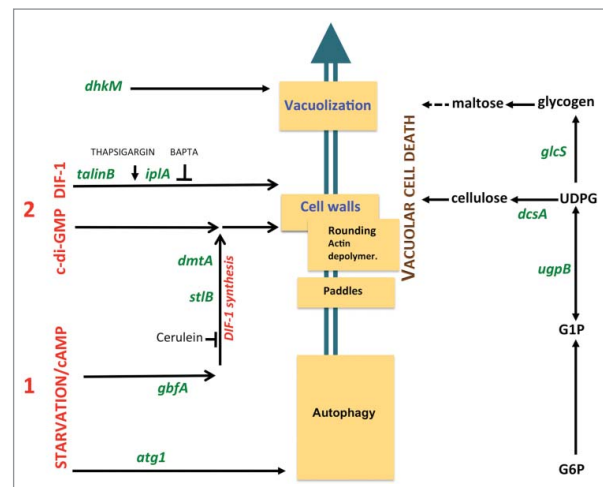

Figure 8. Genes and pathways governing *D. discoideum* vacuolar cell death. The cascade of subcellular cell death events is schematically depicted (*middle*). These include the formation of "paddle" cells, following by their rounding, biogenesis of a cellulose shell and extensive vacuolization. Random insertional mutagenesis and targeted mutagenesis identified a number of genes, here shown in green letters, encoding molecules required for this cell death. Details are given in the main text. These genes in turn helped define pathways to cell death, such as a polysaccharide pathway (*right*), a first signal pathway induced by starvation and cAMP (*lower left*) and second signal pathways (*upper left*). The latter include a DIF-1-induced autonomous pathway and a c-di-GMP pathway requiring endogenously synthesized or exogenous DIF-1. Ca^{2+}-related drugs such as thapsigargin and BAPTA affect DIF-1 signaling leading to cell death.

death. In the presence of autophagy, DIF-1 induces a normal vacuolar cell death. However, in the absence of autophagy, DIF-1 induces necrotic cell death.[153,154] This necrotic death includes mitochondrial uncoupling[155-157] and depends not only on the absence of autophagy upon starvation, but also on given targets of the DIF-1 molecule, distinct from those that induce vacuolar cell death.[158] These results are in line with the known mitochondrial uncoupling effects of DIF-1 treatment[159] and with the recently demonstrated multiplicity of DIF-1-induced effects.[160] Importantly, although both pathways result in programmed death, while vacuolar cell death is part of normal development, necrotic cell death is incompatible with it.[153]

Whether autophagy is also involved at the execution stage of vacuolar cell death has not been unambiguously proven. However, a large amount of debris is observed in the death-accompanying vacuoles indicating active degradation. Autophagy has also been proposed to have a structural role in terminal stalk differentiation.[15] Stalk-cell vacuoles seem to originate from acidic vesicles and autophagosomes, which fuse to form autolysosomes. Their repeated fusion expands the vacuole, accompanied by cellulose wall formation enabling the stalk cells to make the stalk rigid and hold the spores aloft.[15]

DIF-1-induced vacuolar cell death in monolayers has been studied by random insertional mutagenesis. This led to the identification of a number of molecules required for this pathway, including the ITPR/IP3R homolog Ca^{2+} flux-controlling IplA,[161] the UDP-glucose pyrophosphorylase UgpB, the glycogen synthase GlcS,[162] the histidine kinase DhkM,[163] the transcription factor GbfA and the integrin-cytoskeleton intermediate TalB/talinB.[157] These and other studies have contributed to defining molecular pathways required for DIF-1-induced vacuolar cell death (Fig. 8).

An important recent discovery was the demonstration that not only DIF-1, but also the cyclic dinucleotide c-di-GMP are able to induce *D. discoideum* cell death.[164,165] c-di-GMP is a universal bacterial second messenger[166] and can trigger innate immunity in bacterially-infected animal cells.[167] Unexpectedly, experiments using both inducers show marked synergy,[168] although c-di-GMP alone is insufficient to induce cell death in *D. discoideum* cell monolayers, requiring either DIF-1 or a DIF-1-related polyketide. The required DIF-1 can be endogenous, as shown by the inability of c-di-GMP to induce cell death when DIF-1 synthesis was blocked pharmacologically (by cerulenin), and by its rescue upon complementation by exogenous DIF-1.[168] This was confirmed genetically using mutants in the polyketide synthase *stlB* and the methylase *dmtA* genes that are required for DIF-1 biosynthesis.[169,170] The corresponding *stlB⁻* or *dmtA⁻* mutant cells cannot be induced to die by exogenous c-di-GMP, and this can be complemented by exogenous DIF-1.[168] Thus, c-di-GMP can only trigger cell death in the presence of DIF1 or DIF-1-related polyketides, providing an additional level of control to this, and perhaps other c-di-GMP-dependent pathways.

How c-di-GMP synergizes with endogenous DIF-1, to drive cell death is not clear. However, at least part of the c-di-GMP pathway seems to be distinct from the autonomous DIF-1 pathway, since mutants of the latter, *talB⁻* and *iplA⁻*, do not impair the former.[168] Among several cytosolic molecules able to sense c-di-GMP in animal cells, DDX41[171] is especially well

conserved and has a clear *D. discoideum* ortholog. Attempts to inactivate *D. discoideum* DDX41 by targeted mutagenesis have not led to alterations of cell death so far (Y. Song, unpublished) although several other c-di-GMP binding proteins have been reported.[172] Studying not only DIF-1- but also c-di-GMP-induced cell death in *D. discoideum* may provide important detail on the molecular mechanisms, including the role of autophagy, as well as suggestions as to how c-di-GMP acts in animal cells.

Concluding remarks

The strong conservation of the autophagic pathway between *D. discoideum* and mammalian cells justifies the use of this social amoeba as a model system for the study of the molecular mechanisms of autophagy and autophagy-related diseases. For basic studies *D. discoideum* can beautifully complement the enormous wealth of information obtained in *S. cerevisiae*, in particular those genes not conserved in yeast. In recent years, this potential has also become a reality in a wide range of biomedical conditions as exemplified in the use of *D. discoideum* as a surrogate host for studying the role of autophagy in infectious diseases.

Disclosure of potential conflicts of interest

No potential conflicts of interest were disclosed.

Funding

References

[1] Muñoz-Braceras S, Mesquita A, Escalante R. *Dictyostelium discoideum* as a model in biomedical research. In: Romeralo M, Baldauf S, Escalante R, eds. Dictyostelids Evolution, Genomics and Cell Biology. Berlin: Springer, 2013:1-34.

[2] Steinert M. Pathogen-host interactions in Dictyostelium, Legionella, Mycobacterium and other pathogens. Semin Cell Dev Biol 2011; 22:70-6; PMID:21109012; http://dx.doi.org/10.1016/j.semcdb.2010.11.003

[3] Carnell MJ, Insall RH. Actin on disease - Studying the pathobiology of cell motility using *Dictyostelium discoideum*. Semin Cell Dev Biol 2010; 22:82-8; PMID:21145982; http://dx.doi.org/10.1016/j.semcdb.2010.12.003

[4] Francione LM, Annesley SJ, Carilla-Latorre S, Escalante R, Fisher PR. The Dictyostelium model for mitochondrial disease. Semin Cell Dev Biol 2011; 22:120-30; PMID:21129494; http://dx.doi.org/10.1016/j.semcdb.2010.11.004

[5] Ludtmann MH, Boeckeler K, Williams RS. Molecular pharmacology in a simple model system: implicating MAP kinase and phosphoinositide signalling in bipolar disorder. Semin Cell Dev Biol 2011; 22:105-13; PMID:21093602; http://dx.doi.org/10.1016/j.semcdb.2010.11.002

[6] Alexander S, Alexander H. Lead genetic studies in *Dictyostelium discoideum* and translational studies in human cells demonstrate that sphingolipids are key regulators of sensitivity to cisplatin and other anticancer drugs. Semin Cell Dev Biol 2011; 22:97-104; PMID:20951822; http://dx.doi.org/10.1016/j.semcdb.2010.10.005

[7] Myre MA. Clues to gamma-secretase, huntingtin and Hirano body normal function using the model organism *Dictyostelium discoideum*. J Biomed Sci 2012; 19:41; PMID:22489754; http://dx.doi.org/10.1186/1423-0127-19-41

[8] Maniak M. Dictyostelium as a model for human lysosomal and trafficking diseases. Semin Cell Dev Biol 2011; 22:114-9; PMID:21056680; http://dx.doi.org/10.1016/j.semcdb.2010.11.001

[9] Calvo-Garrido J, Carilla-Latorre S, Kubohara Y, Santos-Rodrigo N, Mesquita A, Soldati T, Golstein P, Escalante R. Autophagy in Dictyostelium: genes and pathways, cell death and infection. Autophagy 2010; 6:686-701; PMID:20603609; http://dx.doi.org/10.4161/auto.6.6.12513

[10] Cotter DA, Miura-Santo LY, Hohl HR. Ultrastructural changes during germination of *Dictyostelium discoideum* spores. J Bacteriol 1969; 100:1020-6; PMID:5391047

[11] De Duve C, Wattiaux R. Functions of lysosomes. Annu Rev Physiol 1966; 28:435-92; PMID:5322983; http://dx.doi.org/10.1146/annurev.ph.28.030166.002251

[12] King JS, Gueho A, Hagedorn M, Gopaldass N, Leuba F, Soldati T, Insall RH. WASH is required for lysosomal recycling and efficient autophagic and phagocytic digestion. Mol Biol Cell 2013; 24:2714-26; PMID:23885127; http://dx.doi.org/10.1091/mbc.E13-02-0092

[13] Otto GP, Wu MY, Kazgan N, Anderson OR, Kessin RH. Macroautophagy is required for multicellular development of the social amoeba *Dictyostelium discoideum*. J Biol Chem 2003; 278:17636-45; PMID:12626495; http://dx.doi.org/10.1074/jbc.M212467200

[14] Cabral M, Anjard C, Malhotra V, Loomis WF, Kuspa A. Unconventional secretion of AcbA in Dictyostelium discoideum through a vesicular intermediate. Eukaryot Cell 2010; 9:1009-17; PMID:20472692; http://dx.doi.org/10.1128/ec.00337-09

[15] Uchikawa T, Yamamoto A, Inouye K. Origin and function of the stalk-cell vacuole in Dictyostelium. Dev Biol 2011; 352:48-57; PMID:21256841; http://dx.doi.org/10.1016/j.ydbio.2011.01.014

[16] Cuervo AM, Wong E. Chaperone-mediated autophagy: roles in disease and aging. Cell Res 2014; 24:92-104; PMID:24281265; http://dx.doi.org/10.1038/cr.2013.153

[17] Li WW, Li J, Bao JK. Microautophagy: lesser-known self-eating. Cell Mol Life Sci 2012; 69:1125-36; PMID:22080117; http://dx.doi.org/10.1007/s00018-011-0865-5

[18] Zaffagnini G, Martens S. Mechanisms of selective autophagy. J Mol Biol 2016; 482:1714-24; http://dx.doi.org/10.1016/j.jmb.2016.02.004

[19] Feng Y, He D, Yao Z, Klionsky DJ. The machinery of macroautophagy. Cell Res 2014; 24:24-41; PMID:24366339; http://dx.doi.org/10.1038/cr.2013.168

[20] Parzych KR, Klionsky DJ. An Overview of autophagy: Morphology, mechanism, and regulation. Antioxid Redox Signal 2014; 20:460-73; PMID:23725295; http://dx.doi.org/10.1089/ars.2013.5371

[21] Ktistakis NT, Tooze SA. Digesting the expanding mechanisms of autophagy. Trends Cell Biol 2016; Apr. 2:S0962-8924(16)00045-3

[22] Otto GP, Wu MY, Kazgan N, Anderson OR, Kessin RH. Dictyostelium macroautophagy mutants vary in the severity of their developmental defects. J Biol Chem 2004; 279:15621-9; PMID:14736886; http://dx.doi.org/10.1074/jbc.M311139200

[23] Mesquita A, Tabara LC, Martinez-Costa O, Santos-Rodrigo N, Vincent O, Escalante R. Dissecting the function of Atg1 complex in Dictyostelium autophagy reveals a connection with the pentose phosphate pathway enzyme transketolase. Open Bio 2015; 5:pii: 150088.

[24] Calvo-Garrido J, Carilla-Latorre S, Lazaro-Dieguez F, Egea G, Escalante R. Vacuole membrane protein 1 is an endoplasmic reticulum protein required for organelle biogenesis, protein secretion, and development. Mol Biol Cell 2008; 19:3442-53; PMID:18550798; http://dx.doi.org/10.1091/mbc.E08-01-0075

[25] Tung SM, Unal C, Ley A, Pena C, Tunggal B, Noegel AA, Krut O, Steinert M, Eichinger L. Loss of Dictyostelium ATG9 results in a pleiotropic phenotype affecting growth, development, phagocytosis and clearance and replication of Legionella pneumophila. Cell Microbiol 2010; 12:765-80; PMID:20070309; http://dx.doi.org/10.1111/j.1462-5822.2010.01432.x

[26] Xiong Q, Unal C, Matthias J, Steinert M, Eichinger L. The phenotypes of ATG9, ATG16 and ATG9/16 knock-out mutants imply autophagy-dependent and -independent functions. Open Bio 2015; 5:150008; http://dx.doi.org/10.1098/rsob.150008

[27] Munoz-Braceras S, Calvo R, Escalante R. TipC and the chorea-acanthocytosis protein VPS13A regulate autophagy in Dictyostelium and human HeLa cells. Autophagy 2015; 11:918-27; PMID:25996471; http://dx.doi.org/10.1080/15548627.2015.1034413

[28] Stege JT, Laub MT, Loomis WF. tip genes act in parallel pathways of early Dictyostelium development. Dev Genet 1999; 25:64-77; PMID:10402673; http://dx.doi.org/10.1002/(SICI)1520-6408(1999)25:1%3c64::AID-DVG7%3e3.0.CO;2-1

[29] King JS, Veltman DM, Insall RH. The induction of autophagy by mechanical stress. Autophagy 2011; 7:1490-9; PMID:22024750; http://dx.doi.org/10.4161/auto.7.12.17924

[30] Rosel D, Khurana T, Majithia A, Huang X, Bhandari R, Kimmel AR. TOR complex 2 (TORC2) in Dictyostelium suppresses phagocytic nutrient capture independently of TORC1-mediated nutrient sensing. J Cell Sci 2012; 125:37-48; PMID:22266904; http://dx.doi.org/10.1242/jcs.077040

[31] Kabeya Y, Mizushima N, Ueno T, Yamamoto A, Kirisako T, Noda T, Kominami E, Ohsumi Y, Yoshimori T. LC3, a mammalian homologue of yeast Apg8p, is localized in autophagosome membranes after processing. EMBO J 2000; 19:5720-8; PMID:11060023; http://dx.doi.org/10.1093/emboj/19.21.5720

[32] Matthias J, Messling S, Eichinger L. The two Dictyostelium autophagy eight proteins, ATG8a and ATG8b, associate with the autophagosome in succession. Eur J Cell Biol 2016; 95:15-25; PMID:26697781; http://dx.doi.org/10.1016/j.ejcb.2015.10.007

[33] Krick R, Henke S, Tolstrup J, Thumm M. Dissecting the localization and function of Atg18, Atg21 and Ygr223c. Autophagy 2008; 4:896-910; PMID:18769150; http://dx.doi.org/10.4161/auto.6801

[34] Polson HE, de Lartigue J, Rigden DJ, Reedijk M, Urbe S, Clague MJ, Tooze SA. Mammalian Atg18 (WIPI2) localizes to omegasome-anchored phagophores and positively regulates LC3 lipidation. Autophagy 2010; 6:506-22; PMID:20505359; http://dx.doi.org/10.4161/auto.6.4.11863

[35] Gerstenmaier L, Pilla R, Herrmann L, Herrmann H, Prado M, Villafano GJ, Kolonko M, Reimer R, Soldati T, King JS, et al. The autophagic machinery ensures nonlytic transmission of mycobacteria. Proc Natl Acad Sci U S A 2015; 112:E687-92; PMID:25646440; http://dx.doi.org/10.1073/pnas.1423318112

[36] Kimura S, Noda T, Yoshimori T. Dissection of the autophagosome maturation process by a novel reporter protein, tandem fluorescent-tagged LC3. Autophagy 2007; 3:452-60; PMID:17534139; http://dx.doi.org/10.4161/auto.4451

[37] Mesquita A, Calvo-Garrido J, Carilla-Latorre S, Escalante R. Monitoring autophagy in Dictyostelium. Methods Mol Biol 2013; 983:461-70; PMID:23494324; http://dx.doi.org/10.1007/978-1-62703-302-2_26

[38] Calvo-Garrido J, Carilla-Latorre S, Mesquita A, Escalante R. A proteolytic cleavage assay to monitor autophagy in Dictyostelium discoideum. Autophagy 2011; 7:1063-8; PMID:21876387; http://dx.doi.org/10.4161/auto.7.9.16629

[39] Welter E, Thumm M, Krick R. Quantification of nonselective bulk autophagy in *S. cerevisiae* using Pgk1-GFP. Autophagy 2010; 6:794-7; PMID:20523132; http://dx.doi.org/10.4161/auto.6.6.12348

[40] Lin MG, Hurley JH. Structure and function of the ULK1 complex in autophagy. Curr Opin Cell Biol 2016; 39:61-8; PMID:26921696; http://dx.doi.org/10.1016/j.ceb.2016.02.010

[41] Russell RC, Tian Y, Yuan H, Park HW, Chang YY, Kim J, Kim H, Neufeld TP, Dillin A, Guan KL. ULK1 induces autophagy by phosphorylating Beclin-1 and activating VPS34 lipid kinase. Nat Cell Biol 2013; 15(7):741-50; PMID:23685627

[42] Papinski D, Schuschnig M, Reiter W, Wilhelm L, Barnes CA, Maiolica A, Hansmann I, Pfaffenwimmer T, Kijanska M, Stoffel I, et al. Early steps in autophagy depend on direct phosphorylation of Atg9 by the Atg1 kinase. Mol Cell 2014; 53:471-83; PMID:24440502; http://dx.doi.org/10.1016/j.molcel.2013.12.011

[43] Noda NN, Fujioka Y. Atg1 family kinases in autophagy initiation. Cell Mol Life Sci 2015; 72(16):3083-96; PMID:25948417

[44] Mao K, Chew LH, Inoue-Aono Y, Cheong H, Nair U, Popelka H, Yip CK, Klionsky DJ. Atg29 phosphorylation regulates

coordination of the Atg17-Atg31-Atg29 complex with the Atg11 scaffold during autophagy initiation. Proc Natl Acad Sci U S A 2013; 110:E2875-84; PMID:23858448; http://dx.doi.org/10.1073/pnas.1300064110

[45] Kamada Y, Yoshino K, Kondo C, Kawamata T, Oshiro N, Yonezawa K, Ohsumi Y. Tor directly controls the Atg1 kinase complex to regulate autophagy. Mol Cell Biol 2010; 30:1049-58; PMID:19995911; http://dx.doi.org/10.1128/mcb.01344-09

[46] Kamber RA, Shoemaker CJ, Denic V. Receptor-bound targets of selective autophagy use a scaffold protein to activate the Atg1 kinase. Mol Cell 2015; 59:372-81; PMID:26166702; http://dx.doi.org/10.1016/j.molcel.2015.06.009

[47] Khaminets A, Behl C, Dikic I. Ubiquitin-dependent and independent signals in selective autophagy. Trends Cell Biol 2016; 26:6-16; PMID:26437584; http://dx.doi.org/10.1016/j.tcb.2015.08.010

[48] Hosokawa N, Sasaki T, Iemura S, Natsume T, Hara T, Mizushima N. Atg101, a novel mammalian autophagy protein interacting with Atg13. Autophagy 2009; 5:973-9; PMID:19597335; http://dx.doi.org/10.4161/auto.5.7.9296

[49] Mercer CA, Kaliappan A, Dennis PB. A novel, human Atg13 binding protein, Atg101, interacts with ULK1 and is essential for macroautophagy. Autophagy 2009; 5:649-62; PMID:19287211; http://dx.doi.org/10.4161/auto.5.5.8249

[50] Suzuki H, Kaizuka T, Mizushima N, Noda NN. Structure of the Atg101-Atg13 complex reveals essential roles of Atg101 in autophagy initiation. Nat Struct Mol Biol 2015; 22:572-80; PMID:26030876; http://dx.doi.org/10.1038/nsmb.3036

[51] Qi S, Kim do J, Stjepanovic G, Hurley JH. Structure of the human Atg13-Atg101 HORMA heterodimer: an interaction hub within the ULK1 complex. Structure 2015; 23:1848-57; PMID:26299944; http://dx.doi.org/10.1016/j.str.2015.07.011

[52] Li F, Chung T, Vierstra RD. Autophagy-related 11 plays a critical role in general autophagy- and senescence-induced mitophagy in Arabidopsis. Plant Cell 2014; 26:788-807; PMID:24563201; http://dx.doi.org/10.1105/tpc.113.120014

[53] Rui YN, Xu Z, Patel B, Chen Z, Chen D, Tito A, David G, Sun Y, Stimming EF, Bellen HJ, et al. Huntingtin functions as a scaffold for selective macroautophagy. Nat Cell Biol 2015; 17:262-75; PMID:25686248; http://dx.doi.org/10.1038/ncb3101

[54] Tekinay T, Wu MY, Otto GP, Anderson OR, Kessin RH. Function of the Dictyostelium discoideum Atg1 kinase during autophagy and development. Eukaryot Cell 2006; 5:1797-806; PMID:17031001; http://dx.doi.org/10.1128/ec.00342-05

[55] Calvo-Garrido J, Escalante R. Autophagy dysfunction and ubiquitin-positive protein aggregates in Dictyostelium cells lacking Vmp1. Autophagy 2010; 6:100-9; PMID:20009561; http://dx.doi.org/10.4161/auto.6.1.10697

[56] Heintze J, Costa JR, Weber M, Ketteler R. Ribose 5-phosphate isomerase inhibits LC3 processing and basal autophagy. Cell Signal 2016; 28:1380-8; PMID:27328773; http://dx.doi.org/10.1016/j.cellsig.2016.06.015

[57] Axe EL, Walker SA, Manifava M, Chandra P, Roderick HL, Habermann A, Griffiths G, Ktistakis NT. Autophagosome formation from membrane compartments enriched in phosphatidylinositol 3-phosphate and dynamically connected to the endoplasmic reticulum. J Cell Biol 2008; 182:685-701; PMID:18725538; http://dx.doi.org/10.1083/jcb.200803137

[58] Puri C, Renna M, Bento CF, Moreau K, Rubinsztein DC. Diverse autophagosome membrane sources coalesce in recycling endosomes. Cell 2013; 154:1285-99; PMID:24034251; http://dx.doi.org/10.1016/j.cell.2013.08.044

[59] He S, Ni D, Ma B, Lee JH, Zhang T, Ghozalli I, Pirooz SD, Zhao Z, Bharatham N, Li B, et al. PtdIns(3)P-bound UVRAG coordinates Golgi-ER retrograde and Atg9 transport by differential interactions with the ER tether and the beclin 1 complex. Nat Cell Biol 2013; 15:1206-19; PMID:24056303; http://dx.doi.org/10.1038/ncb2848

[60] Ge L, Zhang M, Schekman R. Phosphatidylinositol 3-kinase and COPII generate LC3 lipidation vesicles from the ER-Golgi intermediate compartment. eLife 2014; 3:e04135; PMID:25432021; http://dx.doi.org/10.7554/eLife.04135

[61] Carlsson SR, Simonsen A. Membrane dynamics in autophagosome biogenesis. J Cell Sci 2015; 128:193-205; PMID:25568151; http://dx.doi.org/10.1242/jcs.141036

[62] Lemus L, Ribas JL, Sikorska N, Goder V. An ER-localized SNARE protein is exported in specific COPII vesicles for autophagosome biogenesis. Cell Rep 2016; 14:1710-22; PMID:26876173; http://dx.doi.org/10.1016/j.celrep.2016.01.047

[63] King JS. Autophagy across the eukaryotes: Is S. cerevisiae the odd one out? Autophagy 2012; 8:1159-62; PMID:22722653; http://dx.doi.org/10.4161/auto.20527

[64] Tenenboim H, Smirnova J, Willmitzer L, Steup M, Brotman Y. VMP1-deficient Chlamydomonas exhibits severely aberrant cell morphology and disrupted cytokinesis. BMC Plant Biol 2014; 14:121; PMID:24885763; http://dx.doi.org/10.1186/1471-2229-14-121

[65] Calvo-Garrido J, King JS, Munoz-Braceras S, Escalante R. Vmp1 regulates PtdIns3P signaling during autophagosome formation in Dictyostelium discoideum. Traffic 2014; 15:1235-46; PMID:25131297; http://dx.doi.org/10.1111/tra.12210

[66] Tian Y, Li Z, Hu W, Ren H, Tian E, Zhao Y, Lu Q, Huang X, Yang P, Li X, et al. C. elegans screen identifies autophagy genes specific to multicellular organisms. Cell 2010; 141:1042-55; PMID:20550938; http://dx.doi.org/10.1016/j.cell.2010.04.034

[67] Itakura E, Mizushima N. Characterization of autophagosome formation site by a hierarchical analysis of mammalian Atg proteins. Autophagy 2010; 6:764-76; PMID:20639694; http://dx.doi.org/10.4161/auto.6.6.12709

[68] Mizushima N, Yoshimori T, Ohsumi Y. The role of Atg proteins in autophagosome formation. Annu Rev Cell Dev Biol 2011; 27:107-32; PMID:21801009; http://dx.doi.org/10.1146/annurev-cellbio-092910-154005

[69] Zhang L, Li J, Ouyang L, Liu B, Cheng Y. Unraveling the roles of Atg4 proteases from autophagy modulation to targeted cancer therapy. Cancer Lett 2016; 373:19-26; PMID:26805760; http://dx.doi.org/10.1016/j.canlet.2016.01.022

[70] Shpilka T, Weidberg H, Pietrokovski S, Elazar Z. Atg8: an autophagy-related ubiquitin-like protein family. Genome Biol 2011; 12:226; PMID:21867568; http://dx.doi.org/10.1186/gb-2011-12-7-226

[71] Weidberg H, Shvets E, Elazar Z. Biogenesis and cargo selectivity of autophagosomes. Annu Rev Biochem 2011; 80:125-56; PMID:21548784; http://dx.doi.org/10.1146/annurev-biochem-052709-094552

[72] Weidberg H, Shpilka T, Shvets E, Abada A, Shimron F, Elazar Z. LC3 and GATE-16 N termini mediate membrane fusion processes required for autophagosome biogenesis. Dev Cell 2011; 20:444-54; PMID:21497758; http://dx.doi.org/10.1016/j.devcel.2011.02.006

[73] Xie Z, Klionsky DJ. Autophagosome formation: core machinery and adaptations. Nat Cell Biol 2007; 9:1102-9; PMID:17909521; http://dx.doi.org/10.1038/ncb1007-1102

[74] Bader CA, Shandala T, Ng YS, Johnson IR, Brooks DA. Atg9 is required for intraluminal vesicles in amphisomes and autolysosomes. Bio Open 2015; 4:1345-55; http://dx.doi.org/10.1242/bio.013979

[75] Jin M, He D, Backues SK, Freeberg MA, Liu X, Kim JK, Klionsky DJ. Transcriptional regulation by Pho23 modulates the frequency of autophagosome formation. Curr Biol 2014; 24:1314-22; PMID:24881874; http://dx.doi.org/10.1016/j.cub.2014.04.048

[76] Mari M, Griffith J, Rieter E, Krishnappa L, Klionsky DJ, Reggiori F. An Atg9-containing compartment that functions in the early steps of autophagosome biogenesis. J Cell Biol 2010; 190:1005-22; PMID:20855505; http://dx.doi.org/10.1083/jcb.200912089

[77] Reggiori F, Shintani T, Nair U, Klionsky DJ. Atg9 cycles between mitochondria and the pre-autophagosomal structure in yeasts. Autophagy 2005; 1:101-9; PMID:16874040; http://dx.doi.org/10.4161/auto.1.2.1840

[78] Yamada T, Carson AR, Caniggia I, Umebayashi K, Yoshimori T, Nakabayashi K, Scherer SW. Endothelial nitric-oxide synthase antisense (NOS3AS) gene encodes an autophagy-related protein (APG9-like2) highly expressed in trophoblast. J Biol

Chem 2005; 280:18283-90; PMID:15755735; http://dx.doi.org/10.1074/jbc.M413957200

[79] Young AR, Chan EY, Hu XW, Kochl R, Crawshaw SG, High S, Hailey DW, Lippincott-Schwartz J, Tooze SA. Starvation and ULK1-dependent cycling of mammalian Atg9 between the TGN and endosomes. J Cell Sci 2006; 119:3888-900; PMID:16940348; http://dx.doi.org/10.1242/jcs.03172

[80] Puri C, Renna M, Bento CF, Moreau K, Rubinsztein DC. ATG16L1 meets ATG9 in recycling endosomes: additional roles for the plasma membrane and endocytosis in autophagosome biogenesis. Autophagy 2014; 10:182-4; PMID:24257061; http://dx.doi.org/10.4161/auto.27174

[81] Tang HW, Wang YB, Wang SL, Wu MH, Lin SY, Chen GC. Atg1-mediated myosin II activation regulates autophagosome formation during starvation-induced autophagy. EMBO J 2011; 30:636-51; PMID:21169990; http://dx.doi.org/10.1038/emboj.2010.338

[82] Arhzaouy K, Strucksberg KH, Tung SM, Tangavelou K, Stumpf M, Faix J, Schroder R, Clemen CS, Eichinger L. Heteromeric p97/p97 (R155C) complexes induce dominant negative changes in wild-type and autophagy 9-deficient Dictyostelium strains. PLoS ONE 2012; 7:e46879; PMID:23056506; http://dx.doi.org/10.1371/journal.pone.0046879

[83] Dai RM, Li CC. Valosin-containing protein is a multi-ubiquitin chain-targeting factor required in ubiquitin-proteasome degradation. Nat Cell Biol 2001; 3:740-4; PMID:11483959; http://dx.doi.org/10.1038/35087056

[84] Lilley BN, Ploegh HL. Multiprotein complexes that link dislocation, ubiquitination, and extraction of misfolded proteins from the endoplasmic reticulum membrane. Proc Natl Acad Sci U S A 2005; 102:14296-301; PMID:16186509; http://dx.doi.org/10.1073/pnas.0505014102

[85] Ye Y, Shibata Y, Yun C, Ron D, Rapoport TA. A membrane protein complex mediates retro-translocation from the ER lumen into the cytosol. Nature 2004; 429:841-7; PMID:15215856; http://dx.doi.org/10.1038/nature02656

[86] Kazamel M, Sorenson EJ, McEvoy KM, Jones LK, Jr., Leep-Hunderfund AN, Mauermann ML, Milone M. Clinical spectrum of valosin containing protein (VCP)-opathy. Muscle Nerve 2016; 54:94-9; PMID:26574898; http://dx.doi.org/10.1002/mus.24980

[87] Kimonis VE, Mehta SG, Fulchiero EC, Thomasova D, Pasquali M, Boycott K, Neilan EG, Kartashov A, Forman MS, Tucker S, et al. Clinical studies in familial VCP myopathy associated with Paget disease of bone and frontotemporal dementia. Am J Med Genet A 2008; 146A:745-57; PMID:18260132; http://dx.doi.org/10.1002/ajmg.a.31862

[88] Tresse E, Salomons FA, Vesa J, Bott LC, Kimonis V, Yao TP, Dantuma NP, Taylor JP. VCP/p97 is essential for maturation of ubiquitin-containing autophagosomes and this function is impaired by mutations that cause IBMPFD. Autophagy 2010; 6:217-27; PMID:20104022; http://dx.doi.org/10.4161/auto.6.2.11014

[89] Schneider JL, Cuervo AM. Autophagy and human disease: emerging themes. Curr Opin Genet Dev 2014; 26C:16-23; http://dx.doi.org/10.1016/j.gde.2014.04.003

[90] Katsuragi Y, Ichimura Y, Komatsu M. p62/SQSTM1 functions as a signaling hub and an autophagy adaptor. FEBS J 2015; 282:4672-8; PMID:26432171; http://dx.doi.org/10.1111/febs.13540

[91] Schmauch C, Claussner S, Zoltzer H, Maniak M. Targeting the actin-binding protein VASP to late endosomes induces the formation of giant actin aggregates. Eur J Cell Biol 2009; 88:385-96; PMID:19324455; http://dx.doi.org/10.1016/j.ejcb.2009.02.185

[92] Maselli AG, Davis R, Furukawa R, Fechheimer M. Formation of Hirano bodies in Dictyostelium and mammalian cells induced by expression of a modified form of an actin-crosslinking protein. J Cell Sci 2002; 115:1939-49; PMID:11956325

[93] Kim DH, Davis RC, Furukawa R, Fechheimer M. Autophagy contributes to degradation of Hirano bodies. Autophagy 2009; 5:44-51; PMID:18989098; http://dx.doi.org/10.4161/auto.5.1.7228

[94] Rampoldi L, Dobson-Stone C, Rubio JP, Danek A, Chalmers RM, Wood NW, Verellen C, Ferrer X, Malandrini A, Fabrizi GM, et al. A conserved sorting-associated protein is mutant in chorea-acanthocytosis. Nat Genet 2001; 28:119-20; PMID:11381253; http://dx.doi.org/10.1038/88821

[95] Ueno S, Maruki Y, Nakamura M, Tomemori Y, Kamae K, Tanabe H, Yamashita Y, Matsuda S, Kaneko S, Sano A. The gene encoding a newly discovered protein, chorein, is mutated in chorea-acanthocytosis. Nat Genet 2001; 28:121-2; PMID:11381254; http://dx.doi.org/10.1038/88825

[96] Foller M, Hermann A, Gu S, Alesutan I, Qadri SM, Borst O, Schmidt EM, Schiele F, vom Hagen JM, Saft C, et al. Chorein-sensitive polymerization of cortical actin and suicidal cell death in chorea-acanthocytosis. FASEB J 2012; 26:1526-34; PMID:22227296; http://dx.doi.org/10.1096/fj.11-198317

[97] Alesutan I, Seifert J, Pakladok T, Rheinlaender J, Lebedeva A, Towhid ST, Stournaras C, Voelkl J, Schaffer TE, Lang F. Chorein sensitivity of actin polymerization, cell shape and mechanical stiffness of vascular endothelial cells. Cell Physiol Biochem 2013; 32:728-42; PMID:24080826; http://dx.doi.org/10.1159/000354475

[98] Park JS, Neiman AM. VPS13 regulates membrane morphogenesis during sporulation in Saccharomyces cerevisiae. J Cell Sci 2012; 125:3004-11; PMID:22442115; http://dx.doi.org/10.1242/jcs.105114

[99] Samaranayake HS, Cowan AE, Klobutcher LA. Vacuolar protein sorting protein 13A, TtVPS13A, localizes to the tetrahymena thermophila phagosome membrane and is required for efficient phagocytosis. Eukaryot Cell 2011; 10:1207-18; PMID:21764909; http://dx.doi.org/10.1128/ec.05089-11

[100] Velayos-Baeza A, Vettori A, Copley RR, Dobson-Stone C, Monaco AP. Analysis of the human VPS13 gene family. Genomics 2004; 84:536-49; PMID:15498460; http://dx.doi.org/10.1016/j.ygeno.2004.04.012

[101] Balikova I, Lehesjoki AE, de Ravel TJ, Thienpont B, Chandler KE, Clayton-Smith J, Traskelin AL, Fryns JP, Vermeesch JR. Deletions in the VPS13B (COH1) gene as a cause of Cohen syndrome. Hum Mutat 2009; 30:E845-54; PMID:19533689; http://dx.doi.org/10.1002/humu.21065

[102] Wang L, Cheng L, Li NN, Yu WJ, Sun XY, Peng R. Association of four new candidate genetic variants with Parkinson's disease in a Han Chinese population. Am J Med Genet B 2016; 171:342-7; http://dx.doi.org/10.1002/ajmg.b.32410

[103] Duleh SN, Welch MD. WASH and the Arp2/3 complex regulate endosome shape and trafficking. Cytoskeleton 2010; 67:193-206; PMID:20175130

[104] Freeman C, Seaman MN, Reid E. The hereditary spastic paraplegia protein strumpellin: characterisation in neurons and of the effect of disease mutations on WASH complex assembly and function. Biochim Biophys Acta 2013; 1832:160-73; PMID:23085491; http://dx.doi.org/10.1016/j.bbadis.2012.10.011

[105] Zavodszky E, Seaman MN, Moreau K, Jimenez-Sanchez M, Breusegem SY, Harbour ME, Rubinsztein DC. Mutation in VPS35 associated with Parkinson's disease impairs WASH complex association and inhibits autophagy. Nat Commun 2014; 5:3828; PMID:24819384; http://dx.doi.org/10.1038/ncomms4828

[106] Xia P, Wang S, Du Y, Zhao Z, Shi L, Sun L, Huang G, Ye B, Li C, Dai Z, et al. WASH inhibits autophagy through suppression of Beclin 1 ubiquitination. EMBO J 2013; 32:2685-96; PMID:23974797; http://dx.doi.org/10.1038/emboj.2013.189

[107] Sarkar S. Regulation of autophagy by mTOR-dependent and mTOR-independent pathways: autophagy dysfunction in neurodegenerative diseases and therapeutic application of autophagy enhancers. Biochem Soc Trans 2013; 41:1103-30; PMID:24059496; http://dx.doi.org/10.1042/BST20130134

[108] Francione L, Smith PK, Accari SL, Taylor PE, Bokko PB, Bozzaro S, Beech PL, Fisher PR. Legionella pneumophila multiplication is enhanced by chronic AMPK signalling in mitochondrially diseased Dictyostelium cells. Dis Model Mech 2009; 2:479-89; PMID:19638422; http://dx.doi.org/10.1242/dmm.003319

[109] Carilla-Latorre S, Gallardo ME, Annesley SJ, Calvo-Garrido J, Grana O, Accari SL, Smith PK, Valencia A, Garesse R, Fisher PR, et al. MidA is a putative methyltransferase that is required for mitochondrial complex I function. J Cell Sci 2010; 123:1674-83; PMID:20406883; http://dx.doi.org/10.1242/jcs.066076

[110] Carilla-Latorre S, Annesley SJ, Munoz-Braceras S, Fisher PR, Escalante R. Ndufaf5 deficiency in the Dictyostelium model: new roles in autophagy and development. Mol Biol Cell 2013; 24:1519-28; PMID:23536703; http://dx.doi.org/10.1091/mbc.E12-11-0796

[111] Peng M, Ostrovsky J, Kwon YJ, Polyak E, Licata J, Tsukikawa M, Marty E, Thomas J, Felix CA, Xiao R, et al. Inhibiting cytosolic translation and autophagy improves health in mitochondrial disease. Hum Mol Genet 2015; 24:4829-47; PMID:26041819; http://dx.doi.org/10.1093/hmg/ddv207

[112] Moran M, Delmiro A, Blazquez A, Ugalde C, Arenas J, Martin MA. Bulk autophagy, but not mitophagy, is increased in cellular model of mitochondrial disease. Biochim Biophys Acta 2014; 1842:1059-70; PMID:24704045; http://dx.doi.org/10.1016/j.bbadis.2014.03.013

[113] Escoll P, Rolando M, Buchrieser C. Modulation of host autophagy during bacterial infection: Sabotaging host munitions for pathogen nutrition. Frontiers Immunol 2016; 7:81; http://dx.doi.org/10.3389/fimmu.2016.00081

[114] Sillo A, Matthias J, Konertz R, Bozzaro S, Eichinger L. Salmonella typhimurium is pathogenic for Dictyostelium cells and subverts the starvation response. Cell Microbiol 2011; 13:1793-811; PMID:21824247; http://dx.doi.org/10.1111/j.1462-5822.2011.01662.x

[115] Pflaum K, Gerdes K, Yovo K, Callahan J, Snyder ML. Lipopolysaccharide induction of autophagy is associated with enhanced bactericidal activity in Dictyostelium discoideum. Biochem Biophys Res Commun 2012; 422:417-22; PMID:22575510; http://dx.doi.org/10.1016/j.bbrc.2012.05.006

[116] Lampe EO, Brenz Y, Herrmann L, Repnik U, Griffiths G, Zingmark C, Sjostedt A, Winther-Larsen HC, Hagedorn M. Dissection of Francisella - host cell interactions in Dictyostelium discoideum. Appl Environ Microbiol 2015; 82:1586-98; PMID:26712555; http://dx.doi.org/10.1128/aem.02950-15

[117] Barisch C, Paschke P, Hagedorn M, Maniak M, Soldati T. Lipid droplet dynamics at early stages of Mycobacterium marinum infection in Dictyostelium. Cell Microbiol 2015; 17:1332-49; PMID:25772333; http://dx.doi.org/10.1111/cmi.12437

[118] Kolonko M, Geffken AC, Blumer T, Hagens K, Schaible UE, Hagedorn M. WASH-driven actin polymerization is required for efficient mycobacterial phagosome maturation arrest. Cell Microbiol 2014; 16:232-46; PMID:24119059; http://dx.doi.org/10.1111/cmi.12217

[119] Schiebler M, Brown K, Hegyi K, Newton SM, Renna M, Hepburn L, Klapholz C, Coulter S, Obregon-Henao A, Henao Tamayo M, et al. Functional drug screening reveals anticonvulsants as enhancers of mTOR-independent autophagic killing of Mycobacterium tuberculosis through inositol depletion. EMBO Mol Med 2014; 7:127-39; PMID:25535254; http://dx.doi.org/10.15252/emmm.201404137

[120] Jaiswal P, Soldati T, Thewes S, Baskar R. Regulation of aggregate size and pattern by adenosine and caffeine in cellular slime molds. BMC Dev Biol 2012; 12:5; PMID:22269093; http://dx.doi.org/10.1186/1471-213X-12-5

[121] Kicka S, Trofimov V, Harrison C, Ouertatani-Sakouhi H, McKinney J, Scapozza L, Hilbi H, Cosson P, Soldati T. Establishment and validation of whole-cell based fluorescence assays to identify anti-mycobacterial compounds using the Acanthamoeba castellanii-Mycobacterium marinum host-pathogen system. PLoS ONE 2014; 9:e87834; PMID:24498207; http://dx.doi.org/10.1371/journal.pone.0087834

[122] Swer PB, Lohia R, Saran S. Analysis of rapamycin induced autophagy in Dictyostelium discoideum. Indian J Exp Biol 2014; 52:295-304; PMID:24772931

[123] Tobin DM, Ramakrishnan L. Comparative pathogenesis of Mycobacterium marinum and Mycobacterium tuberculosis. Cell Microbiol 2008; 10:1027-39; PMID:18298637; http://dx.doi.org/10.1111/j.1462-5822.2008.01133.x

[124] Lerena MC, Colombo MI. Mycobacterium marinum induces a marked LC3 recruitment to its containing phagosome that depends on a functional ESX-1 secretion system. Cell Microbiol 2011; 13:814-35; PMID:21447143; http://dx.doi.org/10.1111/j.1462-5822.2011.01581.x

[125] van der Vaart M, Korbee CJ, Lamers GE, Tengeler AC, Hosseini R, Haks MC, Ottenhoff TH, Spaink HP, Meijer AH. The DNA damage-regulated autophagy modulator DRAM1 links mycobacterial recognition via TLP-MYD88 to authophagic defense. Cell Host Microbe 2014; 15:753-67; PMID:24922577; http://dx.doi.org/10.1016/j.chom.2014.05.005

[126] Sato E, Imafuku S, Ishii K, Itoh R, Chou B, Soejima T, Nakayama J, Hiromatsu K. Vitamin D-dependent cathelicidin inhibits Mycobacterium marinum infection in human monocytic cells. Journal Dermatol Sci 2013; 70:166-72; http://dx.doi.org/10.1016/j.jdermsci.2013.01.011

[127] Hosseini R, Lamers GE, Hodzic Z, Meijer AH, Schaaf MJ, Spaink HP. Correlative light and electron microscopy imaging of autophagy in a zebrafish infection model. Autophagy 2014; 10:1844-57; PMID:25126731; http://dx.doi.org/10.4161/auto.29992

[128] Mohanty S, Jagannathan L, Ganguli G, Padhi A, Roy D, Alaridah N, Saha P, Nongthomba U, Godaly G, Gopal RK, et al. A mycobacterial phosphoribosyltransferase promotes bacillary survival by inhibiting oxidative stress and autophagy pathways in macrophages and zebrafish. J Biol Chem 2015; 290:13321-43; PMID:25825498; http://dx.doi.org/10.1074/jbc.M114.598482

[129] Watson RO, Manzanillo PS, Cox JS. Extracellular M. tuberculosis DNA targets bacteria for autophagy by activating the host DNA-sensing pathway. Cell 2012; 150:803-15; PMID:22901810; http://dx.doi.org/10.1016/j.cell.2012.06.040

[130] Collins CA, De Maziere A, van Dijk S, Carlsson F, Klumperman J, Brown EJ. Atg5-independent sequestration of ubiquitinated mycobacteria. PLoS Pathog 2009; 5:e1000430; PMID:19436699; http://dx.doi.org/10.1371/journal.ppat.1000430

[131] Smith J, Manoranjan J, Pan M, Bohsali A, Xu J, Liu J, McDonald KL, Szyk A, LaRonde-LeBlanc N, Gao LY. Evidence for pore formation in host cell membranes by ESX-1-secreted ESAT-6 and its role in Mycobacterium marinum escape from the vacuole. Infect Immun 2008; 76:5478-87; PMID:18852239; http://dx.doi.org/10.1128/iai.00614-08

[132] Hagedorn M, Rohde KH, Russell DG, Soldati T. Infection by tubercular mycobacteria is spread by nonlytic ejection from their amoeba hosts. Science 2009; 323:1729-33; PMID:19325115; http://dx.doi.org/10.1126/science.1169381

[133] Hagedorn M, Soldati T. Flotillin and RacH modulate the intracellular immunity of Dictyostelium to Mycobacterium marinum infection. Cell Microbiol 2007; 9:2984; http://dx.doi.org/10.1111/j.1462-5822.2007.01064.x

[134] Checroun C, Wehrly TD, Fischer ER, Hayes SF, Celli J. Autophagy-mediated reentry of Francisella tularensis into the endocytic compartment after cytoplasmic replication. Proc Natl Acad Sci U S A 2006; 103:14578-83; PMID:16983090; http://dx.doi.org/10.1073/pnas.0601838103

[135] Steele S, Brunton J, Ziehr B, Taft-Benz S, Moorman N, Kawula T. Francisella tularensis Harvests Nutrients Derived via ATG5-Independent Autophagy to Support Intracellular Growth. PLoS Pathog 2013; 9:e1003562; PMID:23966861; http://dx.doi.org/10.1371/journal.ppat.1003562

[136] Otto GP, Wu MY, Clarke M, Lu H, Anderson OR, Hilbi H, Shuman HA, Kessin RH. Macroautophagy is dispensable for intracellular replication of Legionella pneumophila in Dictyostelium discoideum. Mol Microbiol 2004; 51:63-72; PMID:14651611; http://dx.doi.org/10.1046/j.1365-2958.2003.03826.x

[137] Choy A, Dancourt J, Mugo B, O'Connor TJ, Isberg RR, Melia TJ, Roy CR. The Legionella effector RavZ inhibits host autophagy through irreversible Atg8 deconjugation. Science 2012; 338:1072-6; PMID:23112293; http://dx.doi.org/10.1126/science.1227026

[138] Mack HI, Zheng B, Asara JM, Thomas SM. AMPK-dependent phosphorylation of ULK1 regulates ATG9 localization. Autophagy 2012; 8:1197-214; PMID:22932492; http://dx.doi.org/10.4161/auto.20586

[139] LaRock DL, Chaudhary A, Miller SI. Salmonellae interactions with host processes. Nat Rev Microbiol 2015; 13:191-205; PMID:25749450; http://dx.doi.org/10.1038/nrmicro3420

[140] Garai P, Gnanadhas DP, Chakravortty D. Salmonella enterica serovars Typhimurium and Typhi as model organisms: revealing

paradigm of host-pathogen interactions. Virulence 2012; 3:377-88; PMID:22722237; http://dx.doi.org/10.4161/viru.21087

[141] Skriwan C, Fajardo M, Hagele S, Horn M, Wagner M, Michel R, Krohne G, Schleicher M, Hacker J, Steinert M. Various bacterial pathogens and symbionts infect the amoeba Dictyostelium discoideum. Int J Med Microbiol 2002; 291:615-24; PMID:12008915; http://dx.doi.org/10.1078/1438-4221-00177

[142] Jia K, Thomas C, Akbar M, Sun Q, Adams-Huet B, Gilpin C, Levine B. Autophagy genes protect against Salmonella typhimurium infection and mediate insulin signaling-regulated pathogen resistance. Proc Natl Acad Sci U S A 2009; 106:14564-9; PMID:19667176; http://dx.doi.org/10.1073/pnas.0813319106

[143] Mestre MB, Fader CM, Sola C, Colombo MI. Alpha-hemolysin is required for the activation of the autophagic pathway in Staphylococcus aureus-infected cells. Autophagy 2010; 6:110-25; PMID:20110774; http://dx.doi.org/10.4161/auto.6.1.10698

[144] Schnaith A, Kashkar H, Leggio SA, Addicks K, Kronke M, Krut O. Staphylococcus aureus subvert autophagy for induction of caspase-independent host cell death. J Biol Chem 2007; 282:2695-706; PMID:17135247; http://dx.doi.org/10.1074/jbc.M609784200

[145] O'Keeffe KM, Wilk MM, Leech JM, Murphy AG, Laabei M, Monk IR, Massey RC, Lindsay JA, Foster TJ, Geoghegan JA, et al. Manipulation of Autophagy in Phagocytes Facilitates Staphylococcus aureus Bloodstream Infection. Infect Immun 2015; 83:3445-57; PMID:26099586; http://dx.doi.org/10.1128/iai.00358-15

[146] Klionsky DJ, Abdelmohsen K, Abe A, Abedin MJ, Abeliovich H, Acevedo Arozena A, Adachi H, Adams CM, Adams PD, Adeli K, et al. Guidelines for the use and interpretation of assays for monitoring autophagy (3rd edition). Autophagy 2016; 12:1-222; PMID:26799652; http://dx.doi.org/10.1080/15548627.2015.1100356

[147] Golstein P, Aubry L, Levraud JP. Cell-death alternative model organisms: why and which? Nature Rev Mol Cell Biol 2003; 4:798-807; http://dx.doi.org/10.1038/nrm1224

[148] Whittingham WF, Raper KB. Non-viability of stalk cells in Dictyostelium. Proc Natl Acad Sci USA 1960; 46:642-9; PMID:16590653; http://dx.doi.org/10.1073/pnas.46.5.642

[149] Kay RR. Cell differentiation in monolayers and the investigation of slime mold morphogens. Methods Cell Biol 1987; 28:433-48; PMID:3600415; http://dx.doi.org/10.1016/S0091-679X(08)61661-1

[150] Cornillon S, Foa C, Davoust J, Buonavista N, Gross JD, Golstein P. Programmed cell death in Dictyostelium. J Cell Sci 1994; 107:2691-704; PMID:7876338

[151] Giusti C, Tresse E, Luciani MF, Golstein P. Autophagic cell death: analysis in Dictyostelium. Biochim Biophys Acta 2009; 1793:1422-31; PMID:19133302; http://dx.doi.org/10.1016/j.bbamcr.2008.12.005

[152] Morris HR, Taylor GW, Masento MS, Jermyn KA, Kay RR. Chemical structure of the morphogen differentiation inducing factor from Dictyostelium discoideum. Nature 1987; 328:811-4; PMID:3627228; http://dx.doi.org/10.1038/328811a0

[153] Luciani MF, Giusti C, Harms B, Oshima Y, Kikuchi H, Kubohara Y, Golstein P. Atg1 allows second-signaled autophagic cell death in Dictyostelium. Autophagy 2011; 7:501-8; PMID:21301205; http://dx.doi.org/10.4161/auto.7.5.14957

[154] Kosta A, Roisin-Bouffay C, Luciani MF, Otto GP, Kessin RH, Golstein P. Autophagy gene disruption reveals a non-vacuolar cell death pathway in Dictyostelium. J Biol Chem 2004; 279:48404-9; PMID:15358773; http://dx.doi.org/10.1074/jbc.M408924200

[155] Kosta A, Laporte C, Lam D, Tresse E, Luciani MF, Golstein P. How to assess and study cell death in Dictyostelium discoideum. Methods Mol Biol 2006; 346:535-50; PMID:16957313

[156] Laporte C, Kosta A, Klein G, Aubry L, Lam D, Tresse E, Luciani MF, Golstein P. A necrotic cell death model in a protist. Cell Death

Differ 2007; 14:266-74; PMID:16810325; http://dx.doi.org/10.1038/sj.cdd.4401994

[157] Giusti C, Luciani MF, Klein G, Aubry L, Tresse E, Kosta A, Golstein P. Necrotic cell death: From reversible mitochondrial uncoupling to irreversible lysosomal permeabilization. Exp Cell Res 2009; 315:26-38; PMID:18951891; http://dx.doi.org/10.1016/j.yexcr.2008.09.028

[158] Luciani MF, Kubohara Y, Kikuchi H, Oshima Y, Golstein P. Autophagic or necrotic cell death triggered by distinct motifs of the differentiation factor DIF-1. Cell Death Differ 2009; 16:564-70; PMID:19079140; http://dx.doi.org/10.1038/cdd.2008.177

[159] Shaulsky G, Loomis WF. Mitochondrial DNA replication but no nuclear DNA replication during development of Dictyostelium. Proc Natl Acad Sci USA 1995; 92:5660-3; PMID:7777565; http://dx.doi.org/10.1073/pnas.92.12.5660

[160] Sugden C, Urbaniak MD, Araki T, Williams JG. The Dictyostelium prestalk inducer differentiation-inducing factor-1 (DIF-1) triggers unexpectedly complex global phosphorylation changes. Mol Biol Cell 2015; 26:805-20; PMID:25518940; http://dx.doi.org/10.1091/mbc.E14-08-1319

[161] Lam D, Golstein P. A specific pathway inducing autophagic cell death is marked by an IP3R mutation. Autophagy 2008; 4:349-50; PMID:18196962; http://dx.doi.org/10.4161/auto.5521

[162] Tresse E, Kosta A, Giusti C, Luciani MF, Golstein P. A UDP-glucose derivative is required for vacuolar autophagic cell death. Autophagy 2008; 4:680-91; PMID:18424909; http://dx.doi.org/10.4161/auto.6084

[163] Giusti C, Luciani MF, Ravens S, Gillet A, Golstein P. Autophagic cell death in Dictyostelium requires the receptor histidine kinase DhkM. Mol Biol Cell 2010; 21:1825-35; PMID:20375146; http://dx.doi.org/10.1091/mbc.E09-11-0976

[164] Chen ZH, Schaap P. The prokaryote messenger c-di-GMP triggers stalk cell differentiation in Dictyostelium. Nature 2012; 488:680-3; PMID:22864416; http://dx.doi.org/10.1038/nature11313

[165] Chen ZH, Schaap P. Secreted cyclic-di-GMP induces stalk cell differentiation in the eukaryote Dictyostelium discoideum. J Bacteriol 2016; 198:27-31; PMID:26013485; http://dx.doi.org/10.1128/jb.00321-15

[166] Romling U, Galperin MY, Gomelsky M. Cyclic di-GMP: the first 25 years of a universal bacterial second messenger. Microbiol Mol Biol Rev 2013; 77:1-52; PMID:23471616; http://dx.doi.org/10.1128/mmbr.00043-12

[167] Danilchanka O, Mekalanos JJ. Cyclic dinucleotides and the innate immune response. Cell 2013; 154:962-70; PMID:23993090; http://dx.doi.org/10.1016/j.cell.2013.08.014

[168] Song Y, Luciani MF, Giusti C, Golstein P. c-di-GMP induction of Dictyostelium cell death requires the polyketide DIF-1. Mol Biol Cell 2015; 26:651-8; PMID:25518941; http://dx.doi.org/10.1091/mbc.E14-08-1337

[169] Thompson CRL, Kay RR. The role of DIF-1 signaling in Dictyostelium development. Mol Cell 2000; 6:1509-14; PMID:11163223; http://dx.doi.org/10.1016/S1097-2765(00)00147-7

[170] Saito T, Kato A, Kay RR. DIF-1 induces the basal disc of the Dictyostelium fruiting body. Dev Biol 2008; 317:444-53; PMID:18402932; http://dx.doi.org/10.1016/j.ydbio.2008.02.036

[171] Parvatiyar K, Zhang Z, Teles RM, Ouyang S, Jiang Y, Iyer SS, Zaver SA, Schenk M, Zeng S, Zhong W, et al. The helicase DDX41 recognizes the bacterial secondary messengers cyclic di-GMP and cyclic di-AMP to activate a type I interferon immune response. Nat Immunol 2012; 13:1155-61; PMID:23142775; http://dx.doi.org/10.1038/ni.2460

[172] Chou SH, Galperin MY. Diversity of c-di-GMP-binding proteins and mechanisms. J Bacteriol 2015; 198:32-46; http://dx.doi.org/10.1128/jb.00333-15

The Unfolded Protein Response Pathway in the Yeast *Kluyveromyces lactis*. A Comparative View among Yeast Species

Mariana Hernández-Elvira [1] , **Francisco Torres-Quiroz** [2] , **Abril Escamilla-Ayala** [3],
Eunice Domínguez-Martin [1] , **Ricardo Escalante** [4], **Laura Kawasaki** [1], **Laura Ongay-Larios** [5] and
Roberto Coria [1,*]

1   Departamento de Genética Molecular, Instituto de Fisiología Celular, Universidad Nacional Autónoma de México, 04510 Mexico City, Mexico; melvira@email.ifc.unam.mx (M.H.-E.); edominguez@email.ifc.unam.mx (E.D.-M.); lkawasak@ifc.unam.mx (L.K.)

2   Departamento de Bioquímica y Biología Estructural, Instituto de Fisiología Celular, Universidad Nacional Autónoma de México, 04510 Mexico City, Mexico; ftq@ifc.unam.mx

3   Laboratory for Membrane Trafficking, VIB-KU Leuven Center for Brain & Disease Research and Department of Neurosciences, KU Leuven, 3000 Leuven, Belgium; abril.escamillaayala@kuleuven.vib.be

4   Instituto de Investigaciones Biomédicas "Alberto Sols" (CSIC-UAM), Arturo Duperier 4, 28029 Madrid, Spain; rescalante@iib.uam.es

5   Unidad de Biología Molecular, Instituto de Fisiología Celular, Universidad Nacional Autónoma de México, 04510 Mexico City, Mexico; longay@ifc.unam.mx

*   Correspondence: rcoria@ifc.unam.mx; Tel.: +52-55-56-22-56-52

Abstract: Eukaryotic cells have evolved signalling pathways that allow adaptation to harmful conditions that disrupt endoplasmic reticulum (ER) homeostasis. When the function of the ER is compromised in a condition known as ER stress, the cell triggers the unfolded protein response (UPR) in order to restore ER homeostasis. Accumulation of misfolded proteins due to stress conditions activates the UPR pathway. In mammalian cells, the UPR is composed of three branches, each containing an ER sensor (PERK, ATF6 and IRE1). However, in yeast species, the only sensor present is the inositol-requiring enzyme Ire1. To cope with unfolded protein accumulation, Ire1 triggers either a transcriptional response mediated by a transcriptional factor that belongs to the bZIP transcription factor family or an mRNA degradation process. In this review, we address the current knowledge of the UPR pathway in several yeast species: *Saccharomyces cerevisiae*, *Schizosaccharomyces pombe*, *Candida glabrata*, *Cryptococcus neoformans*, and *Candida albicans*. We also include unpublished data on the UPR pathway of the budding yeast *Kluyveromyces lactis*. We describe the basic components of the UPR pathway along with similarities and differences in the UPR mechanism that are present in these yeast species.

Keywords: yeast; endoplasmic reticulum; stress; UPR; Ire1; Hac1; Kar2

1. Introduction

Secreted and transmembrane proteins are synthesised in ribosomes that are attached to the endoplasmic reticulum (ER) membrane and are co-translationally processed and folded in the lumen of this organelle. Protein folding is accomplished by chemical modification, including the addition of oligosaccharides (*N*-glycosylation) and formation of disulphide bonds. These modifications are essential for the proper function of the proteins. Certain physiological, environmental, or pathogenic conditions can cause the accumulation of unfolded proteins, generating a condition known as ER stress.

Experimentally, ER stress is induced by treatment with agents that either inhibit *N*-glycosylation, such as tunicamycin (Tn) or 2-deoxyglucose (2-DOG), or agents that disrupt the formation of disulphide bonds such as dithiothreitol (DTT) and β-mercaptoethanol (β-ME). In order to respond to these harmful conditions, eukaryotic organisms activate a conserved signalling pathway termed the unfolded protein response (UPR). Many components and mechanisms of this pathway are conserved between species and they are dedicated to restoring ER homeostasis by increasing protein folding capacity and by decreasing the load of new proteins arriving to the ER. In metazoans, the UPR has three branches, each one named after the protein involved in sensing the ER stress stimulus. They are known as IRE1 (inositol-requiring enzyme 1), PERK (protein kinase RNA-like endoplasmic reticulum kinase) and ATF6 (activating transcription factor 6). The presence of these branches is species-dependent; however, the most conserved component of the UPR is the IRE1 branch, which is present in all eukaryotes including yeasts and the social amoeba *Dictyostelium discoideum* [1,2].

The IRE1 branch is composed by Ire1, that acts as a sensor of the ER stress. Under ER stress, Ire1 processes the mRNA of a bZIP transcription factor (in most cases known as Hac1). Once synthesised, the transcription factor is transported into the nucleus where it regulates transcription of a variety of genes such as those that encode chaperones, post-translational modification enzymes and proteins for proteolytic degradation. This pathway was initially described in *Saccharomyces cerevisiae*, and it was later detected in other yeast species, but it is not universally conserved among yeasts. For instance, the fission yeast *Schizosaccharomyces pombe* lacks a Hac1 orthologue and the UPR does not consist of a transcriptional response; instead, Ire1 triggers an ER-targeted mRNAs decay pathway. In this review, we describe the current knowledge regarding the UPR in several yeast species, namely *S. cerevisiae*, *S. pombe*, *Candida glabrata*, *Cryptoccocus neoformans* and *Candida albicans*. In the third section, we present original data (obtained in our group) regarding the UPR in *Kluyveromyces lactis*. To our knowledge, this is the first review that describes the UPR of these six yeast species and we expect that it will be of great interest to researchers in the field.

2. The UPR in *Saccharomyces cerevisiae*

The IRE1 pathway was initially described in *S. cerevisiae*. In this system the *Sc*Ire1 protein has been extensively characterised. In this work we do not intend to describe in detail all the information accumulated regarding *Sc*Ire1, due to space limitations; we will simply refer to the general characteristics that are relevant to this review. *Sc*Ire1 is a 1115 amino acid residue transmembrane protein (Figure 1). This protein has a sensor domain at its N-terminus that lies inside the lumen and interacts with unfolded proteins, while its C-terminus lies in the cytosol and contains a serine-threonine kinase domain and an endoribonuclease domain [3,4]. A single transmembrane segment that lies in a region with very low similarity to the Ire1 of other yeast species connects the luminal N-terminal sensor domain with the cytoplasmic kinase and endoribonuclease domains (Figure 1). The activity of *Sc*Ire1 is regulated by the ER-luminal resident chaperone *Sc*Kar2 (BiP) (see below). Briefly, *Sc*Kar2 is bound to the N-terminus of *Sc*Ire1 under normal conditions and dissociates in response to ER stress [5,6]. Dissociation of *Sc*Kar2 leads to *Sc*Ire1 dimerisation and ultimately to its oligomerisation by binding to unfolded proteins through its core stress-sensing region (CSSR) located in the sensor domain [7–9]. The crystal structure of the *S. cerevisiae* CSSR suggests that it is able to form a groove similar to that present in the histocompatibility complex where the unfolded proteins may be captured [7]. The interaction with unfolded proteins may be essential for *Sc*Ire1 activation [10].

*Sc*Ire1 was initially isolated as essential for growth in the absence of inositol [11]. It was later determined that the null mutant was lethal in the presence of ER stress inducers [12]. An *S. cerevisiae* mutant lacking Ire1 is auxotrophic for inositol because it is unable to induce adequate expression of Ino1, the inositol-1-phosphate synthase that constitutes the rate-limiting step in the *de novo* inositol biosynthesis pathway [11,13]. The absence of inositol induces the UPR in wild-type yeast cells, and treatment with Tn induces *INO1* expression in an *Sc*Ire1-dependent manner [14]. *Sc*Ire1 is not required

for cell growth in normal conditions but it is essential for growth in the presence of ER stress inducers such as Tn and β-ME [14,15].
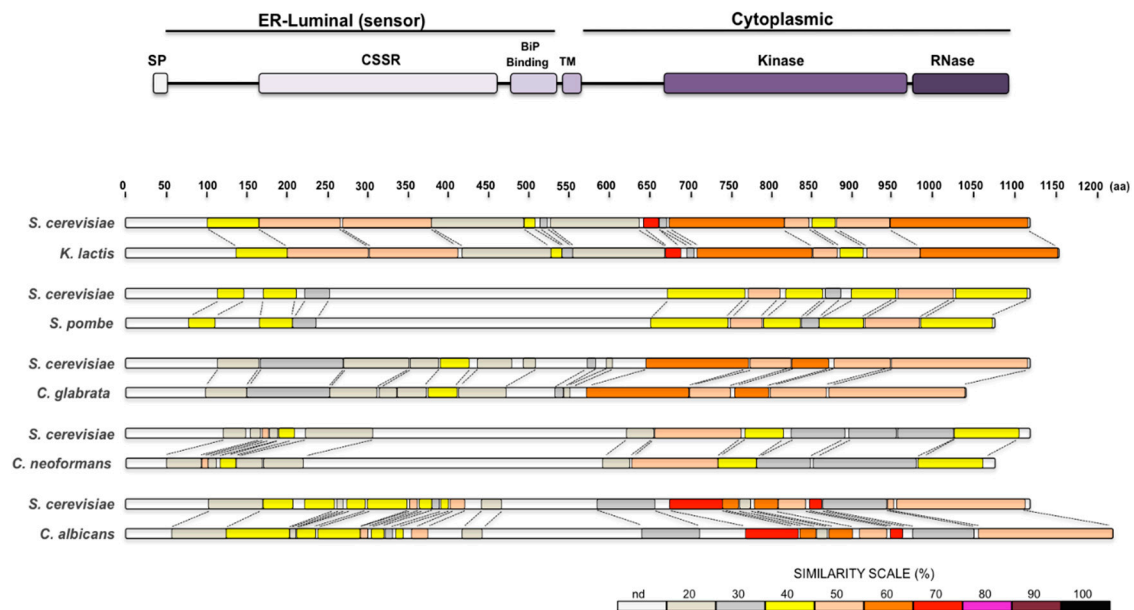

Figure 1. (**Top**) Diagram of the Ire1 protein structure. Signal Peptide (SP), Core Stress Sensing Region (CSSR), BiP Binding domain, Transmembrane segment (TM), and the Kinase and RNase domains were deduced from the *S. cerevisiae* Ire1 protein. (**Bottom**) Pairwise alignments between the *S. cerevisiae*, *K. lactis*, *S. pombe*, *C. glabrata*, *C. neoformans* and *C. albicans*, Ire1 orthologues. The Ire1 protein of each species is compared to the *S. cerevisiae* one. Protein sequences were analysed with SIM local alignment tool and results were visualized with LALNVIEW. Protein schemes are drawn to scale.

Mutations that affect either the groove where unfolded peptides bind ($M^{229}A$, $F^{285}A$, $Y^{301}A$) or those that affect oligomerisation and clustering ($F^{247}A$, $W^{426}A$) affect the response to ER stress-inducing agents [9,10]. Additionally, mutations that substitute K^{702} and N^{1057} abolish kinase and RNase activities respectively and also affect growth in ER stress inducers [3,16–18]. These data indicate that in *S. cerevisiae* all three Ire1 activities, i.e., the unfolded protein sensor, the kinase activity and the RNase activity, are essential for Ire1 function in the UPR pathway and required for proper ER stress response.

Once *Sc*Ire1 is active, it, in turn, activates the transcription factor Hac1p, which comprises 238 amino acids and belongs to the basic-leucine zipper (bZIP) family. It contains a basic DNA binding region of 21 amino acids followed by a leucine zipper motif of 20 amino acids (Figure 2) [19]. In the presence of ER stress, *Sc*Hac1 binds as a homodimer to promoters of UPR targets [19,20] in sequences known as UPRE (unfolded protein response element) motifs. It has been proposed that *Sc*Hac1 binds to long and short UPREs (see below) through at least two different mechanisms, allowing a wide regulation of UPR gene transcription [20]. Conserved N and R residues within the basic DNA binding region of *Sc*Hac1 are essential for recognition of palindromic or semi-palindromic UPRE DNA target sites (Figure 2). These residues make direct contact with the major groove of DNA [21,22]. A lack of Hac1 does not compromise cell growth in normal conditions but it does cause sensitivity to ER-stress-inducing drugs such as Tn and DTT, and also to caffeine [23], and as in the case of an *Sc*Ire1 null mutant, a lack of *Sc*Hac1 causes inositol auxotrophy [13,24].

Although the *ScHAC1* precursor mRNA (*HAC1*ᵘ, for uninduced *HAC1*) is constitutively produced, the *Sc*Hac1 protein is not detected [25]. *ScHAC1* mRNA contains an unconventional 252 nucleotide intron near its 3′ end (Figure 3) that is specifically processed only by the RNase domain of *Sc*Ire1 [4,26,27]. *ScHAC1* pre-mRNA contains a translational attenuator that is located near the 5′ end of the intron [26]. The attenuation of translation is exerted by base pairing between the intron

and the 5′ untranslated region, forming a loop structure where the ribosomes are stalled [28,29] (see the analogous mechanism of *K. lactis* attenuation depicted in Section 3). After splicing, the two exons are joined together by the RNA ligase Rlg1, leading to the formation of a mature mRNA (*HAC1^i*, for induced *HAC1*) [13]. This splicing allows the substitution of the last 10 amino acid residues of *Sc*Hac1^u by 18 residues, rendering a protein of 238 amino acids (*Sc*Hac1^i) [25,27]. The novel 18 amino acids at the C-terminus tail of Hac1 function as the transcription transactivation domain [30]. *ScHAC1* mRNA splicing by *Sc*Ire1 is a highly selective and efficient process that is promoted by the binding of pre-mRNA to a docking site formed by a positively charged motif located in the cytosolic linker domain of Ire1. The R^647 and R^650 residues located within this basic motif appear to play an important role in the binding of *HAC1* pre-mRNA [17]. Additionally, *ScHAC1* mRNA forms a stem-loop structure at its 3′ UTR that contains an important component, the 3′ UTR bipartite element (3′BE), which consists of two juxtaposed short motifs located at the distal end of the loop. This stem structure cooperates with the intron stalling structure to target the *ScHAC1* mRNA to the Ire1 oligomer foci in order to allow efficient splicing of the mRNA. The two short motifs are highly conserved in several yeast *HAC1* orthologues [29].
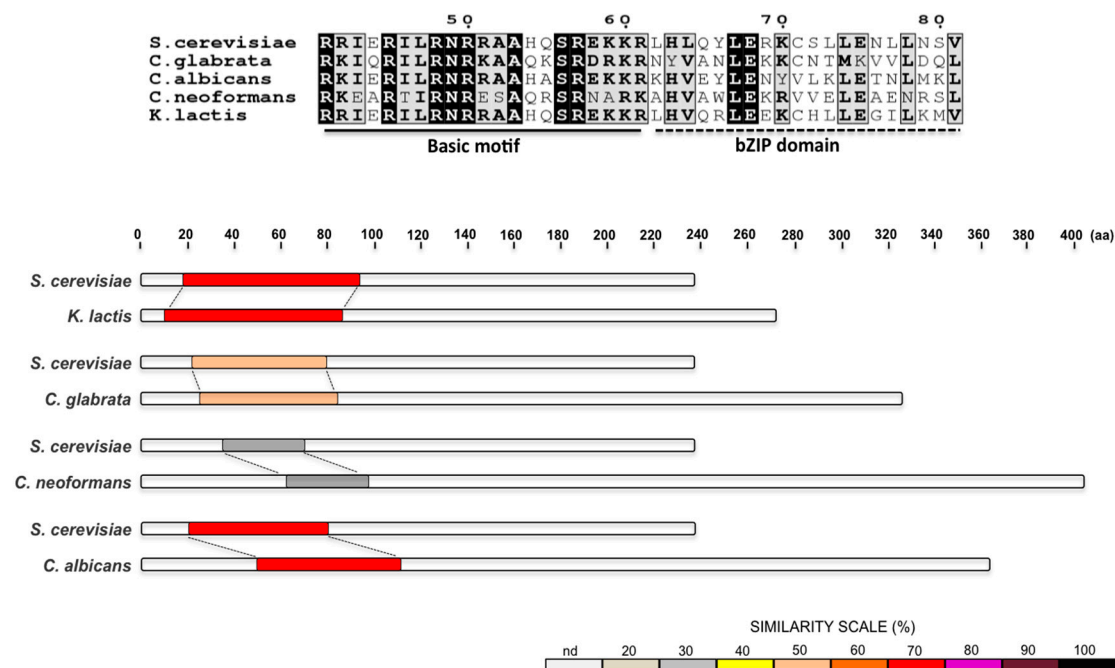
Figure 2. (**Top**) Alignment of the basic motif and the bZIP domain of Hac1 (or Hxl1) of yeast species. Amino acids fully conserved are depicted in black boxes. Amino acid coordinates correspond to the *S. cerevisiae* protein. (**Bottom**) Pairwise alignments between the *S. cerevisiae*, *K. lactis*, *S. pombe*, *C. glabrata*, *C. neoformans* and *C. albicans*, Ire1 orthologues. The Ire1 protein of each species is compared to the *S. cerevisiae* one. Protein sequences were analyzed with SIM local alignment tool and results were visualized with LALNVIEW.

Dissection of promoter sequences in the *ScKAR2* gene allows the identification of a 22-bp unfolded protein response element [31,32] to which *Sc*Hac1 binds directly [19,25]. Within the 22-bp element a central semi-palindromic core of 7 bp (5′-CAGNGTG-3′) known as UPRE-1 motif, is essential for the transcriptional activity of *ScKAR2* under ER stress [19]. The UPRE-1 motif, later determined to comprise from 11 to 13 bp [20], is present in several genes that are UPR targets [33,34]. Genes that are *Sc*Hac1 targets lacking the UPRE-1 motif contain a distinct sequence called UPRE-2 [35]. This sequence is 6 to 7 bp long (5′-TACGTGT-3′) and binds *Sc*Hac1 with high affinity [20].

*Sc*Kar2 is an ER-resident chaperone that belongs to the Hsp70 family. It has an ATPase domain near its N-terminus adjacent to the substrate-binding domain [36]. ATPase activity is required for its

participation in the translocation of proteins across the ER membrane [37]. *Sc*Kar2 also participates in ER-associated protein degradation by maintaining luminal substrates in a retrotranslocation-competent state [38]. *Sc*Kar2 negatively regulates the UPR through its interaction with *Sc*Ire1. Under ER stress conditions, binding of unfolded proteins to *Sc*Kar2 induces its dissociation from *Sc*Ire1, leading to the activation of the UPR pathway [6,39]. *Sc*Kar2 is an essential and abundant protein, the synthesis of which is further induced by the presence of unfolded proteins [32,40].
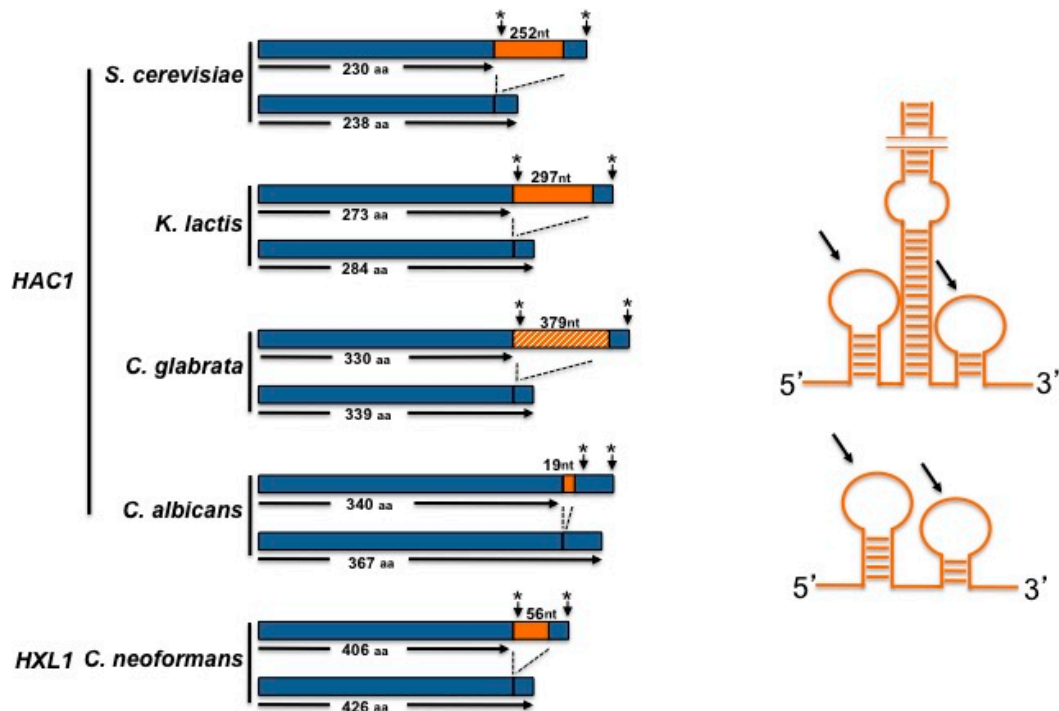
Figure 3. (**Left**) Scheme of un-spliced and spliced *HAC1* (or *HXL1*) RNAs. Sizes of putative protein products from un-spliced and spliced RNAs are depicted. Introns (and their sizes in nucleotides) are shown by the orange boxes. The putative *HAC1* intron of *C. glabrata*, that appears not to be processed is indicated by the slashed box. Stop codons are indicated by asterisk. (**Right**) Scheme of putative stem-loop structures of large and small introns. Arrows indicate 5′ and 3′ exon-intron boundaries. Structures are not drawn to scale.

3. The UPR in *Kluyveromyces lactis*

K. lactis is a biotechnologically important yeast which diverged before the genome duplication that gave rise to the *Saccharomyces* species [41]; thus, it represents a suitable organism for making evolutionary comparisons with *S. cerevisiae*.

The *K. lactis* genome encodes orthologue proteins of the IRE1 branch of the UPR signalling pathway, namely Ire1, Hac1, and Kar2. The KLLA0D13266g ORF of *K. lactis* has been identified as putative homologue of the *IRE1* gene of *S. cerevisiae*. It comprises 3459 nucleotides including the stop codon and codes for a protein of 1152 amino acids. Comparative analysis shows that the putative protein has 48% identity with *Sc*Ire1, and exhibits a structure similar to that of *S. cerevisiae* (Figure 1). From the sequence analysis of *Kl*Ire1, a luminal dimerisation domain at the N-terminal region, a serine/threonine protein kinase catalytic domain, and an endoribonuclease domain located at the C-terminus can be predicted. *Kl*Ire1 conserves the K^{737} and N^{1096} residues, which are essential for the kinase and RNase activities in *S. cerevisiae*. Additionally, *Kl*Ire1 conserves the R residues (673 and 676) that in *S. cerevisiae* participate in the binding of *HAC1* RNA.

Experimental data from our group showed that *Kl*Ire1 is involved in the UPR pathway in *K. lactis*; a *Klire1* mutant is sensitive to ER stress induced by Tn or 2-DOG (Figure 4). However, unlike *S. cerevisiae*,

in *K. lactis IRE1* is not essential for growth in the absence of inositol (Figure 4), indicating that in this species the Ire1 function may differ, or that *K. lactis* may synthesise inositol in the absence of *Kl*Ire1.
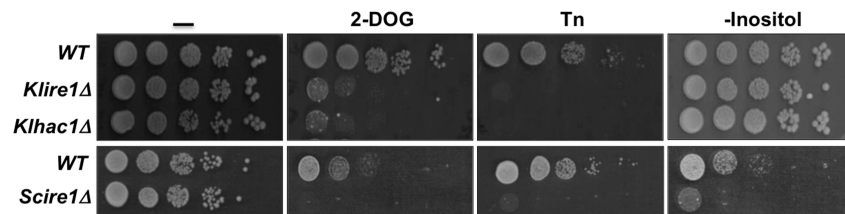

Figure 4. Effect of *IRE1* and *HAC1* inactivation on the *K. lactis* growth properties. *K. lactis* null mutants were obtained by standard homologous recombination introducing in both cases the *URA3* selective cassette. *K. lactis* cells were grown in YPD (1% yeast extract, 2% peptone, and 2% Glucose) until 0.5 OD_{600} then were washed and suspended in fresh YPD. Cells were spotted as 10 fold serial dilutions on YPD plates containing 15 mM 2-DOG or 50 ng/mL Tn and on plates of 2% glucose, 0.5% ammonium sulfate, 0.17% yeast nitrogen base w/o amino acids and w/o inositol. *S. cerevisiae* wild type and *ire1Δ* strains were included as controls. Cells were plated on the same media except that the 2-DOG concentration was 20 mM and the Tn concentration was 500 ng/mL. Plates were incubated at 30 °C and photographed 48 h later.

A *K. lactis HAC1* gene has been identified in the *K. lactis* genome database. *KlHAC1* is a 1152 nucleotide gene that encodes a pre-mRNA formed by two exons of 805 and 50 nucleotides respectively and a long intron of 297 nucleotides (Figure 3), which has been identified as characteristic in several *Saccharomyces* species and some other yeasts [42]. Transcription of the *KlHAC1* gene produces an mRNA that is processed upon ER stress induction. After 30 min of exposure of *K. lactis* cells to 2-DOG, the presence of two forms of the transcript are evident (Figure 5), the larger form corresponds to the unprocessed *KlHAC1* mRNA (*HAC1*[u] mRNA), and the second to the mature form (*HAC1*[i] mRNA). In *K. lactis*, the sequence of the *HAC1*[i] mRNA predicts a 284 amino acids protein that has the features of a bZIP transcriptional factor; namely, a conserved DNA binding domain and a basic leucine zipper domain (Figure 2).
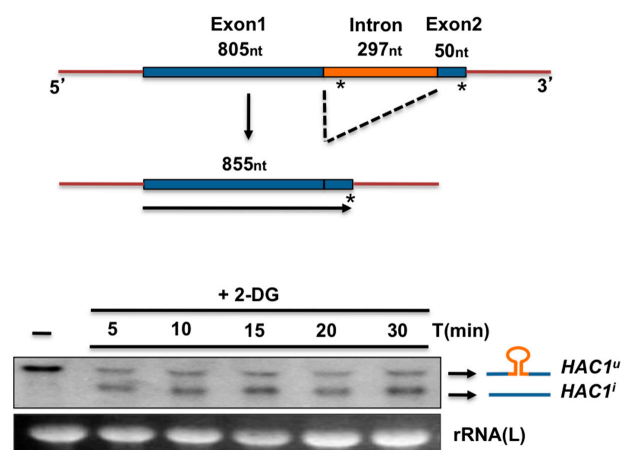

Figure 5. (**Top**) Diagram of the precursor and processed forms of *K. lactis HAC1* RNA. Exon and intron sizes (nucleotides) were determined by sequence analysis. Size of the induced *HAC1* (*HAC1*[i]) includes the stop codon. (**Bottom**) Northern blot analysis of *HAC1* processing. *K. lactis* cells were grown in YPD (1% yeast extract, 2% peptone, and 2% Glucose) until 0.5 OD_{600}. Cells were treated with 20 mM 2-DOG for the indicated times. Total RNA was extracted with the conventional Trizol protocol. Boiled RNA was loaded in a 1% agarose gel, electrophoresed, and transferred to a nylon membrane. The RNA was probed with a fragment containing the first 500 nt of the *HAC1* ORF labelled with ^{32}P and visualized in a phosphorimager. The large rRNA was used as a load control.

Sequence analysis of both the *KlHAC1*[u] and *KlHAC1*[i] revealed that the pre-mRNA contains conserved cleavage motifs at the 5′ and 3′ intron-exon boundaries. Secondary structure analysis showed that these regions are capable of folding in a stem-loop structure (Figure 6). This sort of structure together with the 5′ and 3′ motifs is essential for the recognition and further cleavage of the pre-mRNA. We also found that there is a region in the intron (+909 to +936) that can base-pair with a region in the 5′UTR (−52 to −28) of the mRNA (Figure 6), allowing the formation of a translation attenuation structure like that of the *S. cerevisiae* mRNA and other *HAC1* RNAs with long introns [42,43]. Another interesting feature of the *K. lactis HAC1* mRNA is the presence of a conserved bipartite element, located in the 3′UTR, which in *S. cerevisiae* appears to be important in targeting the mRNA to Ire1 oligomers [29].
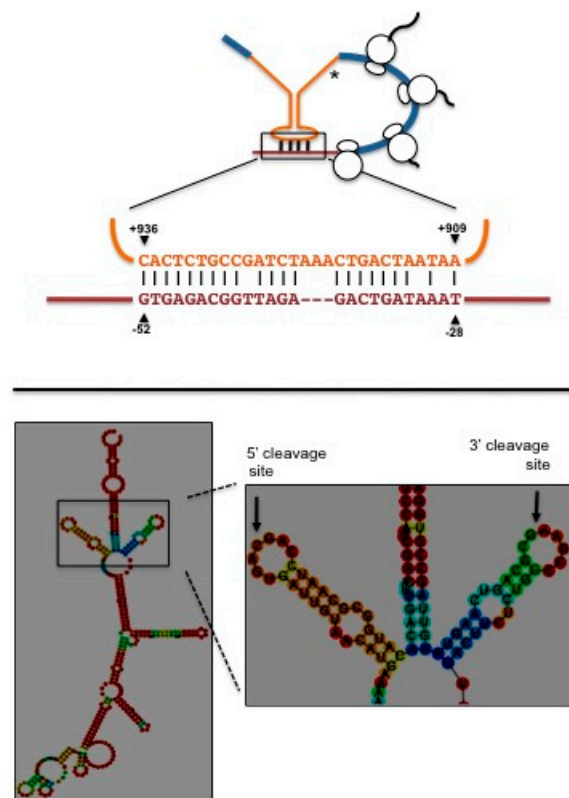
Figure 6. (**Top**) Diagram of a predicted translation attenuation structure formed in the *K. lactis HAC1* pre-mRNA. Exons are indicated in blue, intron is indicated in orange and 5′ untranslated region in brown. Coordinates are relative to the first nucleotide of the translation start codon. Asterisk indicates an in-frame stop codon located within the intron. (**Bottom**) Predicted stem-loop secondary structure of the exon-intron boundaries of *K. lactis HAC1* pre-mRNA. Arrows pinpoint the 5′ and 3′ cleavage sites. The predicted secondary structure was obtained using the RNAfold web server from the ViennaRNA Web Services.

The aforementioned characteristics suggest that *K. lactis HAC1* mRNA is regulated and activated in a similar manner as that of *S. cerevisiae*, and that its translation may be modulated by the regulatory intron which upon ER stress is cleaved by the endonuclease activity of *Kl*Ire1 at the 5′ and 3′ specific splicing sites, and the exons are joined. This would render the *KlHAC1 mRNA* translatable, and the active transcriptional factor Hac1 would be produced.

Like *Kl*Ire1, *Kl*Hac1 is also a key element in the ER stress response pathway of *K. lactis*. A null mutant of *KlHAC1* is sensitive to agents that induce ER stress, such as Tn or 2-DOG (Figure 4). Additionally, as in the case of *KlIRE1*, this gene is dispensable for growth in the absence of inositol (Figure 4).

The *K. lactis KAR2* gene codes for the major ER chaperone, Kar2. The gene was identified by its high similarity with the *S. cerevisiae* gene. It has 2040 nucleotides and predicts a 679 amino acid protein, with 77.3% identity with the *S. cerevisiae* Kar2 [44].

*Kl*Kar2 displays characteristics typical of the Hsp70 type of chaperones such as a hydrophobic leader sequence, and an ER retention signal at its C-terminus, which is important in order to prevent its secretion. In *K. lactis* the retention signal of Kar2 is the tetrapeptide DDLE, while in *S. cerevisiae* it is HDEL; this difference seems to be important for the specificity of the retention system [44,45]. The *K. lactis* Kar2 sequence contains a potential *N*-glycosylation site at the C-terminal region, although it is not known whether it is functional in this budding yeast [45]. Additionally, the *Kl*Kar2 C-terminus shows some sequence conservation with that of *S. pombe* and cross-reacts with an antibody raised against the BiP of this latter species [46].

We found that the *K. lactis KAR*2 gene is upregulated under ER stress. Treatment of *K. lactis* cells with 2-DOG induced over-expression of a GFP reporter gene fused to the *KAR2* promoter (Figure 7). By deletion analyses, we also identified a 211 nucleotide region with promoter activity that responded to 2-DOG induction (from −291 to −479). Within this region, we detected a 22 nucleotide motif (Figure 7) with some identity to the *S. cerevisiae* UPRE [20,31]. Furthermore, inside this motif the heptanucleotide TGACGTG was detected, which exhibits high similarity to UPRE-1 of *S. cerevisiae*. This motif was searched in promoter regions of several *K. lactis* genes that in *S. cerevisiae* have been identified as UPR-responsive genes. This analysis allowed us to identify the consensus sequence T/GG/CANG/CTG/C which may represent the *K. lactis* UPRE responsive element (Figure 8).
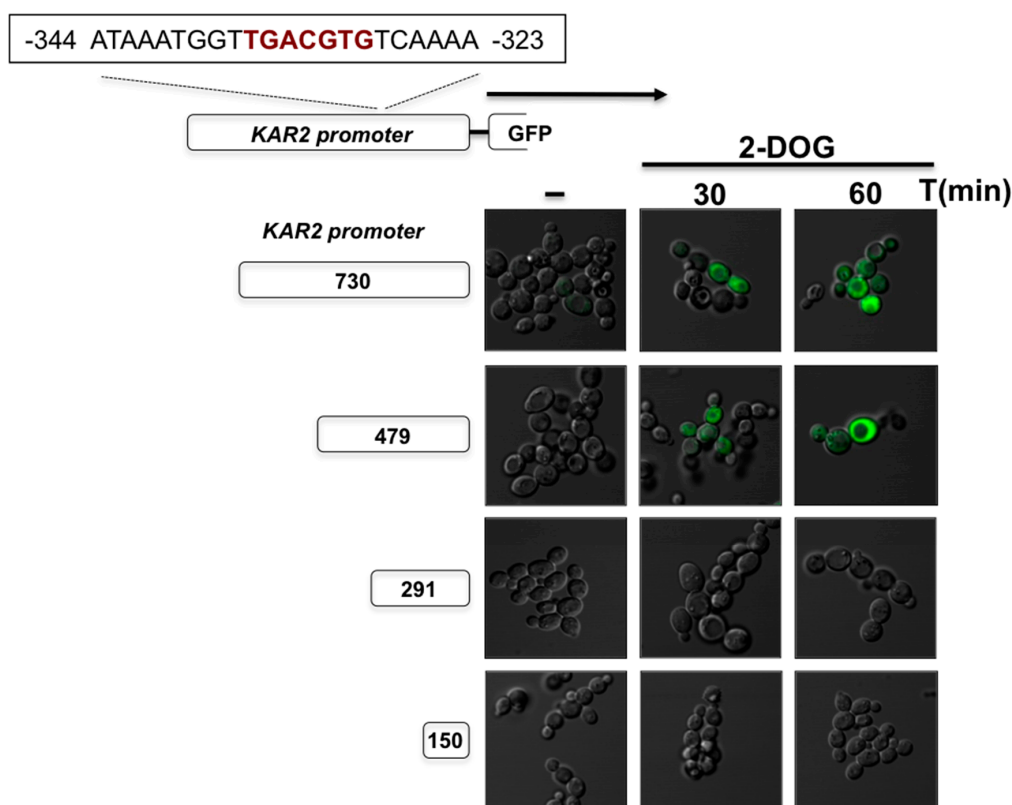

Figure 7. Detection of *K. lactis KAR2* promoter activity upon ER stress. The putative *KlKAR2* promoter (730 nucleotides of the upstream start codon region) and the indicated serial deletions fragments were fused to the *GFP* reporter gene. Constructions were cloned in an episomal multicopy *K. lactis* plasmid and used to transfect wild type cells. Cells were grown in YPD until 0.5 OD_{600} and treated with 2-DOG for the indicated times. Cells were visualized under epi-fluorescence microscopy and photographed.

Figure 8. Blast search of the putative *K. lactis* UPRE motif (shown in brown in Figure 7) in putative ER stress-responsive genes. The search was directed to the indicated 5′ untranslated regions of the indicated genes. Coordinates are relative to the first nucleotide of the respective translation start codon.

4. The UPR in *Schizosaccharomyces pombe*

S. pombe, the fission yeast, is a model organism used to analyse different aspects of cellular physiology. Interestingly, this yeast species lacks *HAC1* and the ER stress response is mediated by an Ire1-dependent mRNA degradation.

The Ire1 of *S. pombe* has the same structural features as *Sc*Ire1 (Figure 1). It has a luminal domain and a cytosolic portion that contains the kinase and endoribonuclease domains. The full length *Sp*Ire1 sequence shows only 24% identity with *Sc*Ire1, which indicates a wide evolutionary distance between the two proteins. *Sp*Ire1 contains the K^{682} and N^{1014} residues, which have been shown to be essential for kinase and RNase activities in *S. cerevisiae* respectively [3,16,17]. However, the R residues that may form the basic motif of the putative RNA docking site [17,18], and that are well conserved in other yeast species are not present in *Sp*Ire1, suggesting that it might not bind a specific RNA molecule.

S. pombe Ire1 null mutants are sensitive to ER stress inducers such as DTT and Tn [47] and since *S. pombe* is a natural auxotroph for inositol due to the absence of the inositol-1-phosphate synthase, the lack of inositol in the medium is lethal to *S. pombe* [48,49]. In this yeast, inositol is essential for mating and sporulation [50]. Although the mechanism remains unknown, it has been proposed that the effect of inositol may be indirect, possibly through regulation of membrane and cell wall composition [51].

Unlike *S. cerevisiae* and other yeast species, no specific substrate has been identified for *Sp*Ire1, suggesting that *S. pombe* lacks a Hac1 orthologue. In contrast to *S. cerevisiae* and other yeast species the UPR in *S. pombe* is not mediated by a transcriptional reprogramming; instead, it has been observed that the *Sp*Ire1 RNase activity is involved in a mechanism termed Regulated Ire-Dependent Decay (RIDD) [52]. This process was first described in *Drosophila* [53] but it has also been observed in plants [54] and mammalian cells [55,56]. In *S. pombe* upon ER-stress, *Sp*Ire1 cleaves ER-localised mRNAs at consensus sites, leading to free 5′ and 3′ end-containing mRNA fragments that are rapidly degraded by exoribonucleases in a 5′-3′ direction [57] and by the exosome in the 3′-5′ direction [53], thus alleviating the ER-protein load. The *Sp*Ire1 mRNA substrates contain a consensus UG/CU sequence flanking the cleavage sites. These cleavage sites reside within the coding sequences of mRNAs, resulting in the stalling of ribosomes engaged in translation. Those ribosomes are then liberated by a ribosome/mRNA decay pathway known as 'no-go decay', which consists of the endonucleolytic cleavage of the RNA and the Dom34/Hbs1-dependent recycling of the ribosome [58].

Approximately 31% of the mRNAs regulated by *Sp*Ire1 code for proteins involved in lipid metabolism, and particularly in sterol metabolism. Sterol has also been shown to induce ER stress and to trigger UPR in *S. cerevisiae* [59]. Despite the fact that it is not known how the reduction in sterol synthesis regulates the toxicity associated with ER stress, it has been suggested that this kind of stress affects vesicular sterol transport and that therefore, when sterol biosynthesis is reduced, ER membrane fluidity may be stabilised [52].

One of the RIDD substrates is the mRNA that codes for the Grp78 chaperone orthologue BiP1 [52,60]. *Sp*Ire1 cleaves the *BiP1* mRNA within the consensus UG/CU sequence located in its 3′-UTR, leading to the loss of the poliA tail. Paradoxically, *Sp*Ire1 activity does not increase the *SpBiP1* mRNA degradation rate; instead, it makes it more stable, possibly due to the elimination of an RNA degradation sequence without affecting its translation efficiency.

In *S. pombe*, Bip1 is a 663 amino acid protein essential for cell viability and its expression is induced by various stresses, such as heat shock and Tn. It contains an ER retention signal [60] and a predicted *N*-glycosylation site [46]. Indeed, a small portion (10%) of *Sp*BiP1 is rapidly N-glycosylated upon synthesis and this glycosylation does not change with time. As one might expect, Tn prevents the appearance of the glycosylated form of BiP1 [46]. Although the synthesis of the mRNA of *Sp*BiP1 is not increased upon ER stress, its extended stability after SpIre1-dependent cleavage following ER stress results in an increase of the *Sp*Bip1 protein [52]. Finally, it appears that elimination of the 3′-UTR mRNA processing site in *Sp*BiP1 induces a significant impairment in the response to ER stress conditions [52].

5. The UPR in *Candida glabrata*

C. glabrata is one of the most common human pathogenic yeasts. It is phylogenetically related to *S. cerevisiae*, and it has the canonical Ire1 kinase and the transcriptional factor Hac1. However, the ER stress response mechanism in this yeast is very different; particularly, *CgHAC1* mRNA is not spliced by *Cg*Ire1, and *Cg*Ire1 regulates the response in an Hac1-independent manner.

C glabrata Ire1 is a 1036 amino acid protein that conserves the typical Ire1 domains: the N-terminal hydrophobic signal sequence, an ER luminal domain, a transmembrane segment, a serine/threonine kinase domain and a nuclease domain. Overall, *Cg*Ire1 displays 49% similarity and 33% identity with *Sc*Ire1 (Figure 1). *Cg*Ire1 is required for cellular response to ER stress inducers such as Tn and DTT, and this function requires its kinase and the ribonuclease activities [61]. However, the ribonuclease activity of *Cg*Ire1 does not seem to be required for the *CgHAC1* RNA splicing (see below); instead it appears to participate in the degradation of ER-associated mRNAs through a RIDD pathway similar to that of *S. pombe* [61]. Accordingly, *Cg*Ire1 does not trigger a transcriptional response to ER stress; instead, transcription is regulated by the calcium signalling pathway which depends on calcineurin phosphatase [61] (see below).

C. glabrata has a single *HAC1* orthologue containing a highly conserved bZIP domain and a conserved DNA binding region [61] (Figure 2). Overall, the *Cg*Hac1 transcription factor shows low similarity and low identity with *Sc*Hac1. The *CgHAC1* pre-mRNA contains a predicted intron of 379 nucleotides (Figure 3), which may potentially form a stem-loop structure, but it apparently lacks the consensus Ire1 splicing recognition sequences [61]. Unlike *Cg*Ire1, a lack of *Cg*Hac1 does not induce sensitivity to ER stress inducers and *Cg*Hac1 remains un-spliced in both stressed and non-stressed conditions. A lack of *HAC1* pre-mRNA splicing under ER stress conditions supports the notion that in *C. glabrata* there is a RIDD pathway that is *Cg*Ire1-dependent but *Cg*Hac1-independent [62]. Nevertheless, un-spliced *Cg*Hac1 is able to induce transcription of UPR genes in *S. cerevisiae*, indicating that it has conserved its structure and function [61].

The transcriptional response to ER stress in *C. glabrata* depends on calcineurin signalling and on the Slt2 MAPK pathway [61]. In this yeast, calcineurin prevents cell death upon ER stress by regulating calcium influx through the Crz1 transcription factor [61]. The calcineurin-Crz1 pathway is also required for the response of *C. glabrata* to various stress stimuli and for virulence [63]. The Stl2 MAPK may also exert an ER stress surveillance function to ensure transmission of healthy ER to daughter cells, as it does it in *S. cerevisiae* [62,64]. In *C. glabrata*, the gene transcription program triggered by ER stress appears to be more closely related to calcineurin-Crz1 regulated genes than to increasing the folding capacity of the ER [61,65]. In fact the *CgKAR2* promoter lacks a consensus UPRE sequence and its expression depends on the Crz1 transcription factor [61]. In summary, *C. glabrata* monitors ER stress by means of three pathways acting in parallel: the Ire1-RIDD pathway, the calcineurin-Crz1 pathway and

the Stl2-surveillance pathway. *Cg*Ire1 is also required for virulence, although its role in the infectious process remains unknown [61].

6. The UPR in *Cryptococcus neoformans*

C. neoformans is a basidiomycetous yeast. It is the most common cause of severe pulmonary infections and meningoencephalitis in immunocompromised patients. This yeast has an unfolded protein response pathway involved in ER stress response and virulence [66–68].

C. neoformans has a conserved Ire1 protein. Overall *Cn*Ire1 displays 25% identity with *Sc*Ire1. It contains the typical Ire1 domains, a sensor-luminal domain, a Ser/Thr protein kinase, and a ribonuclease domain (Figure 1). It also contains the catalytic sites (Lys[641] and Arg[1010]) for kinase and ribonuclease activities. A lack of Ire1 in *C. neoformans* generates sensitivity to ER stress inducers like Tn and DTT, and the *ire1* mutant also shows a variety of pleiotropic effects such as thermosensitivity and sensitivity to cell wall damaging agents [69]. The mutant lacking *Cn*Ire1 is avirulent since it is defective in forming the antiphagocytic capsule that is essential for evading the host immune response [69,70]. Inositol is required for mating and virulence and *C. neoformans* can use myo-inositol as a sole carbon source [71]; but there is no report that *Cn*Ire1 is required for its synthesis.

*Cn*Ire1 processes the *HXL1* pre-mRNA (the *HAC1* orthologue), which encodes a bZIP transcription factor that appears to be phylogenetically distant from *Sc*Hac1 (Figure 2). Hxl1 shows the lowest sequence conservation on the basic DNA binding domain compared to the other bZIP factors described in this work (Figure 2). However, like other *HACs*, *HXL1* contains an unconventional intron of 56 nucleotides whose splicing sites are well conserved with *basidiomycetes* and *ascomycetes* fungi (Figure 3) [70]. Although a small proportion of spliced *HXL1* mRNA coexists with the unspliced molecule in unstressed conditions, most pre-RNA is spliced by *Cn*Ire1 under ER stress conditions [69]. In contrast to *S. cerevisiae* and *K. lactis*, the *CnHXL1* intron does not seem to contain sequences complementary to the 5′-UTR region, disregarding an attenuation mechanism for negative regulation of translation. This suggests that the unspliced mRNA can be translated, yielding a 406 amino acid protein in contrast to the 426 amino acids of the induced Hxl1 protein [70]. In *C. neoformans*, an alternative mechanism of post-transcriptional regulation has been described. Splicing and stability of the *HXL1* mRNA is regulated through binding of Puf4, a component of the pumilio-FBF family of mRNA binding proteins that facilitates splicing under ER-stress conditions and attenuates mRNA degradation during ER stress attenuation [72].

A Kar2/BiP chaperone has been identified in *C. neoformans*, whose expression under ER stress conditions is regulated by the Ire1-Hxl1 pathway [69,73]. *Cn*Kar2 is an essential protein with 679 amino acid residues that displays an Hsp70 domain and an ER retention signal [73,74]. *Cn*Kar2 is required for cellular response to ER stress and high temperature, and for maintenance of cell wall integrity [70,73].

Aside from the ER stress response, *Cn*Ire1 has other functions. It also participates in the biosynthesis of the antiphagocytic capsule, in thermotolerance, in azole drug resistance, partially in the genotoxic stress response and in the maintenance of cell wall integrity [69,70]. Except for capsule production and thermotolerance these functions are at least partially mediated by Hxl1, while capsule biosynthesis seems to be dependent only on *Cn*Ire1 [70]. Furthermore, *Cn*Ire1 has a role in the sexual mating and unisexual differentiation of *C. neoformans*. While sexual mating is dependent on the activity of *Cn*Kar2, the same-sex mating is independent [68,74]. Both, opposite- and uni-sexual reproductions are independent of the Hxl1 transcription factor [68]. This indicates that *C. neoformans* has evolved unique features of the UPR pathway that are not present in other eukaryotic organisms.

7. The UPR in *Candida albicans*

C. albicans is an opportunistic human fungal pathogen. The yeast-mycelia morphological transitions play an important role in its pathogenesis.

C. albicans contains a typical Ire1 protein. Its full length comprises 1224 amino acid residues. By primary sequence comparison *Ca*Ire1 contains the common structural domains, i.e., the sensor-luminal

domain, the protein kinase domain and the ribonuclease domain (Figure 1). Overall CaIre1 displays 45% similarity and 31% identity with *Sc*Ire1. Like other yeasts, *Ca*Ire1 conserves the amino acid residues involved in kinase and RNase activities. Although, no direct evidence of the involvement of *Ca*Ire1 in the ER unfolded protein response has been obtained, its structural features indicate that it may activate a bZIP transcription factor (see below). It also appears that defective *Ca*Ire1 mutants display high sensitivity to cell wall stress inducers such as caspofungin [75] and show defective filamentation that alters their pathogenic capacity [76]. *C. albicans* is able to synthesise inositol *de novo* and can take it up from the media; however, *Ca*Ire1 has not been shown to participate in any of these processes [77].

In *C. albicans* the most studied component of the UPR pathway is the transcription factor Hac1. This protein displays high sequence similarity within the putative DNA-binding region to other yeast Hac1 proteins (Figure 2). Under ER stress conditions, the *CaHAC1* mRNA is processed analogously to the *S. cerevisiae HAC1* [78]. In contrast to other yeast species, however, the *CaHAC1* intron is only 19 bp long and it is located near the 3′ end of the precursor mRNA (Figure 3), although it is apparently capable of forming the stem-loop structure characteristic of this kind of introns. Processing of the intron results in the synthesis of a transcription factor with a novel 27 C-terminus [78] that may form the transactivation domain. The sequence at the intron/exon boundaries in *Ca*Hac1 are well conserved [78], but the unspliced form of *Ca*Hac1 is unable to complement a *Sc*hac1Δ mutant, indicating that *Sc*Ire1 is unable to process the *CaHAC1* intron [78]. However, the fact that the spliced form of *CaHAC1* is able to complement the *S. cerevisiae* mutant indicates that *Ca*Hac1 is the functional homologue of *Sc*Hac1 [78]. Due to the small size of the *CaHAC1* intron, a translation attenuation mechanism similar to that present in *S. cerevisiae* and *K. lactis*, seems to be discarded.

CaHac1 is required in order to trigger a cellular response to ER stress inducers such as Tn and DTT. In fact, it appears that under ER stress, *Ca*Hac1 triggers expression of a group of genes involved in secretion, cell wall biogenesis and vesicle transport among other processes [78].

Like in *C. glabrata*, the ER stress response in *C. albicans* is dependent on the calcineurin-CRZ1 pathway [79]. Nevertheless, it seems that in this species, the calcineurin pathway is required as an assisting mechanism to regulate the Hac1-dependent UPR genes [79]. Additionally, *C. albicans* cells that are defective in calcineurin and Crz1 activities are highly sensitive to Tn and DTT [80].

C. albicans expresses a Kar2 chaperone orthologue, which is essential for cell survival [81] but nothing is known regarding its participation in the ER stress response pathway. It has been determined that *Ca*Kar2 can partially complement a lack of Kar2 in *S. cerevisiae*, alleviating the thermosensitivity displayed by the *Sc*kar2Δ mutant. Additionally, *Ca*Kar2 displays *in vitro* protein translocation activity, suggesting that it may participate in the secretory pathway of *C. albicans* [81].

8. Concluding Remarks

The unfolded protein response (UPR) is a signalling pathway that is activated in response to ER stress to restore and maintain ER homeostasis. In mammalian cells, it is composed by three branches: IRE1, PERK, and ATF6. IRE1 is the most conserved branch of the UPR. It is preserved in all eukaryotes and is the only branch present in yeast species. Even though the Ire1 sensor is highly conserved, the mechanisms to handle the ER stress response varies in different species. The kinase and RNase domains of Ire1 proteins are greatly similar among different species. In particular, the catalytic residues of those domains are highly conserved in all eukaryotes [82]. Upon ER stress, ER homeostasis can be restored in two ways: by increasing the protein folding capacity, and by decreasing the load of proteins arriving to the ER. The folding capacity may be increased through transcriptional upregulation, while the reduction of the protein load can be achieved by selective decay of ER-localised mRNAs. In any case, it seems that the RNase activity of Ire1 has a crucial role in the mechanism of the UPR, either degrading a large set of mRNAs or processing a very specific mRNA to produce a transcriptional response. In mammalian cells, both mechanisms are present, and are triggered depending on cellular conditions and cell type [52,53,56]. However, in yeast species the strategy is different; some yeasts rely on a transcriptional response to regulate genes needed to cope with unfolded protein accumulation,

while others initiate a selective decay of ER-localised mRNAs (Figure 9). In *S. cerevisiae*, *K. lactis*, *C. albicans* and *C. neoformans* Ire1 processes the pre-mRNA of a bZIP transcription factor, Hac1 (in *Sc.*, *Kl.*, and *Ca.*) or Hxl1 (in *Cn.*); while in *S. pombe* and *C. glabrata* the response is mediated by Ire1 through degradation of ER targeted-mRNAs by the RIDD pathway (Figure 9).
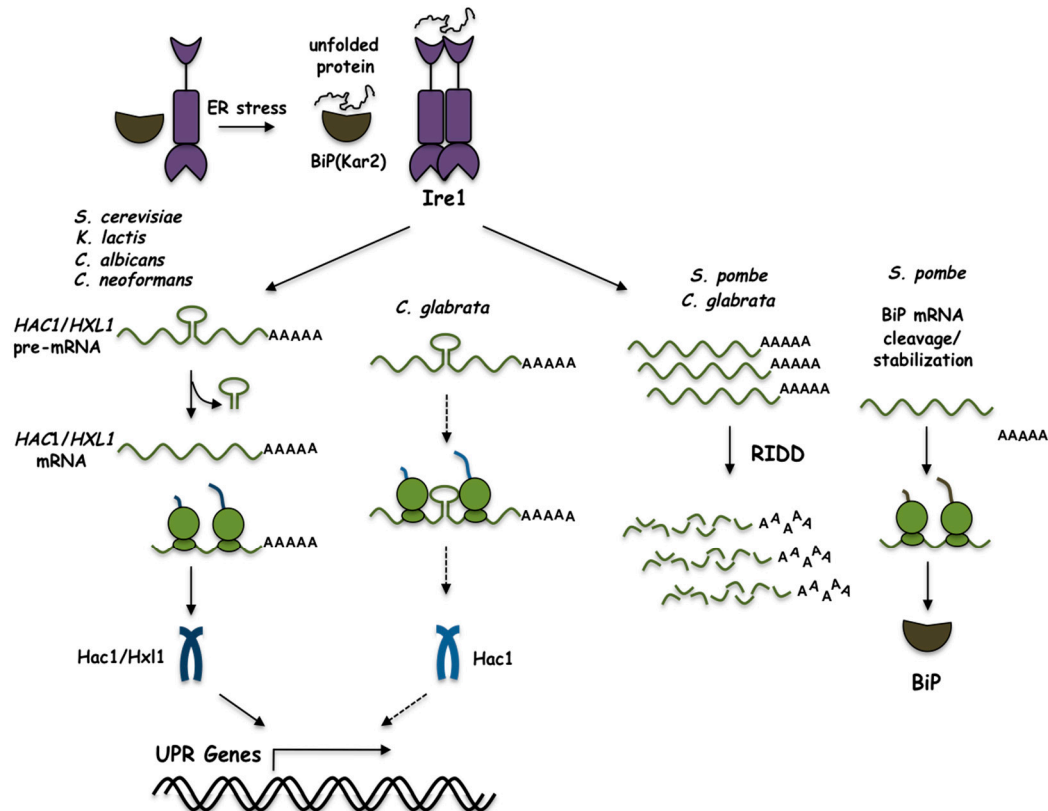

Figure 9. The unfolded protein response pathway in several yeast species. The accumulation of unfolded proteins in the ER leads to the activation of Ire1. In *Sc.*, *Kl.*, *Ca.*, and *Cn.*, Ire1 splices the *HAC1*/*HXL1* pre-mRNA leading to its translation. The synthesised bZIP factor (Hac1/Hxl1), regulates transcription of UPR-responsive genes. In *Sp.*, and *Cg.*, Ire1 cleaves ER-localised mRNAs through the Regulated Ire-Dependent Decay (RIDD) pathway. In *Sp.*, Ire1 also cleaves the BiP mRNA in the 3′ UTR region leading to its stabilization and translation. As described in the text, the unspliced *HAC1* RNA of *Cg* may induce transcription of UPR-responsive genes in *S. cerevisiae* (depicted by the dotted arrows), although there is no evidence that this process can actually occur in *C. glabrata*.

It has been proposed that the RNase activity used in the RIDD process represents the ancestral mechanism, since it is less specific with a broader mRNA degradation capacity. Evolution of this process implied loss of this broad degradation capacity and the acquisition of a more specialised mechanism to splice a specific target [52]. Through this last mechanism Ire1 removes an unconventional intron; interestingly, it has been shown that the sequence of the Hac1/Hxl1 intron is conserved only at the splice recognition sites, while its size and structure vary among different species; it is very short in metazoan, filamentous fungi, and several yeasts, whereas some other yeasts have long introns [83]. The long intron of *S. cerevisiae* is shared by some closely related species, and it is suggested that the translation attenuation mechanism that depends on the 5′ UTR described in *S. cerevisiae* is present only in this kind of long introns [42]. We have found that *K. lactis* presents a long intron containing a sequence complementary to the 5′ UTR, which is similar to that of *S. cerevisiae*, therefore the attenuation mechanism could be conserved in *K. lactis*. Some yeasts lack the regulatory intron or even have lost the ortholog of the bZIP mRNA and therefore have evolved other mechanisms for the induction of the UPR. These different strategies indicate that yeast species have optimized the mechanisms of

their UPR to adapt to their specific lifestyles. The UPR pathways of the yeast species described in this review show intriguing differences that may expand our understanding of their phylogenetic relationships and the utility of the mechanisms present in each organism to deal with and adapt to their particular niche.

Conflicts of Interest: The authors declare no conflict of interest.

References

1. Domínguez-Martín, E.; Ongay-Larios, L.; Kawasaki, L.; Vincent, O.; Coello, G.; Coria, R.; Escalante, R. IreA controls endoplasmic reticulum stress-induced autophagy and survival through homeostasis recovery. *Mol. Cell. Biol.* **2018**, *38*, e00054-18. [CrossRef]

2. Domínguez-Martín, E.; Hernández-Elvira, M.; Vincent, O.; Coria, R.; Escalante, R. Unfolding the endoplasmic reticulum of a social amoeba: *Dictyostelium discoideum* as a new model for the study of endoplasmic reticulum stress. *Cells* **2018**, *7*, 56. [CrossRef] [PubMed]

3. Mori, K.; Ma, W.; Gething, M.J.; Sambrook, J. A transmembrane protein with a cdc2+/CDC28-related kinase activity is required for signaling from the ER to the nucleus. *Cell* **1993**, *74*, 743–756. [CrossRef] [PubMed]

4. Sidrauski, C.; Walter, P. The transmembrane kinase Ire1p is a site-specific endonuclease that initiates mRNA splicing in the unfolded protein response. *Cell* **1997**, *90*, 1031–1039. [CrossRef]

5. Bertolotti, A.; Zhang, Y.; Hendershot, L.M.; Harding, H.P.; Ron, D. Dynamic interaction of BiP and ER stress transducers in the unfolded- protein response. *Nat. Cell Biol.* **2000**, *2*, 326–332. [CrossRef] [PubMed]

6. Okamura, K.; Kimata, Y.; Higashio, H.; Tsuru, A.; Kohno, K. Dissociation of Kar2p/BiP from an ER sensory molecule, Ire1p, triggers the unfolded protein response in yeast. *Biochem. Biophys. Res. Commun.* **2000**, *279*, 445–450. [CrossRef] [PubMed]

7. Credle, J.J.; Finer-Moore, J.S.; Papa, F.R.; Stroud, R.M.; Walter, P. On the mechanism of sensing unfolded protein in the endoplasmic reticulum. *Proc. Natl. Acad. Sci. USA* **2005**, *102*, 18773–18784. [CrossRef] [PubMed]

8. Oikawa, D.; Kimata, Y.; Kohno, K. Self-association and BiP dissociation are not sufficient for activation of the ER stress sensor Ire1. *J. Cell Sci.* **2007**, *120*, 1681–1688. [CrossRef] [PubMed]

9. Kimata, Y.; Ishiwata-Kimata, Y.; Ito, T.; Hirata, A.; Suzuki, T.; Oikawa, D.; Takeuchi, M.; Kohno, K. Two regulatory steps of ER-stress sensor Ire1 involving its cluster formation and interaction with unfolded proteins. *J. Cell Biol.* **2007**, *179*, 75–86. [CrossRef] [PubMed]

10. Gardner, B.M.; Walter, P. Unfolded proteins are Ire1-activating ligands that directly induce the unfolded protein response. *Science* **2011**, *333*, 1891–1894. [CrossRef] [PubMed]

11. Nikawa, J.; Yamashita, S. IRE1 encodes a putative protein kinase containing a membrane-spanning domain and is required for inositol phototrophy in Saccharomyces cerevisiae. *Mol. Microbiol.* **1992**, *6*, 1441–1446. [CrossRef] [PubMed]

12. Cox, J.S.; Shamu, C.E.; Walter, P. Transcriptional induction of genes encoding endoplasmic-reticulum resident proteins requires a transmembrane protein-kinase. *Cell* **1993**, *73*, 1197–1206. [CrossRef]

13. Sidrauski, C.; Cox, J.S.; Walter, P. tRNA ligase is required for regulated mRNA splicing in the unfolded protein response. *Cell* **1996**, *87*, 405–413. [CrossRef]

14. Cox, J.S.; Chapman, R.E.; Walter, P. The unfolded protein response coordinates the production of endoplasmic reticulum protein and endoplasmic reticulum membrane. *Mol. Biol. Cell* **1997**, *8*, 1805–1814. [CrossRef] [PubMed]

15. Chen, Y. Identification of mitogen-activated protein kinase signaling pathways that confer resistance to endoplasmic reticulum stress in *Saccharomyces cerevisiae*. *Mol. Cancer Res.* **2005**, *3*, 669–677. [CrossRef] [PubMed]

16. Shamu, C.E.; Walter, P. Oligomerization and phosphorylation of the Ire1p kinase during intracellular signaling from the endoplasmic reticulum to the nucleus. *EMBO J.* **1996**, *15*, 3028–3039. [PubMed]

17. Van Anken, E.; Pincus, D.; Coyle, S.; Aragón, T.; Osman, C.; Lari, F.; Gómez Puerta, S.; Korennykh, A.V.; Walter, P. Specificity in endoplasmic reticulum-stress signaling in yeast entails a step-wise engagement of HAC1 mRNA to clusters of the stress sensor Ire1. *eLife* **2014**, *3*, e05031. [CrossRef] [PubMed]

18. Goffin, L.; Vodala, S.; Fraser, C.; Ryan, J.; Timms, M.; Meusburger, S.; Catimel, B.; Nice, E.C.; Silver, P.A.; Xiao, C.-Y.; et al. The Unfolded Protein Response transducer Ire1p contains a nuclear localization sequence recognized by multiple β importins. *Mol. Biol. Cell* **2006**, *17*, 5309–5323. [CrossRef] [PubMed]

19. Mori, K.; Kawahara, T.; Yoshida, H.; Yanagi, H.; Yura, T. Signalling from endoplasmic reticulum to nucleus: Transcription factor with a basic-leucine zipper motif is required for the unfolded protein-response pathway. *Genes Cells* **1996**, *1*, 803–817. [CrossRef] [PubMed]

20. Fordyce, P.M.; Pincus, D.; Kimmig, P.; Nelson, C.S.; El-Samad, H.; Walter, P.; DeRisi, J.L. Basic leucine zipper transcription factor Hac1 binds DNA in two distinct modes as revealed by microfluidic analyses. *Proc. Natl. Acad. Sci. USA* **2012**, *109*, E3084–E3093. [CrossRef] [PubMed]

21. Fujii, Y.; Shimizu, T.; Toda, T.; Yanagida, M.; Hakoshima, T. Structural basis for the diversity of DNA recognition by bZIP transcription factors. *Nat. Struct. Biol.* **2000**, *7*, 889–893. [CrossRef] [PubMed]

22. Miller, M. The importance of being flexible: The case of basic region leucine zipper transcriptional regulators. *Curr. Protein Pept. Sci.* **2009**, *10*, 244–269. [CrossRef] [PubMed]

23. Nojima, H.; Leem, S.H.; Araki, H.; Sakai, A.; Nakashima, N.; Kanaoka, Y.; Ono, Y. Hac1: A novel yeast bZIP protein binding to the CRE motif is a multicopy suppressor for cdc10 mutant of *Schizosaccharomyces pombe*. *Nucleic Acids Res.* **1994**, *22*, 5279–5288. [CrossRef] [PubMed]

24. Nikawa, J.I.; Akiyoshi, M.; Hirata, S.; Fukuda, T. *Saccharomyces cerevisiae* IRE2/HAC1 is involved in IRE1-mediated KAR2 expression. *Nucleic Acids Res.* **1996**, *24*, 4222–4226. [CrossRef] [PubMed]

25. Cox, J.S.; Walter, P. A novel mechanism for regulating activity of a transcription factor that controls the unfolded protein response. *Cell* **1996**, *87*, 391–404. [CrossRef]

26. Chapman, R.E.; Walter, P. Translational attenuation mediated by an mRNA intron. *Curr. Biol.* **1997**, *7*, 850–859. [CrossRef]

27. Kawahara, T.; Yanagi, H.; Yura, T.; Mori, K. Endoplasmic reticulum stress-induced mRNA splicing permits synthesis of transcription factor Hac1p/Ern4p that activates the unfolded protein response. *Mol. Biol. Cell* **1997**, *8*, 1845–1862. [CrossRef] [PubMed]

28. Rüegsegger, U.; Leber, J.H.; Walter, P. Block of HAC1 mRNA translation by long-range base pairing is released by cytoplasmic splicing upon induction of the unfolded protein response. *Cell* **2001**, *107*, 103–114. [CrossRef]

29. Aragón, T.; Van Anken, E.; Pincus, D.; Serafimova, I.M.; Korennykh, A.V.; Rubio, C.A.; Walter, P. Messenger RNA targeting to endoplasmic reticulum stress signalling sites. *Nature* **2009**, *457*, 736–740. [CrossRef] [PubMed]

30. Mori, K.; Ogawa, N.; Kawahara, T.; Yanagi, H.; Yura, T. mRNA splicing-mediated C-terminal replacement of transcription factor Hac1p is required for efficient activation of the unfolded protein response. *Proc. Natl. Acad. Sci. USA* **2000**, *97*, 4660–4665. [CrossRef] [PubMed]

31. Mori, K.; Sant, A.; Kohno, K.; Normington, K.; Gething, M.J.; Sambrook, J.F. A 22 bp cis-acting element is necessary and sufficient for the induction of the yeast KAR2 (BiP) gene by unfolded proteins. *EMBO J.* **1992**, *11*, 2583–2593. [PubMed]

32. Kohno, K.; Normington, K.; Sambrook, J.; Gething, M.J.; Mori, K. The promoter region of the yeast KAR2 (BiP) gene contains a regulatory domain that responds to the presence of unfolded proteins in the endoplasmic reticulum. *Mol. Cell. Biol.* **1993**, *13*, 877–890. [CrossRef] [PubMed]

33. Mori, K.; Ogawa, N.; Kawahara, T.; Yanagi, H.; Yura, T. Palindrome with spacer of one nucleotide is characteristic of the cis-acting unfolded protein response element in Saccharomyces cerevisiae. *J. Biol. Chem.* **1998**, *273*, 9912–9920. [CrossRef] [PubMed]

34. Partaledis, J.A.; Berlin, V. The FKB2 gene of *Saccharomyces cerevisiae*, encoding the immunosuppressant-binding protein FKBP-13, is regulated in response to accumulation of unfolded proteins in the endoplasmic reticulum. *Proc. Natl. Acad. Sci. USA* **1993**, *90*, 5450–5454. [CrossRef] [PubMed]

35. Patil, C.K.; Li, H.; Walter, P. Gcn4p and novel upstream activating sequences regulate targets of the unfolded protein response. *PLoS Biol.* **2004**, *2*, e246. [CrossRef] [PubMed]

36. Bukau, B.; Horwich, A.L. The Hsp70 and Hsp60 Chaperone Machines. *Cell* **1998**, *92*, 351–366. [CrossRef]

37. Vogel, J.P.; Misra, L.M.; Rose, M.D. Loss of BiP/GRP78 function blocks translocation of secretory proteins in yeast. *J. Cell Biol.* **1990**, *110*, 1885–1895. [CrossRef] [PubMed]

38. Nishikawa, S.I.; Fewell, S.W.; Kato, Y.; Brodsky, J.L.; Endo, T. Molecular chaperones in the yeast endoplasmic reticulum maintain the solubility of proteins for retrotranslocation and degradation. *J. Cell Biol.* **2001**, *153*, 1061–1070. [CrossRef] [PubMed]

39. Kimata, Y.; Kimata, Y.I.; Shimizu, Y.; Abe, H.; Farcasanu, I.C.; Takeuchi, M.; Rose, M.D.; Kohno, K. Genetic evidence for a role of BiP/Kar2 that regulates Ire1 in response to accumulation of unfolded proteins. *Mol. Biol. Cell* **2003**, *14*, 2559–2569. [CrossRef] [PubMed]

40. Normington, K.; Kohno, K.; Kozutsumi, Y.; Gething, M.J.; Sambrook, J. *S. cerevisiae* encodes an essential protein homologous in sequence and function to mammalian BiP. *Cell* **1989**, *57*, 1223–1236. [CrossRef]

41. Wolfe, K.H.; Shields, D.C. Molecular evidence for an ancient duplication of the entire yeast genome. *Nature* **1997**, *387*, 708–713. [CrossRef] [PubMed]

42. Hooks, K.B.; Griffiths-Jones, S. Conserved RNA structures in the non-canonical Hac1/Xbp1 intron. *RNA Biol.* **2011**, *8*, 1–6. [CrossRef] [PubMed]

43. Mori, T.; Ogasawara, C.; Inada, T.; Englert, M.; Beier, H.; Takezawa, M.; Endo, T.; Yoshihisa, T. Dual functions of yeast tRNA ligase in the Unfolded Protein Response: Unconventional cytoplasmic splicing of HAC1 pre-mRNA is not sufficient to release translational attenuation. *Mol. Biol. Cell* **2010**, *21*, 3722–3734. [CrossRef] [PubMed]

44. Lewis, M.J.; Pelham, H.R. The sequence of the *Kluyveromyces lactis* BiP gene. *Nucleic Acids Res.* **1990**, *18*, 6438. [CrossRef] [PubMed]

45. Lewis, M.J.; Sweet, D.J.; Pelham, H.R. The ERD2 gene determines the specificity of the luminal ER protein retention system. *Cell* **1990**, *61*, 1359–1363. [CrossRef]

46. Pidoux, A.L.; Armstrong, J. The BiP protein and the endoplasmic reticulum of *Schizosaccharomyces pombe*: Fate of the nuclear envelope during cell division. *J. Cell. Sci.* **1993**, *105*, 1115–1120. [PubMed]

47. Frost, A.; Elgort, M.G.; Brandman, O.; Ives, C.; Collins, S.R.; Miller-Vedam, L.; Weibezahn, J.; Hein, M.Y.; Poser, I.; Mann, M.; et al. Functional repurposing revealed by comparing *S. pombe* and *S. cerevisiae* genetic interactions. *Cell* **2012**, *149*, 1339–1352. [CrossRef] [PubMed]

48. Ridgway, G.J.; Douglas, H.C. Unbalanced growth of yeast due to inositol deficiency. *J. Bacteriol.* **1958**, *76*, 163–166. [PubMed]

49. Ingavale, S.S.; Bachhawat, A.K. Restoration of inositol prototrophy in the fission yeast *Schizosaccharomyces pombe*. *Microbiology* **1999**, *145*, 1903–1910. [CrossRef] [PubMed]

50. Voicu, P.-M.; Poitelea, M.; Schweingruber, E.; Rusu, M. Inositol is specifically involved in the sexual program of the fission yeast *Schizosaccharomyces pombe*. *Arch. Microbiol.* **2002**, *177*, 251–258. [CrossRef] [PubMed]

51. Niederberger, C.; Gräub, R.; Schweingruber, A.-M.; Fankhauser, H.; Rusu, M.; Poitelea, M.; Edenharter, L.; Schweingruber, M.E. Exogenous inositol and genes responsible for inositol transport are required for mating and sporulation in *Schizosaccharomyces pombe*. *Curr. Genet.* **1998**, *33*, 255–261. [CrossRef] [PubMed]

52. Kimmig, P.; Diaz, M.; Zheng, J.; Williams, C.C.; Lang, A.; Aragón, T.; Li, H.; Walter, P. The unfolded protein response in fission yeast modulates stability of select mRNAs to maintain protein homeostasis. *eLife* **2012**, *2012*, e00048. [CrossRef] [PubMed]

53. Hollien, J.; Weissman, J.S. Decay of endoplasmic reticulum-localized mRNAs during the unfolded protein response. *Science* **2006**, *313*, 104–107. [CrossRef] [PubMed]

54. Mishiba, K.; Nagashima, Y.; Suzuki, E.; Hayashi, N.; Ogata, Y.; Shimada, Y.; Koizumi, N. Defects in IRE1 enhance cell death and fail to degrade mRNAs encoding secretory pathway proteins in the *Arabidopsis* unfolded protein response. *Proc. Natl. Acad. Sci. USA* **2013**, *110*, 5713–5718. [CrossRef] [PubMed]

55. Han, D.; Lerner, A.G.; Vande Walle, L.; Upton, J.-P.; Xu, W.; Hagen, A.; Backes, B.J.; Oakes, S.A.; Papa, F.R. IRE1alpha kinase activation modes control alternate endoribonuclease outputs to determine divergent cell fates. *Cell* **2009**, *138*, 562–575. [CrossRef] [PubMed]

56. Hollien, J.; Lin, J.H.; Li, H.; Stevens, N.; Walter, P.; Weissman, J.S. Regulated Ire1-dependent decay of messenger RNAs in mammalian cells. *J. Cell Biol.* **2009**, *186*, 323–331. [CrossRef] [PubMed]

57. Iqbal, J.; Dai, K.; Seimon, T.; Jungreis, R.; Oyadomari, M.; Kuriakose, G.; Ron, D.; Tabas, I.; Hussain, M.M. IRE1beta inhibits chylomicron production by selectively degrading MTP mRNA. *Cell Metab.* **2008**, *7*, 445–455. [CrossRef] [PubMed]

58. Pidoux, A.L.; Armstrong, J. Analysis of the BiP gene and identification of an ER retention signal in *Schizosaccharomyces pombe*. *EMBO J.* **1992**, *11*, 1583–1591. [PubMed]

59. Guydosh, N.R.; Kimmig, P.; Walter, P.; Green, R. Regulated Ire1-dependent mRNA decay requires no-go mRNA degradation to maintain endoplasmic reticulum homeostasis in *S. pombe*. *eLife* **2017**, *6*. [CrossRef] [PubMed]

60. Pineau, L.; Colas, J.; Dupont, S.; Beney, L.; Fleurat-Lessard, P.; Berjeaud, J.-M.; Bergès, T.; Ferreira, T. Lipid-induced ER stress: Synergistic effects of sterols and saturated fatty acids. *Traffic* **2009**, *10*, 673–690. [CrossRef] [PubMed]

61. Miyazaki, T.; Nakayama, H.; Nagayoshi, Y.; Kakeya, H.; Kohno, S. Dissection of Ire1 functions reveals stress response mechanisms uniquely evolved in *Candida glabrata*. *PLoS Pathog.* **2013**, *9*, e1003160. [CrossRef] [PubMed]

62. Miyazaki, T.; Kohno, S. ER stress response mechanisms in the pathogenic yeast *Candida glabrata* and their roles in virulence. *Virulence* **2014**, *5*, 365–370. [CrossRef] [PubMed]

63. Miyazaki, T.; Yamauchi, S.; Inamine, T.; Nagayoshi, Y.; Saijo, T.; Izumikawa, K.; Seki, M.; Kakeya, H.; Yamamoto, Y.; Yanagihara, K.; et al. Roles of calcineurin and Crz1 in antifungal susceptibility and virulence of *Candida glabrata*. *Antimicrob. Agents Chemother.* **2010**, *54*, 1639–1643. [CrossRef] [PubMed]

64. Babour, A.; Bicknell, A.A.; Tourtellotte, J.; Niwa, M. A surveillance pathway monitors the fitness of the endoplasmic reticulum to control its inheritance. *Cell* **2010**, *142*, 256–269. [CrossRef] [PubMed]

65. Chen, Y.-L.; Konieczka, J.H.; Springer, D.J.; Bowen, S.E.; Zhang, J.; Silao, F.G.S.; Bungay, A.A.C.; Bigol, U.G.; Nicolas, M.G.; Abraham, S.N.; et al. Convergent Evolution of calcineurin pathway roles in thermotolerance and virulence in *Candida glabrata*. *Genes Genome Genet.* **2012**, *2*, 675–691. [CrossRef] [PubMed]

66. Askew, D.S. Endoplasmic reticulum stress and fungal pathogenesis converge. *Virulence* **2014**, *5*, 331–333. [CrossRef] [PubMed]

67. Krishnan, K.; Askew, D.S. Endoplasmic reticulum stress and fungal pathogenesis. *Fungal Biol. Rev.* **2014**, *28*, 29–35. [CrossRef] [PubMed]

68. Jung, K.W.; So, Y.S.; Bahn, Y.S. Unique roles of the unfolded protein response pathway in fungal development and differentiation. *Sci. Rep.* **2016**, *6*, 1–14. [CrossRef] [PubMed]

69. Cheon, S.A.; Jung, K.-W.; Chen, Y.-L.; Heitman, J.; Bahn, Y.-S.; Kang, H.A. Unique evolution of the UPR pathway with a novel bZIP transcription factor, Hxl1, for controlling pathogenicity of *Cryptococcus neoformans*. *PLoS Pathog.* **2011**, *7*, e1002177. [CrossRef] [PubMed]

70. Cheon, S.A.; Jung, K.W.; Bahn, Y.S.; Kang, H.A. The Unfolded Protein Response (UPR) pathway in *Cryptococcus*. *Virulence* **2014**, *5*, 341–350. [CrossRef] [PubMed]

71. Xue, C.; Liu, T.; Chen, L.; Li, W.; Liu, I.; Kronstad, J.W.; Seyfang, A.; Heitman, J. Role of an expanded inositol transporter repertoire in *Cryptococcus neoformans* sexual reproduction and virulence. *mBio* **2010**, *1*, e00084-10. [CrossRef] [PubMed]

72. Glazier, V.E.; Kaur, J.N.; Brown, N.T.; Rivera, A.A.; Panepinto, J.C. Puf4 regulates both splicing and decay of *HXL1* mRNA encoding the unfolded protein response transcription factor in *Cryptococcus neoformans*. *Eukaryot. Cell* **2015**, *14*, 385–395. [CrossRef] [PubMed]

73. Jung, K.W.; Kang, H.A.; Bahn, Y.S. Essential roles of the Kar2/BiP molecular chaperone downstream of the UPR pathway in *Cryptococcus neoformans*. *PLoS ONE* **2013**, *8*, e58956. [CrossRef] [PubMed]

74. Lee, S.C.; Heitman, J. Function of *Cryptococcus neoformans* KAR7 (SEC66) in karyogamy during unisexual and opposite-sex mating. *Eukaryot. Cell* **2012**, *11*, 783–794. [CrossRef] [PubMed]

75. Blankenship, J.R.; Fanning, S.; Hamaker, J.J.; Mitchell, A.P. An Extensive circuitry for cell wall regulation in *Candida albicans*. *PLoS Pathog.* **2010**, *6*, e1000752. [CrossRef] [PubMed]

76. Azadmanesh, J.; Gowen, A.M.; Creger, P.E.; Schafer, N.D.; Blankenship, J.R. Filamentation involves two overlapping, but distinct, programs of filamentation in the pathogenic fungus *Candida albicans*. *Genes Genome Genet.* **2017**, *7*, 3797–3808. [CrossRef] [PubMed]

77. Chen, Y.-L.; Kauffman, S.; Reynolds, T.B. *Candida albicans* uses multiple mechanisms to acquire the essential metabolite inositol during infection. *Infect. Immun.* **2008**, *76*, 2793–2801. [CrossRef] [PubMed]

78. Wimalasena, T.T.; Enjalbert, B.; Guillemette, T.; Plumridge, A.; Budge, S.; Yin, Z.; Brown, A.J.P.; Archer, D.B. Impact of the unfolded protein response upon genome-wide expression patterns, and the role of Hac1 in the polarized growth, of *Candida albicans*. *Fungal Genet. Biol.* **2008**, *45*, 1235–1247. [CrossRef] [PubMed]

79. Thomas, E.; Sircaik, S.; Roman, E.; Brunel, J.M.; Johri, A.K.; Pla, J.; Panwar, S.L. The activity of RTA2, a downstream effector of the calcineurin pathway, is required during tunicamycin-induced ER stress response in *Candida albicans*. *FEMS Yeast Res.* **2015**, *15*, fov095. [CrossRef] [PubMed]

80. Zhang, J.; Heitman, J.; Chen, Y.-L. Comparative analysis of calcineurin signaling between *Candida dubliniensis* and *Candida albicans*. *Commun. Integr. Biol.* **2012**, *5*, 122–126. [CrossRef] [PubMed]

81. Morrow, M.W.; Janke, M.R.; Lund, K.; Morrison, E.P.; Paulson, B.A. The *Candida albicans* Kar2 protein is essential and functions during the translocation of proteins into the endoplasmic reticulum. *Curr. Genet.* **2011**, *57*, 25–37. [CrossRef] [PubMed]

82. Zhang, L.; Zhang, C.; Wang, A. Divergence and conservation of the major UPR branch IRE1-bZIP signaling pathway across eukaryotes. *Sci. Rep.* **2016**, *6*, 27362. [CrossRef] [PubMed]

83. Montenegro-Montero, A.; Goity, A.; Larrondo, L.F. The bZIP transcription factor HAC-1 is involved in the unfolded protein response and is necessary for growth on cellulose in *Neurospora crassa*. *PLoS ONE* **2015**, *10*, e0131415. [CrossRef] [PubMed]